Nanoparticle-filled micelles as versatile delivery vehicles for TLR4 mediated immunotherapy

Ph.D. Thesis

GIORDANO TRAINI

2019

Nanoparticle-filled micelles as versatile delivery vehicles for TLR4 mediated immunotherapy

Summary

Cancer immunotherapy is a revolutionary new method using the immune system to fight cancer. Immunotherapy is expected to radically change the way cancer is treated due to the multiple advantages it features compared to the traditional pillars of cancer care such as radiotherapy, chemotherapy, and surgery. Cancer immunotherapy "trains" the immune system in discerning and killing cancer cells, being more targeted and having fewer side-effects than chemo- and radiotherapy, and resulting in a long-lasting remission.

Amongst the different cancer immunotherapies developed up until now, checkpoint blockade therapy is an important breakthrough with 5 drugs and antibodies approved by the American food and drug administration (FDA) and hundreds of ongoing clinical trials. This approach consists of inhibiting the immune escape mechanisms of cancer cells, unleashing the full potential of the immune system and in particular of T cells. However, this therapy shows a low response rate (with checkpoint blockade having a success rate of 10-40% in advanced melanoma patients when used as monotherapy). Moreover, immune-related adverse effects, development of resistance and late tumor relapses are emerging.

Another possibility in cancer immunotherapy is represented by therapeutic vaccines, and especially the delivery of antigens and adjuvants by nanoparticles has the potential to improve the efficacy of such treatments. Nanoparticles can make a difference since they can deliver antigen and adjuvant together to the tumor site and lymph nodes, protect the antigen from degradation upon its administration by different routes and sustain the antigen release over time. Moreover, nanoparticles can be used to provide additional treatment modalities such as hyperthermia and photodynamic therapy and multimodal imaging all in a small delivery vehicle.

The need for further developments in cancer immunotherapy led to the concept of combinatorial immunotherapy, where different immunotherapies cooperate together in order to overcome the limitations of monotherapies. A crucial element needed for the proper functioning of checkpoint blockade is the continuous and sustained generation of a population of T cells capable of recognizing the tumor, and for this purpose, cancer vaccines could be considered an ideal partner for immunotherapies.

Amongst the possible vaccine adjuvants, Toll-like receptors (TLR) ligands and in particular TLR4 ligands have been actively investigated due to the known crucial roles of TLRs. TLR4 agonists have the potential to enhance both innate and adaptive immunity to treat cancer; while on the other hand TLR4 antagonists can suppress over-stimulation, and are thus promising for the treatment of auto-immune diseases and sepsis.

The best known TLR4 ligand is lipopolysaccharides (LPS), a major component of the cell surface of gram-negative bacteria, featuring the amphipathic domain known as lipid A responsible for the immunogenic activity of LPS. The FDA approved monophosphoryl lipid A (MPLA) and other lipid-A derivatives with reduced toxicity have been targets for the development of human vaccine adjuvants, with the former being evaluated as a cancer vaccine adjuvant in a number of clinical trials. These molecules achieved effective stimulation of cellular Th1 immune responses and $CD8^+$ T cell responses required to mediate immunity in cancer immunotherapy. However, the application of TLR agonists as monotherapies and their success in clinical trials has been impaired by dose-limiting toxicities owing to systemic cytokine induction and inefficient delivery to tumors and draining lymph nodes.

Lipooligosaccharides (LOS), LPS not possessing the O-antigen chain (also named rough LPS), have been investigated less for oncological applications and especially as adjuvants. The immune stimulatory effects and toxicity of LPS and LOS greatly vary due to structural differences and their "state of aggregation". The structure of TLR4 ligands also plays an important role in determining whether they behave as TLR4 agonists or antagonists. One important aspect is the number of hydrophobic chains contained in the Lipid A moiety: whereas agonists are generally characterized by having 6 acyl chains, molecules with 4 or 5 of these chains mainly behave as antagonists.

The **first chapter** of this thesis is a general introduction presenting the scientific background and some of the concepts behind this work.

The **second chapter** focuses on the development of nanoplatforms loaded with different TLR4 ligands. The LOS from Escherichia Coli (*E. coli* LOS) and from the plant pathogen *Xanthomonas campestris* pv. *Campestris* (*Xcc* LOS) were used as anticancer vaccine adjuvants, with the hypothesis that due to the structural

differences from the more known LPS and MPLA they could behave differently and change the assembly and the characteristics of the resulting systems. Besides, IAXO 102, a new synthetic TLR4 antagonist was loaded on nanoparticles and tested as an immune modulator to test the possibilities attainable by suppressing TLR4 stimulation.

In order to improve the delivery of these ligands, quantum dots (QDs), upconverting nanoparticles (UCNPs), and iron oxide nanospheres and nanocubes (IONPsp and IONPc) characterized by different properties, biocompatibility, complexity of synthesis and efficacy, were screened. By taking advantage of a self-assembly process and the amphiphilic character of the TLR4 modulators, several formulations exploiting nanoparticle encapsulation in polyethylene glycol-phospholipid micelles were prepared. Aiming to examine how the various TLR4 ligands could interact with the different nanoparticles, the pathogen-like structures derived from the hydrophobic interaction of ligand and nanoparticle were characterized, and amongst these, the best adjuvant based on in vitro results was chosen for further studies in vivo. The best adjuvant, mIONPsp-*Xcc* LOS, was generated by loading *Xcc* LOS onto 7 nm iron oxide nanospheres (IONPsp), a biocompatible and biodegradable material which has been already used clinically as an iron supplement, in magnetic resonance imaging (MRI) as contrast agent, in hyperthermia treatments and holds potential for use in further cancer immunotherapy approaches. Besides, the small size and the negative charge of the construct have the ideal characteristics for lymph-node delivery, and these nanoconstructs can feature multimodal imaging and boast intrinsic therapeutical modalities.

The **third chapter** describes how the model antigen ovalbumin (OVA) was attached to the IONPsp by using a covalent chemistry based on a hydrazone bonding that has an optimal reaction yield and fast kinetics. Moreover, it works at low concentrations and can be monitored by UV-Vis spectroscopy to obtain live feedback. This approach therefore overcomes the drawbacks of the conventional conjugation strategies such as 1-ethyl-3-(3-dimethylaminopropyl)carbodiimide (EDC) chemistry, generally being cross-linking and the need for a large excess of reagents. It was also explored how this covalent binding strategy can be applied on the iron oxide side of gold-iron oxide Janus nanoparticles (JanusNPs) to exploit their unique properties contributing towards the development of a unique theranostic system with specific

applications in cancer treatment. Moreover, a system where both OVA as antigen and LPS as an adjuvant were loaded into a IONPsp was developed. The resulting nanosystems featured hydrodynamic diameters within the 20-100 nm range ideal for lymph node delivery.

The **fourth chapter** investigates the OVA linked to mIONPsp via hydrazone bond (mIONPsp-HyNic-FB-OVA) formulated with the pathogen-mimicking mIONPsp-*Xcc* LOS as vaccine adjuvant in mice against B16-F10 melanoma expressing OVA, together with a strategy to evaluate the effect of immune checkpoint blockade for the immunosuppressive programmed death-ligand 1 (PD-L1). When this nanovaccine was administered in the mouse melanoma model combined to the checkpoint-blockade strategy, complete rejection of the tumor and the capacity to clear a tumor re-challenge were observed, which could be explained by the increase in the number of SIINFEKL-specific CD8$^+$ T cells. Moreover, by formulating mIONPsp-HyNic-FB-OVA with mIONPsp-Poly(I:C)-imiquimod, an adjuvant previously developed in our laboratory, its antitumor activity improved compared to the same adjuvant delivered with the mIONPsp-OVA prepared using electrostatic adsorption.

The importance of these results is not only related to the complete rejection of the tumor observed with our combined vaccine + checkpoint blockade approach, but also to the simple and modular assembly of the developed delivery vehicles and the potential applications of nanoparticles such as hyperthermia, photodynamic therapy and multimodal imaging that haven't been explored in this thesis.

Resumen

Desde su descubrimiento en 1995, se espera que la inmunoterapia para el cáncer, un método revolucionario que utiliza el propio sistema inmunológico como arma para combatir el cáncer, cambie radicalmente la manera en la que se tratan los tumores. Esto método tiene múltiples ventajas en comparación con la radioterapia, la quimioterapia y la cirugía, los pilares tradicionales de la oncología. La inmunoterapia para el cáncer "entrena" al sistema inmunológico en el discernimiento y la eliminación de las células cancerosas, siendo más específica, resultando en una remisión duradera e induciendo menos efectos secundarios que las maneras tradicionales de tratamiento del cáncer.

Un avance importante entre las diferentes inmunoterapias contra el cáncer desarrolladas está representado por el bloqueo de puntos de control inmunitario, un método que consiste en inhibir los mecanismos de escape de las células cancerosas desde la vigilancia del sistema inmunológico liberando todo su potencial y en particular el de las células T. Hasta ahora, 5 medicamentos y anticuerpos para el bloqueo de puntos de control inmunitario han sido aprobados por la Administración de Alimentos y Medicamentos de los Estados Unidos (FDA) y cientos de ensayos clínicos se están llevando a cabo. Desafortunadamente, esta terapia muestra una baja tasa de respuesta (con una tasa de éxito del 10-40% en pacientes con melanoma avanzado cuando se usa como monoterapia). Además, están surgiendo efectos adversos relacionados con el sistema inmunológico, desarrollo de resistencia a la terapia y recaídas tardías del tumor.

Otra posibilidad en la inmunoterapia del cáncer está representada por las vacunas terapéuticas, y especialmente la administración de antígenos y adyuvantes mediante nanopartículas tiene el potencial de mejorar la eficacia de un tratamiento convencional de este tipo. Las nanopartículas pueden marcar la diferencia ya que pueden suministrar antígeno y adyuvante juntos al tumor y ganglios linfáticos, proteger el antígeno de la degradación al momento de su administración por diferentes vías y mantener la liberación del antígeno con el tiempo. Además, las nanopartículas presentan modalidades de tratamiento adicionales, como la terapia de hipertermia, la terapia fotodinámica y pueden ser usadas para la adquisición de

imagen multimodal, todo ello en un pequeño vehículo de transporte. Este concepto ha tomado el nombre de nanomedicina teranóstica.

La necesidad de nuevos desarrollos en la inmunoterapia oncológica llevó al concepto de inmunoterapia combinatoria, en el que diferentes modalidades inmunoterapéuticas cooperan entre sí para superar las limitaciones de las monoterapias. Un elemento crucial para el éxito de la terapia de bloqueo de los puntos de control inmunitario es la generación continua y sostenida de una población de células T capaces de reconocer el tumor, y para ello, las vacunas contra el cáncer se consideran un socio ideal para las inmunoterapias.

Entre los posibles adyuvantes de la vacuna, los ligandos de los receptores de tipo Toll (TLRs) se han investigado activamente debido a las funciones cruciales conocidas de los TLR y, en particular, se han investigado los que modulan el TLR4. Los agonistas del TLR4 son capaces de potenciar la respuesta inmune y una de sus posibles aplicaciones es el tratamiento del cáncer; mientras que, por otro lado, los antagonistas de TLR4 pueden suprimir respuestas inmunitarias demasiado fuertes y, por lo tanto, son prometedores para el tratamiento de enfermedades autoinmunes.

El ligando TLR4 más conocido es el lipopolisacárido (LPS), un componente importante de la superficie celular de las bacterias gramnegativas, que presenta el dominio anfipático conocido como lípido A, responsable de la actividad inmunogénica del LPS. La FDA aprobó el uso del monofosforil lípido A (MPLA) como adyuvante en Cervarix, una vacuna contra el cáncer cervical, siendo el primer ligando de origen sintética de TLR aprobado para el uso en seres humanos. Además, el lípido A y sus derivados con toxicidad reducida han sido objetivos para el desarrollo de adyuvantes de vacunas humanas en una serie de ensayos clínicos. Estas moléculas han conseguido estimular la producción de respuestas inmunitarias de tipo Th1 por la inducción de citocinas proinflamatorias y moléculas coestimuladoras en células dendríticas (DCs). Sin embargo, han tenido un éxito limitado debido a su inducción sistémica de citocinas que limita la dosis suministrable y su incapacidad de alcanzar el tumor y los ganglios linfáticos. Además, nuevos estudios han demostrado que pueden inducir la producción de factores que inhiben la respuesta inmunológica. Por esa razón, la combinación del bloqueo de puntos de control inmunitario con ligandos del TLR4 representa una

excelente oportunidad de incrementar la eficacia terapéutica de estas moléculas en el tratamiento del cáncer.

Dentro de los agonistas del TLR4, los lipooligosacáridos (LOS), LPS que no poseen la cadena del antígeno O, han sido menos investigados para aplicaciones en oncología y especialmente como adyuvantes. Los efectos inmunoestimulantes y la toxicidad del LPS y del LOS varían mucho debido a las diferencias estructurales y a su "estado de agregación". La estructura de los ligandos TLR4 también juega un papel importante para determinar si se comportan como agonistas o antagonistas de TLR4. Un aspecto importante es el número de cadenas hidrofóbicas contenidas en la fracción lípido A: mientras que los agonistas se caracterizan generalmente por tener 6 cadenas acílicas, las moléculas con 4 o 5 de estas cadenas se comportan principalmente como antagonistas.

Dentro de lo posibles antígenos, la ovoalbúmina (OVA), la principal proteína presente en la clara de huevo de gallina, es un candidato ideal para el uso como antígeno modelo debido a su disponibilidad comercial y bajo coste. Varios modelos tumorales que expresan OVA se han desarrollado específicamente para probar la eficacia de diferentes estrategias inmunoterapéuticas contra el cáncer y melanomas, y varios trabajos han usado el antígeno OVA como prueba de concepto.

Muchos estudios han explotado la entrega de antígenos por nanopartículas y diferentes estrategias han sido utilizadas para la formación de enlaces entre la nanopartícula y el antígeno, entre ellas la activación de la carbodiimida (por ejemplo, 1-etil-3-(3 dimetilaminopropil)carbodiimida, o EDC). Esta estrategia sufre de pobre quimioselectividad, requiere un exceso de reactivos para funcionar de una manera adecuada, es sensible a las variaciones de temperatura y pH y sufre de reticulación, que resulta en agregación y perdida de la estabilidad coloidal. Adicionalmente, la falta de métodos analíticos adecuados para caracterizar rápidamente el producto de la conjugación y su estequiometría comporta que no hay respuesta directa sobre el progreso de la reacción y consecuentemente su optimización es complicada. Aquí se aplicó un enlace de bis-arilhidrazona para el acoplamiento de nanoesferas de hierro al antígeno modelo ovoalbúmina (OVA), usando anilina como catalizador nucleófilo. La reacción de formación de hidrazona se pudo monitorizar por UV-vis, demostró una cinética de reacción rápida, alto rendimiento químico de conjugación

(>85% en pocos minutos) a concentraciones micromolares (0.5- 3 µM) y pH neutro, produciendo nanoplataformas estables y proporcionando ventajas significativas en la formación de conjugados antígeno-nanopartícula.

- El primer capítulo de esta tesis es una introducción general que pretende discutir los antecedentes científicos y algunos de los conceptos que subyacen a este trabajo.

- El segundo capítulo se centra en el desarrollo de nanoplataformas funcionalizadas con diferentes ligandos TLR4. Se utilizaron los LOS de Escherichia Coli (*E. Coli* LOS) y el del patógeno vegetal Xanthomonas campestris pv. campestris (*Xcc* LOS) como adyuvantes de la vacuna contra el cáncer, con la hipótesis de que, debido a sus diferencias estructurales con respecto a los más conocidos *E. Coli* LPS y MPLA, podrían comportarse de forma diferente afectando el ensamblaje y las características de los sistemas resultantes. Debido a nuestro interés tanto en la estimulación como en la regulación de la respuesta inmune alcanzable con la modulación del TLR4, se probó también el ligando IAXO 102, un nuevo antagonista sintético como inmunosupresor del TLR4. Con el fin de mejorar la entrega de estos ligandos, se examinaron puntos cuánticos (QDs), nanopartículas de conversión ascendente (UCNPs) y nanoesferas y nanocubos de óxido de hierro (IONPsp y IONPc) caracterizadas por diferentes propriedades, biocompatibilidad, complejidad de síntesis y eficacia. Aprovechando de un proceso de autoensamblaje y de la hidrofobicidad de los moduladores TLR4, se prepararon varias formulaciones aprovechando la encapsulación de nanopartículas en micelas de polietilenglicol-fosfolípidos. Con el objetivo de examinar cómo los distintos ligandos TLR4 podrían interactuar con las diferentes nanopartículas, se caracterizaron las estructuras similares a patógenos únicas derivadas de la interacción hidrofóbica entre ligando y nanopartícula. Entre ellas, se eligió el mejor adyuvante basado en resultados "in vitro" para estudios posteriores "in vivo", basándose en la toxicidad y en las propiedades inmunoestimulantes, medidas por la liberación de la interleucina 6 (IL-6), tras administración de las nanoplataformas a los

macrófagos murinos J774A.1. El mejor adyuvante, mIONPsp-Xcc LOS, resultante de la funcionalización de IONPsp con el ligando *Xcc* LOS, fue generado usando IONPsp con un tamaño de 7 nm, un material biocompatible y biodegradable que ya ha sido usado clínicamente como suplemento de hierro, en agentes de contraste de imagen por resonancia magnética (IRM) y en tratamientos de hipertermia. Además, el pequeño tamaño y la carga negativa de los sistemas obtenidos constituyen características ideales para la administración en ganglios linfáticos y pueden potencialmente ofrecer modalidades terapéuticas intrínsecas e imagen multimodal.

- El tercer capítulo describe cómo el antígeno modelo OVA se unió a las IONPsp utilizando la formación del enlace covalente hidrazona, rendiendo mIONPsp-HyNic-FB-OVA. También se exploró cómo esta estrategia de unión covalente puede aplicarse en el lado de óxido de hierro de nanopartículas Janus (JanusNPs) para explotar las propiedades únicas de estas nanopartículas y contribuir al desarrollo de un sistema teranóstico único con aplicaciones específicas en el tratamiento del cáncer. Además, también se desarrolló y probó in vitro un sistema en el que tanto E. Coli LPS como adyuvante y OVA como antígeno se unieron a una IONPsp. Todas las nanoplataformas resultantes fueron caracterizadas por un tamaño en el rango de 20-100 nm ideal para administración a los ganglios linfáticos.

- El cuarto capítulo investiga la actividad antitumoral de la formulación compuesta por mIONPsp-HyNic-FB-OVA y mIONPsp-*Xcc* LOS en ratones contra el melanoma B16-F10 que expresa OVA (B16-F10(OVA)), junto con una estrategia para evaluar el efecto del bloqueo del punto de control inmunológico, apuntando el ligando del receptor de muerte programada 1 (PD-L1). Cuando esta nanovacuna fue administrada en el modelo de melanoma de ratones y combinado con la estrategia de bloqueo de puntos de control, se observó un rechazo completo del tumor y la capacidad de eliminar un nuevo desafío tumoral, lo que podría explicarse por el aumento en el número de células T CD8$^+$ específicas para el SIINFEKL. Además, la formulación de las mIONPsp-HyNic-FB-OVA con mIONPsp-Poly(I:C)-

imiquimod, un adyuvante desarrollado precedentemente en nuestro laboratorio, consiguió mejorar el efecto antitumoral del mismo adyuvante formulado con mIONPsp-OVA obtenidas por anclaje electrostático.

La importancia de estos resultados no sólo está relacionada con el rechazo completo del tumor observado con nuestro enfoque de vacuna combinada + bloqueo de puntos de control en modelos de melanoma cutáneo para ratones, sino también con el ensamblaje simple y modular de los vehículos de transporte desarrollados y las aplicaciones potenciales de nanopartículas como la adquisición de imágenes y las modalidades intrínsecas de terapia que no han sido exploradas en esta tesis.

CHAPTER 1

Introduction

This chapter provides a general introduction to this thesis, presenting and discussing some of the concepts and the scientific background behind this work.

1.1: Cancer immunotherapy

Immunotherapy is a new treatment modality that uses the immune system as a weapon to fight cancer[1,2,3]. This new approach holds the biggest promise for cancer treatment since the development of the first chemotherapies in the 1940s[4] and has recently been reported as one of the main pillars of cancer care, alongside surgery, radiotherapy, and chemotherapy[5] (**Figure 1**).
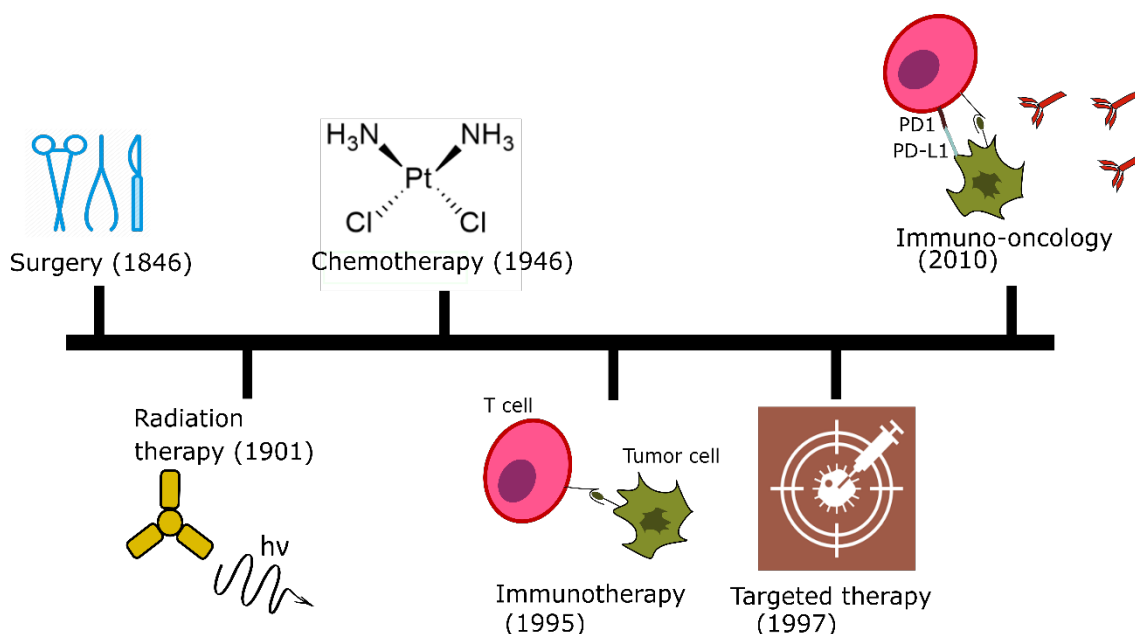
Figure 1: *Development timeline of specific cancer treatment modalities.*

Immunotherapy dates back to China's third century BC Qin dynasty, where it was used to prevent smallpox[6], but only in the second half of the 19th century the German physicians Busch and Fehleisen independently noticed regression of tumors in cancer patients after accidental infections by a pathogen[7]. In 1890 William B. Coley developed the scientific notion that tumors express specific antigens which could render them naturally immunogenic in case adequate immunostimulation is provided and reported a significant number of tumor regressions and cures in more than 1,000 patients[6]. The next step in the development of cancer vaccines would take a century, impaired by the lack of knowledge of tumor antigens: in 1976 Morales et al. reported[8] that the bacterium known as "Bacillus Calmette-Guérin" (BCG) was effective in the treatment of superficial bladder cancer, and BCG was approved by the American

food and drug administration (FDA) 14 years later[9] to treat such disease. In 1985, Hoover et al.[10] showed that BCG could be used also to treat colorectal cancer, showing modest clinical benefit in a small number of patients. Important breakthroughs in the understanding of anticancer cancer immunity were reported separately by Steinman et al.[11] in 1973 with the discovery of dendritic cells (DCs) and by van der Bruggen et al.[12] in 1991, which discovered the first human tumor-associated antigen: MAGE1. Years later, in 2010, the FDA approved the first-ever DC-based prostate cancer vaccine Sipuleucel-T (Provenge; Dendreon) for therapeutical use in humans[13]. More specifically targeted cancer immunotherapies were approved in recent times and include the first immune checkpoint inhibitors: the three antibodies nivolumab[14], ipilimumab[15], and pembrolizumab[16,17], a bi-specific T-cell engager targeting a specific antigen (Blinatumomab)[18], and an oncolytic virus to enhance systemic antitumor immune responses (Talimogene Laherparepvec)[19]. Consequently, immunotherapy treatments have been classified according to the mechanisms they follow, each of which exhibits different characteristics as well as advantages and disadvantages. This thesis will mainly concentrate on checkpoint inhibition and cancer vaccines. However there are other immunotherapy approaches and approved immunotherapeutic drugs[5].

1.1.1: Programmed cell death protein 1 (PD-1) and programmed death-ligand 1 (PD-L1) checkpoint blockade strategies in cancer immunotherapy

Targeting the programmed death protein 1 (PD-1)/ programmed death-ligand 1 (PD-L1) axis, immune checkpoint inhibitors have been reported to reactivate CD8$^+$ T cells to perform an attack against cancer cells hence "releasing the brakes" of anti-tumor immunity[20,21,22]. In fact, it has been recently reported that expression of immune-inhibitory checkpoints such as PD-1/PD-L1 is a potent mediator for the balance and escape phases of cancer immune editing[21]. PD-1 (also called CD279) is one of the co-inhibitory receptors expressed on a variety of immune cells, such as monocytes, T cells, B cells, DCs, and tumor-infiltrating lymphocytes (TILs), and it interacts with two ligands, PD-L1 and PD-L2[23] (*Figure 2*). However, PD-L1 is expressed in tumor cells and antigen-presenting cells (APCs), and the engagement of their PD-L1 with the PD-1 of T cells creates T cell dysfunction, exhaustion, neutralization, and IL-10 production in a tumor mass[24]. Additionally, the PD-1 inhibitory receptor is expressed

by T cells during long-term antigen exposure[25]. Therefore, the function of a tumor overexpressing PD-L1 is to protect itself from CD8^{+} T cell-mediated cell killing. Physiologically, the PD-1/PD-L1 pathway developed as a result of the need to control inflammation and secure normal tissue from damage[26].
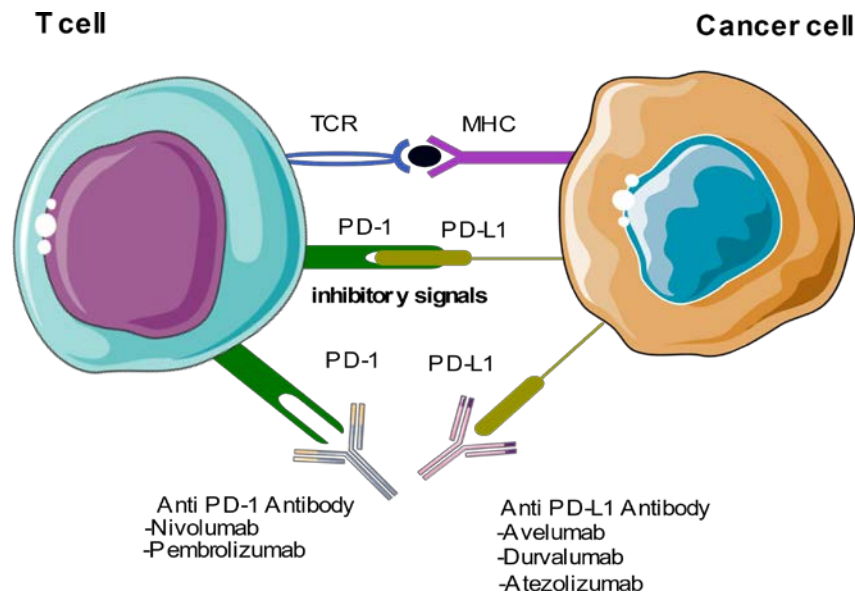
Figure. 2: PD-1/ PD-L1 axis checkpoint blockade mechanism: T cell receptors (TCR) interact with the major histocompatibility complex (MHC) on tumor cells. On the other hand, PD-1 interacts with PD-L1 inhibiting T cells. Using anti-PD-1 antibodies and anti-PD-L1 antibodies suppresses these interactions "unleashing" the full T cell potential.

Recently, many antibody-based checkpoint inhibitors targeting PD-1 or PD-L1 have been developed. To date five PD-1/PD-L1 inhibitors (PD-1 – nivolumab, PD-1 – pembrolizumab, PD-L1 – atezolizumab, PD-L1 – durvalumab, PD-L1 – avelumab)[23] have been FDA approved for the treatment of a wide spectrum of cancers including a large number of malignancies[27]. Those diseases include melanoma, non-small cell lung cancer (NSCLC), renal cell carcinoma (RCC), Hodgkin's lymphoma, bladder cancer, head and neck squamous cell carcinoma (HNSCC), Merkel-cell carcinoma, and microsatellite instable-high (MSI-H) or mismatch repair-deficient (dMMR) solid tumors. Furthermore, as of March 2018, more than 1000 clinical trials of antibodies targeting the PD-1/PD-L1 axis are ongoing[23].

Despite the huge clinical success of PD-1/PD-L1 antibodies and the improvement in patient outcome, some deficiencies of this therapy have been described recently. First of all, only a minority of patients have shown durable responses, with the frequency of rapid tumor shrinkage from single-agent anti-PD-1/PD-L1 antibodies ranging from 10–40% in advanced melanoma patients[28]. Moreover, intrinsic therapy resistance is common, and acquired resistance is emerging, suggesting that a broader view of cancer immunity is required[29,23]. Besides, anti-PD-1/PD-L1 therapy is limited to a few specific types of cancers, attributed to the heterogeneous and insufficient expression of such receptors in the tumor microenvironment[21]. A variety of factors contribute to determining whether an efficient response to the therapy occurs and appear to be associated with the diverse tumor phenotypes revealed by clinical studies. Differences between the phenotypes depend on whether the tumors host an inflammatory microenvironment, which can reflect variations in a number of cellular and other factors such as age, genetics, microbiome, viral infections, and immune-modifying drugs[28].

The context is key for the PD-1 pathway, with factors such as timing, location, T cell differentiation state, inflammation levels and antigen burden having an impact on the functional outcome of PD-1 engagement[30]. The activity of this immunotherapy strategy strictly depends on the generation of a population of T cells capable of recognizing the tumor through APCs. If this process does not occur, PD-1/PD-L1 blockade is inefficient, because of the lack of an appropriate immune response that can trigger the effective killing of the tumor cells[21]. Therefore, even after successful anti-PD-1/PD-L1 therapy, a self-renewing or expanding memory T cell compartment may be too little to keep pace with tumor growth. In such occurrences, continued priming of naive T cells is necessary to replenish and support the antitumor response[28]. This is the reason for which a PD-L1 checkpoint blockade strategy was chosen and coupled to an anti-cancer vaccine in this thesis.

1.1.2: Vaccines for cancer immunotherapy

The combination of immune checkpoint blockade approaches and vaccines offers intriguing opportunities to overcome their limitations and make therapies more widely effective amongst patients[31,32]. Before discussing the use of vaccines in cancer immunotherapy, a small introduction to the immune system together with its basic working principles is presented below.

The immune system is mainly composed of two different arms, known as innate immunity and adaptive immunity. The former is the first line of defense and displays a nonspecific immune response against "danger" signals coming from external threats such as bacteria and toxins or internal ones such as growing tumors. Ideally, such conditions induce inflammation, activate innate effector cells with antitumor activity and stimulate professional APCs, especially DCs. These engulf tumor-derived antigens and finally migrate to the draining lymph nodes to trigger an adaptive response by T and B lymphocytes, involving the adaptive immune system (*Figure 3*).

As reported by Mellman et al., three distinct steps take part in generating effective antitumor immunity:

1: Dendritic cells must sample tumor-associated antigens (TAAs), process and finally present them. TAAs can be either captured "in situ" or received from an external source such as therapeutic vaccines. These antigens might reflect one or more of the many mutated proteins that are typical of cancer or differentiation antigens associated with the cancer's tissue of origin, but against which thymic or peripheral tolerance has not been completely established (for example, melanosome-associated proteins in melanoma)[33]. Antigen processing and presentation is also known as maturation and makes them differentiate extensively to promote immunity instead of tolerance[34,35].
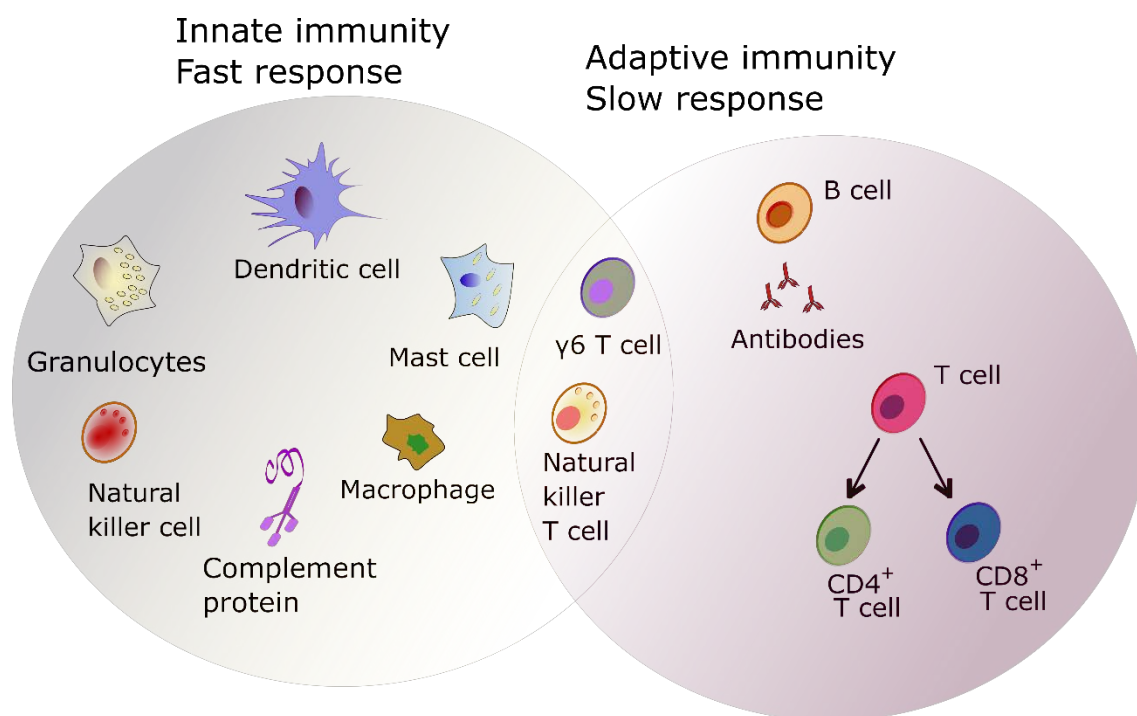
Figure 3: *Innate and adaptive immune response. The former is the first line of defense against infection while the second is slower but more antigen-specific and keeps memory.*

Maturation should be performed by a stimulatory adjuvant to elicit the desired T cells. Activation signals for therapy could be supplied exogenously (for example, Toll-like receptor (TLR) ligands) or endogenously, enabling tumor antigens presentation on MHC class I and class II molecules. Recently, it was claimed that MHC class II epitopes are the driving force for cancer immunotherapy[37], but discussing that is not the objective of this thesis.

2: Tumor-antigen-loaded dendritic cells must migrate to lymphoid organs and promote T cell expansion[38], to an extent that makes detection and elimination of cancer cells possible. Amongst T cells, expansion of CD81 effector T cells with cytotoxic potential, antibody and natural killer (NK) or natural killer T (NKT)- cell responses are desirable since they may contribute to antitumor immunity.

3: Finally, educated cancer-specific T cells must enter the tumor bed and persist there long enough to kill the malignant cells. At this moment, tumors can release

immunosuppressive factors enabling T_{regs} cells to accumulate or expand, which could oppose the activity of effector T cells downregulating the expression of target tumor antigens. The tumor might also produce a variety of surface molecules (for example, PD-L1 or PD-L2) that engage receptors on the surfaces of activated T cells (PD-1), causing T cell anergy or exhaustion[39].

After having discussed the basis of the immune system functioning, and according to the current understanding of how antigen-specific immune responses are generated, the key components of cancer vaccines can be summarized in three components: tumor antigens, immune adjuvants, and delivery vehicles[40,32] and will be described herein.

But how does a vaccine work? First of all, APCs such as DCs must encounter the antigen, and this happens at the injection site. Antigen-loaded APCs then traffic through the lymphatic system to the draining lymph nodes, the main site of T cell priming. Here, mature DCs present the tumor-derived peptides on MHC class I molecules and MHC class II molecules to CD8^{+} and CD4^{+} T cells, respectively, of both naive and memory phenotypes. Additionally, tumor-specific responses are promoted by the delivery of costimulatory signals (CD80-CD28, CD86–CD28, CD70–CD27 and CD40–CD40L interactions) and co-stimulation is increased by DC releasing IL-12 and type I interferons (IFNs). Finally, T cells traffic to the tumor site and kill tumor cells through cytotoxicity and production of effector cytokines. The lysed tumor cells release tumor antigen causing epitope spreading thus increasing the antigenic breadth of the antitumor immune response (**Figure 4**).
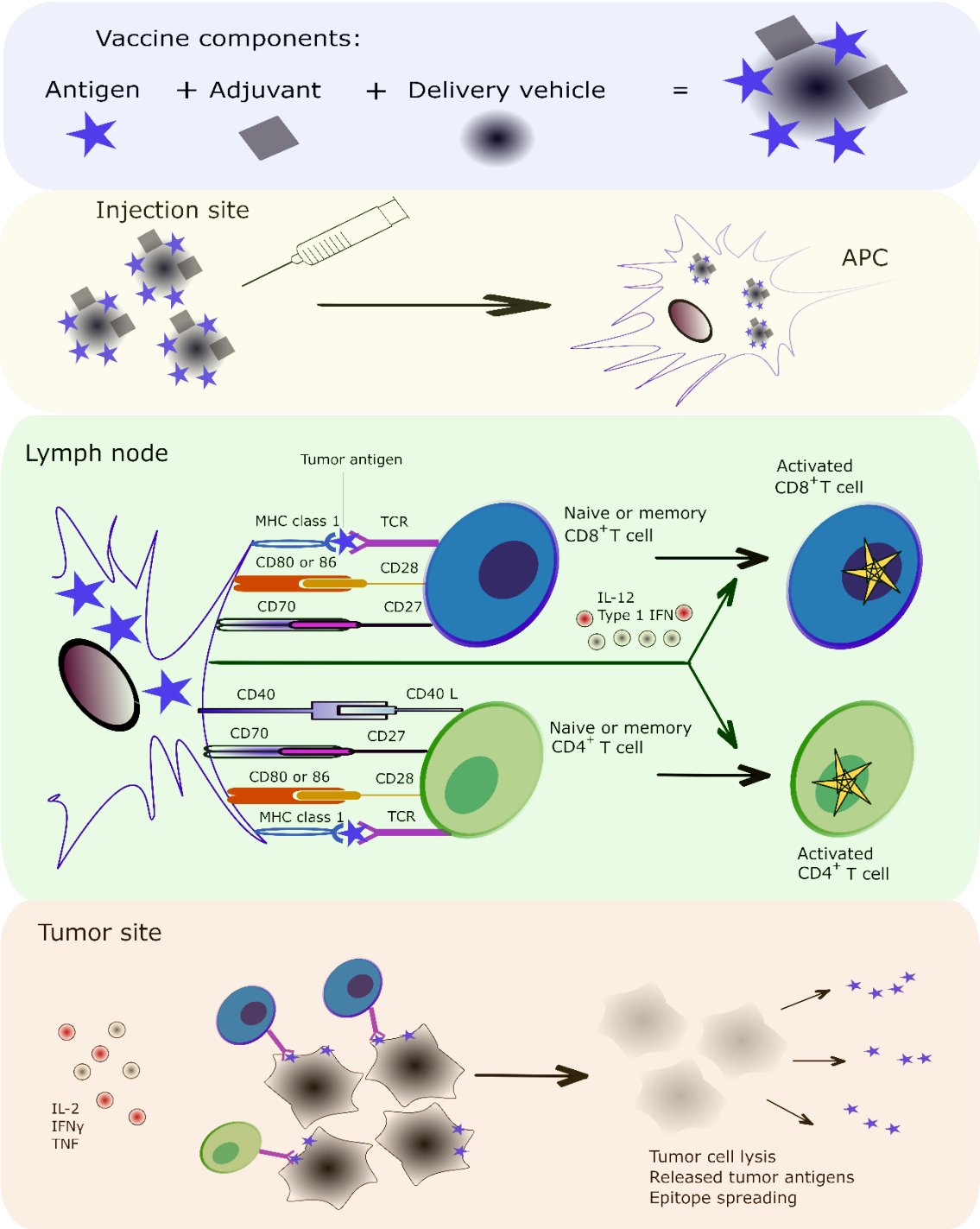
Figure 4: *Components and mechanism of an effective vaccine.*

1.1.2.1: Tumor antigens

According to Coulie et al., each tumor is characterized by the presence of several tumor antigens[31]. Generally, two broad categories of antigens can be recognized: TAAs and tumor-specific antigens (TSAs). The former are the ones that are overexpressed, involved in tissue differentiation or preferentially expressed by cancer cells but not normal tissue. Although TAAs are commonly associated with malignant cells, they can also be expressed by healthy ones[41]. On the other hand, tumor-specific antigens are expressed only by cancer cells and therefore they are tumor specific. TSAs are profitable targets for cancer immunotherapy because they generate T lymphocytes-mediated responses. First, T cell responses elicited against such antigens in cancer patients leave normal tissues completely unharmed. Second, our natural tolerance mechanisms should not prevent or repress these responses. In fact, vaccines using these antigens have already shown efficacy in both preventive and therapeutic settings for HPV-associated cancers[42]. Amongst them, tumor neoantigens are generated as products of somatic mutations, and hence they are not only fully tumor specific but also highly immunogenic, lacking central tolerance. However, it should be taken into account that some procedures used to generate responder T cells against tumor-specific antigens do generate T cells that crossreact with other antigens present on normal cells. This can result in harmful side effects[31]. In general, antitumoral T cells are more likely to attack normal tissues when low tumoral specificity antigens are involved, such as differentiation antigens or overexpressed ones. Amongst the many antigens that have been reported in the literature, selecting an effective one was not the objective of this thesis, it was rather to study the efficiency of the developed vaccine. For this purpose, ovalbumin (OVA) was selected as a proof of concept antigen. OVA is the main protein present in chicken egg white and can act as a tumor neoantigen[43]. Its low cost and commercial availability make OVA an ideal candidate for use as a model antigenic molecule. Several OVA-expressing tumor models have been developed specifically to test the efficacy of different immunotherapeutic strategies against cancer and several papers have reported the use of OVA as a model antigen[44,45,46,47]. Moreover, several OVA-expressing tumor models have been developed specifically to test the efficacy in different melanomas.

1.1.2.2: Vaccine adjuvants

Adjuvants are substances or interventions that, when combined with an antigen, enhance antigen immunogenicity and elicit the desired immune response[40]. On their own, adjuvants do not provide immunity, but rather stimulate the immune system to respond to a defined antigen and play a key role in improving the humoral and/or cell-mediated immune response to vaccine antigens and in eliciting protective and long-lasting immunity[48,49] (**Figure 5**). Indeed, the word "adjuvant" comes from the Latin "adiuvare" and means "to help/aid". Adjuvants can be classified according to their mode of action, as reported in 1997 by Cox et al.[50]: (i) immunomodulation (modification of cytokine networks); (ii) presentation (maintenance of antigen conformation); (iii) CD8^{+} T cells induction; (iv) targeting specific cells; (v) depot generation. A list of the advantages related to the use of vaccine adjuvants is given below[48]:

1: They decrease the dose of antigen and the number of vaccine doses needed;

2: Improve vaccine efficiency in infants, elderly and immunocompromised people;

3: Increase functional antibody titer;

4: Promote more rapid and long-lasting immune responses;

5: Induce robust cell-mediated immunity;

6: Provide broad protection (cross-reactivity);

7: Facilitate mucosal immunity;

8: Overcome antigen competition in combination vaccines.

The discovery of adjuvants was first reported in 1926 by Alexander T. Glenny and colleagues, who reported that antigen precipitation onto insoluble particles of aluminum potassium sulfate (named "potash alum") could improve antibody responses with respect to the soluble antigen alone. Aluminum salts were used in vaccine preparations with tetanus and diphtheria toxoids to protect against C. tetani and C. diphtheriae respectively, and still, nowadays insoluble aluminum salts are used worldwide as the principal adjuvants in clinical vaccines[51]. Unfortunately, despite aluminum-based adjuvants being capable of eliciting a good Th2-type response (i.e., antibody production-based response optimal for fighting extracellular

pathogens), they are not able to induce potent cell-mediated immunity (Th1-type response), which is a fundamental requisite for developing a successful anticancer vaccine[52]. On the other hand, TLR agonists such as polyinosinic: polycytidylic acid (Poly(I:C)), monophosphoryl lipid A (MPLA), and imiquimod (respectively TLR3, TLR4, and TLR7 ligands) have recently been used to enhance the immunogenicity of vaccines[53,54,55] especially because of the Th1-type immune response that they stimulate. The use of TLR4-based vaccine adjuvants is part of the strategy used in this thesis and will be discussed later in this chapter.
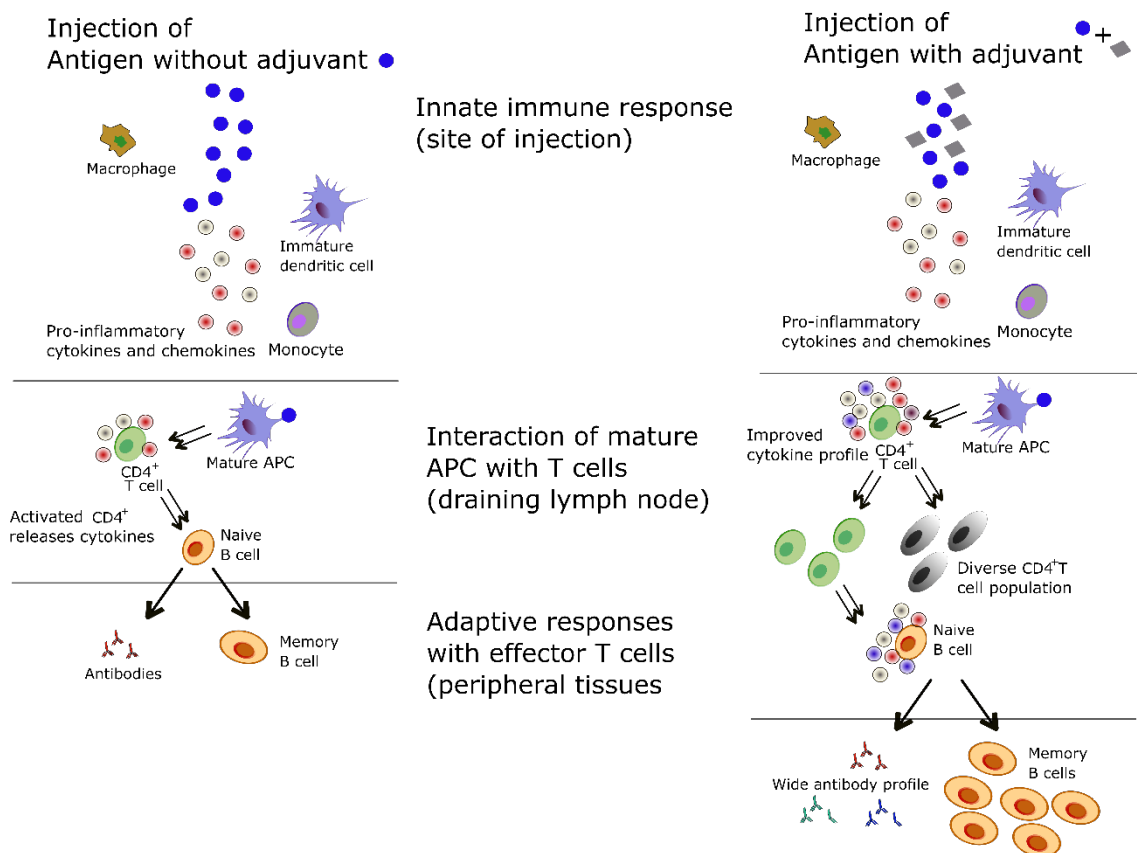
Figure 5: *The immune response to vaccination with and without adjuvant.*

1.1.2.3: Delivery vehicles

The process of developing an effective vaccine formulation requires careful selection of a potent antigen, efficient adjuvant and delivery vehicle.

Traditional vaccines such as killed microbes, live attenuated microbes, or microbes' components have had a main role in the past to control infectious diseases. However, they have many drawbacks: require multiple doses, may show side effects like inflammation at the site of vaccination and some do not confer good protection against disease. Besides, in nowadays' society some live vaccines might not be safe to be used in the growing population of immunocompromised individuals. There is also a wide range of infectious diseases for which no licensed vaccines are available. An important advance is in the development of subunit vaccines, but they feature poor immunogenicity and inability to cross intestinal mucosal tissues due to degradation by metabolic enzymes[56,57]. It is also known that antigen and adjuvant should be together at the same site since APCs which process the antigen are also responsible for the activation of naïve T cells. This is where carriers can make a difference since they can deliver both antigen and adjuvant to the cell, protect the antigen from degradation upon its administration by different routes and sustain the antigen release over time[58,59]. Several particle-based vaccine delivery systems such as polymeric, lipid-based and chitosan nanoparticles have been investigated[57], and Gregory et al. subdivided the different kinds of vaccine carriers used up until now in 5 different categories (***Table 1***). This thesis will focus on the delivery of antigens and adjuvants with different kinds of nanoparticles with unique properties. Nanoparticles are attractive delivery vehicles for vaccines. Due to their unique chemical, physical and biological properties, nanoparticles are considered to be efficient delivery vectors for drugs, proteins, peptides, and nucleic acids. Besides, they can improve DC-mediated antigen uptake, direct DCs stimulation, stimulate cross-presentation, and act as an adjuvant on their own. Conjugation of antigens onto nanoparticles can allow presentation of the immunogen to the immune system in much the same way that it would be presented by the pathogen, thereby provoking a similar response[56,60,40]. Florindo et al. reported that upon associating an antigen with

nanoparticles, a stronger immune response is generated compared to the soluble antigen alone[61].
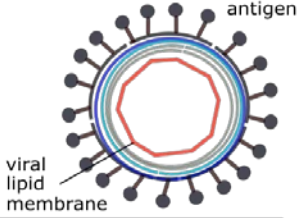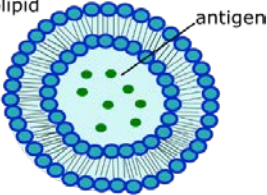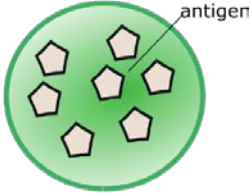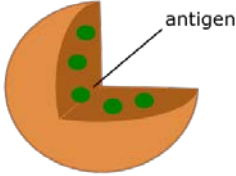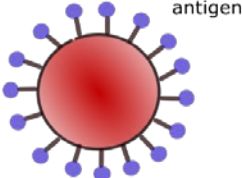
	Size range	Loading examples (drug, antigen)	Schematic representation
VLP	50- 200 nm	Human papillomavirus (HPV) Human immunodeficiency virus (HIV)	
Liposomes	50- 500 nm	Vibrio cholerae (Cholera) Plasmodium falciparum (Malaria)	
ISCOMs	40 nm	Human immunodeficiency virus (HIV) Feline immunodeficiency virus (FIV)	
Polymeric NPs	100 nm- 5 um	Docetaxel Clostridium tetani (Tetanus) Hepatitis B virus (HBV)	
Inorganic NPs	2- 400 nm	Influenza Hepatitis B virus (HBV)	

Table 1: Brief summary and pictorial representation of different types of carriers for delivery of anticancer vaccines.

1.1.3: Combinatorial immunotherapy

Since the different kinds of immunotherapies have advantages and disadvantages, several new approaches target combinatorial immunotherapy or immunotherapeutic synergy, which can be defined as a therapeutic effect superior to the additive effect of each of the components in a combination and is nowadays seen as the most promising method for progress in cancer treatment[62,63,64]. Numerous clinical trials of immunotherapy combinations are ongoing and can be found in (Clinical Trials.gov). One of the first attempts was performed by Schwartzenruber et al.[65], that used a combination of high-dose IL-2 and a peptide vaccine in a Phase III trial obtaining improved clinical responses. However, it should be pointed out that hospitalizing patients is required for high-dose IL-2 due to the toxicity associated with the administration of this therapy[63]. Many different combinations of checkpoint inhibitors have been reported, and especially combinations of checkpoint blockade with other strategies are very promising[54,20,9]. Although the drug ipilimumab, blocking Cytotoxic T-lymphocyte-associated protein 4 (CTLA-4) has been FDA approved for use in metastatic melanoma patients[15] and is currently being evaluated in two Phase III clinical trials for the treatment of advanced castration-resistant prostate cancer[66], CTLA-4 blockade can cause autoimmune adverse effects[67,68,69]. Another way to increment the effectiveness of cancer immunotherapy is the combined administration of PD-1-blocking antibodies and CTLA-4-blocking antibodies. Despite having already been approved for melanoma treatment and being investigated in many other malignancies, the combination of ipilimumab with pembrolizumab or nivolumab has a drawback, leading to substantially higher toxicity in both melanoma and non-small cell lung cancer[70,9]. Other possible combinatorial approaches that will be discussed in this thesis include the partnership between strategies targeting checkpoint blockade and cancer vaccines. Since cancer vaccines possess potential to both generate new antigen-specific T cell responses against tumor cells and amplify existing responses, they may be an effective combinatorial partner with checkpoint blockade because they can presensitize the host's immune system to the tumor[32]. By picking suitable antigen targets, a strong tumor-specific immune response can be induced while minimizing autoimmunity. Recent studies have shown that tumor

neoantigens are key targets for adoptive cell transfer, checkpoint blockade and therapeutic vaccination[71,72,37,73].

1.2: Toll-like receptors-based cancer immunotherapy

1.2.1: An introduction to Toll-like receptors (TLRs) and their importance

TLRs are a family of transmembrane pattern recognition receptors (PRRs) capable of detecting conserved pathogen-associated molecular patterns (PAMPs) expressed on a wide array of microorganisms as well as endogenous damage-associated molecular patterns (DAMPs) released from stressed or dying cells. They are well-known for the role they play in host defense against infection. Lately, there has been some interest in TLRs since they play a role in tissue repair and tissue injury-induced inflammation, and more importantly for this thesis, in activating and mediating antitumor immune responses[74,75,76,77,78].

The TLRs that recognize lipids and protein as ligands are localized on the plasma membrane (TLR1, TLR2, TLR4, TLR5, and TLR6), whereas TLRs detecting viral nucleic acids are expressed on endolysosomal compartments (TLR3, TLR7 and TLR9) (**Figure 6**). TLRs transmit signals through one or more of four adaptor proteins: myeloid differentiation factor 88 (MyD88), Toll-interleukin 1 (TIR) receptor domain-containing adapter-inducing interferon-β (TRIF), TIR-domain containing adaptor protein (TIRAP), and TIR-containing adapter molecule 2 (TICAM2). All TLRs signal through MyD88, except for TLR3, which signals through TICAM1, and TLR4 signals through both the MyD88 and TRIF pathways[74,79].

TLRs are critical for the activation and maturation of the B-cell response during infection and vaccination due to their role to mediate the adaptive immunity[80,74]. Indeed, TLRs-mediated activation of professional antigen-presenting cells has a fundamental role in immunotherapy since it is necessary for processes such as antigen processing and presentation[81], T cell activation[82,83,84], activation of naive CD4 T cells[85], and the inhibition of regulatory T cell activity[86].

Purified TLR ligands have been demonstrated to induce potent anticancer effects against established tumors both in mice and humans. Amongst them, CpG oligodeoxynucleotide (CpG ODN), a TLR9 agonist, has been reported to induce strong Th1 adaptive and innate immune responses when used as a vaccine adjuvant and a number of CpG ODN-based vaccine adjuvants are ongoing clinical trials since TLR9 activation has been reported to enhance tumor vaccination in humans[87]. This thesis will mainly focus on the stimulation of TLR4 but the antitumor activity of other TLRs is reviewed elsewhere[74].
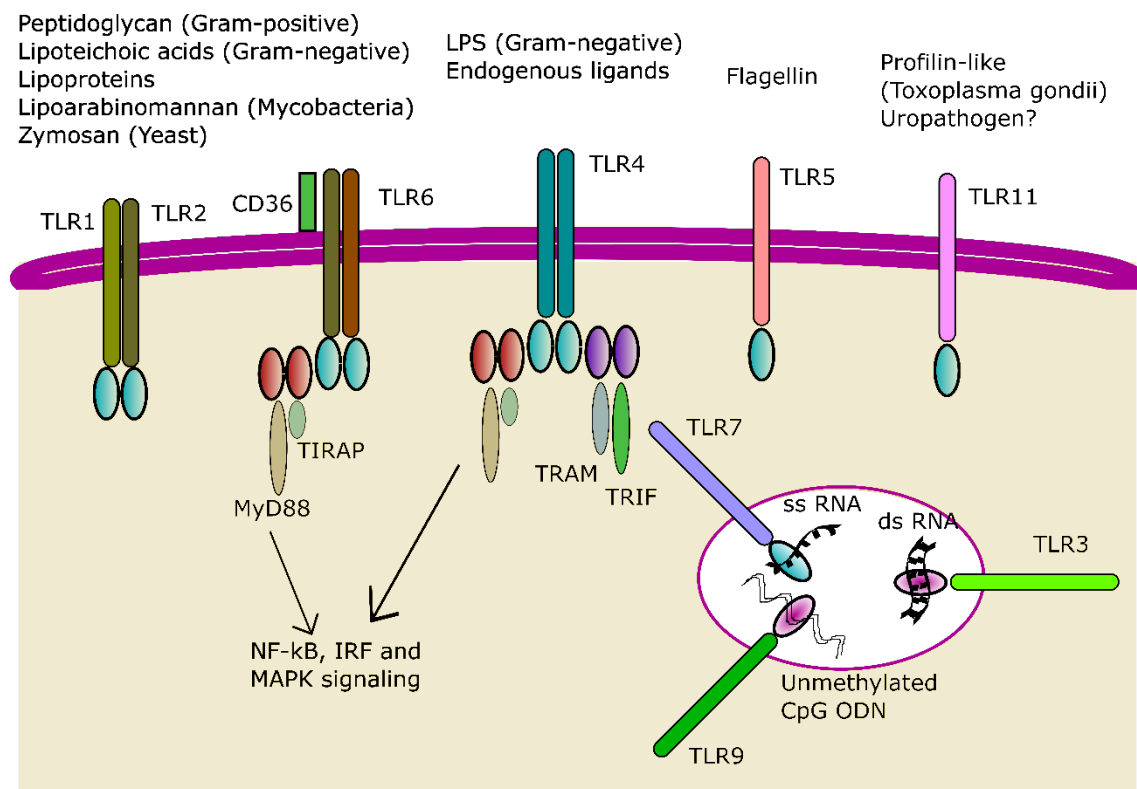
Figure 6*: TLRs take part in the recognition of PAMPs and DAMPs. After ligation of TLR ligands either directly or with the help of accessory molecules, TLRs lead to the activation of a signaling cascade, which in turn activates the regulation of innate and adaptive immune responses, inflammation and tissue repair.*

1.2.2: Toll-like receptor 4 (TLR4) stimulation in cancer immunotherapy

TLR4 strongly activates inflammatory pathways, thus making it an ideal target for therapeutic intervention and adjuvant development[88]. This receptor has long been involved in the quest for the development of antitumor therapies: at the end of the

19th century, Dr. William Coley reported that the injection of killed bacteria (Streptococcus pyogenes) into inoperable tumors reduced tumor growth in some patients[89]. However, the scientific community had to wait almost one century until Beutler and colleagues identified TLR4 as a receptor of Lipopolysaccharides (LPS)[90]. More recently, the mechanism of LPS binding to TLR4 has been reported[91]: this receptor heterodimerizes together with the help of his cofactors, cluster of differentiation 14 (CD14) and MD-2, and needs LPS to be presented by an LPS binding protein (*Figure 7*).
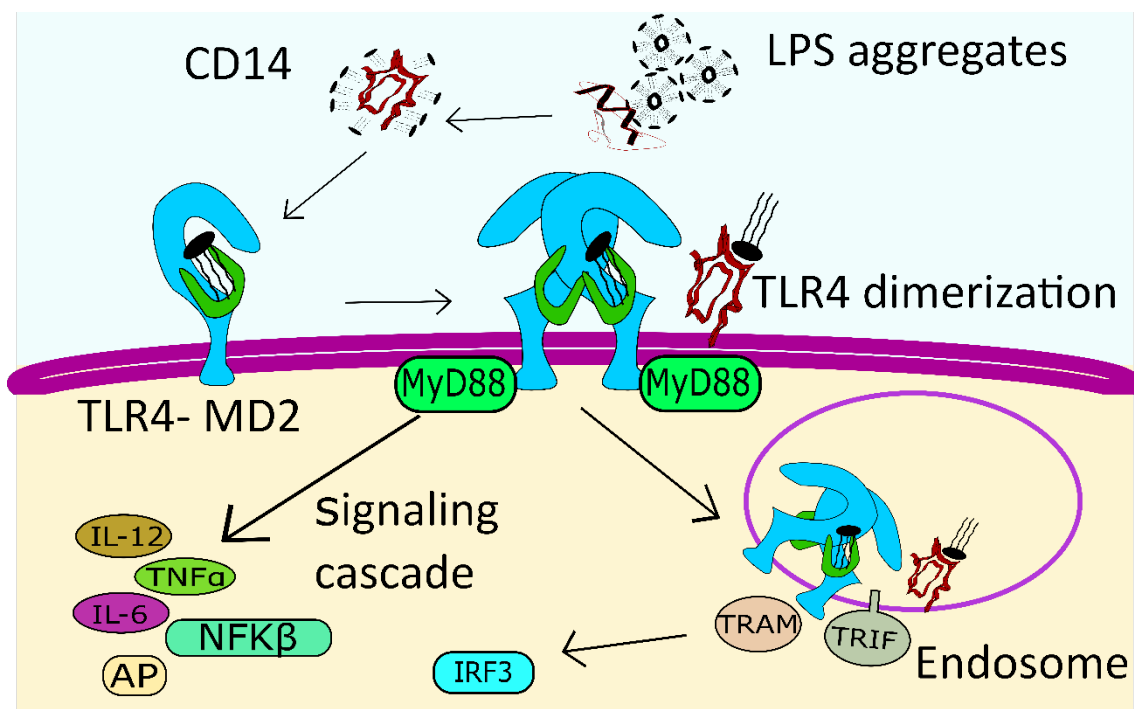
Figure 7*: Activation of TLR4 and its dimerization. LPS is taken by the LPS binding protein and cofactors CD14 and MD-2 are needed to activate the receptor.*

Nowadays, it is known that Coley's toxin's proinflammatory activity is due to the various bacterial components it contains such as the strongly immunostimulatory LPS and the TLR4 engagement on immune cells.

Immunologically, the importance of TLR4 relates to the fact that upon stimulation with LPS, it is able to activate and promote T cell proliferation by stimulating APCs. Besides, it induces production of various proinflammatory cytokines such as tumor necrosis factor α (TNF-α), IL-6, pro-IL-1β, and IL-12[74], corresponding to a Th1 type response[88], promoting nonspecific or bystander T cell expansion and activation[92].

Moreover, CD4^{+} and CD8^{+} T cells too can respond to TLR4 stimulation with LPS. A study from Vogel et al. reported that a cloned murine IL-2-dependent cytotoxic T cell line, CT 6, proliferated in response to LPS[93]. TLR4 engagement on human CD8^{+} T cells has also been proved to induce the release of TNF-α, IFN-γ, perforin and granzyme B[94,75]. An interesting paper by Bauer et al. showed that the expression of TLR4 on lung epithelium can have a protective effect against lung cancer development[95].

Some recent studies have suggested additional roles of TLRs in inducing anti-tumor T cell responses. Apetoh et al. have suggested that TLR4 provide an important contribution to chemotherapy and radiotherapy. The authors studied the effect of those two conventional treatment methods in TLR4- and MyD88-deficient mice and noted that the ability of numerous chemotherapeutic agents to kill established tumors was decreased. They demonstrated that the high-mobility-group box 1 alarmin protein (HMGB1) binds to TLR4 and that HMGB1, which is released by chemotherapy-induced cell death, can activate TLR4 and induce anti-tumor T cell immunity[96]. Another study by Yusuf et al. shows that C3H/HeJ mice with a TLR4 mutation causing loss-of-function developed more tumors than wild-type mice when treated with 7,12-dimethylbenz(a)anthracene (DMBA) to induce skin tumors, probably owing to decreased activation of interferon-γ-dependent anti-tumor T cell responses[97]. Hsiao et al. found that TLR4 agonistic treatment inhibits migration and invasion of Hepatoblastoma HepG2 cells "in vitro" and can thus be a potential therapeutic target for control of this kind of tumor's progression[98].

However, to date TLR modulators have shown modest antitumor effects in the clinic, and that is the reason for which it is important to improve their efficiency by different strategies such as combination with other agents to synergistically enhance their immunostimulatory capacity[79]. Another viable option, since TLR expression and its costimulatory effects on T cells depend on TCR stimulation, consists in fine-tuning the timing and capacity of the ligand to make it to the tumor site[75], and this is what this thesis aims to accomplish by developing NP-based delivery vehicles for TLR4 ligands offering new and unique features.

1.2.2.1: TLR4 agonists as vaccine adjuvants

TLR modulators, especially TLR4 agonists, have been studied intensively in the last few years due to the role they play in modulating the innate and adaptive immune response[99,100] and as a class of promising anticancer vaccines and therapeutics [96,101,102].

To date only MPLA (*Figure 8*), a TLR4 agonist and much less toxic derivative of LPS, has been FDA approved for use in humans. It is used as an adjuvant in Cervarix, a vaccine to prevent cervical cancer caused by human papillomavirus types 16 and 18[103], and it is in phase I clinical trial for patients with colorectal cancer[76]. MPLA has also been approved in Europe as an adjuvant for a hepatitis B vaccine, Fendrix[104]. An old TLR agonist approved by the FDA for use in cancer patients is BCG which stimulates TLR2, TLR3 and possibly TLR9 other than TLR4[75].

LPS and many of its less toxic derivatives, such as its active component Lipid A, aminoalkyl glucosamidine-4-phosphates (AGP) (*Figure 8*) and Corixa 675 (an aqueous formulation of Lipid A) are being extensively studied due to the strong inflammatory response they cause and their capacity to induce and activate antitumor responses[105,103]. Besides, also synthetic compounds mimicking the LPS structure like glucopyranosyl lipid A (GLA) (*Figure 8*) and compounds D1 and D7[106,107] have been prepared and tested. As Cui et al. reported[108], despite Lipid A being less toxic than LPS, the latter induces a much larger fraction of LPS-primed CD8$^+$ T cells in the memory cell pool compared with the former. Unfortunately, despite many new adjuvants are being studied and developed[109], finding an effective and safe one remains a challenge since many cause an unwanted systemic production of cytokines and toxicity[110,111]. To efficiently face this issue, control of the adjuvant's pharmacodynamics and biodistribution will be fundamental to modulate and focalize its activity to further improve them[112,113,114]. That is why one of the objectives of this thesis was to find a suitable NP-based delivery vehicle for TLR4 ligands.

MPLA

AGP

$R_2 = $ fatty acid chain

GLA
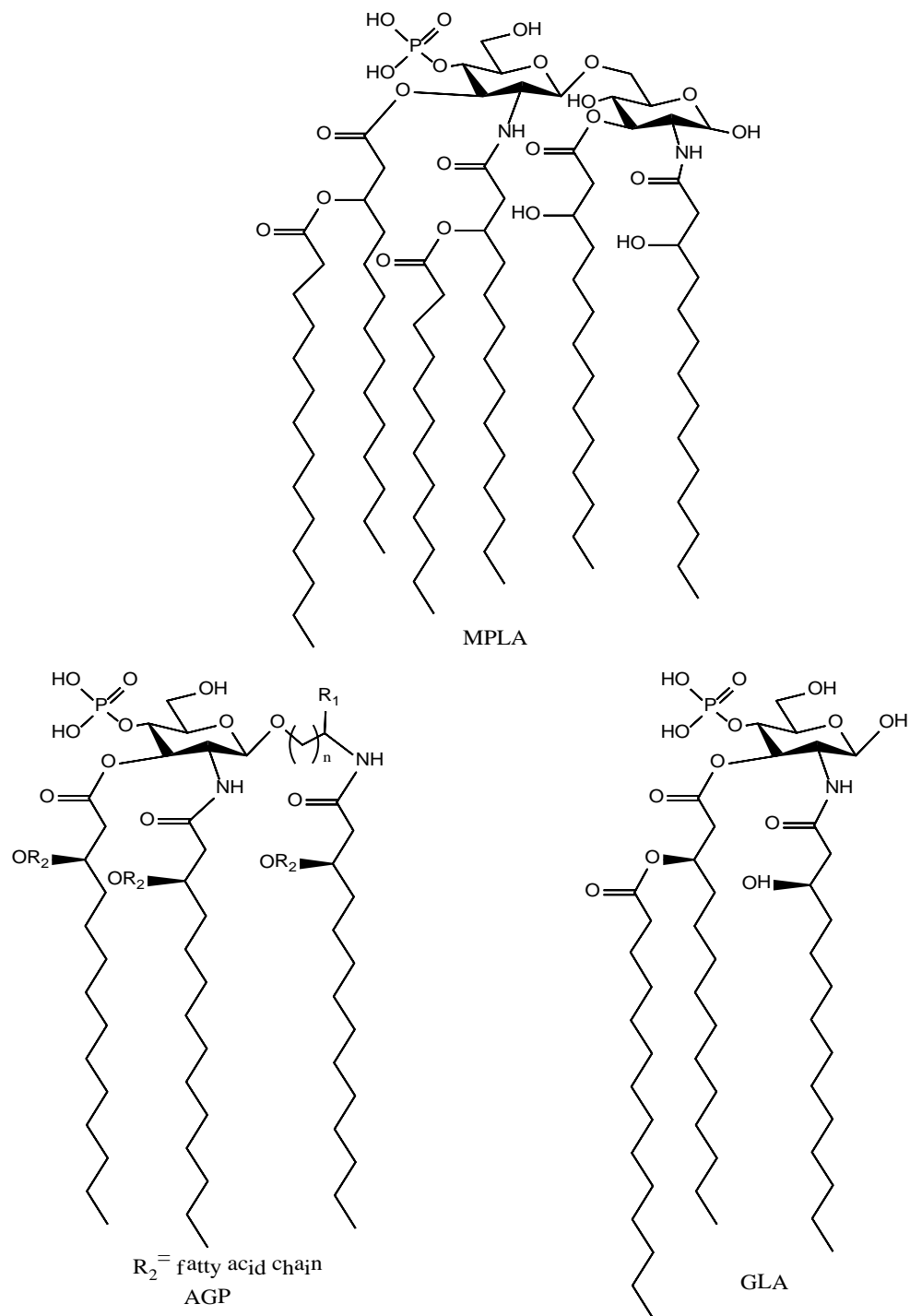
Figure 8: Structures of some TLR4 agonists.

1.2.2.2: The importance of Lipopolysaccharide (LPS): its characteristics and derivatives

LPS, or Endotoxin, was first reported by Richard Pfeiffer in 1892 as a heat-stable, cell-associated material isolated from *Vibrio cholerae* which induced toxic reactions in guinea-pigs. He recognized this material to be clearly distinguishable from the heat-labile exotoxins which are secreted by bacteria[115]. However, it took approximately 60 years to discover the hot phenol-water procedure that allowed extraction of rather pure LPS[116]. LPS is commonly found in the outer leaflet of the outer membrane of most Gram-negative bacteria, (with some exceptions such as *Treponema pallidum, Borrelia burgdorferi, B. hispanica, Sphingomonas capsulata and S. paucimobili, Thermus thermophilus, and Meiothermus taiwanensis*)[117] covering up to 75% of the total cell surface. The remainder surface is constituted by integral membrane proteins such as porins that serve as channels to let small hydrophilic molecules enter and exit[118]. LPS is a fundamental macromolecule for growth and survival of many Gram-negative bacteria as it protects them from harmful bile acids, hydrophobic antibiotics, cellular host defense strategies[119] and helps to provide the correct assembly of the outer membrane and the right positioning of porins[111]. LPS was named as such since it consists of poly-saccharides and a lipid part. The general structure of LPS was discovered back in 1971 by Liideritz et al.[120] which observed that different forms of LPS from different strains of bacteria have common features: all of them are made up by a polysaccharide or oligosaccharide portion covalently linked to a specific glycolipid component called Lipid A.

According to the size of the saccharide portion, LPS can be subdivided into smooth-form LPS (S-form) and rough-form LPS (R-form, also called lipooligosaccharides, LOS)[121,122]. In S-form LPS, the core saccharide portion is replaced by the O-specific polysaccharide. This LPS is mainly found in naturally occurring, or wild type, species of bacteria and composed by a structure of up to 50 repeating oligosaccharide units mainly formed by two to eight monomers and the core region, closest to the lipid A part[123] (**Figure 9**).
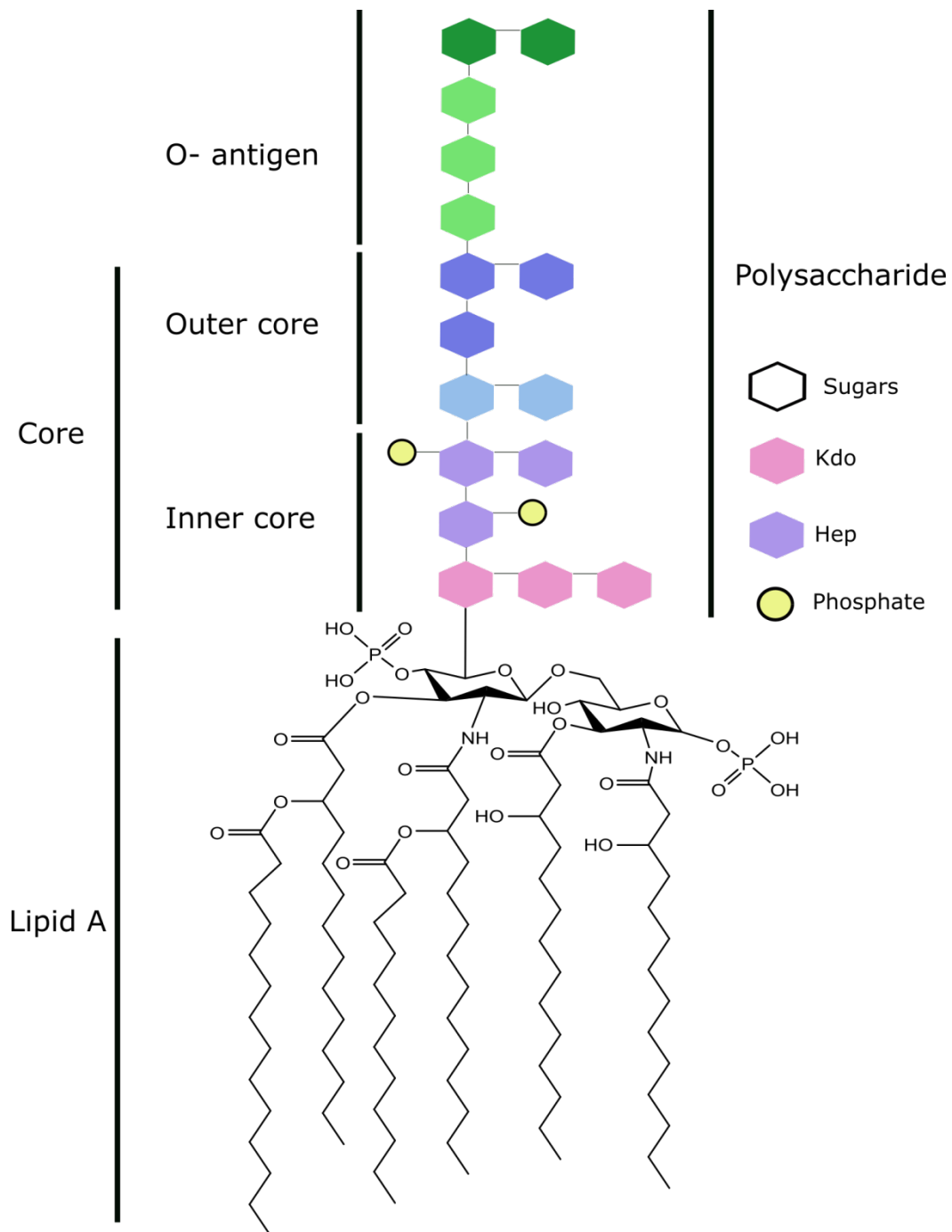
Figure 9: Schematic representation of S- form LPS from Escherichia Coli, composed by the Lipid A moiety, the inner core, the outer core, and the O-antigen chain.

Whereas both the lipid portion and polysaccharide of LPS contribute to the pathogenic potential of Gram-negative bacteria, it is the lipid component (lipid A) which determines the endotoxic properties of LPS. As LPS are surface structures, they play a big part in the interaction of Gram-negative bacteria with higher organisms. The host's defense system recognizes invading bacteria by the LPS and

reacts with the formation of antibacterial antibodies directed against LPS regions. Therefore, they were also called O-antigens since they are immune-reactive surface agents. On the other hand, free LPS can be released killing the bacteria, and when this happens, they exhibit a broad spectrum of biological activities such as pyrogenicity and lethal shock. They are thus held responsible for certain Gram-negative infection and accused as causative agents of the sepsis syndrome. Finally, LPS activate B lymphocytes, granulocytes and mononuclear cells and, hence, are potent immunostimulators. By virtue of this property, they are also believed to be involved in the physiological development and activation of the immune system[124].

1.2.2.3: LPS and its derivatives: structure-activity correlation

It is known that molecules such as MPLA have a common feature: they include the chemical determinant (or pharmacophore) essential for MD-2 recognition and binding, a disaccharide core (GlcNAc–GlcNAc) with six lipid chains, and two negatively charged phosphates at positions C1 and C4 of the disaccharide. All these compounds are sparingly soluble and have poor pharmacokinetic in vivo[125]. In the past few years, an important effort has been made in order to study the correlation between the structure and the activity of LPS and parent molecules to get a deeper understanding of their immune-stimulating properties and sepsis-related toxicity. This knowledge is leading also to the development of new LPS-based immune-therapies for prevention and treatment of diseases such as cancer and to strengthen immune resistance to bacterial and viral infections. However, all the LPS derived from bacterial cell wall are a mixture of chemically different LPS molecules that range from rough LPS to LPS with varying core length to LPS having a high number of O-chain oligosaccharide repeats. Additionally, some might be differently substituted with acyl chains. This represents a problem when studying the mechanisms by which those molecules are recognized[126]. Therefore, accurate purification and characterization are fundamental to study their biochemical properties. It has been observed that a simple variation in the structure of such molecules might dramatically change the way they fit into the TLR4 complex and thus the way they interact with the immune system. Synthesizing a panel of LOS with slight structural differences using modular synthesis, Stöver et al.[127] found that the ideal structure of an agonist LPS-like molecule, both to human and mouse cells, is hexa-acylated and has a secondary

acyl chain with a length of 10 carbon atoms. A similar study using bacterial enzymatic combinatorial chemistry (BECC) was done in 2017[128], and could to some extent correlate the difference in the structure of the prepared LOS with the cytokine secretion induced, which in turn guided the immune response over Th1, Th2, (T_{regs}) or Th17 cells. Choi et al.[129] verified that the elongation of the oligosaccharide chain and the deletion of phosphorylcholine (PCho) at the Heptose I can attenuate the release of inflammatory cytokines such as TNF-α and IL-1β. Other examples worth mentioning are the variation of an ethylamine group on a synthetic analog of the lipid A from *H. Pylori* (HPLAEA). In fact, Fujimoto et al.[130] noticed that the compound HPLAEA was a much stronger antagonist of LPS than HPLA. The former could inhibit secretion of some cytokines, such as IL-6, IL-8, IL-18, IL-1β, and TNF-α up to 10-fold with respect to the latter at a concentration of 5 µg/mL when E. Coli LPS was used as a stimulus at a concentration of 500 pg/mL.

1.2.2.4: Lipooligosaccharides (LOS) and their structure-activity correlation

Two different kinds of LPS have been found and isolated, R-form and S-form LPS. The main difference consists in the fact that R- form LPS, or LOS, show similar Lipid A structures but lack O-antigen units and the oligosaccharide core is limited to around ten units. LOS are the major glycolipids expressed on mucosal Gram-negative bacteria such as the ones from the genera Neisseria, Haemophilus, Bordetella, and Branhamella. Those differences between LPS and LOS are probably due to the fact that different forms can benefit the survival of the pathogens in different conditions and environments[131,132]. Huber et al.[133] reported that R-form LPS are the key to the activation of TLR4/MD-2-positive cells: they can activate mouse cells which lack expression of the LPS-binding protein CD14. They also stated that up-regulation of soluble CD14 due to S-form LPS in the course of an inflammatory response might provoke an enhanced risk of endotoxin shock[134], or lead to acute allergic reactions. LOS have shown very promising results as vaccine adjuvants, both against pathogens and diseases. Ko et al.[135] have recently explored the combination of a de-O-acylated lipooligosaccharide (dLOS, a TLR4 agonist derived from an E. Coli LPS mutant strain) combined with Alum and Liposomes as an adjuvant against Japanese encephalitis (JE) in a mice model. Both formulations

significantly increased the serum IgG antibody titers 2 weeks after a single vaccination and were comparable to those obtained 2 weeks after two immunizations with the alum-adjuvanted vaccine. Besides, dLOS combined with liposomes promoted both antibody and Th1-type cellular responses to JE vaccine. Notably, dLOS coupled to Alum and used as a vaccine against H1N1 Pandemic Influenza in mice stimulated Th1 cytokine release together with activating CD4$^+$ and CD8$^+$ T cells reducing mortality and morbidity of mice, as described by Ryu et al.[136]. Similar results were observed some years before by Han et al.[137], which also assessed that dLOS has low toxicity up to a dose of 1 mg/kg of body weight in mice and is a more potent activator than MPLA in human monocytes and DCs. With respect to bacterial infections, LOS showed efficacy against P. aeruginosa infection in mice, increasing the survival rate up to 100% with the right immunization dosage and thus showed potential against other gram-negative bacteria infections[138]. In 2003, Hirano et al.[139] have used a LOS-based conjugate vaccine from nontypeable *Haemophilus Influenza* and administered it by the intranasal route to enhance bacterial clearance in mouse nasopharynx generating mainly IgA antibodies in lymphoid tissues. The most important result of the biological characterization of LPS fractions isolated from wild-type E. Coli is the fact that the R-forms of LPS had a broader capacity to activate human macrophages in vitro compared with the isolated S-form of LPS, which required the presence of serum for the induction of TNF-α as a central mediator of the pro-inflammatory response to bacterial infection. Independently of the route of activation, the physicochemical properties of S-LPS (such as hydrophobicity, aggregate structure, and stability) are likely to be different from those of R-LPS and could explain the observed differences in the biologic activity[126].

Another well-known and used LOS is 3-deoxy-D-manno-octulosonic acid-lipid A (Kdo$_2$-Lipid A). This molecule was first prepared by Raetz et al.[140] and obtained by chromatographic purification from a heptose-deficient Escherichia coli mutant. They verified that this LOS is fully active as an endotoxin by stimulating RAW 264.7 macrophage-like tumor cells to produce eicosanoids and TNF-α. One advantage of this molecule with respect to LPS is the high purity[141].

In this thesis, the activity of two different LOS was investigated. These LOS respectively named E. Coli LOS (*Figure 10*) and Xcc LOS (*Figure 11*) were

extracted from natural sources by the group of Professor Alba Silipo at the University of Naples Federico II.
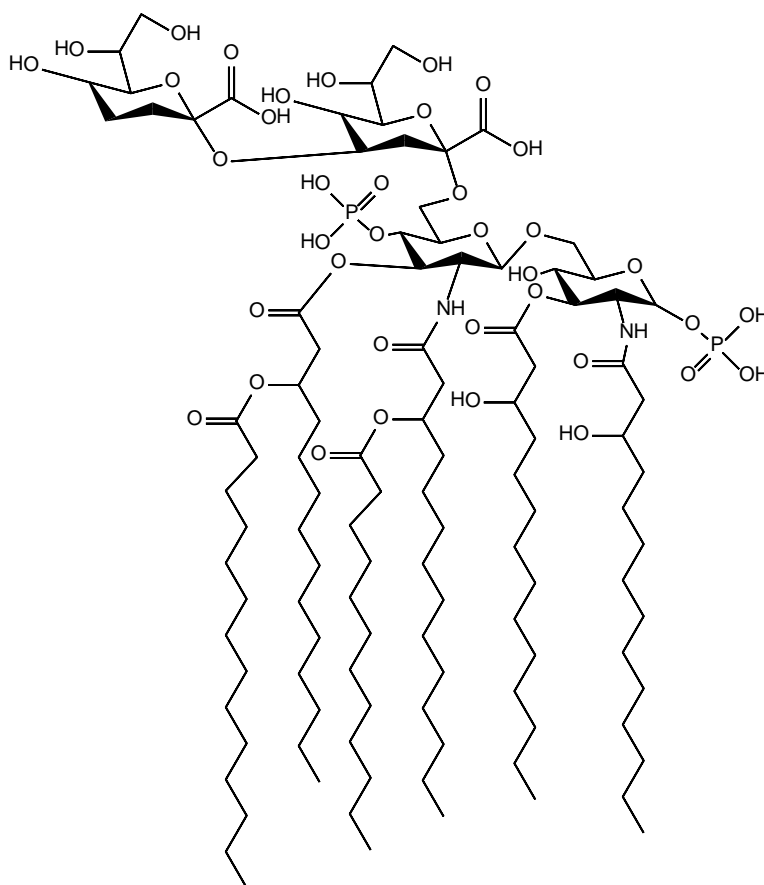
Figure 10*: E. Coli LOS, the first LOS investigated in this thesis.*

The latter is a purified lipid obtained from the plant pathogen Xanthomonas campestris pv. campestris (strain 8004). Its structure presents a strong negative charge density in the lipid A-inner core region and has a number of interesting features, such as a galacturonyl phosphate attached at a 3-deoxy-D-manno-oct-2-ulosonic acid residue and a unique phosphoramide group in the inner core region[142]. Besides that, it presents a 3-3 symmetry in the distribution of the acyl chains in the Lipid A moiety, compared with the usual 2-4 of conventional LPS.
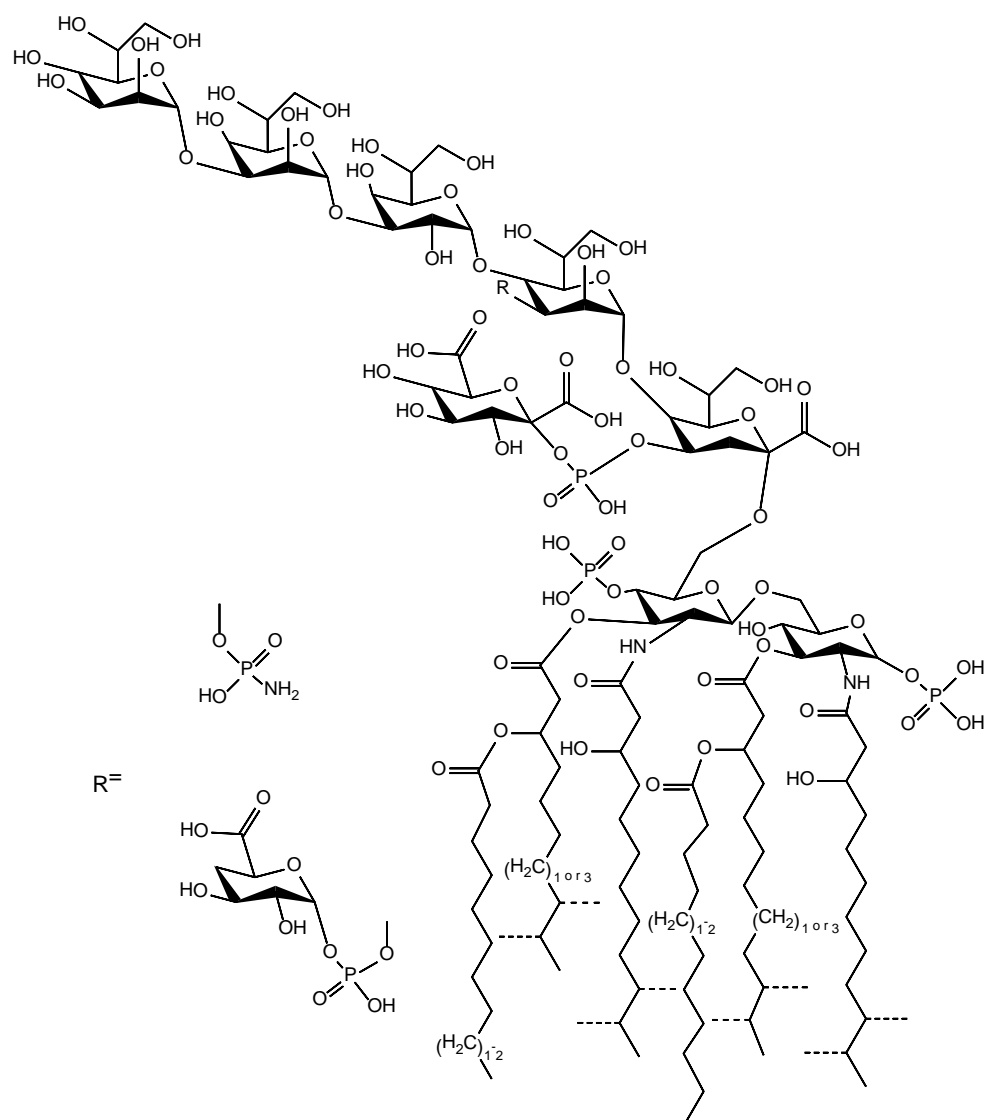
Figure 11: *Xcc LOS, the second LOS examined in this thesis. The dotted lines indicate nonstoichiometric substitutions. The dotted methyl groups on fatty acids are present as possible single substitutions. Adapted from*[142].

1.2.3: Therapeutic TLR4 suppression

TLR4 can be potentially used as a target for anti-cancer immunotherapy. Interestingly, PAMPs- and DAMPs-mediated overactivation of TLRs, TLR4 included, can be harmful since it unbalances immune homeostasis by sustained pro-inflammatory cytokines and chemokines production. As a consequence, TLR4 can take part in the development of autoimmune diseases and inflammation[143]. From this point of view, TLR4 is related to a broad spectrum of contemporary diseases including allergies, asthma, chronic inflammations, autoimmune disorders. TLR4 has

also been suggested as a promising therapeutic target for depressive disorder and amyotrophic lateral sclerosis[125]. Especially, DAMPs have been implicated in TLR4 overstimulation causing atherosclerosis, rheumatoid arthritis (RA) and neurodegenerative diseases such as Alzheimer's disease (AD), amyotrophic lateral sclerosis (ALS) and many others[144,145].

Indeed, TLR4 activation and signaling contribute to the progression of the afore-mentioned diseases and therefore inhibitors and/or antagonists targeting TLR signals may be beneficial to treat these disorders[146,147]. Amongst these diseases, the most severe one is sepsis, deriving from excessive TLR4 activation. It consists of a dysregulated response of the host organism to outer pathogens, leading to acute life-threatening organ dysfunction. Sepsis has a very high fatality rate (20%) and accounts for 5.3 million deaths annually worldwide[148]. Up until now, only two sepsis drugs made it to phase 3 clinical trials, Eritoran and TAK-242, but failed to show significant results and block acute sepsis[145] and did not get the FDA approval[125]. Nevertheless, as the vast majority of the mentioned pathologies still lack a specific pharmacological treatment, molecules active in inhibiting TLR4 activation have attracted increasing interest in a wide range of possible clinical settings[149]. However, manipulation of TLR mediated immune responses needs to be balanced and requires further studies[150,151]. In this context, the manipulation or intervention of TLR-mediated immune responses by nanomaterials is a potential approach to treat these diseases.

1.2.3.1: TLR4 antagonists for immune suppression

As already mentioned, the variable composition of natural products belonging to the LPS family are unpure or show different composition, which is an obstacle when determining the immune stimulating properties of such compounds[126]. As a result, different TLR4 antagonists have been developed also following a synthetic route.
Amongst them, a notable example is Eritoran (E5564) (*Figure 12*), a synthetic analog of lipid A with four acyl chains of different length and nature. Structural studies of the TLR4–MD2 complexation to Eritoran showed that it binds directly to the hydrophobic pocket of MD2, competitively inhibits LPS from binding to MD2, and prevents dimerization of TLR4 and consequently TLR4-signaling, acting as a TLR4 antagonist[152]. An interesting study was reported by Czeslick et al. in 2006, who

demonstrated that Eritoran inhibited the production of LPS-induced TNF-α and IL-6 In human monocytes[153]. Despite the favorable results obtained in animal sepsis models[152] and its safety in humans[154], Eritoran did not reduce the patient mortality at 28 days and 1 year from the statistical analysis[143] and therefore didn't get the FDA approval for use in the clinic to treat sepsis. Nonetheless, Eritoran could still be therapeutically beneficial for other inflammatory diseases. Indeed, it has been shown to prevent influenza-induced death in mice, to reduce cardiac hypertrophy in a mouse model and to attenuate inflammatory cytokine production and myocardial ischemia/ reperfusion injury in a rat model.

Resatorvid (TAK-242) (*Figure 12*) is a small molecule with a chemical structure different from lipid A that directly targets TLR4 with a non-classical mechanism of action and made it to clinical investigations due to its preclinical success. Specifically, two phase III clinical trials for severe sepsis and for sepsis-induced cardiovascular and respiratory failure were performed. In the first trial, the results were unfortunately not satisfactory due to failure to effectively suppress serum cytokine levels (IL-6, IL-8, and TNF-α)[149] when compared to controls, even with the drug showing a good tolerability profile[155]. The second trial, however, was terminated due to a business decision, and no further clinical development of this drug has been conducted ever since[143].

Lipid IVa (*Figure 12*) is a biosynthetic precursor that has been intensively studied and reported in 2003 by Onto et al.[156] and pioneered the studies of the structural interaction amongst the TLR4 complex and its modulators. Interestingly, this molecule acts as an agonist in mice and antagonist in human, a difference which has been attributed to the difference in the shape between the human and murine MD2 pocket and to variations in the electrostatic potential at the rim of the binding cavity of MD-2 and at the dimerization interface[156,157].

Ibudilast (AV411) (*Figure 12*), another small molecule TLR4 antagonist, has been shown to suppress pro-inflammatory cytokines such as TNF-α and IL-6 in neuroinflammation[158] and is already used in Asia to treat asthma and post-stroke disorders[88]. Phase II clinical trials looking at AV411 for treatment of neuropathic pain in 2008 demonstrated that the antagonist was well tolerated in humans[159]. At

present, Ibudilast is in Phase II clinical trials for the treatment of asthma and poststroke disorders[125].

Perrin-Cocon et al.[144] reported that FP7, a synthetic small-molecule TLR4 antagonist, could modulate the "in vitro" secretion of proinflammatory cytokines (IL-6, IL-8, and MIP-1β) by monocytes and DCs (half maximal inhibitory concentration (IC50) < 1 μM) and prevented DC maturation upon TLR4 activation by ultrapure LPS and blocked influenza-induced lethality in a mice model. Its mechanism of action is based on the direct competition with LPS for MD-2 binding probably reinforced by direct binding to CD14 co-receptor[125].

Other compounds such as VIPER and NI-0101 have shown promising experimental results: the former is a peptide inhibitor derived from vaccinia virus protein A46 described to inhibit TLR4-dependent signaling via blocking TIR–TIR domain interactions[160], which showed the attenuation of blood pressure and inflammatory responses in hypertensive rats[88]. NI-0101 is a TLR4 targeted monoclonal antibody that inhibits dimerization reducing pro-inflammatory cytokine production and has several potential applications including in asthma. It is the first TLR4-targeting antibody to pass Phase I clinical trials for safety and tolerability[88].
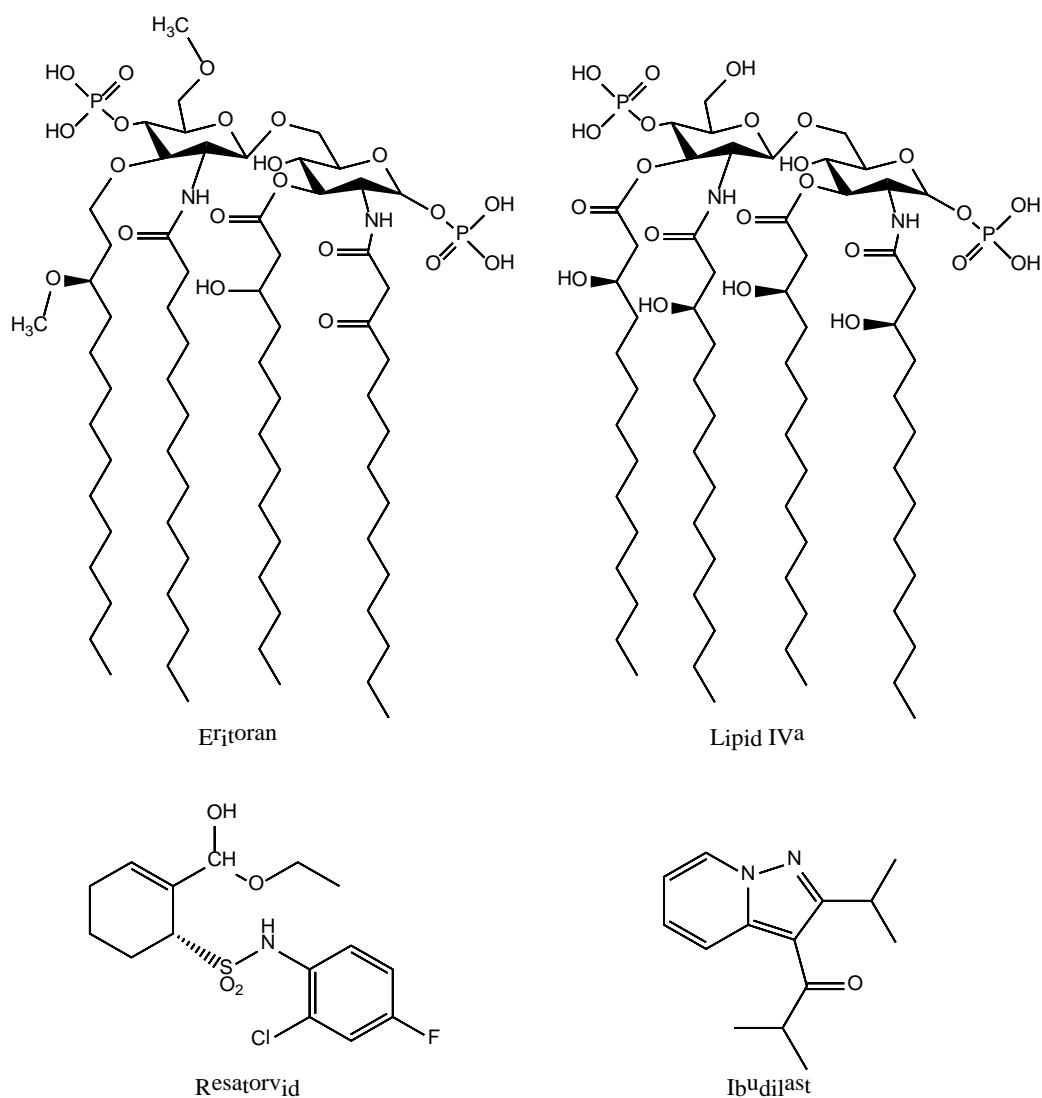
Figure 12: *Structures of synthetic TLR4 antagonists.*

1.2.3.2: Structure-biological activity correlation in TLR4 antagonists

The common features (or pharmacophore) that the TLR4 agonists have in common have already been discussed. New insights into the ligand-receptor interaction mechanisms were discovered recently by studying the structures of Eritoran and lipid IVa and the way these agonists bind to MD-2, which helped to understand the different mechanism of action of TLR4 agonists and adjuvants. Indeed, the molecular structures of Eritoran and lipid IVa, well known TLR4 antagonists, share four lipid chains that fit in and fill the available space in the hydrophobic MD-2 pocket. On the other hand, E. coli LPS and other TLR4 agonists have two or more additional lipid chains than these. It was proposed at first that some structural changes in the MD-2

pocket could account for the capacity of accommodating the extra lipid chain. However, Park et al.[91] later found that the size of the MD-2 pocket doesn't change and that additional space for lipid binding is generated by displacing the glucosamine backbone upwards by 5.5 A° (**Figure 13**). This repositions the phosphate groups so that they are allowed to interact with positively charged residues of the two TLR4 heterodimers, TLR4 and TLR4*, therefore promoting dimerization and activation of the receptor complex. Hence, the total number of lipid chains is the most important factor in determining whether a TLR4 ligand is an agonist or an antagonist, according to Park et al. Indeed, molecules such as Eritoran featuring four lipid chains completely lack agonistic activity and are antagonists that prevent binding of agonists to TLR4. Increasing the number of chains, Lipid As with five lipid chains behave as agonists and Lipid A, with six lipid chains, has optimal inflammatory activity, 100 fold higher than five lipid chains lipid As[161]. Nonetheless, other molecules having different structures from the well-known lipids can inhibit the TLR4. For example, the aforementioned Resatorvid selectively inhibits TLR4 signal by covalently binding Cys747 in the intracellular domain of TLR4 which blocks the interaction between TLR4 and the adaptor proteins TIRAP and TRIF-related adaptor molecule (TRAM), thereby diminishing LPS-induced TLR4 signaling and inflammation[149,143]. An interesting example of synthesis and biological study of small structural differences was performed by Piazza et al.[162], which reported the synthesis of six different glycolipids and a benzylammonium lipid rationally varying the chemical structure of a D-glucose-derived compound active as lipid A antagonist. In vitro studies confirmed their activity as lipid A antagonists on HEK cells, and the capacity to inhibit LPS-induced septic shock "in vivo" upon injection of a lethal LPS dose per mice. Particularly, one of the reported compounds, IAXO 102 (**Figure 14**), could block the effect of the LPS injection and all the mice receiving compound 5 + LPS survived, while the control group mice, which only received LPS injection, died after 2 days. According to their data, IAXO 102 has a potency comparable to that of the best antisepsis agents developed to date such as Resatorvid, which showed comparable activity in the same in vivo test with a similar effective dose (ED). In this thesis, the antagonistic activity of IAXO 102 was assessed in J774 murine macrophages, and the results are reported in chapter 2.
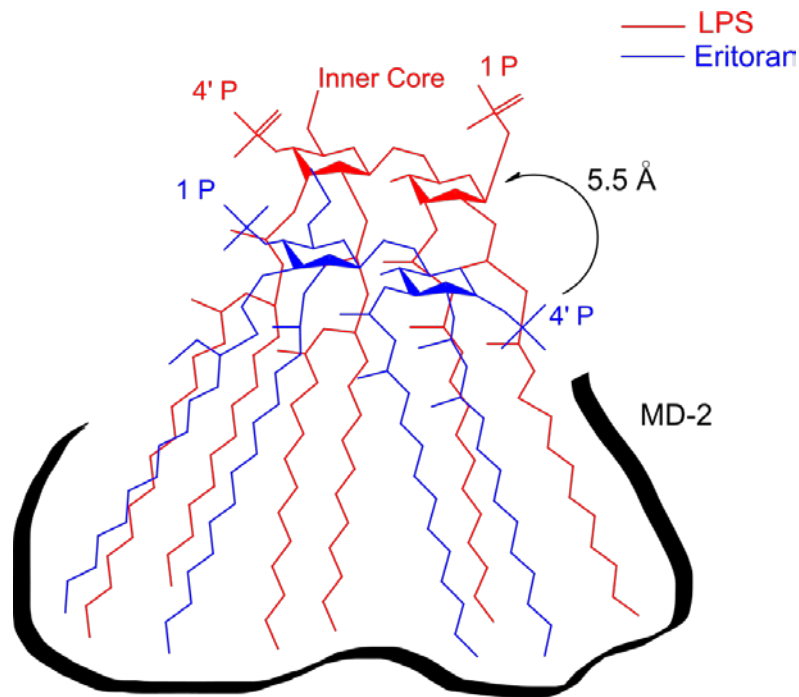
Figure 13: *Differences in the binding of Eritoran and LPS into the hydrophobic pocket of MD-2.*
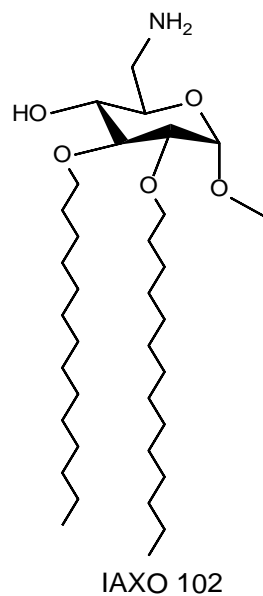
IAXO 102

Figure 14: *Structure of IAXO 102, the TLR4 modulator used in this thesis.*

1.3: Nanochemistry for drug delivery: an introduction

Nanoparticles are of great interest for biomedical applications due to their unique physicochemical properties. The interest towards nanotechnology was kicked off by Richard Feynman's talk in 1959 when he first pronounced the famous sentence ''there is plenty of room at the bottom'', also stating that to complement the interest in ''big science'' scientists should study and understand phenomena on a small scale[163]. The term "nanotechnology" itself was first defined by Norio Taniguchi in 1974. This field of science deals with the development, handling, characterization, and use of materials, devices, and structures with at least one dimension less than 100 nanometers [164]. The FDA also refers to nanomaterials as "materials that have at least one dimension in the range of approximately 1 to 100 nm and exhibit dimension-dependent phenomena[165] (**Figure 15**).
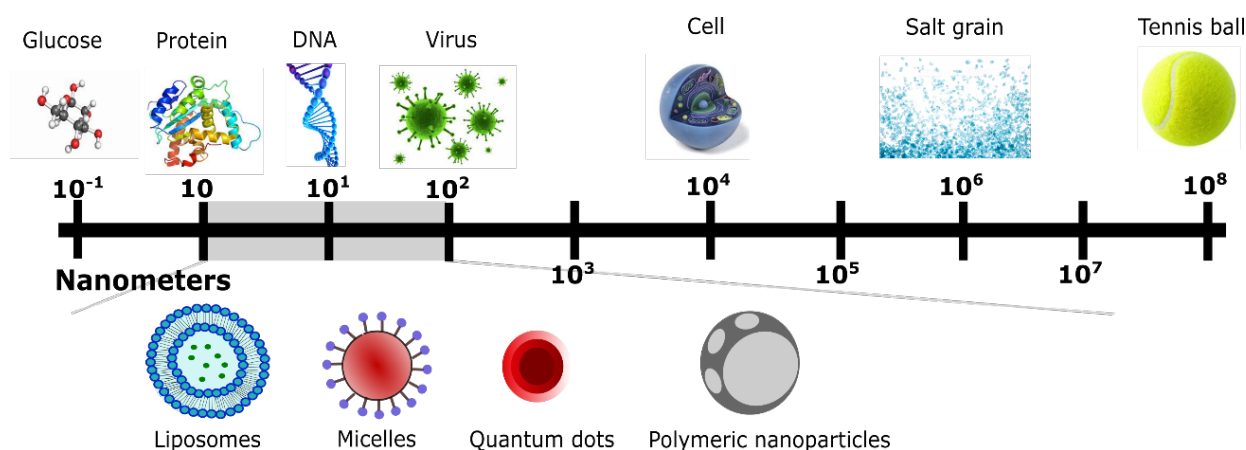
Figure 15: Comparison of the size of nanomaterials with those of other common materials.

Since the beginning of the 21st century, a plethora of nanomaterials have been reported in the literature due to their versatility (**Figure 16**), and the focus on such materials is expected to grow significantly in the future[166], and nanotechnology promises to revolutionize cancer diagnosis and therapy[167,168,169].

Nanomaterials-based medicine hugely developed in the last years, with numerous nanomedicines approved by the FDA for different clinical applications[170]. Amongst nanomaterials, paramagnetic iron oxide nanoparticles, quantum dots, nanoshells,

and nanosomes have been extensively used for diagnostic purposes[171]. Many nanosystems for drug delivery have been used as therapeutic tools[172,173], for early detection of cancer cells and/or specific tumor biomarkers[174] and to enhance the efficacy of applied treatments[175]. The use of nanoparticles as delivery systems for cancer therapies[176,177] and vaccine adjuvants[178] also holds huge potential.
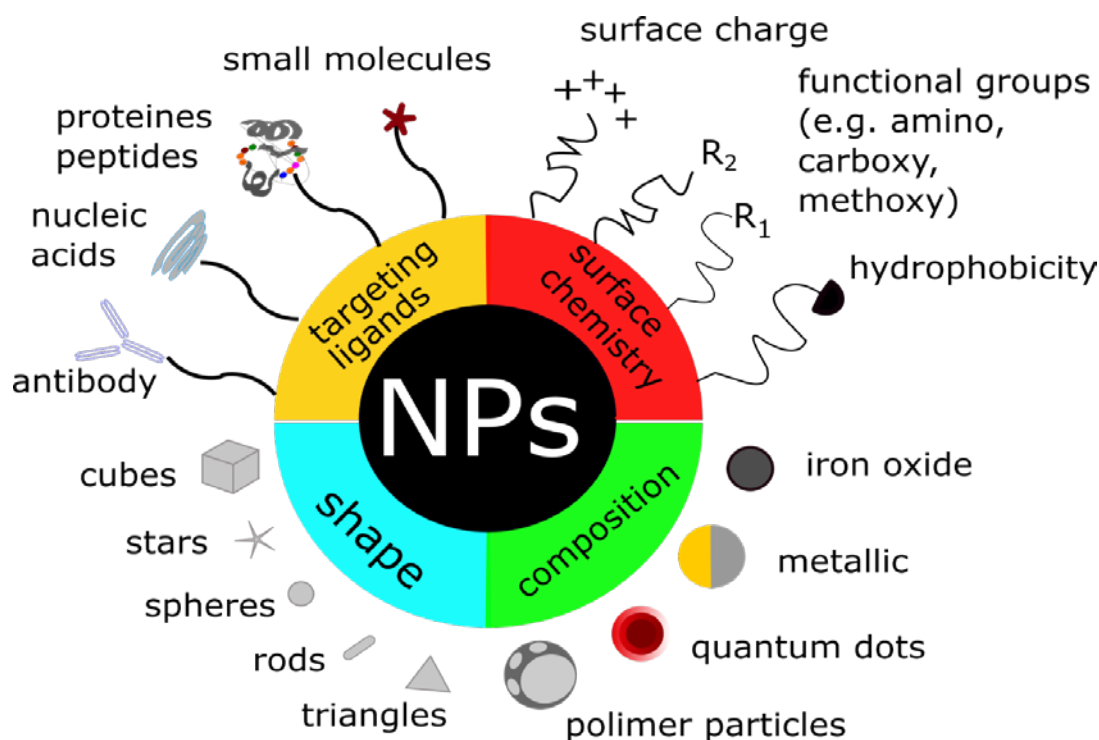
Figure 16: A pictorial representation summarizing some of the nanoparticles' shapes, compositions and surface properties.

Improved drug delivery and reduced toxicity and side effects arise from a combination of unique properties such as their high loading surface area, their capacity to specifically present the payload to its binding sites, alter its biodistribution and slowly release it over time[179,180,181,172,171]. Indeed, small molecule therapeutics showed limited clinical efficacy due to many limiting factors such as poor solubility, inefficiently timed release and inability to target or directly accumulate in the desired locations[182,183,184,169,185]. Size, shape, composition and surface chemistry of nanoparticles are all factors that affect the toxicity, in vivo biodistribution, biological fate and targeting ability of these systems, thus being key factors to their use as carriers. Recent advances in nanochemistry, biomedicine and the concurrence of these disciplines have now expanded the ability to design and construct "multifunctional" nanoparticles, combining different functions such as targeted

therapy and diagnostic functions in a single entity allowing multimodal approaches[112,174,173,186,187]. Thus, nanotheranostics (nanotherapy + nanodiagnosis) emerged as an alternative to the separate administration of diagnostic probes and pharmacologically active molecules. Nanotheranostics provides an unprecedented opportunity to integrate various components along with customized therapeutic agents, controlled-release mechanisms, targeting strategies, and reporting functionality for therapeutic detection/ visualization within a nano-scaled architecture[188]. The combination of such different functionalities eventually looks to the establishment of "personalized nanomedicine", which refers to the use of these nanosystems to elaborate specific and optimized treatment protocols fitting to each specific patient, or in administering "the right drug to the right patient"[189].

1.3.1: Different types and properties of theranostic nanomaterials

Nanoparticles can be widely subdivided into inorganic and organic nanoparticles according to the chemical composition of their core[190], or polymer and nonpolymer nanoparticles according to the presence or absence of a polymeric component. Although an astonishing variety of nanoparticles featuring different properties is available, the main objective of this thesis was to investigate specific types of metallic nanoparticles for their intrinsic imaging and therapeutic properties, which will be discussed in the following chapters. In general, it is considered that nanoparticles within a size of 10–100 nm are ideal for use as delivery vehicles or cancer therapeutics[191,192,193] and in vivo applications[194]. Particles bigger than 200 nm can accumulate in the liver and spleen[191], might not be uptaken at all[195] or be lethal depending on the dose[196]. Zauner et al.[197] and Rejman et al.[198] discovered a trend in the uptake of differently sized nanoparticles in different kinds of cells: as the particle size increases beyond the range of 20- 50 nm, their likeliness to be uptaken in cells decreases. Additionally, Wilhelm et al. performed a literature survey and found that particles with a hydrodynamic diameter smaller than 100 nm tend to show higher delivery efficiency to solid tumors than larger particles (0.7% and 0.6% of the injected dose, respectively)[199]. Nanoparticles within a size of 25–40 nm penetrate tissue barriers and traffic to the draining lymph nodes more rapidly than nanoparticles larger than 100 nm in size[200]. The high surface-to-volume ratio is another advantage

of nanosized materials, especially when it comes to surface functionalization and drug delivery[201].

1.3.1.1: Iron oxide nanoparticles

Within all the nanomaterials currently used for medical applications, superparamagnetic iron oxide nanoparticles (IONPs) are very versatile as they have been used for many in vivo applications such as hyperthermia, drug delivery, MRI contrast agents[202,203,164,] and cancer diagnosis and treatment[173,204,205,166]. Many magnetic nanoparticle-based cancer therapy systems are still at the research stage, but according to Yigit et al.[206], their routine clinical application is getting near. This affirmation is supported by the number of IONPs-based nanomedicines that have been approved for use in humans as iron deficiency therapeutics and as MRI contrast agents by the FDA, such as Feraheme™/ferumoxytol, Feridex®/Endorem®, GastroMARK™/Lumirem® and by the European Medicines Agency (EMA) such as Endorem/Feridex[170,207,204,208]. Besides, it has been demonstrated that IONPs have a very good tolerance profile, by undergoing in vivo biotransformation to be turned into iron species stored into ferritin proteins[209,210]. Nowadays, the level of knowledge acquired in the field of nanoscience allows easy control over the size and shape of IONPs and fine-tuning of their properties and cargos[211]: It is considered important for those particles to be smaller than 100 nm to increase blood circulation time, and at the same time have a high surface area and a narrow particle size distribution[212].

The interest in IONPs derives from their magnetic properties, which are strongly depending on the size and morphology of the particles. In the bulk state, magnetic materials are constituted of multi-domains, but as particle size decreases to the sub-micron range, the particles become monodomains, leading to a ferromagnetic behavior. If size is reduced even further, the resulting nanoparticles become superparamagnetic[213]: IONPs smaller than 25 nm are superparamagnetic, meaning that when a magnetic field is applied, the magnetic moments align to the magnetic field leading to a net magnetization[214] (**Figure 17**). Indeed, when the particle size goes below 25 nm the nanoparticle acts as a single monodomain, with all the spins aligned in the same direction, and when the applied magnetic field disappears, magnetization is completely lost. These magnetic properties make IONPs ideal candidates as contrast agents for MRI and possible candidates for performing

hyperthermia therapy, a form of cancer therapy which will be explained deeper later in the introduction. Since imaging is not the main objective of this thesis, it is important to note that their biocompatibility, stability, and the possibility of modulating their surface according to the chemical needs also made them an ideal choice for this thesis' purpose and for many other biomedical applications.[215–217].
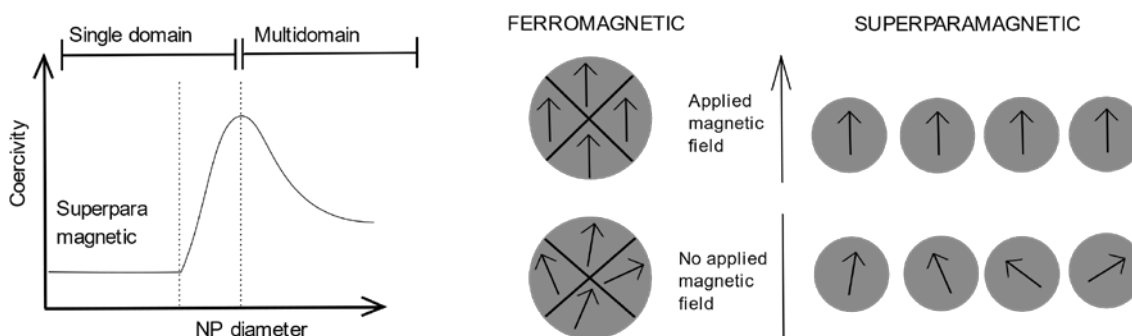
Figure 17: Size-dependent properties of IONPs.

1.3.1.2: Quantum dots

Quantum dots (QDs) feature unique optical and electronic properties such as a narrow size-tunable emission spectrum with light emission, and a broad absorption spectrum enabling the simultaneous excitation of multiple fluorescence colors. QDs also show about 10 - 100 times brighter emission than organic fluorophores and are 100 - 1000 times more stable against photobleaching[218]. These properties are well suited for dynamic imaging at the single-molecule level and for multiplexed biomedical diagnostics at ultrahigh sensitivity[219]. Different strategies have been developed to conjugate QDs to a variety of bioactive molecules such as enzymes, proteins, peptides, antibodies, and oligonucleotides[220]. QDs are thus widely used nanomaterials for biological applications[221]. Recent advances have led to the development of luminescent QDs for multiplexed molecular diagnosis and in vivo imaging[222,223,224,225] and high specificity cancer targeting, as shown by Gao et al.[226].

The unique photophysical properties of QDs and their popularity derive from size-dependent fluorescent emission (*Figure 18*): their small size, which is close or even smaller than the energy level spacing between excited electrons and their corresponding electron holes, leads to discrete quantized energies. The band gap is

inversely proportional to the radius of the QDs (an effect also known as quantum confinement), with the emission wavelength shifting to the blue as QDs get smaller and changing their composition and crystal structure allows fine-tuning of their emission[227].
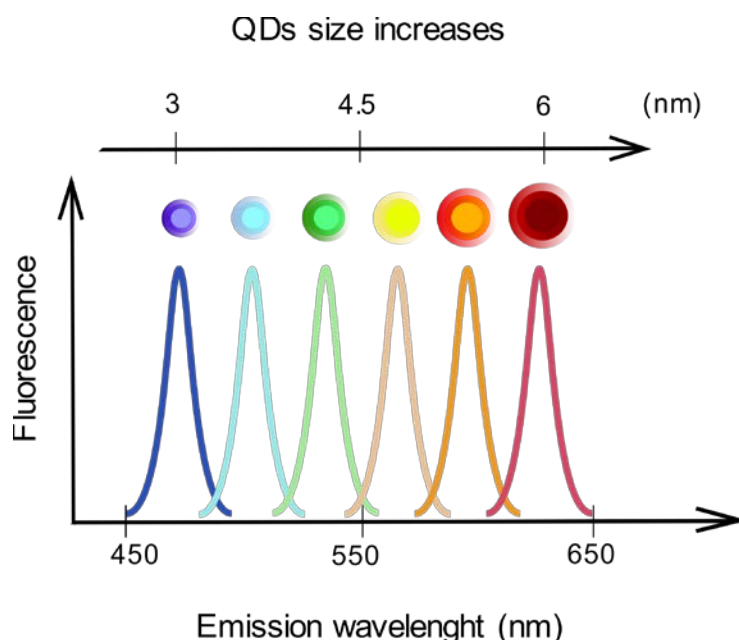
Figure 18: Size-dependent fluorescent emission of QDs.

1.3.1.3: Upconverting nanoparticles

Upconverting nanoparticles serve as an excellent substitute for traditional fluorescent labels, even for medical applications. Especially, rare earth-doped upconverting nanoparticles are able to turn long-wavelength radiation (e.g., NIR light) into short-wavelength fluorescence (e.g., visible light) via a two-photon or multiphoton mechanism, thus emerging as a new class of fluorophores. These particles possess several advantages with respect to conventional fluorescent biolabels, such as the utilization of NIR excitation light which not only allows for deeper light penetration in tissues but also offer lower autofluorescence, reduced light scattering and phototoxicity[228,229], an excellent signal to noise ratio (SNR) and improved detection sensitivity owing to the absence of autofluorescence. Additional advantages of upconverting nanoparticles include good chemical and physical stability, narrow emission peaks, resistance to photobleaching and low toxicity[230,231,232]. Lanthanide-doped upconversion nanoparticles (UCNPs) have promisingly been used for

bioimaging, antigen-delivery[233], photodynamic therapy[234,235,236] and could potentially be used for targeted cancer therapy[237,238].

UCNPs feature the capacity of emitting visible light from near infrared radiation (NIR) by a process called upconversion (UC) (*Figure 19*). It is a nonlinear optical process by which excitation of lower electronic levels with low-energy radiation (NIR light) results in higher energy emission (visible or UV light) at higher electronic levels and can, therefore, be ascribed as an anti-Stokes mechanism, as opposed to a stokes mechanism, where excitation of electronic levels leads to a lower-energy emission. Anti-Stokes mechanisms require the sequential absorption of two or more photons to provide sufficient energy for the emission to occur[232]. Three different classes of UC processing mechanisms can lead to multi-photon absorption and are discussed in detail elsewhere[231].
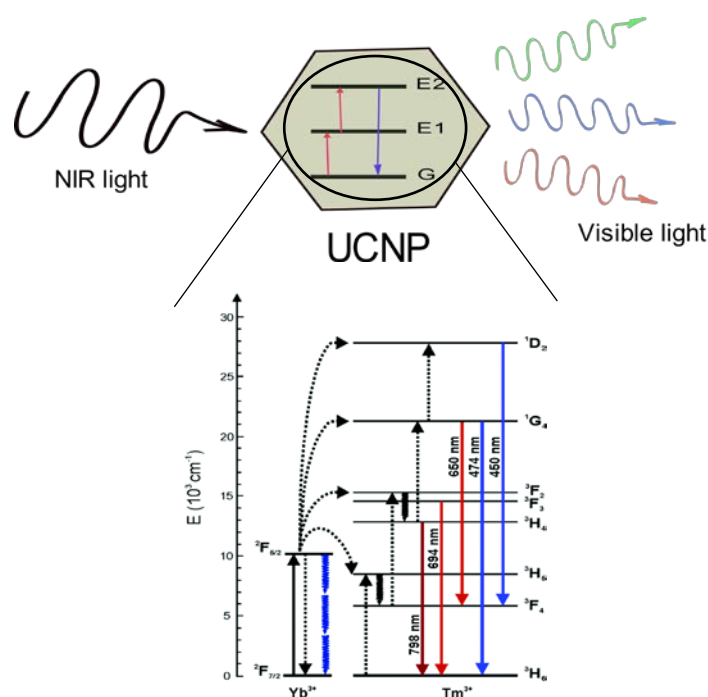
Figure 19: Schematic representation of the upconversion process and graphical explanation. Solid, dotted and wavy arrows in the graph represent photon absorption or emission, energy transfer and relaxation processes, respectively. The blue wavy arrows denote the increased multiphonon relaxations caused by OH vibrations. Graph published by the Royal Society of Chemistry[239].

UCNPs are also advantageous because of the biocompatibility of their material composition and usefulness in optical diagnostic applications due to their high

photostability, weak background signal, and long luminescence lifetimes (micro- to milliseconds)[237].

1.3.1.4: Janus nanoparticles

Janus particles (JanusNPs) are named after the Roman god Janus (typically represented by a double-faced head) and are characterized by the presence of two chemically different surface regions within a single particle,[240,241] which generates asymmetry and confers properties unconceivable for homogeneous, core-shell and patchy nanoparticles. Indeed, JanusNPs are a special type of patchy particles presenting only one patch that covers half of the particle[242]. These are of particular interest in applications where a spatial separation of functionalities is required, such as interfaces stabilization, catalysis, assembly of higher order suprastructures with new properties arising by the collaborative effect of the nano-objects and biomedical application that could combine targeted drug delivery, molecular imaging or biomolecular biosensing in a single platform[243]. The interest in this kind of nanoparticles was promoted by the Nobel laureate P. G. de Gennes who talked about them in his Nobel lecture entitled "Soft Matter" in 1991[244]. Different particle architectures bridging from simple spherical to different kinds of dumbbell shapes to vesicles/capsules and highly anisotropic architectures, such as cylinders or disks have been attained so far[240]. Not only that, but diverse morphologies too have been reported for JanusNPs which combine gold with other nanomaterials, including iron oxides, QDs, and UCNPs[245,246,247].

In this thesis, JanusNPs composed of a spherical IONPs and a gold nanostar were used, due to the interesting surface functionalization possibilities of both gold and IONPs and the useful combination of magnetic and plasmonic properties. Nanoparticles with a branched gold structure, also known as nanostars, show a strong light absorption and plasmon resonance at the visible-NIR window and a high photothermal generation. The resulting JanusNPs allow photothermal therapy (PTT) together with the outstanding magnetic properties, multimodal imaging capabilities and biocompatibility of IONPs[248]. Moreover, both the heat coming from photothermal and hyperthermia therapy can potentially be applied to treat cancer.

1.3.2: Nanoparticle-based delivery: functionalization strategies

The surface of nanocarriers can be modified to introduce either functional groups, hydrophobic or hydrophilic ligands or targeting moieties and cargos like antibodies, small molecules, drugs or proteins depending on the specific needs, which can also allow controlled release strategies by using stimuli-responsive nanocarriers[249,250].

Three are the major conjugation strategies that have been adopted for cargo loading on nanoparticles: adsorption, encapsulation, and conjugation (**Figure 20**), all of which are dependent on the nature of both the carrier and the particle. Adsorption is generally based on either electrostatic or hydrophobic interactions retaining the drug in the nanoparticle[251,252,253,] while encapsulation is most commonly applied in the case of organic nanoparticles such as liposomes or polymeric nanoparticles[254,255,256].

Encapsulation   Conjugation   Adsorption
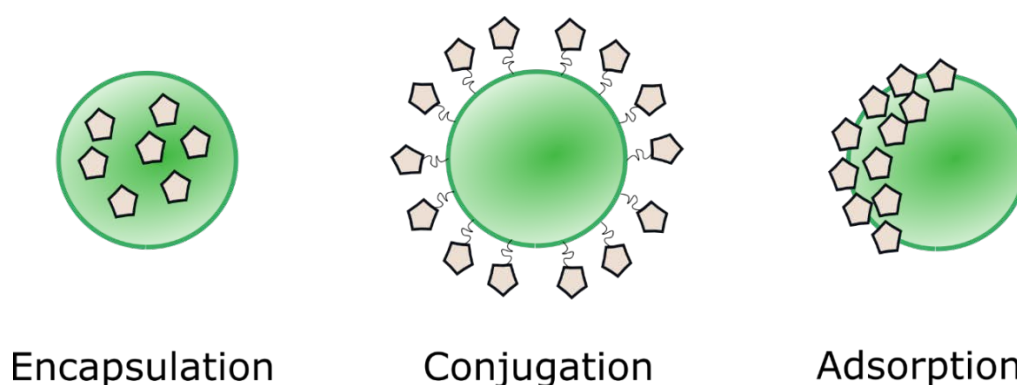
Figure 20: *Cartoon representing the different ligand loading strategies on nanoparticles.*

1.3.2.1: Covalent strategies for nanoparticle conjugation

Conjugation of bioactive molecules (e.g. OVA as a tumor antigen) to nanostructures has been one of the objectives of this thesis. The conjugation approach consists of creating a chemical bond between the drug and the nanoparticle by the means of organic or click chemistry, usually mediated by chosen ligands or linker molecules. In all cases, the delivery vectors must not only transport the payload but also be able to release it in a specific location.

The first strategies developed for the conjugation of bioactive molecules to nanoparticles are the ones that drew inspiration from standard protein labeling chemistries: maleimide-thiol reaction, succinimidyl ester-amine reaction and carbodiimide activation followed by reaction to an amine[257] (*Figure 21*).

A popular cross-linking reaction is the one that uses amines and carboxylic acids as reactive functional groups, taking advantage of the process known as carbodiimide activation (e.g., 1-ethyl- 3-(3-dimethylaminopropyl) carbodiimide, or EDC). This method presents some disadvantages, one is the instability of the o-acylisourea intermediate formed through the activation of carboxylic acids, bringing to the use of a large excess of reagents and loss of colloidal stability. This has been only partially ameliorated by converting the o-acylisourea to a more stable reactive intermediate using N-hydroxysuccinimide (NHS), which helps maintain colloidal stability during the reaction[258]. Despite the improvement, this method is still limited by its sensitivity to reaction conditions such as pH and temperature. Furthermore, these reactions require very high concentrations of reagents, biomolecules, and nanoparticles, do not achieve control on the stoichiometry and display of the biomolecule loaded on the nanoparticles and can cause crosslinking and precipitation of the nanoparticles, with permanent loss of their properties[259,260].

Maleimide-thiol reaction

maleimide — thiol — thioether bond

Succinimidyl ester-amine reaction

succinimidyl ester — 1° amine — amide bond

Carbodiimide activation and reaction to an amine

carboxyl — carbodiimide — O-acylisourea intermediate — amide bond
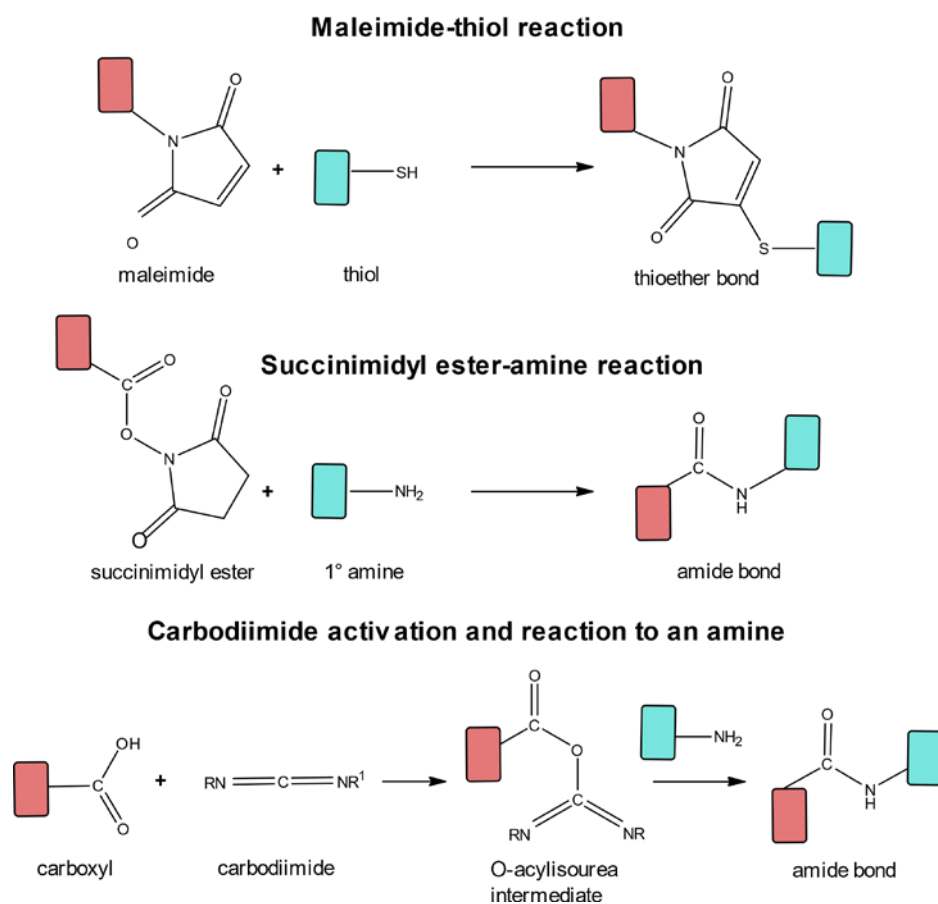
Figure 21: Standard bioconjugation reactions, including maleimide-thiol, succinimidyl ester-amine, and carbodiimide-mediated coupling between carboxyls and amines.

Another example is the monofunctional conjugation of avidin to pcQDs[261]: conjugation of large molecules to QDs is still challenging because steric hindrance, geometry, the stoichiometry of the conjugate, and its final functional activity have to be addressed.

In the last few years, cleaner and more efficient biorthogonal chemistry has been used to tackle this challenge. It exploits functional groups not having significant reactivity toward the functional groups intrinsic to biomolecules such as amine, carboxyl, hydroxyl, and thiol groups. This approach offers the potential to eliminate undesirable side reactions, minimize nonspecific NP-bioconjugate activity, improve reproducibility in production, and maximize efficacy[262,257]. In particular, hydrazone ligations have proven to be chemoselective and fast, yielding stable products and reactions that can be monitored by UV-Visible spectroscopy due to the formation of the hydrazone cromophore[263]. Besides, this chemistry is suitable for applications in

the drug delivery field, since the hydrazone bond hydrolyzes at a pH of 5-6, corresponding with the one in the acidic environment of endosomes and lysosomes, releasing any biologically active molecule that is bound to the nanoparticle[257].

Different strategies have been used to achieve successful functionalization of nanoparticles with biomolecules and drugs. Some examples are reported below. Doxorubicin (DOX) is one of the main anticancer drugs that have been coupled to IONPs. This drug can both be covalently and electrostatically bound to functionalized IONPs. An example of the first approach is the paper by Wu et al.[264] in which 1,2-ethanediamine (EDA)-azo (4,4-azobis (4-cyanovaleric acid))-functionalized magnetic nanoparticles were conjugated to DOX. When this system was injected in tumor challenged mice, the delivery of DOX by the nanoparticle reduced the tumor volume by 6.8 times compared with the free drug. Additionally, upon exposure to NIR irradiation, IONPs could reach a temperature of 43°C which could break the bond and achieve controlled release of DOX.

Dutta et al.[265] reported an example of sulfate moieties-mediated electrostatic conjugation of DOX to IONPs based on a self-assembled system consisting of an anionic surfactant and sodium dodecyl sulfate (SDS) on hydrophobic nanoparticles. These particles showed internalization in cells and heating ability under a magnetic field is thus suitable for hyperthermia treatment of cancer.

A notable example is the yolk-shell $Fe_3O_4@MgSiO_3$ nanoplatform developed by Wang et al.[266], where the magnetic Fe_3O_4 core contributes to magnetic targeting, the magnesium silicate shell provides a hollow cavity for drug loading and finally, the polymer poly(ethylene glycol) (PEG) guarantees in vivo biocompatibility and biostability. This nanocarrier was able to improve the activity of a conventional anticancer drug by taking advantage of the rational design. It was loaded with folic acid for targeting and the application of a magnetic field allowed to further enhance the delivery efficacy. Nevertheless, the presence of the nanoparticle alone without using the intrinsic properties could already improve the antitumor effect in mice increasing tumor growth inhibition rate to 40% compared to 27% obtained with the drug alone.

Another interesting example of delivery is reported by Xiang et al.[233], who took a model antigen, OVA, and loaded it via electrostatic interaction on the surface of dual-polymer-coated UCNPs, forming nanoparticle-antigen complexes that were efficiently engulfed by DCs and induced DCs maturation and cytokine release.

1.4: Nanotheranostics: exploiting the intrinsic therapeutic modalities of nanoparticles

Even though this thesis focuses on the use of nanoparticles as delivery vehicles for immune therapies, it must be noted that the chosen nanoparticles feature different intrinsic properties that will allow them to be used for various therapeutic modalities and imaging (but these studies are beyond the scope of this thesis). This combination of intrinsic and extrinsic therapeutic elements, previously discussed in this chapter, is called nanotheranostics and aims in integrating various components along with customized therapeutic agents, controlled-release mechanisms and targeting strategies within a nano-scaled architecture[188]. This section summarizes some of the applications that have been reported for IONPs, QDs, UCNPs and JanusNPs together with the most recent effects and results obtained with these nanoparticles within the nanotheranostics field.

1.4.1: Photothermal therapy (PTT)

Photothermal therapy (PTT) is a non-invasive cancer therapy approach utilizing visible or NIR light, performed in the presence of photo-absorbers such as nanoparticles that convert absorbed light energy into thermal energy. More specifically, the excited conduction band electrons decay to the ground state by releasing their energy as heat to the surrounding medium leading to thermal ablation of cancer[267,268,269] (***Figure 22***). Compared with the conventional therapeutic modalities, PTT exhibits unique advantages in cancer therapy such as high specificity to biological tissues when coupled with targeting methods and drug delivery coming from the same nanoparticle[270]. Besides, minimal invasiveness and precise spatial-temporal selectivity constitute an improvement with respect to conventional therapies such as the use of visible lasers[270,271.272,273].

In PTT, the cells can be killed by either necrosis or apoptosis depending on applied parameters such as laser power and time of exposure, which will, in turn, affect the temperature in the targeted area[274]. Right now, PTT is in a clinical trial, and AuroShell (Nanospectra Biosciences Inc., Texas), a gold nanoshells-based formulation (GNs), was recently approved for clinical evaluation in patients with refractory and/or recurrent tumors of the head and neck[275,276].
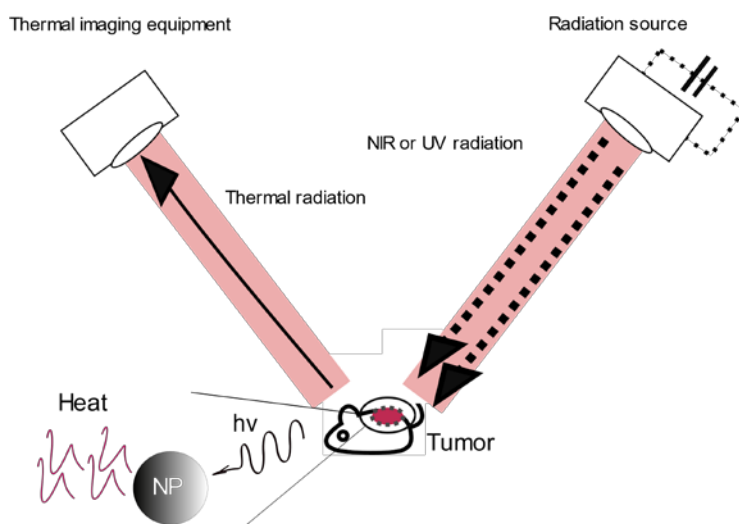
Figure 22: *A cartoon illustrating photothermal therapy.*

IONPs can play important roles within nanosystems used for photothermal therapy. Zhou et al.[277] reported PEGylated Fe@Fe$_3$O$_4$ nanoparticles, presenting a combination of targeting, PTT, and imaging in one entity. These nanocrystals demonstrated an excellent in vivo magnetic targeting effect upon application of an external magnetic field by MRI and showed a high photothermal conversion efficiency (~20%, comparable to gold nanorods). Strikingly, fourteen days after tumor challenge in mice, PBS-treated mice showed a 20-fold bigger tumor compared with the group treated using magnetically guided PEGylated Fe@Fe$_3$O$_4$ nanoparticles when photothermal treatment was applied[276].

UCNPs too have been used in the field of photothermal therapy. Lv et al.[278] reported the preparation of mesoporous silica-coated core-shell UCNPs loaded with dopamine (abbreviated as UCNP@mSiO$_2$-Dopa). Upon activation of the dopamine by the polyethyleneimine containing silica, this nanosystem is able to strongly absorb light under single 980 nm irradiation producing a photothermal effect and emitting

upconverted luminescence. The gadolinium core enabled the use of computed tomography (CT) and MRI. The UCNP@mSiO$_2$-Dopa agent was shown to be reasonably biocompatible and could slow tumor growth two times better than the well-known anticancer drug DOX.

Chu et al.[279] showed an example of photothermal therapy using 10 nm silica-coated CdTe QDs emitting at a wavelength of 710 nm. Interestingly, scanning a series of increasing dimensions QDs, they found that the larger the QD sizes the higher the increase in temperature after irradiation is. To prove the "in vivo" efficiency, mice were challenged with A375 melanoma cells. Upon administration of QDs to mice and irradiation at 671 nm, they showed that the QDs significantly inhibited tumor growth.

1.4.2: Hyperthermia

Hyperthermia consists in the treatment of malignant diseases by administering heat in various ways[280]. This treatment modality also aims at improving the outcome of conventional treatment strategies within the framework of multimodal treatments. Indeed, its efficacy is not enough to replace the already established therapy modalities when applied alone but can work complementary to, for instance, chemotherapy in difficult to treat tumors[281]. Magnetic hyperthermia consists of raising the temperature of tumor tissues to 40–43°C[282], but not higher than 46°C[283]. This temperature range might slightly change since the thermal dose-response relation varies among different cell lines and depends on microenvironmental factors such as pH[284]. This method is effective against cancer cells because of their higher sensitivity to elevated temperatures[285]. Hyperthermia with small magnetite nanoparticles was first reported by Gilchrist in 1957[286] and further developed by Gordon 20 years later[287]. The first heating technique using magnetic nanoparticles to have entered clinical trials is called magnetic nanoparticle thermotherapy, a minimally invasive method developed for interstitial thermal therapy[288]. In this technique, a dispersion of IONPs is injected directly into the target tissue and heated in an alternating magnetic field. This technology, named NanoTherm®, is the only nanotechnology-based therapy approved by the European Union for the treatment of brain tumors[289].

The heating efficiency of nanomaterials depends on different parameters such as the size and shape of magnetic nanoparticles: Fortin et al.[290] discussed the effect of size in regulating the efficiency of maghemite nanoparticles as heat mediators and found that magnetization decreases with the size, being increased by 3 orders of magnitude (4 to 1650 W/g) for particles with sizes ranging from 5.3 to 16.5 nm.

On the other hand, the effect of shape vas studied by Samia and co-workers which recently published a study comparing spherical and cubic IONPs (IONPsp and IONPc) as well as the effect of a zinc doped composition in both cases. Zn-doped IONPc were the most efficient heat producers, with a 5-fold improvement compared to undoped IONPsp[291].

Moreover, many applications have been reported in the literature where hyperthermia was combined with other strategies. Quinto et al.[292] prepared 14 nm PEG-coated IONPs and showed their potential to concurrently deliver DOX and generate heat for an enhanced multimodal cancer treatment, reducing in half viability of a HeLa cell line with respect to the single effect of DOX being released from the particle and reducing it three times with respect to the drug free IONPs without using hyperthermia.

1.4.3: Photodynamic Therapy

Photodynamic therapy (PDT) is a minimally invasive and clinically approved cancer therapy exerting a selective cytotoxic activity toward malignant cells. It is constituted by the combination of non-toxic components known as photosensitizers (PS) and a laser source irradiating at a frequency corresponding to the absorption band of the photosensitizers. This activates the release of reactive oxygen species (ROS), but requires sufficient molecular oxygen to be present in the cells to work effectively (*Figure 23*). PDT acts in three steps: excitation of PS followed by the activation of oxygen-species which ultimately lead to cell death by apoptosis, triggered by signaling pathways such as caspase activation or mitochondrial release of proapoptotic factors and cysteine-aspartic acid proteases activation[293]. It is different from PTT which utilizes heat for thermal ablation. Even though the therapeutic effect of light was known to the ancient Egyptian for repigmentation of Vitiligo, the first

clinical application of PDT was demonstrated in 1903 by Von Tappeiner and Jesionek using basal cell carcinomas and nowadays PDT has been approved to treat various cancers such as gastric cancer, esophagus, and melanoma[294,295].

A problem of PDT is in the PSs, which have limitations, such as limited delivery to target tissues and poor penetration of excitation wavelength, non-specific targeting, easy photodecomposition, hydrophobicity, and toxicity. NPs can be used to deliver the PS to effectively overcome these limitations[296,297]. Amongst them, IONPs can act as PS carriers for imaging-guided PDT overcoming most of the limitations of classic PS due to their diverse and non- toxic nature. IONPs can also be used with inorganic PS (TiO_2) for PDT and imaging[164].
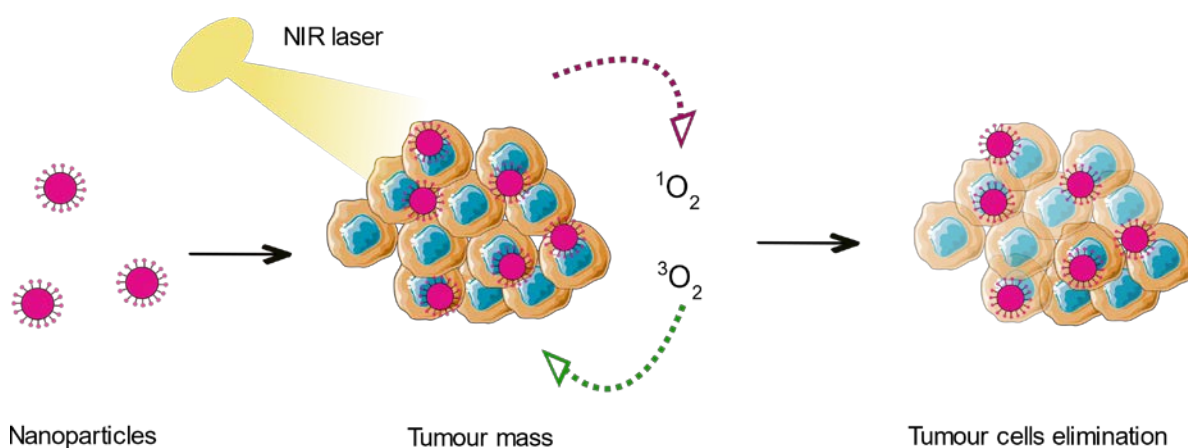
Figure 23: Pictorial representation of PDT.

More relevant to this thesis, PDT could combine well with immunotherapy by compensating for ineffective antigen delivery or presentation and overcoming the intratumoral immunosuppressive microenvironment[298]. Exogenous light can be controlled by different means to ensure precise tumor tissue targeting[299,300, 301,302] and the in-situ release of tumor antigens due to PDT cytotoxicity could significantly initiate immune response[298,303,297,304,305]. Notable examples of PDT performed using nanoparticles have been reported in the literature recently.

Cui et al. showed an UCNPs-based construct functionalized with a phthalocyanine zinc PS and coated by a folic acid modified chitosan (FASOC-UCNP-ZnPc). Upon intravenous injection in mice, the nanosystems accumulated mainly in the tumor thanks to folate receptors and were used to effectively perform PDT therapy to shrink

the tumors. Specifically, the mice treated with 660 nm PDT showed a tumor inhibition ratio of 77% with respect to the control group[235].

On the other hand, Xu et al.[297] were capable of developing an UCNP combining PDT to the delivery of R837, a TLR7 agonist as an adjuvant, and adding CTLA-4 checkpoint blockade to potentiate the anticancer activity. These multitasking nanoparticles could use NIR-induced PDT to destroy tumor cells and stimulate immune responses by triggering the maturation of DCs and secretion of cytokines. The combined activity of the nanoparticles and the checkpoint blockade strategy conferred complete immunity to a tumor challenge in a period of 60 days in the primary tumor and 44 days in secondary tumors (*Figure 24*). Besides, mice were protected from tumor reoccurrence from the development of a long-term immune memory[297] by the development of CD8$^+$ T cells and T$_{regs}$ cells.
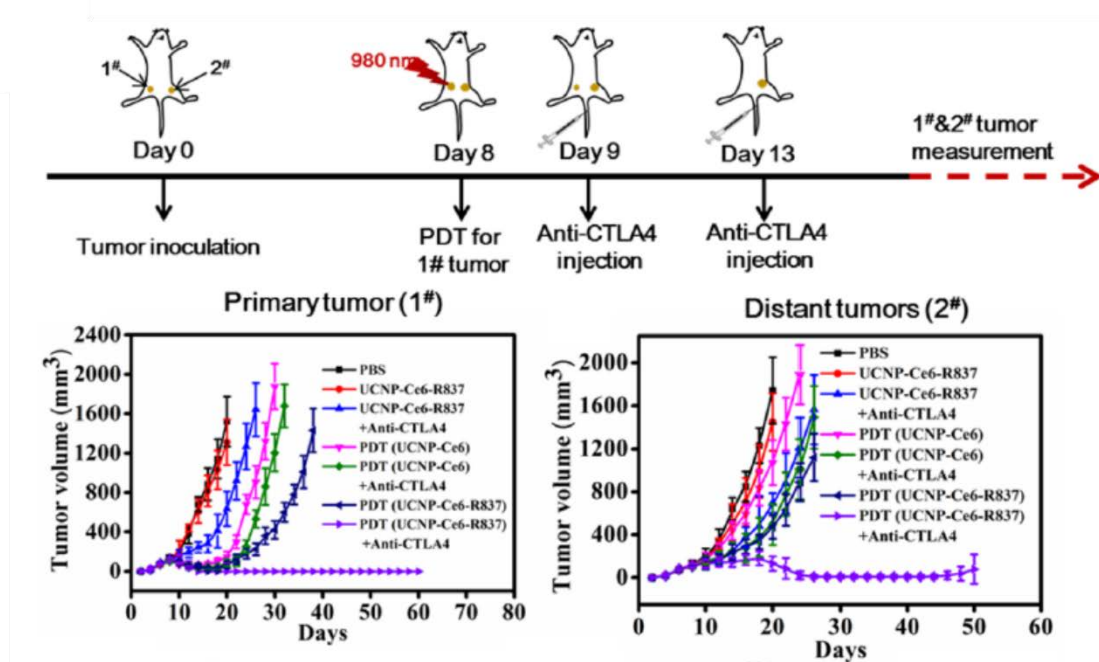
Figure 24: *Tumor challenge and primary and secondary tumor regression as shown in reference n.[297]. -Reprinted with permission from reference n.[297]. Copyright 2017 American Chemical Society-.*

Park et al.[234] showed a similar system using hexagonal-phase NaYF$_4$:Yb,Er/NaGdF$_4$ core-shell UCNPs conjugated with Ce6, a PDT drug. UCNP–Ce6 nanoparticles were readily accumulated in tumor sites by the EPR effect. Upon irradiation by a 980 nm

laser, UCNPs were able to provide complete tumor protection until day 14 after tumor injection. UCNP–Ce6 could as well be used as dual-modal imaging probes for accurate diagnosis clearly making tumor visible by MRI and upconversion luminescence imaging.

Another example of a combined activity is reported by Di Corato et al., that coupled PDT to magnetic hyperthermia. The authors prepared 9 nm magnetic nanoparticles-filled liposomes and stimulated them both by an alternating magnetic field, to induce local hyperthermia, and by a light source, to generate highly toxic ROS, obtaining complete tumor rejection by mice after 9 days of treatment only applying both treatment modalities[306].

1.5: References

(1)   American Cancer Society (www.cancer.org). What Is Cancer Immunotherapy?

(2)   National Cancer Institute (www.cancer.org). Immunotherapy to Treat Cancer.

(3)   Nature Reviews Immunology (www.nature.com). Cancer immunotherapy.

(4)   Cancer Research Institute (www.canceresearch.org). What is immunotherapy.

(5)   Farkona, S.; Diamandis, E. P.; Blasutig, I. M. Cancer Immunotherapy: The Beginning of the End of Cancer? *BMC Med.* **2016**, *14* (1), 1.

(6)   Decker, W. K.; da Silva, R. F.; Sanabria, M. H.; Angelo, L. S.; Guimarães, F.; Burt, B. M.; Kheradmand, F.; Paust, S. Cancer Immunotherapy: Historical Perspective of a Clinical Revolution and Emerging Preclinical Animal Models. *Front. Immunol.* **2017**, *2* (8), 829.

(7)   Oiseth, S. J.; Aziz, M. S. Cancer Immunotherapy: A Brief Review of the History, Possibilities, and Challenges Ahead. *J. Cancer Metastasis Treat.* **2017**, *3* (10), 250.

(8)   Morales, A.; Eidinger, D.; Bruce, A. W. Intracavitary Bacillus Calmette-Guerin in the Treatment of Superficial Bladder Tumors. *J. Urol.* **1976**, *116* (2), 180.

(9)   Emens, L. A.; Ascierto, P. A.; Darcy, P. K.; Demaria, S.; Eggermont, A. M. M.; Redmond, W. L.; Seliger, B.; Marincola, F. M. Cancer Immunotherapy: Opportunities and Challenges in the Rapidly Evolving Clinical Landscape. *Eur. J. Cancer* **2017**, *81*, 116.

(10)   Hoover, H. C.; Surdyke, M. G.; Dangel, R. B.; Peters, L. C.; Hanna, M. G. Prospectively Randomized Trial of Adjuvant Active-specific Immunotherapy for Human Colorectal Cancer. *Cancer* **1985**, *15* (55), 1236.

(11)   Steinman, R. M.; Cohn, Z. A. Identification of a Novel Cell Type in Peripheral Lymphoid Organs of Mice. I. Morphology, Quantitation, Tissue Distribution. *J. Exp. Med.* **1973**, *1* (137), 1142.

(12)   Van Der Bruggen, P.; Traversari, C.; Chomez, P.; Lurquin, C.; De Plaen, E.; Van Den Eynde, B.; Knuth, A.; Boon, T. A Gene Encoding an Antigen Recognized by Cytolytic T Lymphocytes on a Human Melanoma. *Science.*

1991, *13* (254), 1643.

(13)   Kantoff, P. W.; Higano, C. S.; Shore, N. D.; Berger, E. R.; Small, E. J.; Penson, D. F.; Redfern, C. H.; Ferrari, A. C.; Dreicer, R.; Sims, R. B.; et al. Sipuleucel-T Immunotherapy for Castration-Resistant Prostate Cancer. *N. Engl. J. Med.* **2010**, *29* (363), 411.

(14)   Topalian, S. L.; Sznol, M.; McDermott, D. F.; Kluger, H. M.; Carvajal, R. D.; Sharfman, W. H.; Brahmer, J. R.; Lawrence, D. P.; Atkins, M. B.; Powderly, J. D.; Leming P.D.; Lipson E.J.; Puzanov I.: Smith D.C.; Taube J.M.; Wigginton J.M.; Kollia G.D.; Gupta A.; Pardoll D.M.; Sosman J.A.; Hodi F.S. Survival, Durable Tumor Remission, and Long-Term Safety in Patients with Advanced Melanoma Receiving Nivolumab. *J. Clin. Oncol.* **2014**, *1* (32), 1020.

(15)   Hodi, F. S.; O'Day, S. J.; McDermott, D. F.; Weber, R. W.; Sosman, J. A.; Haanen, J. B.; Gonzalez, R.; Robert, C.; Schadendorf, D.; Hassel, J. C.; Akerley W.; van den Eertwegh A.J.; Lutzky J.; Lorigan P.; Vaubel J.M.; Linette G.P.; Hogg D.; Ottensmeier C.H.; Lebbé C.; Peschel C.; Quirt I.; Clark J.I.; Wolchok J.D.; Weber J.S.; Tian J.; Yellin M.J.; Nichol G.M.; Hoos A.; Urba W.J. Improved Survival with Ipilimumab in Patients with Metastatic Melanoma. *N. Engl. J. Med.* **2010**, *19* (363), 711.

(16)   Robert, C.; Schachter, J.; Long, G. V.; Arance, A.; Grob, J. J.; Mortier, L.; Daud, A.; Carlino, M. S.; McNeil, C.; Lotem, M.; Larkin J.; Lorigan P.; Neyns B.; Blank C.U.; Hamid O.; Mateus C.; Shapira-Frommer R.; Kosh M.; Zhou H.; Ibrahim N.; Ebbinghaus S.; Ribas A. Pembrolizumab versus Ipilimumab in Advanced Melanoma. *N. Engl. J. Med.* **2015**, *25* (372), 2521.

(17)   Ribas, A.; Puzanov, I.; Dummer, R.; Schadendorf, D.; Hamid, O.; Robert, C.; Hodi, F. S.; Schachter, J.; Pavlick, A. C.; Lewis, K. D.; Cranmer L.D.; Blank C.U.; O'Day S.J.; Ascierto P.A.; Salama A.K.; Margolin K.A.; Loquai C.; Eigentler T.K.; Gangadhar T.C.; Carlino M.S.; Agarwala S.S.; Moschos S.J.; Sosman J.A.; Goldinger S.M.; Shapira-Frommer R.; Gonzalez R.; Kirkwood J.M.; Wolchok J.D.; Eggermont A.; Li X.N.; Zhou W.; Zernhelt A.M.; Lis J.; Ebbinghaus S.; Kang S.P.; Daud A. Pembrolizumab versus Investigator-Choice Chemotherapy for Ipilimumab-Refractory Melanoma (KEYNOTE-002): A Randomised, Controlled, Phase 2 Trial. *Lancet Oncol.*

2015, *16*, 918.

(18) Topp, M. S.; Kufer, P.; Gökbuget, N.; Goebeler, M.; Klinger, M.; Neumann, S.; Horst, H. A.; Raff, T.; Viardot, A.; Schmid, M.; Schaich M.; Degenhard E.; Köhne-Volland R.; Brüggemann M.; Ottmann O.; Pfeifer H.; Burmeister T.; Nagorsen D.; Schmidt M.; Lutterbuese R.; Reinhardt C.; Baeuerle P.A.; Kneba M.; Einsele H.; Riethmüller G.; Hoelzer D.; Zugmaier G.; Bargou R.C. Targeted Therapy with the T-Cell - Engaging Antibody Blinatumomab of Chemotherapy-Refractory Minimal Residual Disease in B-Lineage Acute Lymphoblastic Leukemia Patients Results in High Response Rate and Prolonged Leukemia-Free Survival. *J. Clin. Oncol.* **2011**, *20* (29), 2493.

(19) Andtbacka, R. H. I.; Kaufman, H. L.; Collichio, F.; Amatruda, T.; Senzer, N.; Chesney, J.; Delman, K. A.; Spitler, L. E.; Puzanov, I.; Agarwala, S. S.; Milhem M.; Cranmer L.; Curti B.; Lewis K.; Ross M.; Guthrie T.; Linette G.P.; Daniels G.A.; Harrington K.; Middleton M.R.; Miller W.H. Jr; Zager J.S.; Ye Y.; Yao B[1], Li A.; Doleman S.; VanderWalde A.; Gansert J.; Coffin R.S. Talimogene Laherparepvec Improves Durable Response Rate in Patients with Advanced Melanoma. *J. Clin. Oncol.* **2015**, *1* (33), 2780.

(20) Lipson, E. J. Antagonists of PD-1 and PD-L1 in Cancer Treatment. **2016**, *179* (110), 95.

(21) Alsaab, H. O.; Sau, S.; Alzhrani, R.; Tatiparti, K.; Bhise, K.; Kashaw, S. K.; Iyer, A. K. PD-1 and PD-L1 Checkpoint Signaling Inhibition for Cancer Immunotherapy: Mechanism, Combinations, and Clinical Outcome. *Front. Pharmacol.* **2017**, *23* (8), 561.

(22) Shukuya, T.; Carbone, D. P. Predictive Markers for the Efficacy of Anti-PD-1/PD-L1 Antibodies in Lung Cancer. *J. Thorac. Oncol.* **2016**, *11* (7), 976.

(23) Sun, C.; Mezzadra, R.; Schumacher, T. N. Regulation and Function of the PD-L1 Checkpoint. *Immunity* **2018**, *48* (3), 434.

(24) Sun, Z.; Fourcade, J.; Pagliano, O.; Chauvin, J. M.; Sander, C.; Kirkwood, J. M.; Zarour, H. M. IL10 and PD-1 Cooperate to Limit the Activity of Tumor-Specific CD8+ T Cells. *Cancer Res.* **2015**, *15* (75), 1635.

(25) Singh, P. P.; Sharma, P. K.; Krishnan, G.; Lockhart, A. C. Immune Checkpoints and Immunotherapy for Colorectal Cancer. *Gastroenterol. Rep.* **2015**, *3* (4), 289.

(26) Mahoney, K. M.; Rennert, P. D.; Freeman, G. J. Combination Cancer Immunotherapy and New Immunomodulatory Targets. *Nat. Rev. Drug Discov.* **2015**, *14* (8), 561.

(27) Gong, J.; Chehrazi-Raffle, A.; Reddi, S.; Salgia, R. Development of PD-1 and PD-L1 Inhibitors as a Form of Cancer Immunotherapy: A Comprehensive Review of Registration Trials and Future Considerations. *J. Immunother. Cancer* **2018**, *6* (1), 1.

(28) Chen, D. S.; Mellman, I. Elements of Cancer Immunity and the Cancer-Immune Set Point. *Nature* **2017**, *541* (7637), 321.

(29) Maleki Vareki, S.; Garrigós, C.; Duran, I. Biomarkers of Response to PD-1/PD-L1 Inhibition. *Crit. Rev. Oncol. Hematol.* **2017**, *116*, 116.

(30) Sharpe, A. H.; Pauken, K. E. The Diverse Functions of the PD1 Inhibitory Pathway. *Nat. Rev. Immunol.* **2018**, *18* (3), 153.

(31) Coulie, P. G.; Van Den Eynde, B. J.; Van Der Bruggen, P.; Boon, T. Tumour Antigens Recognized by T Lymphocytes: At the Core of Cancer Immunotherapy. *Nat. Rev. Cancer* **2014**, *14* (2), 135.

(32) Hu, Z.; Ott, P. A.; Wu, C. J. Towards Personalized, Tumour-Specific, Therapeutic Vaccines for Cancer. *Nat. Rev. Immunol.* **2018**, *18* (3), 168.

(33) Boon, T.; Coulie, P. G.; Eynde, B. J. Van den; Bruggen, P. van der. Human T Cell Responses against Melanoma. *Annu. Rev. Immunol.* **2006**, *24*, 175.

(34) Trombetta, E. S.; Mellman, I. Cell Biology of Antigen Processing in Vitro and in Vivo. *Annu. Rev. Immunol.* **2005**, *23*, 975.

(35) Takenaka M. C.; Quintana F. C. Tolerogenic Dendritic Cells. *Semin. Immunopathol.* **2017**, *39*, 113.

(36) Dranoff, G. Cytokines in Cancer Pathogenesis and Cancer Therapy. *Nat. Rev. Cancer* **2004**, *4* (1), 11.

(37) Kreiter, S.; Vormehr, M.; Van De Roemer, N.; Diken, M.; Löwer, M.; Diekmann, J.; Boegel, S.; Schrörs, B.; Vascotto, F.; Castle, J. C.; Tadmor A.D.; Schoenberger S.P.; Huber C.; Türeci Ö.; Sahin U. Mutant MHC Class II Epitopes Drive Therapeutic Immune Responses to Cancer. *Nature* **2015**, *520* (7549), 692.

(38) Palucka, K.; Banchereau, J.; Mellman, I. Designing Vaccines Based on Biology of Human Dendritic Cell Subsets. *Immunity* **2010**, *29* (33), 464.

(39) Hamanishi, J.; Mandai, M.; Iwasaki, M.; Okazaki, T.; Tanaka, Y.; Yamaguchi, K.; Higuchi, T.; Yagi, H.; Takakura, K.; Minato, N.; Honjo T.; Fujii S. Programmed Cell Death 1 Ligand 1 and Tumor-Infiltrating CD8+ T Lymphocytes Are Prognostic Factors of Human Ovarian Cancer. *Proc. Natl. Acad. Sci. U. S. A.* **2007**, *27* (104), 3360.

(40) Melero, I.; Gaudernack, G.; Gerritsen, W.; Huber, C.; Parmiani, G.; Scholl, S.; Thatcher, N.; Wagstaff, J.; Zielinski, C.; Faulkner, I.; Mellstedt H. Therapeutic Vaccines for Cancer: An Overview of Clinical Trials. *Nat. Rev. Clin. Oncol.* **2014**, *11* (9), 509.

(41) Alatrash, G.; Molldrem, J. J. Tumor-Associated Antigens. In *Immune Biology of Allogeneic Hematopoietic Stem Cell Transplantation*; 2013.

(42) Melief, C. J. M.; Hall, T. Van; Arens, R.; Ossendorp, F.; Burg, S. H. Van Der. Therapeutic Cancer Vaccines. *J. Clin. Invest.* **2015**, *125* (9), 3401.

(43) Evans, R. A.; Diamond, M. S.; Rech, A. J.; Chao, T.; Richardson, M. W.; Lin, J. H.; Bajor, D. L.; Byrne, K. T.; Stanger, B. Z.; Riley, J. L.; Markosyan N.; Winograd R.; Vonderheide R.H. Lack of Immunoediting in Murine Pancreatic Cancer Reversed with Neoantigen. *JCI Insight* **2016**, *8* (1), 1.

(44) Bocanegra Gondan, A. I.; Ruiz-de-Angulo, A.; Zabaleta, A.; Gómez Blanco, N.; Cobaleda-Siles, B. M.; García-Granda, M. J.; Padro, D.; Llop, J.; Arnaiz, B.; Gato, M.; Escors D.; Mareque-Rivas J.C. Effective Cancer Immunotherapy in Mice by PolyIC-Imiquimod Complexes and Engineered Magnetic Nanoparticles. *Biomaterials* **2018**, *170*, 95.

(45) Ruiz-De-Angulo, A.; Zabaleta, A.; Gómez-Vallejo, V.; Llop, J.; Mareque-Rivas,

J. C. Microdosed Lipid-Coated (67)Ga-Magnetite Enhances Antigen-Specific Immunity by Image Tracked Delivery of Antigen and CpG to Lymph Nodes. *ACS Nano* **2016**, *26* (10), 1602.

(46) Hutzler, S.; Erbar, S.; Jabulowsky, R. A.; Hanauer, J. R. H.; Schnotz, J. H.; Beissert, T.; Bodmer, B. S.; Eberle, R.; Boller, K.; Klamp, T.; Sahin U.; Mühlebach M.D. Antigen-Specific Oncolytic MV-Based Tumor Vaccines through Presentation of Selected Tumor-Associated Antigens on Infected Cells or Virus-like Particles. *Sci. Rep.* **2017**, *4* (7), 16892.

(47) Basto, A. P.; Badenes, M.; Almeida, S. C. P.; Martins, C.; Duarte, A.; Santos, D. M.; Leitão, A. Immune Response Profile Elicited by the Model Antigen Ovalbumin Expressed in Fusion with the Bacterial OprI Lipoprotein. *Mol. Immunol.* **2015**, *64*, 36.

(48) Lee, S.; Nguyen, M. T. Recent Advances of Vaccine Adjuvants for Infectious Diseases. *Immune Netw.* **2015**, *15* (2), 51.

(49) Mellman, I.; Coukos, G.; Dranoff, G. Cancer Immunotherapy Comes of Age. *Nature* **2011**, *480* (7378), 480.

(50) Cox, J. C.; Coulter, A. R. Adjuvants - A Classification and Review of Their Modes of Action. *Vaccine* **1997**, *15* (3), 248.

(51) Marrack P, McKee AS, M. M. Towards an Understanding of the Mechanism of Action of Praziquantel. *Mol. Biochem. Parasitol.* **2009**, *164* (1), 57.

(52) Grun, J. L.; Maurer, P. H. Different T Helper Cell Subsets Elicited in Mice Utilizing Two Different Adjuvant Vehicles: The Role of Endogenous Interleukin 1 in Proliferative Responses. *Cell. Immunol.* **1989**, *121*, 134.

(53) Coffman, R. L.; Sher, A.; Seder, R. A. Vaccine Adjuvants: Putting Innate Immunity to Work. *Immunity* **2010**, *33* (4), 492.

(54) Ott, P. A.; Hodi, F. S.; Kaufman, H. L.; Wigginton, J. M.; Wolchok, J. D. Combination Immunotherapy: A Road Map. *J. Immunother. Cancer* **2017**, *5* (1), 1.

(55) Pasquale, A.; Preiss, S.; Silva, F.; Garçon, N. Vaccine Adjuvants: From 1920 to 2015 and Beyond. *Vaccines* **2015**, *3* (2), 320.

(56) Gregory, A. E.; Titball, R.; Williamson, D. Vaccine Delivery Using Nanoparticles. *Front. Cell. Infect. Microbiol.* **2013**, *25* (3), 13.

(57) Mody, K. T.; Popat, A.; Mahony, D.; Cavallaro, A. S.; Yu, C.; Mitter, N. Mesoporous Silica Nanoparticles as Antigen Carriers and Adjuvants for Vaccine Delivery. *Nanoscale* **2013**, *21* (5), 5167.

(58) Verma, P.; Biswas, S.; Mohan, T.; Ali, S.; Rao, D. N. Novel Adjuvants and Delivery Vehicles for Vaccines Development: A Road Ahead. *Indian J Med Res.* **2013**, *138* (5), 779.

(59) Saroja C. H.; Lakshmi P. K.; Bhaskaran S. Recent Trends in Vaccine Delivery Systems: A Review. *Int. J. Pharm. Investig.* **2011**, *1* (2), 64.

(60) Salem, A. K. Nanoparticles in Vaccine Delivery. *AAPS J.* **2015**, *17* (2), 289.

(61) Florindo, H. F.; Pandit, S.; Gonçalves, L. M. D.; Alpar, H. O.; Almeida, A. J. Surface Modified Polymeric Nanoparticles for Immunisation against Equine Strangles. *Int. J. Pharm.* **2010**, *390* (1), 25.

(62) Whiteside, T. L.; Demaria, S.; Rodriguez-Ruiz, M. E.; Zarour, H. M.; Melero, I. Emerging Opportunities and Challenges in Cancer Immunotherapy. *Clin. Cancer Res.* **2016**, *22* (8), 1845.

(63) Sharma, P.; Wagner, K.; Wolchok, J. D.; Allison, J. P. Recent Successes and Next Steps. *Nat. Publ. Gr.* **2011**, *11* (11), 805.

(64) Chen, D. S.; Mellman, I. Oncology Meets Immunology: The Cancer-Immunity Cycle. *Immunity* **2013**, *39* (1), 1.

(65) Schwartzenruber, D.; Lawson, D.; Richards J. M.; Conry R. M.; Miller D. M.; J., T.; Gailani F.; Riley L.; Conlon K.; Pockaj B.; Kendra K.L.; White R.L.; Gonzalez R.; Kuzel T.M.; Curti B.; Leming P.D.; Whitman E.D.; Balkissoon J.; Reintgen D.S.; Kaufman H.; Marincola F.M.; Merino M.J.; Rosenberg S.A.; Choyke P.; Vena D.; Hwu P. Gp100 Peptide Vaccine and Interleukin-2 in Patients with Advanced Melanoma. **2012**, *364* (22), 2119–2127.

(66) Yaddanapudi, K.; Mitchell, R. A.; Eaton, J. W. Cancer Vaccines: Looking to the Future. *Oncoimmunology* **2013**, *2* (3), 1.

(67) van Elsas, A.; Hurwitz, a a; Allison, J. P. Combination Immunotherapy of B16 Melanoma Using Anti-Cytotoxic T Lymphocyte-Associated Antigen 4 (CTLA-4) and Granulocyte/Macrophage Colony-Stimulating Factor (GM-CSF)-Producing Vaccines Induces Rejection of Subcutaneous and Metastatic Tumors Accompanied . *J. Exp. Med.* **1999**, *190* (3), 355.

(68) A.J. Korman; Peggs, K. S.; Allison J. P. Checkpoint Blockade in Cancer Immunotherapy. *Adv Immunol.* **2006**, *90*, 297.

(69) O'Day, S. J.; Hamid, O.; Urba, W. J. Targeting Cytotoxic T-Lymphocyte Antigen-4 (CTLA-4): A Novel Strategy for the Treatment of Melanoma and Other Malignancies. *Cancer* **2007**, *110* (12), 2614.

(70) Postow, M. A.; Chesney, J.; Pavlick, A. C.; Robert, C.; Grossmann, K.; McDermott, D.; Linette, G. P.; Meyer, N.; Giguere, J. K.; Agarwala, S. S.; Montaser S.; Ernstoff M.S.; Minor D.; M.D., Salama K.A.; M.D., Taylor M.; Ott P.A.; Rollin L.M.; Horak C.; Gagnier P.; Wolchok J.D.; Hodi F.S. Nivolumab and Ipilimumab versus Ipilimumab in Untreated Melanoma. *N. Engl. J. Med.* **2015**, *372* (21), 2006.

(71) Tran, E.; Turcotte, S.; Gros, A.; Robbins, P. F.; Lu, Y.-C.; Dudley, M. E.; Wunderlich, J. R.; Somerville, R. P.; Hogan, K.; Hinrichs, C. S.; Parkhurst M.R.; Yang J.C.; Rosenberg S.A. Cancer Immunotherapy Based on Mutation-Specific CD4+ T Cells in a Patient with Epithelial Cancer. *Science* **2014**, *344* (6184), 641.

(72) Gubin, M. M.; Zhang, X.; Schuster, H.; Caron, E.; Ward, J. P.; Noguchi, T.; Ivanova, Y.; Hundal, J.; Arthur, C. D.; Krebber, W. J.; Mulder G.E.; Toebes M.; Vesely M.D.; Lam S.S.; Korman A.J.; Allison J.P.; Freeman G.J.; Sharpe A.H.; Pearce E.L.; Schumacher T.N.; Aebersold R.; Rammensee H.G.; Melief C.J.; Mardis E.R.; Gillanders W.E.; Artyomov M.N.; Schreiber R.D. Checkpoint Blockade Cancer Immunotherapy Targets Tumour-Specific Mutant Antigens. *Nature* **2014**, *515* (7528), 577.

(73) Yadav, M.; Jhunjhunwala, S.; Phung, Q. T.; Lupardus, P.; Tanguay, J.; Bumbaca, S.; Franci, C.; Cheung, T. K.; Fritsche, J.; Weinschenk, T.; Modrusan Z.; Mellman I.; Lill J.R.; Delamarre L. Predicting Immunogenic

Tumour Mutations by Combining Mass Spectrometry and Exome Sequencing. *Nature* **2014**, *515* (7528), 572.

(74) Rakoff-Nahoum, S.; Medzhitov, R. Toll-like Receptors and Cancer. *Nat. Rev. Cancer* **2009**, *9* (1), 57.

(75) Kaczanowska, S.; Joseph, A. M.; Davila, E. TLR Agonists: Our Best Frenemy in Cancer Immunotherapy. *J. Leukoc. Biol.* **2013**, *93* (6), 847.

(76) Shi, M.; Chen, X.; Ye, K.; Yao, Y.; Li, Y. Application Potential of Toll-like Receptors in Cancer Immunotherapy: Systematic Review. *Medicine (Baltimore).* **2016**, *95* (25), 3951.

(77) Du, B.; Jiang, Q.-L.; Cleveland, J.; Liu, B.-R.; Zhang, D. Targeting Toll-like Receptors against Cancer. *J. Cancer Metastasis Treat.* **2016**, *2* (12), 463.

(78) Huggins, C.; Pearce, S.; Peri, F.; Neumann, F.; Cockerill, G.; Pirianov, G. A Novel Small Molecule TLR4 Antagonist (IAXO-102) Negatively Regulates Non-Hematopoietic Toll like Receptor 4 Signalling and Inhibits Aortic Aneurysms Development. *Atherosclerosis* **2015**, *242* (2), 563.

(79) Adams, S. Toll-like Receptor Agonists in Cancer Therapy. **2009**, *1* (6), 949.

(80) Schnare, M.; Barton, G. M.; Holt, A. C.; Takeda, K.; Akira, S.; Medzhitov, R. Toll-like Receptors Control Activation of Adaptive Immune Responses. *Nat. Immunol.* **2001**, *2* (10), 947.

(81) Iwasaki, A.; Medzhitov, R. Toll-like Receptor Control of the Adaptive Immune Responses. *Nat. Immunol.* **2004**, *5* (10), 987.

(82) Sallusto, F.; Schaerli, P.; Loetscher, P.; Schaniel, C.; Lenig, D.; Mackay, C. R.; Qin, S.; Lanzavecchia, A. Rapid and Coordinated Switch in Chemokine Receptor Expression during Dendritic Cell Maturation. *Eur. J. Immunol.* **1998**, *28* (9), 2760.

(83) Gunn, M. D.; Kyuwa, S.; Tam, C.; Kakiuchi, T.; Matsuzawa, A.; Williams, L. T.; Nakano, H. Mice Lacking Expression of Secondary Lymphoid Organ Chemokine Have Defects in Lymphocyte Homing and Dendritic Cell Localization. *J. Exp. Med.* **1999**, *1* (189), 451.

(84) Förster, R.; Schubel, A.; Breitfeld, D.; Kremmer, E.; Renner-Müller, I.; Wolf, E.; Lipp, M. CCR7 Coordinates the Primary Immune Response by Establishing Functional Microenvironments in Secondary Lymphoid Organs. *Cell* **1999**, *1* (99), 23.

(85) Medzhitov, R.; Preston-Hurlburt, P.; Janeway, C. A. A Human Homologue of the Drosophila Toll Protein Signals Activation of Adaptive Immunity. *Nature* **1997**, *24* (388), 394.

(86) Pasare, C.; Medzhitov, R. Toll Pathway-Dependent Blockade of CD4+CD25+ T Cell-Mediated Suppression by Dendritic Cells. *Science.* **2003**, *299* (5609), 1033.

(87) Krieg, A. M. Development of TLR9 Agonists for Cancer Therapy. *J. Clin. Invest.* **2007**, *117* (5), 1184.

(88) Dowling, J. K.; Mansell, A. Toll-like Receptors: The Swiss Army Knife of Immunity and Vaccine Development. *Clin. Transl. Immunol.* **2016**, *5* (5), 85.

(89) Coley, W. B. The Treatment of Malignant Tumors by Repeated Inoculations of Erysipelas. With a Report of Ten Original Cases. 1893. *Clin orthop relat res* **1991**, *262*, 3.

(90) Beutler, B.; Greenwald, D.; Hulmes, J. D.; Chang, M.; Pan, Y. C. E.; Mathison, J.; Ulevitch, R.; Cerami, A. Identity of Tumour Necrosis Factor and the Macrophage-Secreted Factor Cachectin. *Nature* **1985**, *316*, 552.

(91) Park, B. S.; Song, D. H.; Kim, H. M.; Choi, B. S.; Lee, H.; Lee, J. O. The Structural Basis of Lipopolysaccharide Recognition by the TLR4-MD-2 Complex. *Nature* **2009**, *458* (7242), 1191.

(92) Yadav, R.; Zammit, D. J.; Lefrancois, L.; Vella, A. T. Effects of LPS-Mediated Bystander Activation in the Innate Immune System. *J. Leukoc. Biol.* **2006**, *80* (6), 1251.

(93) S N Vogel; Hilfiker, M. L.; Caulfield, M. J. Endotoxin-Induced T Lymphocyte Proliferation. *J Immunol* **1983**, *130* (4), 1774.

(94) Komia-Koma, M.; Gildchrist, D. S.; Xu, D. Direct Recognition of LPS by Human but Not Murine CD8+ T Cells via TLR4 Complex. *Eur. J. Immunol.* **2009**, *39*

(6), 1564.

(95)   Bauer, A. K.; Dixon, D.; DeGraff, L. M.; Cho, H. Y.; Walker, C. R.; Malkinson, A. M.; Kleeberger, S. R. Toll-like Receptor 4 in Butylated Hydroxytoluene-Induced Mouse Pulmonary Inflammation and Tumorigenesis. *J. Natl. Cancer Inst.* **2005**, *97* (23), 1778.

(96)   Apetoh, L.; Ghiringhelli, F.; Tesniere, A.; Obeid, M.; Ortiz, C.; Criollo, A.; Mignot, G.; Maiuri, M. C.; Ullrich, E.; Saulnier, P.; Yang H.; Amigorena S.; Ryffel B.; Barrat F.J.; Saftig P.; Levi F.; Lidereau R.; Nogues C.; Mira J.P.; Chompret   A.; Joulin   V.; Clavel-Chapelon   F.; Bourhis   J.; André F.; Delaloge S.; Tursz T.; Kroemer G.; Zitvogel L. Toll-like Receptor 4-Dependent Contribution of the Immune System to Anticancer Chemotherapy and Radiotherapy. *Nat. Med.* **2007**, *13* (9), 1050.

(97)   Yusuf, N.; Nasti, T. H.; Long, J. A.; Naseemuddin, M.; Lucas, A. P.; Xu, H.; Elmets, C. A. Protective Role of TLR4 during the Initiation Stage of Cutaneous Chemical Carcinogenesis. *Cancer Res.* **2008**, *68* (2), 615.

(98)   Chih-Cheng Hsiao, M.; Ying-Hsien Kao, P.; Shun-Chen Huang, M.; Jiin-Haur Chuang, M. Toll-Like Receptor-4 Agonist Inhibits Motility and Invasion of Hepatoblastoma HepG2 Cells In Vitro. *Pediatr. Blood Cancer* **2009**, *53* (2008), 13.

(99)   Vacchelli, E.; Galluzzi, L.; Eggermont, A.; Fridman, W. H.; Galon, J.; Sautès-Fridman, C.; Tartour, E.; Zitvogel, L.; Kroemer, G. Trial Watch: FDA-Approved Toll-like Receptor Agonists for Cancer Therapy. *Oncoimmunology* **2012**, *1* (6), 894.

(100) McKee, A. S.; Munks, M. W.; Marrack, P. How Do Adjuvants Work? Important Considerations for New Generation Adjuvants. *Immunity* **2007**, *27* (5), 687.

(101) Mancek-Keber, M.; Jerala, R. Postulates for Validating TLR4 Agonists. *Eur. J. Immunol.* **2015**, *45* (2), 356.

(102) Mata-Haro, V.; Cekic, C.; Martin, M.; Chilton, P. M.; Casella, C. R.; Mitchell, T. C. The Vaccine Adjuvant Monophosphoryl Lipid A as a TRIF-Biased Agonist of TLR4. *Science.* **2007**, *316* (5831), 1628.

(103) Baldridge, J. R.; McGowan, P.; Evans, J. T.; Cluff, C.; Mossman, S.; Johnson, D.; Persing, D. Taking a Toll on Human Disease: Toll-like Receptor 4 Agonists as Vaccine Adjuvants and Monotherapeutic Agents. *Expert Opin. Biol. Ther.* **2004**, *4* (7), 1129–1138.

(104) www.ema.europa.eu.

(105) Zigler M.; Shir A.; Levitzki A. Targeted Cancer Immune Therapy. *Curr Opin Pharmacol* **2009**, *13* (4), 504.

(106) Pantel, A.; Cheong, C.; Dandamudi, D.; Shrestha, E.; Mehandru, S.; Brane, L.; Ruane, D.; Teixeira, A.; Bozzacco, L.; Steinman, R. M.; Longhi P.M. A New Synthetic TLR4 Agonist, GLA, Allows Dendritic Cells Targeted with Antigen to Elicit Th1 T-Cell Immunity in Vivo. *Eur. J. Immunol.* **2012**, *42* (1), 101.

(107) Piazza, M.; Calabrese, V.; Damore, G.; Cighetti, R.; Gioannini, T.; Weiss, J.; Peri, F. A Synthetic Lipid A Mimetic Modulates Human TLR4 Activity. *ChemMedChem* **2012**, *7* (2), 213.

(108) Cui, W.; Joshi, N. S.; Liu, Y.; Meng, H.; Kleinstein, S. H.; Kaech, S. M. TLR4 Ligands Lipopolysaccharide and Monophosphoryl Lipid A Differentially Regulate Effector and Memory CD8+ T Cell Differentiation. *J. Immunol.* **2014**, *192* (9), 4221.

(109) Reed, S. G.; Hsu, F. C.; Carter, D.; Orr, M. T. The Science of Vaccine Adjuvants: Advances in TLR4 Ligand Adjuvants. *Curr. Opin. Immunol.* **2016**, *41*, 85.

(110) Baxevanis, C. N.; Voutsas, I. F.; Tsitsilonis, O. E. Toll-like Receptor Agonists: Current Status and Future Perspective on Their Utility as Adjuvants in Improving Anticancer Vaccination Strategies. *Immunotherapy* **2013**, *5* (5), 497.

(111) Alexander, C.; Rietschel, E. T. Bacterial Lipopolysaccharides and Innate Immunity. *J. Endotoxin Res.* **2001**, *7* (3), 167.

(112) Caldorera-Moore, M. E.; Liechty, W. B.; Peppas, N. A. Responsive Theranostic Systems: Integration of Diagnostic Imaging Agents and Responsive Controlled Release Drug Delivery Carriers. *Acc. Chem. Res.* **2011**, *44* (10), 1061.

(113) Mancini, R. J.; Stutts, L.; Ryu, K. A.; Tom, J. K.; Esser-Kahn, A. P. Directing

the Immune System with Chemical Compounds. *ACS Chem. Biol.* **2014**, *9* (5), 1075.

(114) Brito, L. A.; O'Hagan, D. T. Designing and Building the next Generation of Improved Vaccine Adjuvants. *J. Control. Release* **2014**, *190*, 563.

(115) Pfeiffer, R. Untersuchungen Uber Das Choleragift. *Zeitschrift fur Hyg. und Infekt.* **1892**, *11* (1), 393.

(116) Westphal, O. and Jann, K. Bacterial Lipopolysaccharide-Extraction with Phenol Water and Further Application of Procedure. *Methods Carbohydr. Chem.* **1965**, No. 5, 83.

(117) Holst, O. *Bacterial Lipopolysaccharides*; 2011.

(118) Molinaro, A.; Holst, O.; Lorenzo, F. Di; Callaghan, M.; Nurisso, A.; D'Errico, G.; Zamyatina, A.; Peri, F.; Berisio, R.; Jerala, R.; Jiménez-Barbero J.; Silipo A.; Martín-Santamaría S. Chemistry of Lipid a: At the Heart of Innate Immunity. *Chem. - A Eur. J.* **2015**, *21* (2), 500.

(119) Holst, O.; Ulmer, A. J.; Brade, H.; Flad, H.; Rietschel, E. T. Biochemistry and Cell Biology of Bacterial Endotoxins. **1996**, *16* (2), 83.

(120) Liideritz O, Westphal O, Staub AM, N. H. Isolation and Chemical and Immunological Characterization of Bacterial Lipopolysaccharides. In *Bacterial Endotoxins*; 1971; p 145.

(121) Rietschel, E. T.; Brade, H.; Holst, O.; Brade, L.; Müller-Loennies, S.; Mamat, U.; Zähringer, U.; Beckmann, F.; Seydel, U.; Brandenburg, K.; Ulmer A.J.; Mattern T.; Heine H.; Schletter J.; Loppnow H.; Schönbeck U.; Flad H.D.; Hauschildt S.; Schade U.F.; Di Padova F.; Kusumoto S.; Schumann R.R. Bacterial Endotoxin: Chemical Constitution, Biological Recognition, Host Response, and Immunological Detoxification. *Curr. Top. Microbiol. Immunol.* **1996**, *216*, 39.

(122) Wilkinson, S. G. Bacterial Lipopolysaccharides - Themes and Variations. *Prog. Lipid Res.* **1996**, *35* (3), 283.

(123) Alexander, C.; Zahringer, U. Chemical Structure of Lipid A- The Primary Immunomodulatory Center of Bacterial Lipopolysaccharides. *Trends Glycosci.*

Glycotechnol. **2002**, *14* (76), 69.

(124) Rietschel, E. T.; Kirikae, T.; Schade, F. U.; Ulmer, A. J.; Holst, O.; Brade, H.; Schmidt, G.; Mamat, U.; Grimmecke, H. D.; Kusumoto, S.; Zähringer U. The Chemical Structure of Bacterial Endotoxin in Relation to Bioactivity. *Immunobiology* **1993**, *187* (3), 169.

(125) Zaffaroni, L.; Peri, F. Recent Advances on Toll-like Receptor 4 Modulation : New Therapeutic Perspectives. *Futur. Med Chem* **2018**, *10* (4), 461.

(126) Pupo, E.; Lindner, B.; Brade, H.; Schromm, A. B. Intact Rough- and Smooth-Form Lipopolysaccharides from Escherichia Coli Separated by Preparative Gel Electrophoresis Exhibit Differential Biologic Activity in Human Macrophages. *FEBS J.* **2013**, *280* (4), 1095.

(127) Stöver, A. G.; Da Silva Correia, J.; Evans, J. T.; Cluff, C. W.; Elliott, M. W.; Jeffery, E. W.; Johnson, D. A.; Lacy, M. J.; Baldridge, J. R.; Probst, P.; Ulevitch R.J.; Persing D.H.; Hershberg R.M.; Structure-Activity Relationship of Synthetic Toll-like Receptor 4 Agonists. *J. Biol. Chem.* **2004**, *279* (6), 4440.

(128) Gregg, K. A.; Harberts, E.; Gardner, F. M.; Pelletier, M. R.; Cayatte, C.; Yu, L.; McCarthy, M. P.; Marshall, J. D.; Ernst, R. K. Rationally Designed TLR4 Ligands for Vaccine Adjuvant Discovery. *MBio* **2017**, *8* (3), 1.

(129) Choi, J.; Cox, A. D.; Li, J.; McCready, W.; Ulanova, M. Activation of Innate Immune Responses by Haemophilus Influenzae Lipooligosaccharide. *Clin. Vaccine Immunol.* **2014**, *21* (5), 769.

(130) Fujimoto, Y.; Shimoyama, A.; Suda, Y.; Fukase, K. Synthesis and Immunomodulatory Activities of Helicobacter Pylori Lipophilic Terminus of Lipopolysaccharide Including Lipid A. *Carbohydr. Res.* **2012**, *356*, 37.

(131) Preston, A.; Mandrell, R. E.; Gibson, B. W.; Apicella, M. A. The Lipooligosaccharides of Pathogenic Gram-Negative Bacteria. *Crit. Rev. Microbiol.* **1996**, *22* (3), 139.

(132) Griffiss, J. M.; Schneider, H.; Mandrell, R. E.; Yamasaki, R.; Jarvis, G. a; Kim, J. J.; Gibson, B. W.; Hamadeh, R.; Apicella, M. A. Lipooligosaccharides: The Principal Glycolipids of the Neisserial Outer Membrane. *Rev. Infect. Dis.* **2014**,

10 (2), S287.

(133) Huber, M.; Kalis, C.; Keck, S.; Jiang, Z.; Georgel, P.; Du, X.; Shamel, L.; Sovath, S.; Mudd, S.; Beutler, B.; Galanos C.; Freudenberg M.A.; R-Form LPS, the Master Key to the Activation of TLR4/MD-2-Positive Cells. *Eur. J. Immunol.* **2006**, *36* (3), 701.

(134) Landmann, R.; Zimmerli, W.; Sansano, S.; Link, S.; Hahn, A.; Glauser, M. P.; Calandra, T. Increased Circulating Soluble Cd14 Is Associated with High Mortality in Gram-Negative Septic Shock. *J. Infect. Dis.* **1995**, *171* (3), 639.

(135) Ko, A.; Wui, S. R.; Ryu, J. I.; Do, H. T. T.; Lee, Y. J.; Lim, S. J.; Rhee, I.; Jung, D. I.; Park, J. A; Choi, J. A; Song M.K.; Lee N.G.; Comparison of the Adjuvanticity of Two Adjuvant Formulations Containing De-O-Acylated Lipooligosaccharide on Japanese Encephalitis Vaccine in Mice. *Arch. Pharm. Res.* **2017**, *41* (2), 1.

(136) Ryu, J. I.; Park, S. A.; Wui, S. R.; Ko, A.; Han, J. E.; Choi, J. A.; Song, M. K.; Kim, K. S.; Cho, Y. J.; Lee, N. G. A De-O-Acylated Lipooligosaccharide-Based Adjuvant System Promotes Antibody and Th1-Type Immune Responses to H1N1 Pandemic Influenza Vaccine in Mice. *Biomed Res. Int.* **2016**, *2016*, 3713656.

(137) Han, J. E.; Wui, S. R.; Kim, K. S.; Cho, Y. J.; Cho, W. J.; Lee, N. G. Characterization of the Structure and Immunostimulatory Activity of a Vaccine Adjuvant, de-O-Acylated Lipooligosaccharide. *PLoS One* **2014**, *9* (1), e85838.

(138) Stanislavsky, E. S.; Makarenko, T. A.; Kholodkova, E. V.; Lugowski, C. R-Form Lipopolysaccharides (LPS) of Gram-Negative Bacteria as Possible Vaccine Antigens. *FEMS Immunol. Med. Microbiol.* **1997**, *18* (3), 139.

(139) Hirano, T.; Hou, Y.; Jiao, X.; Gu, X. X. Intranasal Immunization with a Lipooligosaccharide-Based Conjugate Vaccine from Nontypeable Haemophilus Influenzae Enhances Bacterial Clearance in Mouse Nasopharynx. *FEMS Immunol. Med. Microbiol.* **2003**, *35* (1), 1.

(140) Raetz, C. R. H.; Garrett, T. A.; Reynolds, C. M.; Shaw, W. A.; Moore, J. D.; Smith, D. C.; Ribeiro, A. A.; Murphy, R. C.; Ulevitch, R. J.; Fearns, C.; Reichart

D.; Glass C.K.; Benner C.; Subramaniam S.; Harkewicz R.; Bowers-Gentry R.C.; Buczynski M.W.; Cooper J.A.; Deems R.A.; Dennis E.A.; Kdo2-Lipid A of Escherichia Coli , a Defined Endotoxin That Activates Macrophages via TLR-4. *J. Lipid Res.* **2006**, *47* (5), 1097.

(141) Wang, X.; Quinn, P. J.; Yan, A. Kdo2-Lipid A: Structural Diversity and Impact on Immunopharmacology. *Biol. Rev.* **2015**, *90* (2), 408.

(142) Silipo, A.; Molinaro, A.; Sturiale, L.; Dow, J. M.; Erbs, G.; Lanzetta, R.; Newman, M. A.; Parrilli, M. The Elicitation of Plant Innate Immunity by Lipooligosaccharide of Xanthomonas Campestris. *J. Biol. Chem.* **2005**, *280* (39), 33660.

(143) Gao, W.; Xiong, Y.; Li, Q.; Yang, H. Inhibition of Toll-like Receptor Signaling as a Promising Therapy for Inflammatory Diseases: A Journey from Molecular to Nano Therapeutics. *Front. Physiol.* **2017**, *8*, 508.

(144) Perrin-Cocon, L.; Aublin-Gex, A.; Sestito, S. E.; Shirey, K. A.; Patel, M. C.; André, P.; Blanco, J. C.; Vogel, S. N.; Peri, F.; Lotteau, V. TLR4 Antagonist FP7 Inhibits LPS-Induced Cytokine Production and Glycolytic Reprogramming in Dendritic Cells, and Protects Mice from Lethal Influenza Infection. *Sci. Rep.* **2017**, *7*, 1.

(145) Kuzmich, N.; Sivak, K.; Chubarev, V.; Porozov, Y.; Savateeva-Lyubimova, T.; Peri, F. TLR4 Signaling Pathway Modulators as Potential Therapeutics in Inflammation and Sepsis. *Vaccines* **2017**, *5* (4), 34.

(146) Molteni, M.; Gemma, S.; Rossetti, C. The Role of Toll-Like Receptor 4 in Infectious and Noninfectious Inflammation. *Mediators Inflamm.* **2016**, *2016*, 6978936.

(147) Heneka, M. T.; Carson, M. J.; Khoury, J. El; Landreth, G. E.; Brosseron, F.; Feinstein, D. L.; Jacobs, A. H.; Wyss-Coray, T.; Vitorica, J.; Ransohoff, R. M.; Herrup K.; Frautschy S.A.; Finsen B.; Brown G.C.; Verkhratsky A.; Yamanaka K.; Koistinaho J.; Latz E.; Halle A.; Petzold G.C.; Town T.; Morgan D.; Shinohara M.L.; Perry V.H.; Holmes C.; Bazan N.G.; Brooks D.J.; Hunot S.; Joseph B.; Deigendesch N.; Garaschuk O.; Boddeke E.; Dinarello C.A.; Breitner J.C.; Cole G.M.; Golenbock D.T.; Kummer M.P.

Neuroinflammation in Alzheimer's Disease. *Lancet Neurol.* **2015**, *14* (4), 388.

(148) Van Der Poll, T.; Van De Veerdonk, F. L.; Scicluna, B. P.; Netea, M. G. The Immunopathology of Sepsis and Potential Therapeutic Targets. *Nat. Rev. Immunol.* **2017**, *17* (7), 407.

(149) Peri, F.; Calabrese, V. Toll-like Receptor 4 (TLR4) Modulation by Synthetic and Natural Compounds: An Update. **2015**, *57* (9), 3612.

(150) Leon, C. G.; Tory, R.; Jia, J.; Sivak, O.; Wasan, K. M. Discovery and Development of Toll-like Receptor 4 (TLR4) Antagonists: A New Paradigm for Treating Sepsis and Other Diseases. *Pharm. Res.* **2008**, *25* (8), 1751.

(151) Ishii, K. J.; Uematsu, S.; Akira, S. "Toll" Gates for Future Immunotherapy. *Curr. Pharm. Des.* **2006**, *12* (32), 4135.

(152) Opal, S. M.; Laterre, P. F.; Francois, B.; LaRosa, S. P.; Angus, D. C.; Mira, J. P.; Wittebole, X.; Dugernier, T.; Perrotin, D.; Tidswell, M.; Jauregui L.; Krell K.; Pachl J.; Takahashi T.; Peckelsen C.; Cordasco E.; Chang C.S.; Oeyen S.; Aikawa N.; Maruyama T.; Schein R.; Kalil A.C.; Van Nuffelen M.; Lynn M.; Rossignol D.P.; Gogate J.; Roberts M.B.; Wheeler J.L.; Vincent J.L. ACCESS Study Group. Effect of Eritoran, an Antagonist of MD2-TLR4, on Mortality in Patients with Severe Sepsis: The ACCESS Randomized Trial. *JAMA* **2013**, *309* (11), 1154.

(153) Czeslick, E.; Struppert, A.; Simm, A.; Sablotzki, A. E5564 (Eritoran) Inhibits Lipopolysaccharide-Induced Cytokine Production in Human Blood Monocytes. *Inflamm. Res.* **2006**, *55* (11), 511.

(154) Rossignol, D. P.; Wong, N.; Noveck, R.; Lynn, M. Continuous Pharmacodynamic Activity of Eritoran Tetrasodium, a TLR4 Antagonist, during Intermittent Intravenous Infusion into Normal Volunteers. *Innate Immun.* **2008**, *14* (6), 383.

(155) Rice, T. W.; Wheeler, A. P.; Bernard, G. R.; Vincent, J.-L.; Angus, D. C.; Aikawa, N.; Demeyer, I.; Sainati, S.; Amlot, N.; Cao, C.; Li M.; Matsuda H.; Mouri K.; Cohen J. A Randomized, Double-Blind, Placebo-Controlled Trial of TAK-242 for the Treatment of Severe Sepsis. *Crit. Care Med.* **2010**, *38* (8),

1685.

(156) Onto, U.; Fukase, K.; Miyake, K.; Satow, Y. Crystal Structures of Human MD-2 and Its Complex with Antiendotoxic Lipid IVa. *Science.* **2007**, *316* (5831), 1632.

(157) Walsh, C.; Gangloff, M.; Monie, T.; Smyth, T.; Wei, B.; McKinley, T. J.; Maskell, D.; Gay, N.; Bryant, C. Elucidation of the MD-2/TLR4 Interface Required for Signaling by Lipid IVa. *J. Immunol.* **2008**, *181* (2), 1245.

(158) Awasthi, S. Toll-like Receptor-4 Modulation for Cancer Immunotherapy. *Front. Immunol.* **2014**, *5*, 328.

(159) Rolan, P.; Gibbons, J. A.; He, L.; Chang, E.; Jones, D.; Gross, M. I.; Davidson, J. B.; Sanftner, L. M.; Johnson, K. W. Ibudilast in Healthy Volunteers: Safety, Tolerability and Pharmacokinetics with Single and Multiple Doses. *Br. J. Clin. Pharmacol.* **2008**, *66* (6), 792.

(160) Lysakova-Devine, T.; Keogh, B.; Harrington, B.; Nagpal, K.; Halle, A.; Golenbock, D. T.; Monie, T.; Bowie, A. G. Viral Inhibitory Peptide of TLR4, a Peptide Derived from Vaccinia Protein A46, Specifically Inhibits TLR4 by Directly Targeting MyD88 Adaptor-Like and TRIF-Related Adaptor Molecule. *J. Immunol.* **2010**, *185* (7), 4261.

(161) Teghanemt, A.; Zhang, D.; Levis, E. N.; Weiss, J. P.; Gioannini, T. L. Molecular Basis of Reduced Potency of Underacylated Endotoxins. *J. Immunol.* **2005**, *175* (7), 4669.

(162) Piazza, M.; Rossini, C.; Fiorentina, S. D.; Pozzi, C.; Comelli, F.; Bettoni, I.; Fusi, P.; Costa, B.; Peri, F. Glycolipids and Benzylammonium Lipids as Novel Antisepsis Agents: Synthesis and Biological Characterization. *J. Med. Chem.* **2009**, *52* (4), 1209.

(163) Feynman, R. P. There ' s Plenty of Room at the Bottom. *Eng. Sci.* **1960**, *23* (5), 22.

(164) Saeed, M.; Ren, W.; Wu, A. Therapeutic Applications of Iron Oxide Based Nanoparticles in Cancer: Basic Concepts and Recent Advances. *Biomater. Sci.* **2018**, *6* (4), 708.

(165) USFDA. Guidance for Industry Considering Whether an FDA-Regulated Product Involves the Application of Nanotechnology. *Biotechnol. Law Rep.* **2011**, *30* (5), 613.

(166) Martins, P.; Rosa, D.; Fernandes, A.; Baptista, P. V. Nanoparticle Drug Delivery Systems: Recent Patents and Applications in Nanomedicine. *Recent Patents Nanomed.* **2014**, *3* (2), 105.

(167) Petros, R. A.; Desimone, J. M. Strategies in the Design of Nanoparticles for Therapeutic Applications. *Nat. Rev. Drug Discov.* **2010**, *9* (8), 615.

(168) Sharma, A.; Goyal, A. K.; Rath, G. Recent Advances in Metal Nanoparticles in Cancer Therapy. *J. Drug Target.* **2018**, *26* (8), 617.

(169) Peer, D.; Karp, J. M.; Hong, S.; Farokhzad, O. C.; Margalit, R.; Langer, R. Nanocarriers as an Emerging Platform for Cancer Therapy. *Nat. Nanotechnol.* **2007**, *2* (12), 751.

(170) Bobo, D.; Robinson, K. J.; Islam, J.; Thurecht, K. J.; Corrie, S. R. *Nanoparticle-Based Medicines: A Review of FDA-Approved Materials and Clinical Trials to Date*; Pharmaceutical Research, 2016.

(171) Bhatia, S. Nanoparticles Types, Classification, Characterization, Fabrication Methods and Drug Delivery Applications. In *Natural Polymer Drug Delivery Systems*; 2016.

(172) Sonali; Viswanadh, M. K.; Singh, R. P.; Agrawal, P.; Mehata, A. K.; Pawde, D. M.; Narendra; Sonkar, R.; Muthu, M. S. Nanotheranostics: Emerging Strategies for Early Diagnosis and Therapy of Brain Cancer. *Nanotheranostics* **2018**, *2* (1), 70.

(173) Park, K.; Lee, S.; Kang, E.; Kim, K.; Choi, K.; Kwon, I. C. New Generation of Multifunctional Nanoparticles for Cancer Imaging and Therapy. *Adv. Funct. Mater.* **2009**, *19* (10), 1553.

(174) Janib, S. M.; Moses, A. S.; MacKay, J. A. Imaging and Drug Delivery Using Theranostic Nanoparticles. *Adv. Drug Deliv. Rev.* **2010**, *62* (11), 1052.

(175) Zhang, R. X.; Li, J.; Zhang, T.; Amini, M. A.; He, C.; Lu, B.; Ahmed, T.; Lip, H.; Rauth, A. M.; Wu, X. Y. Importance of Integrating Nanotechnology with

Pharmacology and Physiology for Innovative Drug Delivery and Therapy - An Illustration with Firsthand Examples. *Acta Pharmacol. Sin.* **2018**, *39* (5), 825.

(176) Bertrand, N.; Wu, J.; Xu, X.; Kamaly, N.; Farokhzad, O. C. Cancer Nanotechnology: The Impact of Passive and Active Targeting in the Era of Modern Cancer Biology. *Adv. Drug Deliv. Rev.* **2014**, *66*, 2.

(177) Steichen, S. D.; Caldorera-Moore, M.; Peppas, N. A. A Review of Current Nanoparticle and Targeting Moieties for the Delivery of Cancer Therapeutics. *Eur. J. Pharm. Sci.* **2013**, *48* (3), 416.

(178) Johnson, D. A. TLR4 Agonists as Vaccine Adjuvants : A Chemist ' s Perspective. **2013**, *12* (7), 711.

(179) Moghimi, S. M. Recent Developments in Polymeric Nanoparticle Engineering and Their Applications in Experimental and Clinical Oncology. *Anticancer. Agents Med. Chem.* **2006**, *6* (6), 553.

(180) Langer, R. Drug Delivery and Targeting. *Nature* **1998**, *392* (6679), 5.

(181) Luo, L.; Shu, R.; Wu, A. Nanomaterial-Based Cancer Immunotherapy. *J. Mater. Chem. B* **2017**, *5* (28), 5517.

(182) Byrne, J. D.; Betancourt, T.; Brannon-Peppas, L. Active Targeting Schemes for Nanoparticle Systems in Cancer Therapeutics. *Adv. Drug Deliv. Rev.* **2008**, *60* (15), 1615.

(183) Vlieghe, P.; Lisowski, V.; Martinez, J.; Khrestchatisky, M. Synthetic Therapeutic Peptides: Science and Market. *Drug Discov. Today* **2010**, *15* (1), 40.

(184) Lipinski, C. A.; Lombardo, F.; Dominy, B. W.; Feeney, P. J. Experimental and Computational Approaches to Estimate Solubility and Permeability in Drug Discovery and Development Settings. *Adv. Drug Deliv. Rev.* **2001**, *23*, 3.

(185) Gao, N.; Bozeman, E. N.; Qian, W.; Wang, L.; Chen, H.; Lipowska, M.; Staley, C. A.; Andrew Wang, Y.; Mao, H.; Yang, L. Tumor Penetrating Theranostic Nanoparticles for Enhancement of Targeted and Image-Guided Drug Delivery into Peritoneal Tumors Following Intraperitoneal Delivery. *Theranostics* **2017**, *7* (6), 1689.

(186) Xie, J.; Lee, S.; Chen, X. Nanoparticle-Based Theranostic Agents. *Adv. Drug Deliv. Rev.* **2010**, *62* (11), 1064.

(187) Yuk, S. H.; Choi, K.; Kim, K.; Kwon, I. C. K. C. In Vivo Targeted Delivery of Nanoparticles for Theranosis. *Society* **2011**, *44* (10), 1018.

(188) Wang, J.; Tao, W.; Chen, X.; Farokhzad, O. C.; Liu, G. Emerging Advances in Nanotheranostics with Intelligent Bioresponsive Systems. *Theranostics* **2017**, *7* (16), 3915.

(189) Bates, S. Progress towards Personalized Medicine. *Drug Discov. Today* **2010**, *15* (3), 115.

(190) Xing, Y.; Zhao, J.; Conti, P. S.; Chen, K. Radiolabeled Nanoparticles for Multimodality Tumor Imaging. *Theranostics* **2014**, *4* (3), 290.

(191) Blanco, E.; Shen, H.; Ferrari, M. Principles of Nanoparticles Design for Overcoming Biological Barriers for Drug Delivery. *Nat Biotechnol* **2015**, *33* (9), 941.

(192) Cataldi, M.; Vigliotti, C.; Mosca, T.; Cammarota, M. R.; Capone, D. Emerging Role of the Spleen in the Pharmacokinetics of Monoclonal Antibodies, Nanoparticles and Exosomes. *Int. J. Mol. Sci.* **2017**, *18* (6), E1249.

(193) Davis, M. E.; Chen, Z.; Shin, D. M. Nanoparticle Therapeutics: An Emerging Treatment Modality for Cancer. *Nat. Rev. Drug Discov.* **2008**, *7* (9), 771.

(194) Kamaly, N.; Xiao, Z.; Valencia, P. M.; Radovic-Moreno, A. F.; Farokhzad, O. C. Targeted Polymeric Therapeutic Nanoparticles: Design, Development and Clinical Translation. *Chem. Soc. Rev.* **2012**, *41* (7), 2971.

(195) Singh, R.; Lillard J. W. Nanoparticle-Based Targeted Drug Delivery. *Exp. Mol .Pathol.* **2009**, *86* (3), 215.

(196) Illum, L.; Davis, S. S.; Wilson, C. G.; Thomas, N. W.; Frier, M.; Hardy, J. G. Blood Clearance and Organ Deposition of Intravenously-Administered Colloidal Particles. The Effects of Particle Size, Nature and Shape. *Int. J. Pharm.* **1982**, *12* (2–3), 135.

(197) Zauner, W.; Farrow, N. A.; Haines, A. M. In Vitro Uptake of Polystyrene

Microspheres: Effect of Particle Size, Cell Line and Cell Density. *J Control Release* **2001**, *71* (1), 39.

(198) Rejman, J.; Oberle, V.; Zuhorn, I. S.; Hoekstra, D. Size-Dependent Internalization of Particles via the Pathways of Clathrin- and Caveolae-Mediated Endocytosis. *Biochem. J.* **2004**, *377* (1), 159.

(199) Wilhelm, S.; Tavares, A. J.; Dai, Q.; Ohta, S.; Audet, J.; Dvorak, H. F.; Chan, W. C. W. Analysis of Nanoparticle Delivery to Tumors. *Nat. Rev. Mater.* **2016**, *1*, 1.

(200) Smith, D. M.; Simon, J. K.; Baker, J. R. Applications of Nanotechnology for Immunology. *Nat. Rev. Immunol.* **2013**, *13* (8), 592.

(201) Doane, T. L.; Burda, C. The Unique Role of Nanoparticles in Nanomedicine: Imaging, Drug Delivery and Therapy. *Chem. Soc. Rev.* **2012**, *41* (7), 2885.

(202) Stephen, Z. R.; Kievit, F. M.; Zhang, M. Magnetite Nanoparticles for Medical MR Imaging. *Mater. Today* **2011**, *14* (7–8), 330.

(203) Rümenapp, C.; Gleich, B.; Haase, A. Magnetic Nanoparticles in Magnetic Resonance Imaging and Diagnostics. *Pharm. Res.* **2012**, *29* (5), 1165.

(204) Revia, R. A.; Zhang, M. Magnetite Nanoparticles for Cancer Diagnosis, Treatment, and Treatment Monitoring: Recent Advances. *Mater. Today* **2016**, *19* (3), 157.

(205) Rosen, J. E.; Chan, L.; Shieh, D. Bin; Gu, F. X. Iron Oxide Nanoparticles for Targeted Cancer Imaging and Diagnostics. *Nanomedicine Nanotechnology, Biol. Med.* **2012**, *8* (3), 275.

(206) Yigit, M. V.; Moore, A.; Medarova, Z. Magnetic Nanoparticles for Cancer Diagnosis and Therapy. *Pharm. Res.* **2012**, *29* (5), 1180.

(207) Laurent, S.; Forge, D.; Port, M.; Roch, A.; Robic, C.; Vander Elst, L.; Muller, R. N. Magnetic Iron Oxide Nanoparticles: Synthesis, Stabilization, Vectorization, Physicochemical Characterizations and Biological Applications. *Chem. Rev.* **2008**, *108* (6), 2064.

(208) Wang, Y.-X. J. Superparamagnetic Iron Oxide Based MRI Contrast Agents:

Current Status of Clinical Application. *Quant Imaging Med Surg* **2011**, *1*, 35.

(209) Levy, M.; Luciani, N.; Alloyeau, D.; Elgrabli, D.; Deveaux, V.; Pechoux, C.; Chat, S.; Wang, G.; Vats, N.; Gendron, F.; et al. Long Term in Vivo Biotransformation of Iron Oxide Nanoparticles. *Biomaterials* **2011**, *32* (16), 3988.

(210) Brigger, I.; Dubernet, C.; Couvreur, P. Nanoparticles in Cancer Therapy and Diagnosis. *Adv. Drug Deliv. Rev.* **2012**, *54* (5), 631.

(211) Gupta, A. K.; Gupta, M. Synthesis and Surface Engineering of Iron Oxide Nanoparticles for Biomedical Applications. *Biomaterials* **2005**, *26* (18), 3995.

(212) Caldorera-Moore, M.; Guimard, N.; Shi, L.; Roy, K. Designer Nanoparticles: Incorporating Size, Shape and Triggered Release into Nanoscale Drug Carriers. *Expert Opin. Drug Deliv.* **2010**, *7* (4), 479.

(213) Colombo, M.; Carregal-Romero, S.; Casula, M. F.; Gutiérrez, L.; Morales, M. P.; Böhm, I. B.; Heverhagen, J. T.; Prosperi, D.; Parak, W. J. Biological Applications of Magnetic Nanoparticles. *Chem. Soc. Rev.* **2012**, *41* (11), 4306.

(214) Krishnan, K. M. Biomedical Nanomagnetics: A Spin through Possibilities in Imaging, Diagnostics, and Therapy. *IEEE Trans. Magn.* **2010**, *46* (7), 2523.

(215) Shin, T.-H.; Choi, Y.; Kim, S.; Cheon, J. Recent Advances in Magnetic Nanoparticle-Based Multi-Modal Imaging. *Chem. Soc. Rev.* **2015**, *44* (14), 2501.

(216) Santhosh, P. B.; Ulrih, N. P. Multifunctional Superparamagnetic Iron Oxide Nanoparticles: Promising Tools in Cancer Theranostics. *Cancer Lett.* **2013**, *336* (1), 8.

(217) Mahmoudi, M.; Sant, S.; Wang, B.; Laurent, S.; Sen, T. Superparamagnetic Iron Oxide Nanoparticles (SPIONs): Development, Surface Modification and Applications in Chemotherapy. *Adv. Drug Deliv. Rev.* **2011**, *63* (1–2), 24.

(218) Luo, G.; Long, J.; Zhang, B.; Liu, C.; Ji, S.; Xu, J.; Yu, X.; Ni, Q. Quantum Dots in Cancer Therapy. *Expert Opin Drug Deliv* **2012**, *9* (1), 47.

(219) Kairdolf, B. A.; Smith, A. M.; Stokes, T. H.; Wang, M. D.; Young, A. N.; Nie, S.

Semiconductor Quantum Dots for Bioimaging and Biodiagnostic Applications. *Annu. Rev. Anal. Chem.* **2013**, *6* (1), 143.

(220) Petryayeva, E.; Algar, W. R.; Medintz, I. L. Quantum Dots in Bioanalysis: A Review of Applications across Various Platforms for Fluorescence Spectroscopy and Imaging. *Appl. Spectrosc.* **2013**, *67* (3), 215.

(221) Rosenthal, S. J.; Chang, J. C.; Kovtun, O.; McBride, J. R.; Tomlinson, I. D. Biocompatible Quantum Dots for Biological Applications. *Chem. Biol.* **2011**, *18* (1), 10.

(222) Wu, X.; Liu, H.; Liu, J.; Haley, K. N.; Treadway, J. A.; Larson, J. P.; Ge, N.; Peale, F.; Bruchez, M. P. Immunofluorescent Labeling of Cancer Marker Her2 and Other Cellular Targets with Semiconductor Quantum Dots. *Nat. Biotechnol.* **2003**, *21* (1), 41.

(223) Xing, Y.; Chaudry, Q.; Shen, C.; Kong, K. Y.; Zhau, H. E.; Chung, L. W.; Petros, J. A.; O'Regan, R. M.; Yezhelyev, M. V.; Simons, J. W.; et al. Bioconjugated Quantum Dots for Multiplexed and Quantitative Immunohistochemistry. *Nat. Protoc.* **2007**, *2* (5), 1152.

(224) Kim, S.; Lim, Y. T.; Soltesz, E. G.; De Grand, A. M.; Lee, J.; Nakayama, A.; Parker, J. A.; Mihaljevic, T.; Laurence, R. G.; Dor, D. M.; Cohn L.H.; Bawendi M.G.; Frangioni J.V. Near-Infrared Fluorescent Type II Quantum Dots for Sentinel Lymph Node Mapping. *Nat. Biotechnol.* **2004**, *22* (1), 93.

(225) Rhyner, M. N.; Smith, A. M.; Yang, L.; Gao, X.; Mao, H.; Nie, S. Quantum Dots and Multifunctional Nanoparticles: New Contrast Agents for Tumor Imaging. *Nanomedicine London Engl.* **2006**, *1* (2), 209.

(226) Gao, X.; Cui, Y.; Levenson, R. M.; Chung, L. W. K.; Nie, S. In Vivo Cancer Targeting and Imaging with Semiconductor Quantum Dots. *Nat. Biotechnol.* **2004**, *22* (8), 969.

(227) Bera, D.; Qian, L.; Tseng, T. K.; Holloway, P. H. Quantum Dots and Their Multimodal Applications: A Review. *Materials (Basel).* **2010**, *3* (4), 2260.

(228) Chen, G.; Shen, J.; Ohulchanskyy, T. Y.; Patel, N. J.; Kutikov, A.; Li, Z.; Song, J.; Pandey, R. K.; Agren, H.; Prasad, P. N.; Han G. (α-

NaYbF4:Tm(3+))/CaF2core/Shell Nanoparticles with Efficient near-Infrared to near-Infrared Upconversion for High-Contrast Deep Tissue Bioimaging. *ACS Nano* **2012**, *6* (9), 8280.

(229) Chen, G.; Ohulchanskyy, T. Y.; Kumar, R.; Ågren, H.; Prasad, P. N. Ultrasmall Monodisperse NaYF4:Yb3+/Tm3+nanocrystals with Enhanced near-Infrared to near-Infrared Upconversion Photoluminescence. *ACS Nano* **2010**, *4* (6), 3163.

(230) Zhou, J.; Yu, M.; Sun, Y.; Zhang, X.; Zhu, X.; Wu, Z.; Wu, D.; Li, F. Fluorine-18-Labeled Gd3+/Yb3+/Er3+ Co-Doped NaYF4 Nanophosphors for Multimodality PET/MR/UCL Imaging. *Biomaterials* **2011**, *32* (4), 1148.

(231) Wang, M.; Abbineni, G.; Clevenger, A.; Mao, C.; Xu, S. Upconversion Nanoparticles: Synthesis, Surface Modification and Biological Applications. *Nanomedicine Nanotechnology, Biol. Med.* **2011**, *7* (6), 710.

(232) Chen, G.; Qiu, H.; Prasad, P. N.; Chen, X. Upconversion Nanoparticles: Design, Nanochemistry, and Applications in Theranostics. *Chem. Rev.* **2014**, *114* (10), 5161.

(233) Xiang, J.; Xu, L.; Gong, H.; Zhu, W.; Wang, C.; Xu, J.; Feng, L.; Cheng, L.; Peng, R.; Liu, Z. Antigen-Loaded Upconversion Nanoparticles for Dendritic Cell Stimulation, Tracking, and Vaccination in Dendritic Cell-Based Immunotherapy. *ACS Nano* **2015**, *9* (6), 6401.

(234) Park, Y. II; Kim, H. M.; Kim, J. H.; Moon, K. C.; Yoo, B.; Lee, K. T.; Lee, N.; Choi, Y.; Park, W.; Ling, D.; Na K.; Moon W.K.; Choi S.H.; Park H.S.; Yoon S.Y.; Suh Y.D.; Lee S.H.; Hyeon T. Theranostic Probe Based on Lanthanide-Doped Nanoparticles for Simultaneous in Vivo Dual-Modal Imaging and Photodynamic Therapy. *Adv. Mater.* **2012**, *24* (42), 5755.

(235) Cui, S.; Yin, D.; Chen, Y.; Di, Y.; Chen, H.; Ma, Y.; Achilefu, S.; Gu, Y. In Vivo Targeted Deep- Tissue Photodynamic Therapy Based on Near- Infrared Light Triggered Upconversion Nanoconstruct--Supporting Information. *ACS Nano* **2013**, *7* (1), 676.

(236) Tian, G.; Ren, W.; Yan, L.; Jian, S.; Gu, Z.; Zhou, L.; Jin, S.; Yin, W.; Li, S.; Zhao, Y. Red-Emitting Upconverting Nanoparticles for Photodynamic Therapy

in Cancer Cells under near-Infrared Excitation. *Small* **2013**, *9* (11), 1929.

(237) Fedoryshin, L. L.; Fedoryshin, L. L. Near-Infrared Triggered Anti-Cancer Drug Release from Upconverting Nanoparticles. *ACS Appl. Mater. Interfaces* **2014**, *6* (16), 13600.

(238) Haase, M.; Schäfer, H. Upconverting Nanoparticles. *Angew. Chemie - Int. Ed.* **2011**, *50* (26), 5808.

(239) Arppe, R.; Hyppänen, I.; Perälä, N.; Peltomaa, R.; Kaiser, M.; Würth, C.; Christ, S.; Resch-Genger, U.; Schäferling, M.; Soukka, T. Quenching of the Upconversion Luminescence of NaYF4:Yb3+,Er3+ and NaYF4:Yb3+,Tm3+ Nanophosphors by Water: The Role of the Sensitizer Yb3+ in Non-Radiative Relaxation. *Nanoscale* **2015**, *7* (27), 11746.

(240) Walther, A.; Mueller, A. H. E. Janus Particles : Synthesis , Self-Assembly , Physical Properties , and Applications. *Chem. Rev.* **2013**, *113*, 5194.

(241) Reguera, J.; Jiménez De Aberasturi, D.; Winckelmans, N.; Langer, J.; Bals, S.; Liz-Marzán, L. M. Synthesis of Janus Plasmonic-Magnetic, Star-Sphere Nanoparticles, and Their Application in SERS Detection. *Faraday Discuss.* **2016**, *191*, 47.

(242) Rodríguez-Fernández, D.; Liz-Marzán, L. M. Metallic Janus and Patchy Particles. *Part. Part. Syst. Charact.* **2013**, *30* (1), 46.

(243) Reguera, J.; Kim, H.; Stellacci, F. Advances in Janus Nanoparticles. *Chim. Int. J. Chem.* **2013**, *67* (11), 811.

(244) De Gennes, P. G. Soft Matter. *Rev. Mod. Phys.* **1992**, *64* (3), 645.

(245) Zhou, H.; Zou, F.; Koh, K.; Lee, J. Multifunctional Magnetoplasmonic Nanomaterials and Their Biomedical Applications. *J. Biomed. Nanotechnol.* **2014**, *10* (10), 2921.

(246) Sun, M.; Xu, L.; Ma, W.; Wu, X.; Kuang, H.; Wang, L.; Xu, C. Hierarchical Plasmonic Nanorods and Upconversion Core-Satellite Nanoassemblies for Multimodal Imaging-Guided Combination Phototherapy. *Adv. Mater.* **2016**, *28* (5), 898.

(247) Zhao, X.; Xu, L.; Sun, M.; Ma, W.; Wu, X.; Kuang, H.; Wang, L.; Xu, C. Gold-Quantum Dot Core-Satellite Assemblies for Lighting Up MicroRNA In Vitro and In Vivo. *Small* **2016**, *12* (34), 4662.

(248) Reguera, J.; Jiménez De Aberasturi, D.; Henriksen-Lacey, M.; Langer, J.; Espinosa, A.; Szczupak, B.; Wilhelm, C.; Liz-Marzán, L. M. Janus Plasmonic-Magnetic Gold-Iron Oxide Nanoparticles as Contrast Agents for Multimodal Imaging. *Nanoscale* **2017**, *9* (27), 9467.

(249) Torchilin, V. Multifunctional and Stimuli-Sensitive Pharmaceutical Nanocarriers. *Eur. J. Pharm. Biopharm.* **2009**, *71* (3), 431.

(250) Jhaveri, A.; Deshpande, P.; Torchilin, V. Stimuli-Sensitive Nanopreparations for Combination Cancer Therapy. *J. Control. Release* **2014**, *190*, 352.

(251) Hoshino, Y.; Jibiki, T.; Nakamoto, M.; Miura, Y. Reversible PKa Modulation of Carboxylic Acids in Temperature-Responsive Nanoparticles through Imprinted Electrostatic Interactions. *ACS Appl. Mater. Interfaces* **2018**, *10* (37), 31096.

(252) Keles, E.; Song, Y.; Du, D.; Dong, W. J.; Lin, Y. Recent Progress in Nanomaterials for Gene Delivery Applications. *Biomater. Sci.* **2016**, *4* (9), 1291.

(253) Loh, X. J.; Lee, T. C.; Dou, Q.; Deen, G. R. Utilising Inorganic Nanocarriers for Gene Delivery. *Biomater. Sci.* **2016**, *4* (1), 70.

(254) Deng, W.; Chen, W.; Clement, S.; Guller, A.; Zhao, Z.; Engel, A.; Goldys, E. M. Controlled Gene and Drug Release from a Liposomal Delivery Platform Triggered by X-Ray Radiation. *Nat. Commun.* **2018**, *9* (1), 1.

(255) Malam, Y.; Loizidou, M.; Seifalian, A. M. Liposomes and Nanoparticles: Nanosized Vehicles for Drug Delivery in Cancer. *Trends Pharmacol. Sci.* **2009**, *30* (11), 592.

(256) Allen, T. M.; Cullis, P. R. Liposomal Drug Delivery Systems: From Concept to Clinical Applications. *Adv. Drug Deliv. Rev.* **2013**, *65* (1), 36.

(257) Algar, W. R.; Prasuhn, D. E.; Stewart, M. H.; Jennings, T. L.; Blanco-Canosa, J. B.; Dawson, P. E.; Medintz, I. L. The Controlled Display of Biomolecules on Nanoparticles: A Challenge Suited to Bioorthogonal Chemistry. *Bioconjug.*

Chem. **2011**, *22* (5), 825.

(258) Lockett, M. R.; Phillips, M. F.; Jarecki, J. L.; Peelen, D.; Smith, L. M. A Tetrafluorophenyl Activated Ester Self-Assembled Monolayer for the Immobilization of Amine-Modified Oligonucleotides. *Langmuir* **2008**, *24* (1), 69.

(259) Medintz, I. Universal Tools for Biomolecular Attachment to Surfaces. *Nat. Mater.* **2006**, *5*, 842.

(260) Prasuhn, D. E.; Blanco-canosa, J. B.; Vora, G. J.; Delehanty, J. B.; Susumu, K.; Mei, B. C.; Dawson, P. E.; Medintz, I. L. Combining Chemoselective Ligation with Quantum Dots. *ACS Nano* **2010**, *4* (1), 267.

(261) Pinaud, F.; Clarke, S.; Sittner, A.; Dahan, M. Probing Cellular Events, One Quantum Dot at a Time. *Nat. Methods* **2010**, *7* (4), 275.

(262) Iyer, G.; Pinaud, F.; Xu, J.; Ebenstein, Y.; Li, J.; Chang, J.; Dahan, M.; Weiss, S. Aromatic Aldehyde and Hydrazine Activated Peptide Coated Quantum Dots for Easy Bioconjugation and Live Cell Imaging. *Bioconjug. Chem.* **2011**, *22* (6), 1006.

(263) Blanco-Canosa, J. B.; Medintz, I. L.; Farrel, D.; Mattoussi, H.; Dawson, P. E. Rapid Covalent Ligation of Fluorescent Peptides to Water Solubilized Quantum Dots. *J. Am. Chem. Soc.* **2010**, *132* (29), 10027.

(264) Wu, L.; Chen, L.; Liu, F.; Qi, X.; Ge, Y.; Shen, S. Remotely Controlled Drug Release Based on Iron Oxide Nanoparticles for Specific Therapy of Cancer. *Colloids Surfaces B Biointerfaces* **2017**, *152*, 440.

(265) Dutta, B.; Shetake, N. G.; Barick, B. K.; Barick, K. C.; Pandey, B. N.; Priyadarsini, K. I.; Hassan, P. A. PH Sensitive Surfactant-Stabilized Fe3O4 Magnetic Nanocarriers for Dual Drug Delivery. *Colloids Surfaces B Biointerfaces* **2018**, *162*, 163.

(266) Wang, Y.; Zhao, R.; Wang, S.; Liu, Z.; Tang, R. In Vivo Dual-Targeted Chemotherapy of Drug Resistant Cancer by Rationally Designed Nanocarrier. *Biomaterials* **2016**, *75*, 71.

(267) Zou, L.; Wang, H.; He, B.; Zeng, L.; Tan, T.; Cao, H.; He, X.; Zhang, Z.; Guo, S.; Li, Y. Current Approaches of Photothermal Therapy in Treating Cancer

Metastasis with Nanotherapeutics. *Theranostics* **2016**, *6* (6), 762.

(268) O'Neal, D. P.; Hirsch, L. R.; Halas, N. J.; Payne, J. D.; West, J. L. Photo-Thermal Tumor Ablation in Mice Using near Infrared-Absorbing Nanoparticles. *Cancer Lett.* **2004**, *209* (2), 171.

(269) Li, J. L.; Wang, L.; Liu, X. Y.; Zhang, Z. P.; Guo, H. C.; Liu, W. M.; Tang, S. H. In Vitro Cancer Cell Imaging and Therapy Using Transferrin-Conjugated Gold Nanoparticles. *Cancer Lett.* **2009**, *274* (2), 319.

(270) Shanmugam, V.; Selvakumar, S.; Yeh, C. S. Near-Infrared Light-Responsive Nanomaterials in Cancer Therapeutics. *Chem. Soc. Rev.* **2014**, *43* (17), 6254.

(271) Huang, X.; Jain, P. K.; El-Sayed, I. H.; El-Sayed, M. A. Plasmonic Photothermal Therapy (PPTT) Using Gold Nanoparticles. *Lasers Med. Sci.* **2008**, *23* (3), 217.

(272) Hu, S. H.; Fang, R. H.; Chen, Y. W.; Liao, B. J.; Chen, I. W.; Chen, S. Y. Photoresponsive Protein-Graphene-Protein Hybrid Capsules with Dual Targeted Heat-Triggered Drug Delivery Approach for Enhanced Tumor Therapy. *Adv. Funct. Mater.* **2014**, *24* (26), 4144.

(273) Ma, Y.; Liang, X.; Tong, S.; Bao, G.; Ren, Q.; Dai, Z. Gold Nanoshell Nanomicelles for Potential Magnetic Resonance Imaging, Light-Triggered Drug Release, and Photothermal Therapy. *Adv. Funct. Mater.* **2013**, *23* (7), 815.

(274) Melamed, J. R.; Edelstein, R. S.; Day, E. S. Elucidating the Fundamental Mechanisms of Cell Death Triggered by Photothermal Therapy. *ACS Nano* **2015**, *9* (1), 6.

(275) Hu, Y.; Chi, C.; Wang, S.; Wang, L.; Liang, P.; Liu, F.; Shang, W.; Wang, W.; Zhang, F.; Li, S.; Shen H.; Yu X.; Liu H.; Tian J. A Comparative Study of Clinical Intervention and Interventional Photothermal Therapy for Pancreatic Cancer. *Adv. Mater.* **2017**, *29* (33), 1.

(276) Rai, P.; Mallidi, S.; Zheng, X.; Rahmanzadeh, R.; Mir, Y.; Elrington, S.; Khurshid, A.; Hasan, T. Development and Applications of Photo-Triggered Theranostic Agents. *Adv. Drug Deliv. Rev.* **2010**, *62* (11), 1094.

(277) Zhou, Z.; Sun, Y.; Shen, J.; Wei, J.; Yu, C.; Kong, B.; Liu, W.; Yang, H.; Yang,

S.; Wang, W. Iron/Iron Oxide Core/Shell Nanoparticles for Magnetic Targeting MRI and near-Infrared Photothermal Therapy. *Biomaterials* **2014**, *35* (26), 7470.

(278) Lv, R.; Yang, P.; Chen, G.; Gai, S.; Xu, J.; Prasad, P. N. Dopamine-Mediated Photothermal Theranostics Combined with up-Conversion Platform under near Infrared Light. *Sci. Rep.* **2017**, *7* (1), 1.

(279) Chu, M.; Pan, X.; Zhang, D.; Wu, Q.; Peng, J.; Hai, W. The Therapeutic Efficacy of CdTe and CdSe Quantum Dots for Photothermal Cancer Therapy. *Biomaterials* **2012**, *33* (29), 7071.

(280) Hildebrandt, B. The Cellular and Molecular Basis of Hyperthermia. *Crit. Rev. Oncol. Hematol.* **2002**, *43* (1), 33.

(281) Mahmoudi, K.; Bouras, A.; Bozec, D.; Ivkov, R.; Hadjipanayis, C. Magnetic Hyperthermia Therapy for the Treatment of Glioblastoma: A Review of the Therapy's History, Efficacy and Application in Humans. *Int. J. Hyperth.* **2018**, *0* (0), 1.

(282) Wust, P.; Hildebrandt, B.; Sreenivasa, G.; Rau, B.; Gellermann, J.; Riess, H.; Felix, R.; Schlag, P. M. Hyperthermia in Combined Treatment of Cancer. *The Lancet-Oncology* **2002**, *3* (August), 487.

(283) Arvizo, R. R.; Bhattacharyya, S.; Kudgus, R. A.; Giri, K.; Bhattacharya, R.; Mukherjee, P. Intrinsic Therapeutic Applications of Noble Metal Nanoparticles: Past, Present and Future. *Chem. Soc. Rev.* **2012**, *41* (7), 2943.

(284) Dewhirst, M. W.; Ozimek, E. J.; Gross, J.; Cetas, T. C. Will Hyperthermia Conquer the Elusive Hypoxic Cell? Implications of Heat Effects on Tumor and Normal-Tissue Microcirculation. *Radiology* **1980**, *137*, 811.

(285) Behrouzkia, Z.; Joveini, Z.; Keshavarzi, B.; Eyvazzadeh, N.; Aghdam, R. Z. Hyperthermia: How Can It Be Used? In *Oman Med J*; 2007; Vol. 31, p 89.

(286) Jordan A, Maier-Hauff K, Wust P, J. M. Nanoparticles for Thermotherapy. In *Biofunctionalization of Nanomaterials*; 2007.

(287) Gordon, R. T.; Hines, J. R.; Gordon, D. Intracellular Hyperthermia a Biophysical Approach to Cancer Treatment via Intracellular Temperature and

Biophysical Alterations. *Med. Hypotheses* **1979**, *5* (1), 83.

(288) Gneveckow, U.; Jordan, A.; Scholz, R.; Brüß, V.; Waldöfner, N.; Ricke, J.; Feussner, A.; Hildebrandt, B.; Rau, B.; Wust, P. Description and Characterization of the Novel Hyperthermia- and Thermoablation-System MFH®300F for Clinical Magnetic Fluid Hyperthermia. *Med. Phys.* **2004**, *31* (6), 1444.

(289) Magforce® (http://www.magforce.de/en/unternehmen/ueber-uns.html).

(290) Fortin, J. P.; Wilhelm, C.; Servais, J.; Ménager, C.; Bacri, J. C.; Gazeau, F. Size-Sorted Anionic Iron Oxide Nanomagnets as Colloidal Mediators for Magnetic Hyperthermia. *J. Am. Chem. Soc.* **2007**, *129* (9), 2628.

(291) Bauer, L. M.; Situ, S. F.; Griswold, M. A.; Samia, A. C. S. High-Performance Iron Oxide Nanoparticles for Magnetic Particle Imaging-Guided Hyperthermia (HMPI). *Nanoscale* **2016**, *8* (24), 12162.

(292) Quinto, C. A.; Mohindra, P.; Tong, S.; Bao, G. Multifunctional Superparamagnetic Iron Oxide Nanoparticles for Combined Chemotherapy and Hyperthermia Cancer Treatment. *Nanoscale* **2015**, *7* (29), 12728.

(293) Celli, J. P.; Spring, B. Q.; Rizvi, I.; Evans, C. L.; Samkoe, K. S.; Verma, S.; Pogue, B. W.; Hasan, T. Imaging and Photodynamic Therapy: Mechanisms, Monitoring and Optimization. **2011**, *110* (5), 2795.

(294) Triesscheijn, M.; Baas, P.; Schellens, J. H. M.; Stewart, F. A. Photodynamic Therapy in Oncology. *Expert Opin Pharmacother* **2001**, *2* (6), 917.

(295) Dolmans D. E.; Fukumura, D.; Jain, R. K. Photodynamic Therapy for Cancer. *Nat. Rev. Cancer* **2003**, *3* (5), 380.

(296) Sneider, A.; VanDyke, D.; Paliwal, S.; Rai, P. Remotely Triggered Nano-Theranostics for Cancer Applications. *Nanotheranostics* **2017**, *1* (1), 1.

(297) Xu, J.; Xu, L.; Wang, C.; Yang, R.; Zhuang, Q.; Han, X.; Dong, Z.; Zhu, W.; Peng, R.; Liu, Z. Near-Infrared-Triggered Photodynamic Therapy with Multitasking Upconversion Nanoparticles in Combination with Checkpoint Blockade for Immunotherapy of Colorectal Cancer. *ACS Nano* **2017**, *11* (5), 4463.

(298) Lu, K.; He, C.; Guo, N.; Chan, C.; Ni, K.; Weichselbaum, R. R.; Lin, W. Chlorin-Based Nanoscale Metal-Organic Framework Systemically Rejects Colorectal Cancers via Synergistic Photodynamic Therapy and Checkpoint Blockade Immunotherapy. *J. Am. Chem. Soc.* **2016**, *138* (38), 12502.

(299) Liu, L. H.; Qiu, W. X.; Zhang, Y. H.; Li, B.; Zhang, C.; Gao, F.; Zhang, L.; Zhang, X. Z. A Charge Reversible Self-Delivery Chimeric Peptide with Cell Membrane-Targeting Properties for Enhanced Photodynamic Therapy. *Adv. Funct. Mater.* **2017**, *27* (25), 1700220.

(300) Han, K.; Wang, S. B.; Lei, Q.; Zhu, J. Y.; Zhang, X. Z. Ratiometric Biosensor for Aggregation-Induced Emission-Guided Precise Photodynamic Therapy. *ACS Nano* **2015**, *9* (10), 10268.

(301) Li, S. Y.; Cheng, H.; Xie, B. R.; Qiu, W. X.; Zeng, J. Y.; Li, C. X.; Wan, S. S.; Zhang, L.; Liu, W. L.; Zhang, X. Z. Cancer Cell Membrane Camouflaged Cascade Bioreactor for Cancer Targeted Starvation and Photodynamic Therapy. *ACS Nano* **2017**, *11* (7), 7006.

(302) Zheng, D. W.; Li, B.; Li, C. X.; Fan, J. X.; Lei, Q.; Li, C.; Xu, Z.; Zhang, X. Z. Carbon-Dot-Decorated Carbon Nitride Nanoparticles for Enhanced Photodynamic Therapy against Hypoxic Tumor via Water Splitting. *ACS Nano* **2016**, *10* (9), 8715.

(303) Yang, G.; Xu, L.; Chao, Y.; Xu, J.; Sun, X.; Wu, Y.; Peng, R.; Liu, Z. Hollow MnO2as a Tumor-Microenvironment-Responsive Biodegradable Nano-Platform for Combination Therapy Favoring Antitumor Immune Responses. *Nat. Commun.* **2017**, *8* (1), 902.

(304) Chen, Q.; Xu, L.; Liang, C.; Wang, C.; Peng, R.; Liu, Z. Photothermal Therapy with Immune-Adjuvant Nanoparticles Together with Checkpoint Blockade for Effective Cancer Immunotherapy. *Nat. Commun.* **2016**, *7*, 1.

(305) Song, W.; Kuang, J.; Li, C. X.; Zhang, M.; Zheng, D.; Zeng, X.; Liu, C.; Zhang, X. Z. Enhanced Immunotherapy Based on Photodynamic Therapy for Both Primary and Lung Metastasis Tumor Eradication. *ACS Nano* **2018**, *12* (2), 1978.

(306) Di Corato, R.; Béalle, G.; Kolosnjaj-Tabi, J.; Espinosa, A.; Clément, O.; Silva, A. K. A.; Ménager, C.; Wilhelm, C. Combining Magnetic Hyperthermia and Photodynamic Therapy for Tumor Ablation with Photoresponsive Magnetic Liposomes. *ACS Nano* **2015**, *9* (3), 2904.

CHAPTER 2

Screening of nanoparticles for the delivery of TLR4 ligands and their immunomodulatory properties

In this chapter, different types of nanoparticles (IONPsp, IONPc, QDs, and UCNPs) were explored for the delivery of different TLR4 ligands (the TLR4 agonists E. Coli LOS, E. Coli LPS and Xcc LOS and the synthetic TLR4 antagonist IAXO 102) and the immunomodulatory properties of the resulting systems were investigated in macrophages.

2.1: Introduction

Combinatorial immunotherapy, and especially the combination of checkpoint blockade with vaccines and its promising applications in cancer treatment is increasingly being discussed in the scientific literature[1]. Since cancer vaccines can both generate new antigen-specific T cell responses against tumor cells and amplify existing responses, they can counterbalance one of the main drawbacks of checkpoint blockade, which is the requirement for continuous generation of T cells[1].

TLR agonists are of clinical relevance as vaccine adjuvants due to their capacity to modulate innate and adaptive immunity[2,3], and nanoparticle delivery allows to overcome the limitations of conventional vaccines by presenting a ligand similarly to the way a pathogen would[4,5]. Nanoparticles can also promote cross-presentation and act as adjuvants on their own[6]. Besides, the usage of nanoparticles as carriers improves the therapeutic effectiveness of drugs by site-specific delivery and longer circulation half-life when compared to the free drug counterpart[7,8,9]. Additionally, the different intrinsic properties of nanoparticles allowing multimodal imaging and use in hyperthermia, photodynamic or photothermal therapy, further encourage their use as delivery vehicles for TLR ligands.

There is a growing literature of nanoparticle-mediated delivery of TLR ligands. In relation to this thesis approach Ruiz-de-Angulo et al. described the preparation of CpG ODN-loaded IONPsp with ideal size for accurate delivery to DCs in the lymph nodes. IONPsp-mediated co-delivery of adjuvant and antigen was observed to enhance Th1-cytokine secretion and DC maturation, leading to strong CD8$^+$ T cells activation, in turn developing enhanced protection against an aggressive melanoma tumor challenge[10].

Bocanegra-Gondan et al. used Zn-doped spherical iron oxide nanoparticles to deliver both poly(I:C) and imiquimod, co-administering this system with an OVA-loaded IONPsp. They took advantage of synergistic TLR stimulation and enhanced MRI properties to provide improved activation of macrophages and dendritic cells and in vivo tracking of the nanovaccine delivery. Immunization of mice with small amounts of OVA and poly(I:C)-imiquimod (5 µg) delivered by the different IONPsp lead to long term protection against melanoma, with 100 % of nanoparticle-immunized mice rejecting tumor re-challenge 70 days after the last immunization[11].

The literature also reports some cases where nanoparticles were specifically functionalized with TLR4 ligands. Barr et al.[12] loaded Kdo_2-Lipid A on the surface of QDs reporting the first pathogen-like nanostructure. This delivery system was tracked in vitro by the use of confocal microscopy and exerted a strong immunostimulatory activity when injected together with the model antigen dinitrophenylated-ovalbumin (DNP-OVA) by increasing antibody titers (total Ab, IgG1 and IgG2c) (*Figure 1*) in mice. This system proved to be a better adjuvant than LPS subcutaneously injected with the widely used incomplete Freund's adjuvant (IFA), which is considered as the "gold standard" for T-cell vaccination but suffers from considerable adverse effects.
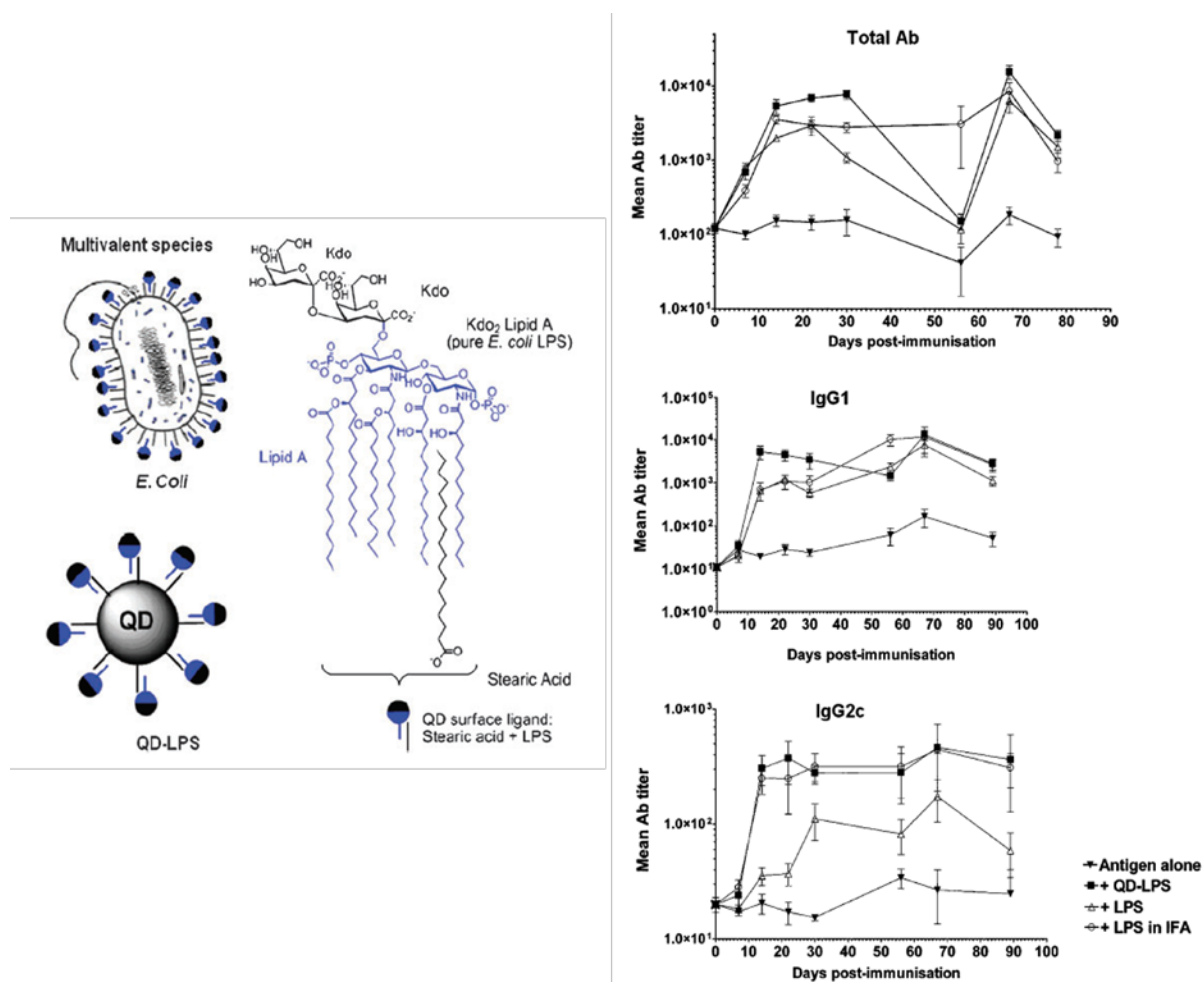

Figure 1: Pathogen-like LPS-loaded QDs and their capacity to increase total Ab, IgG1 and IgG2 titers "in vivo". Adapted from reference[12]. Reproduced by permission of The Royal Society of Chemistry

Another example in functionalization of nanoparticles with TLR4 agonists was reported by Piazza et al., which loaded IONPsp with LPS. The "in vitro" immunostimulatory properties of the nanoparticles were monitored by the accumulation of extracellular TNF-α using innate immune system cells, respectively murine bone marrow-derived dendritic cells (BMDCs) and bone marrow-derived macrophages (BMDMs). These LPS-loaded IONPsp produced dose- and TLR4-dependent activation of both cell types derived from mice[13].

While the QDs used in this thesis were purchased, IONPsp and cubic iron oxide nanoparticles (IONPc) were prepared by Dr. Gomez-Blanco using the method known as thermal decomposition, due to the good size control and high crystallinity of the resulting product[14]. The synthesis and the characterization of UCNPs is reported in the results and discussion section of this chapter.

Monodisperse IONPsp were obtained by thermal decomposition of a metallic precursor, $Fe(acac)_3$, in the presence of oleic acid and oleylamine as surfactants in diphenyl ether (a high boiling point solvent) using 1,2 hexadecanediol as a reducing agent. This procedure has been used several times in our research group, yielding uniform and biocompatible 7 nm IONPsp that have been functionalized with TLR ligands and used for biomedical applications and in vivo imaging[10,15]. This synthetic method is very versatile since it allows precise control over the size of the final product by modulating the reaction conditions. The chosen solvent, reaction temperature, and temperature ramps affect the final size of the IONPsp obtained and are key factors to a monodisperse size distribution[14]. The size of the IONPsp used in this thesis was chosen to be 7 nm as this specific size yields hydrophilic micelles having a size between 20-100 nm, which is ideal for lymph node delivery[16]. Besides, these IONPsp exhibit superparamagnetic behavior at room temperature and their magnetization value (M_s) was measured by Dr. Cobaleda-Siles to be of 91 emu g^{-1}, among the highest reported so far in the literature for IONPsp-based MR contrast agents of this size[17,18,19]. Moreover, the r_2 relaxivity value of the drug-free 25 nm micellar IONPsp (mIONPsp), obtained from self-assembly of PEG-phospholipids around 7 nm IONPsp, was 68.8 mM^{-1}s^{-1}, at 11.7 T and 25 ℃[20], which makes it a very good T_2-weighted MRI contrast agent. Thus, a size of 7 nm was chosen as an ideal compromise between the hydrodynamic diameter of the resulting micelles, suitable for lymph node delivery, and magnetization value for MRI.

On the other hand, IONPc, despite being bigger than IONPsp, yielded mIONPc that were still within the ideal values for lymph node targeting but featuring more promising magnetic properties than IONPsp, which can be used to obtain improved MRI contrast. The improved magnetic properties of IONPc originate from the fact that IONPs bigger than 25 nm behave as randomly distributed stationary objects (static dephasing regime, SDR) and are predicted to exhibit the highest r_2 relaxivity. However, the magnetic dipole interaction among these ferrimagnetic nanoparticles results in poor colloidal stability causing aggregation and impairing their use for biomedical applications. Therefore, obtaining single-core IONPc within the SDR is fundamental for this purpose[21].

The 27 nm IONPc used in this thesis were synthesized by thermal decomposition of iron (III) acetylacetonate in benzyl ether at high temperatures, with oleic acid as surfactant and 4-biphenyl carboxylic acid as reducing agent. This method has been widely used and yields highly uniform and monodisperse nanoparticles by a one-step reaction[22]. Moreover, Dr. Gomez-Blanco prepared 77 nm mIONPc incorporating 27 nm IONPc in PEG-phospholipids and the r_2 relaxivity of the resulting micelles was measured to be 408 mM^{-1}s^{-1} (unpublished data). These are very promising results since this value is almost four times higher than the commercial and clinically used benchmarks[23].

The transmission electron microscopy (TEM) characterization of the synthesized IONPs (***Figure 2***) shows IONPsp with a mean core diameter of 6.6 ± 0.9 nm and IONPc with a mean edge of 26.68 ± 2.6 nm. The nanoparticles prepared by thermal decomposition resulted in hydrophobic materials that needed further functionalization to achieve the water solubility required for biomedical applications. Among all the polymers and ligands suitable, PEG and its derivatives are a very interesting class of polymers that have been widely used to impart water solubility and biocompatibility to hydrophobic nanoparticles[24,25]. These polymers have low toxicity and immunogenicity and several PEGylated products have been approved by the FDA for clinical use[26] and many PEG-encapsulated nanoparticles have been used for biomedical applications. One of the advantages of PEG as a coating for nanoparticles is the increased resistance of the resulting nanoparticles to unspecific interactions with proteins ending up in the formation of the protein corona[27], further affected by the density of the PEG grafting[28]. Additionally, PEG confers stealth

properties to nanoparticles increasing their circulation time and retention in the body[29]. In this thesis, PEG-phospholipids were used to functionalize the hydrophobic nanoparticles used.
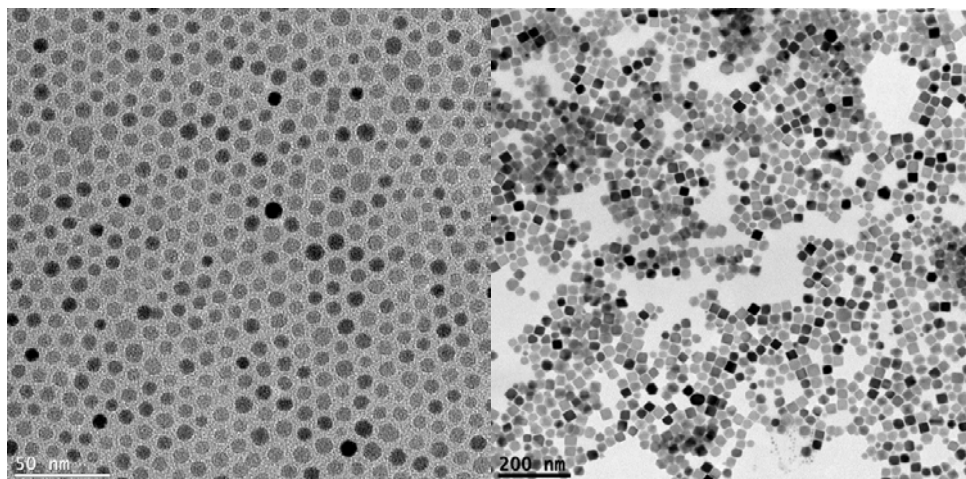
Figure 2: *Representative TEM images of the hydrophobic IONPsp and IONPc used for micelle preparation.*

LOS, or R-form LPS, have been investigated less than LPS for various applications, despite showing very promising results as vaccine adjuvants, both against pathogens and diseases[30,31,32]. To the best of our knowledge, the nanostructures formed by the interaction of our nanoparticles with the two LOS (*E. Coli* LOS and *Xcc* LOS) haven't been investigated previously. These LOS feature structural differences from the conventional LPS, such as the lack of the O-antigen chain and possess a shorter oligosaccharide core, with around ten saccharide units.

The complete structure of *Xcc* LOS was determined by Silipo et al. and it was found to be a unique molecule with high negative charge in the lipid A-inner core region. The unique features include a galacturonyl phosphate attached at a 3-deoxy-D-manno-oct-2-ulosonic acid residue and a unique phosphoramide group in the inner core region[33]. It also shows a 3+3 symmetry in the distribution of the acyl chains in the Lipid A moiety, while conventional LPS typically show a 2+4 distribution. Interested in exploring new TLR4 agonists and improving their adjuvanticity, and in how the structural differences of the two TLR4 agonists might affect their incorporation, these were loaded on different kinds of nanoparticles. Besides, the

structural differences that distinguish these two LOS from the known *E. Coli* LPS and the FDA approved MPLA yielded unique nanoplatforms with distinctive chemical and biological properties.

This chapter will also report the attempts made towards the development of a light-triggered delivery vehicle for suppression of TLR4 signaling.

Recently, an interesting application of the TLR7 agonist imiquimod and TLR7/ 8 agonist resiquimod has been reported in the literature. By applying a protecting group that could be cleaved by light, Ah Ryu et al. developed photo-controlled versions of both these immunomodulators[34] which were biologically inactive and could be activated upon irradiation with UV light (**Figure 3**). We reasoned that UNCPs, with their UC emissions could potentially be used to trigger TLR4 signaling using NIR light. Indeed some recent studies have shown the utility of UCNPs for the release of the active molecule, both by overcoming the pharmacokinetic problems of small molecules[35] and the poor tissue penetration of UV light when compared to NIR irradiation[36].

To the best of our knowledge, prior to this thesis UCNPs had not been exploited for the delivery of TLR4 modulators.
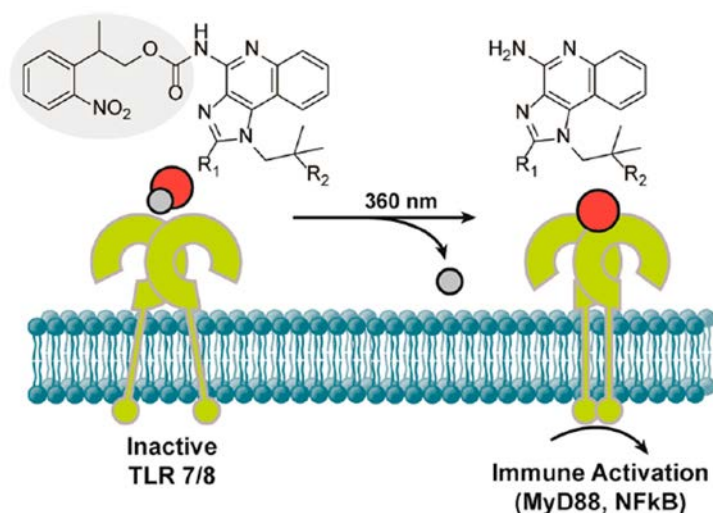

Figure 3: *TLR7/8 activation and subsequent MyD88 signaling cascade by the deprotection of photocaged small-molecule agonists imiquimod and resiquimod. Adapted from reference*[34].

Core-shell UCNPs were chosen for their enhanced UC photoluminescence, as the addition of a shell creates a homogeneous interface between the core and the outer shell. This suppresses surface-related deactivations by the elimination of the quenching sites on the surface of the core nanoparticle as well as spatial isolation of the core from surrounding deactivators (ligands, solvents, etc.), increasing the efficiency of the upconversion process[37]. It is reported that the visible UC emissions in hexagonal phase $NaYF_4{:}Yb^{3+}/Tm^{3+}$ were enhanced 29.6 times by growing a thin layer of $NaYF_4$[38].

The chosen TLR4 ligand for UCNPs functionalization, IAXO 102, was designed, synthesized and characterized by the Peri group at UNIMIB[39]. This molecule had showed promising results when tested as a TLR4 antagonist in vitro.

Looking to ultimately develop a light-triggered system by photo-caging the synthetic TLR4 modulator IAXO 102, un-caged IAXO 102 was loaded onto UCNPs-filled micelles. The immunomodulatory activity of this system was studied in macrophages.

2.2: Results and discussion

2.2.1: Self-assembly of pathogen-mimicking TLR4 agonist-functionalized nanoparticle-filled micelles

Hydrophobic IONPsp, QDs and IONPc were successfully encapsulated in PEG-phospholipids with incorporation of the two TLR4 agonists Xcc LOS and E. Coli LOS (with a molar ratio of 20% *Xcc* LOS to PEG-phospholipids and 27.5% *E. Coli* LOS to PEG-phospholipids). The PEG-phospholipids and the LOS are amphiphilic molecules, which reduce NP/ water surface tension by associating with the surface of the original hydrophobic nanoparticles through interdigitation of their acyl chains by van der Waals attractive interactions. The organization of hydrophilic components/ precursors at the surfactant/ water interface through electrostatic and hydrogen bonding interactions resulted in the encapsulation of the nanoparticles in a shell formed by the polar head groups. The self-assembly process of the amphiphilic PEG-phospholipids and TLR4 agonists with the hydrophobic nanoparticles yielded pathogen-mimicking micellar nanoparticles (mNPs) that are soluble and stable in

water (*Figure 4*) and could be stored in aqueous solution for weeks without major aggregation and size changes. In contrast, the incorporation of the FDA approved MPLA immediately afforded insoluble aggregates. Hence, it seems lack of the hydrophilic O-antigen polysaccharide and core oligosaccharide chain makes the micelle surface less hydrophilic and thus increases the surface hydrophobicity, leading to the formation of large and insoluble aggregates. To remove NP-free micelles the samples were centrifuged and the supernatants were kept for quantification of drug loading and the pelleted mNPs were redissolved in aqueous solution (3 cycles). The drug-free mNPs prepared as controls and the pathogen-mimicking mNPs incorporating the TLR4 agonists were characterized by TEM, dynamic light scattering (DLS) and by measuring the ζ-potential of the particles (*Figure 5*, *Figure 6* and *Figure 7*). The TEM images of these bacteria-like nanoplatforms show mNPs with size distributions corresponding to a number-averaged hydrodynamic diameter of *ca.* 20 nm for IONPsp and QDs and of *ca.* 70 nm for IONPc, which are in the ideal range (20-100 nm) for lymphatic delivery[16] and with rather uniform size distribution (polydispersity index between 0.16 and 0.39). Moreover, they showed a more negative ζ-potential than the drug-free control mNPs, consistent with the high negative charge density of the LOS molecules provided by the high density of phosphate and carboxylate groups and the phosphoramide group uniquely present in *Xcc* LOS. Also consistent with their different structures, the bacteria-like mNPs functionalized with *Xcc* LOS had a more negative surface charge than mNPs functionalized with *E. Coli* LOS (-11.42 ± 2.17 mV for mIONPsp-*Xcc* LOS, -8.17 ± 1.55 mV for mIONPsp-*E. Coli* LOS and -6.71± 0.87 mV for drug free mIONPsp); (-7.48 ± 0.58 for mQDs-*Xcc* LOS, -3.91 ± 0.33 for mQDs-*E. Coli* LOS and -3.53 ± 0.11 for drug-free mQDs); (-9.10 ± 0.85 for mIONPc-*Xcc* LOS, -8.68 ± 0.69 for mIONPc-*E. Coli* LOS and -4.44 ± 0.53 for drug-free mIONPc). Their negative surface charge constitutes an advantage for lymph node targeting. This is because negatively charged particles move faster through the interstitium and are accumulated more efficiently in draining lymph nodes[40,41] due to the electrostatic repulsion with the negatively charged interstitial matrix. Moreover, hydrophobicity has been reported to facilitate uptake by antigen presenting cells and delivery to the lymph nodes[40,42,43] and here bound LOS and the oleic acid chains of the nanoparticles provide hydrophobic components to the micelle, which upon exposure to the surface can facilitate interaction with the membrane of antigen

presenting cells. The mIONPsp-LOS, therefore, possess all the key features of materials that can effectively target lymph nodes, specifically a size of 20-100 nm, an appropriate level of hydrophobicity and a negative surface.

Two sets of experiments were carried out to quantify TLR4 agonist loading onto the mNPs. After pelleting the mNP-LOS systems by three cycles of centrifugation, IL-6 cytokine production in the macrophage cell line J774A.1 upon incubation with the supernatants was compared with the dose-response curves obtained with the corresponding LOS. To check the efficacy of the used quantification method, mNPs-*E. Coli* LPS were prepared and characterized (**Figure 8**) and the LPS left in the supernatants was quantified using both the FDA-approved Limulus amebocyte lysate (LAL) test and the cell stimulation-based method, with the two assays producing almost identical results (**Table 1**). The prepared mNPs-*E. Coli* LPS showed uniform size distributions and negative ζ-potentials higher than the control micelles, proving the incorporation of the negatively charged LPS (-7.10 ± 1.04 mV for mIONPsp-*E. Coli* LPS and -6.71± 0.87 mV for drug free mIONPsp; -9.15 ± 2.71 mV for mIONPc-*E. Coli* LPS and -4.44 ± 0.53 mV for drug-free mIONPc; -4.59 ± 0.86 mV for mQDs-*E. Coli* LPS and -3.53 ± 0.11 mV for drug-free mQDs) (**Figure 8**g). Moreover, mIONPc-*E. Coli* LPS had a much bigger size than mQDs-*E. Coli* LPS and mIONPsp-*E. Coli* LPS (218.5 ± 47.29 for mIONPc-*E. Coli* LPS, 20.63 ± 7.11 for mQDs-*E. Coli* LPS and 27.08 ± 9.30 for mIONPsp-*E. Coli* LPS), due to the bigger number of LPS molecules incorporated in the larger IONPc (78 ± 14 LPS molecules/ mIONPc vs. 53 ± 6 LPS molecules/ mIONPsp and 15 ± 3 LPS molecules/ mQDs) (**Figure 8**g).
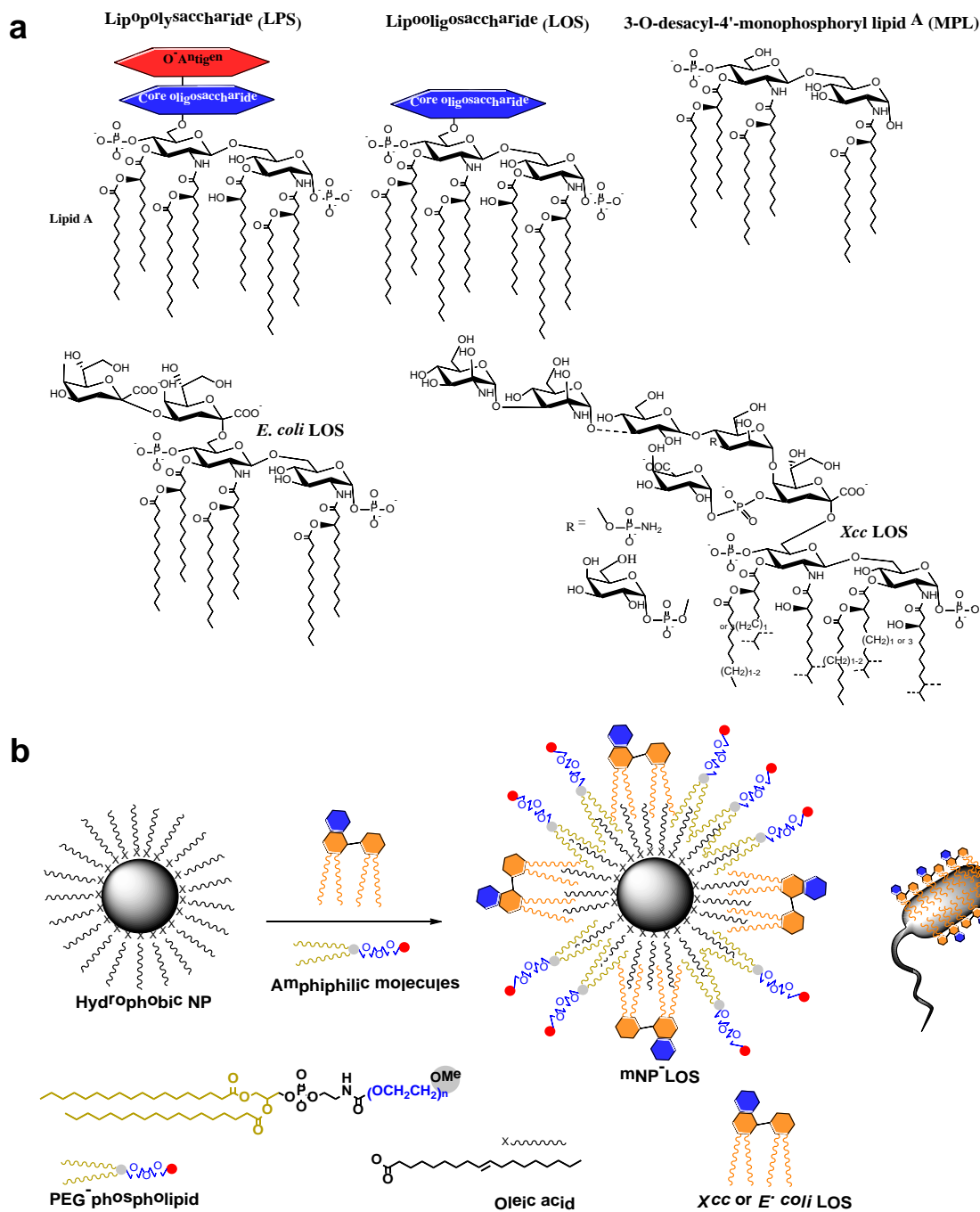
Figure 4: *a) Chemical structures of the TLR4 agonists and b) schematic of the self-assembly process for the synthesis of the water-soluble mNPs incorporating Xcc or E. coli LOS molecules.*

The results showed that *Xcc* LOS is incorporated in the mIONPsp and mIONPc better than *E. coli* LOS (76 ± 6 % *vs* 22.2 ± 5.1 % and 44 ± 11 % *vs* 25 ± 9 %, respectively, (**Figure 9**). The mIONPsp could be loaded with 79 ± 5 and 41 ± 2 molecules of *Xcc* LOS and *E. coli* LOS per particle, respectively (**Figure 5**g). The larger NP core size of the mIONPc allowed to increase the loading to 240 ± 26 *Xcc* LOS molecules/particle and 76 ± 7 molecules of *E. coli* LOS/particle (**Figure 7**g). Both types of nanoparticles are stabilized with an oleic acid/ oleylamine surfactant layer. In contrast, the commercial QDs with a similar core size to the mIONPsp showed a preference for incorporating *E. coli* LOS over *Xcc* LOS (29 ± 1 *Xcc* LOS molecules/particle *vs* 155 ± 11 molecules of *E. coli* LOS/particle) (**Figure 6**g).

g	Diameter			- potential (mV)	/
	nm)	(nm)	(PDI)		ratio
	± 1.19	± 3.53	± 0.015	6.71 ± 0.86	
-*E. coli* LOS	± 1.19	± 7.02	± 0.017	8.17 ± 1.55	± 2
-*Xcc* LOS	± 1.19	± 6.49	± 0.087	11.42 ± 2.17	± 5

Figure 5: *Size and ζ-potential of mIONPsp with and without LOS incorporation. (a-c) TEM images and (d-f) DLS analysis. g) Main characterization data: IONPsp core diameter from TEM images and counting more than 200 nanoparticles, number-average hydrodynamic diameter and polydispersity index obtained by DLS, ζ-potential and number of biomolecules per IONPsp based on n > 10 formulation replicates.*

Figure 6: Size and ζ-potential of mQDs with and without LOS incorporation. (a-c) TEM images and (d-f) DLS analysis. g) Main characterization data: QDs core diameter from TEM images and counting more than 200 nanoparticles, number-average hydrodynamic diameter and polydispersity index obtained by DLS, ζ-potential and number of biomolecules per QDs based on n > 5 formulation replicates.

These results might be explained in term of the differences in the hydrophobic chains, where specific chain lengths etc. contributed to forming more extensive van der Waals interactions with the surfactants stabilizing the nanoparticles[33,44].
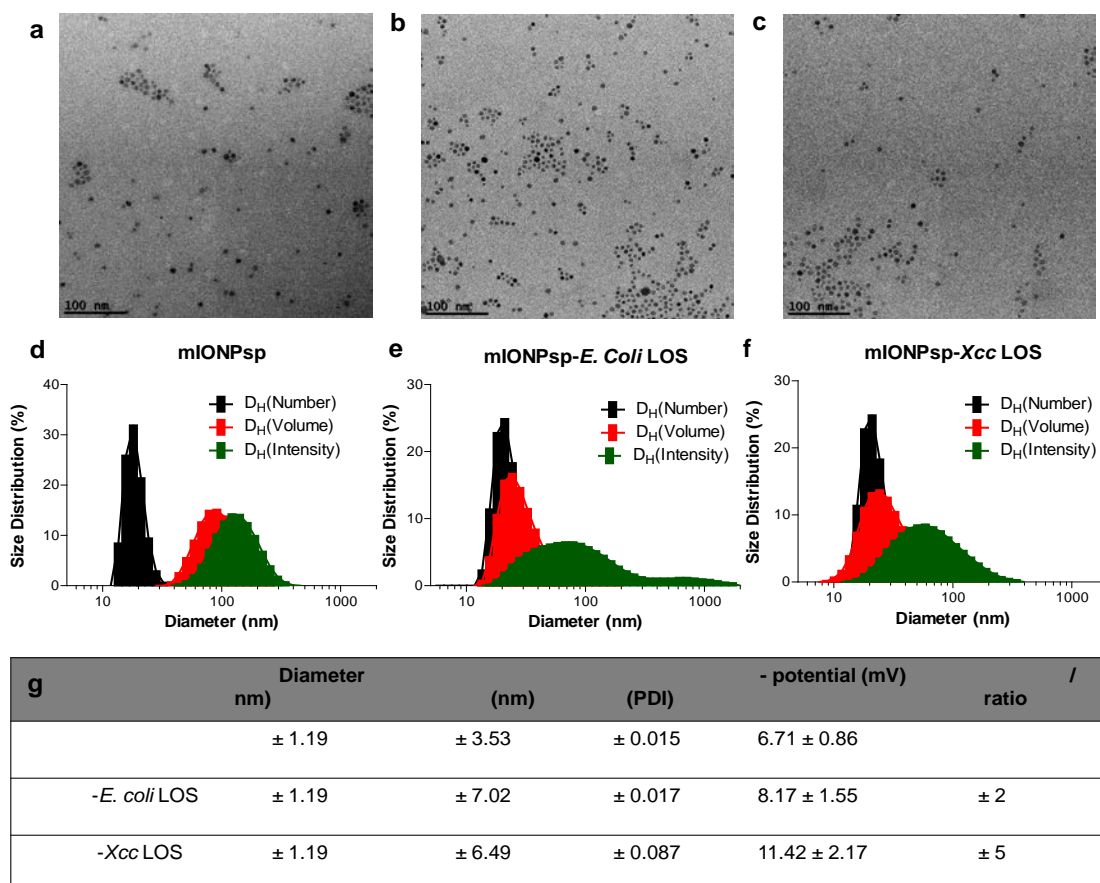
Figure 7: *Size and ζ-potential of mIONPc with and without LOS incorporation. (a-c) TEM images and (d-f) DLS analysis. g) Main characterization data: IONPc core diameter from TEM images and counting more than 200 nanoparticles, number-average hydrodynamic diameter and polydispersity index obtained by DLS, ζ-potential and number of biomolecules per IONPc based on n > 5 formulation replicates.*
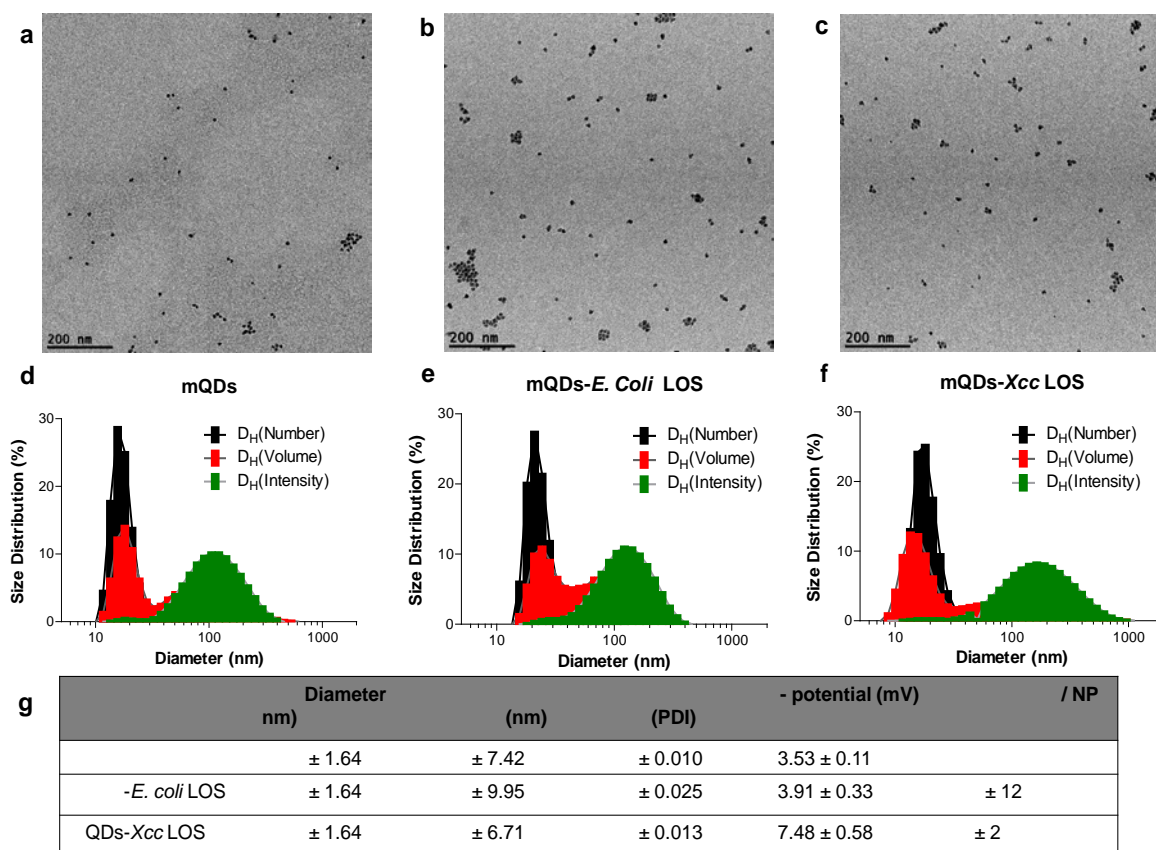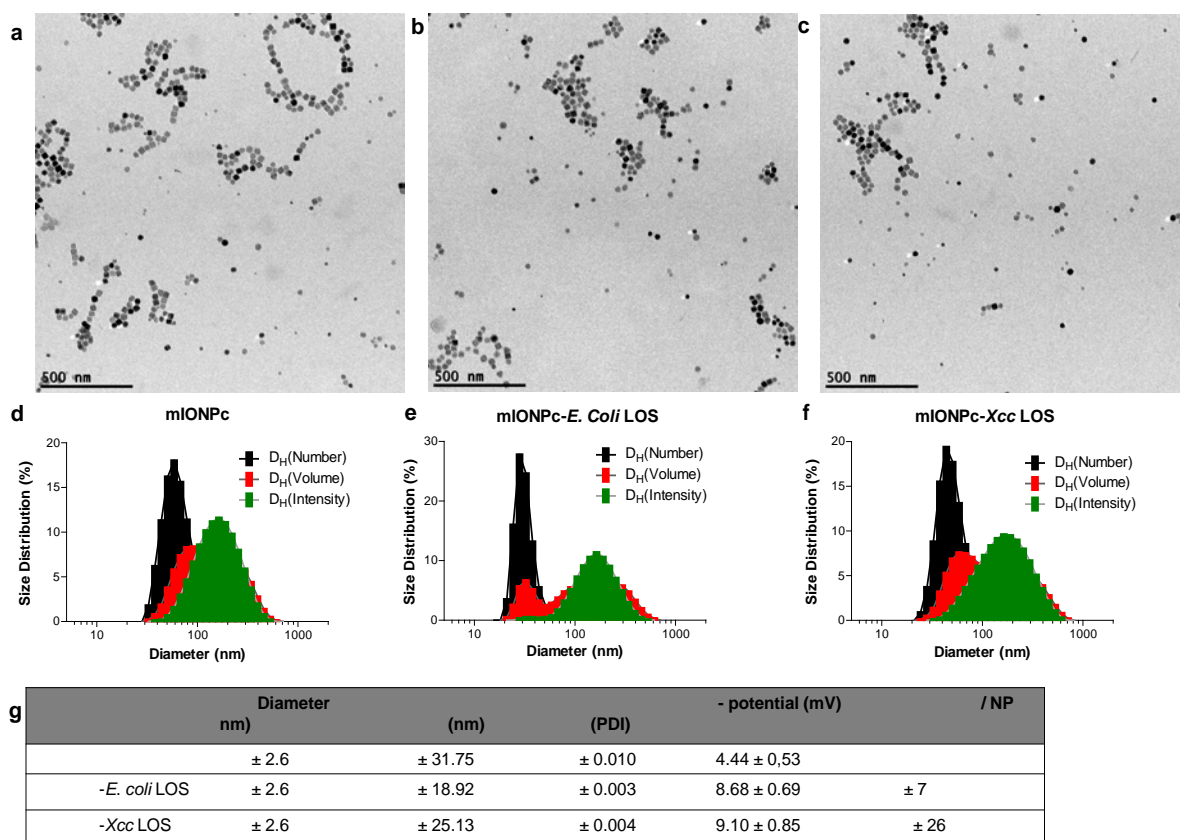
	Diameter			- potential (mV)	/ NP
	nm)	(nm)	(PDI)		
	± 2.6	± 31.75	± 0.010	4.44 ± 0,53	
-*E. coli* LOS	± 2.6	± 18.92	± 0.003	8.68 ± 0.69	± 7
-*Xcc* LOS	± 2.6	± 25.13	± 0.004	9.10 ± 0.85	± 26

% LPS	Micelles		Supernatant 1		Supernatant 2		Supernatant 3	
	CC	LAL	CC	LAL	CC	LAL	CC	LAL
mIONPs-LPS	77.60 ± 6.19	70.09 ± 4.64	11.06 ± 1.66	12.15 ± 3.09	7.35 ± 2.61	8.73 ± 1.01	3.96 ± 3.15	9.01 ± 1.60
mQDs-LPS	27.52 ± 8.78	22.86 ± 3.80	22.81 ± 5.70	25.69 ± 1.69	28.62 ± 7.23	30.64 ± 0.79	21.04 ± 2.56	20.79 ± 2.90
mIONPc-LPS	16.12 ± 6.17	39.55 ± 17.98	39.58 ± 19.07	28.42 ± 11.72	24.27 ± 8.88	20.17 ± 5.64	20.03 ± 14.27	11.88 ± 3.78

Table 1: *Comparison of results from two LPS quantitation methods. IL-6 cytokine production in the macrophage cell line J774A.1 after incubation with the supernatants isolated from the purification of the different mNP-LPS systems: cell-culture-based method and LAL assay. Data are presented as mean ± SEM of three independent experiments each performed in triplicate.*

g	Core Diameter (nm)	Hydrodynamic Diameter (nm)	Polydispersity Index (PDI)	ζ-Potential (mV)	Biomolecule/ NP ratio
mIONPsp	6.56± 1.19	18.70 ± 3.53	0.26 ± 0.015	-6.71 ± 0.86	-
mIONPsp-*E. Coli* LPS	6.56± 1.19	27.08 ± 9.30	0.33 ± 0.07	-7.10 ± 1.04	53 ± 6
mIONPc	26.68 ± 2.57	63.79 ± 31.75	0.16 ± 0.010	-4.44 ± 0,53	-
mIONPc-*E. Coli* LPS	26.68 ± 2.57	218.5 ± 47.29	0.33 ± 0.15	-9.13 ± 2.71	78 ± 14
mQDs	10.41± 1.64	19.59 ± 7.42	0.23 ± 0.010	-3.53 ± 0.11	-
mQDs-*E. Coli* LPS	10.41± 1.64	20.63 ± 7.11	0.38 ± 0.02	-4.59 ± 0.86	15 ± 3
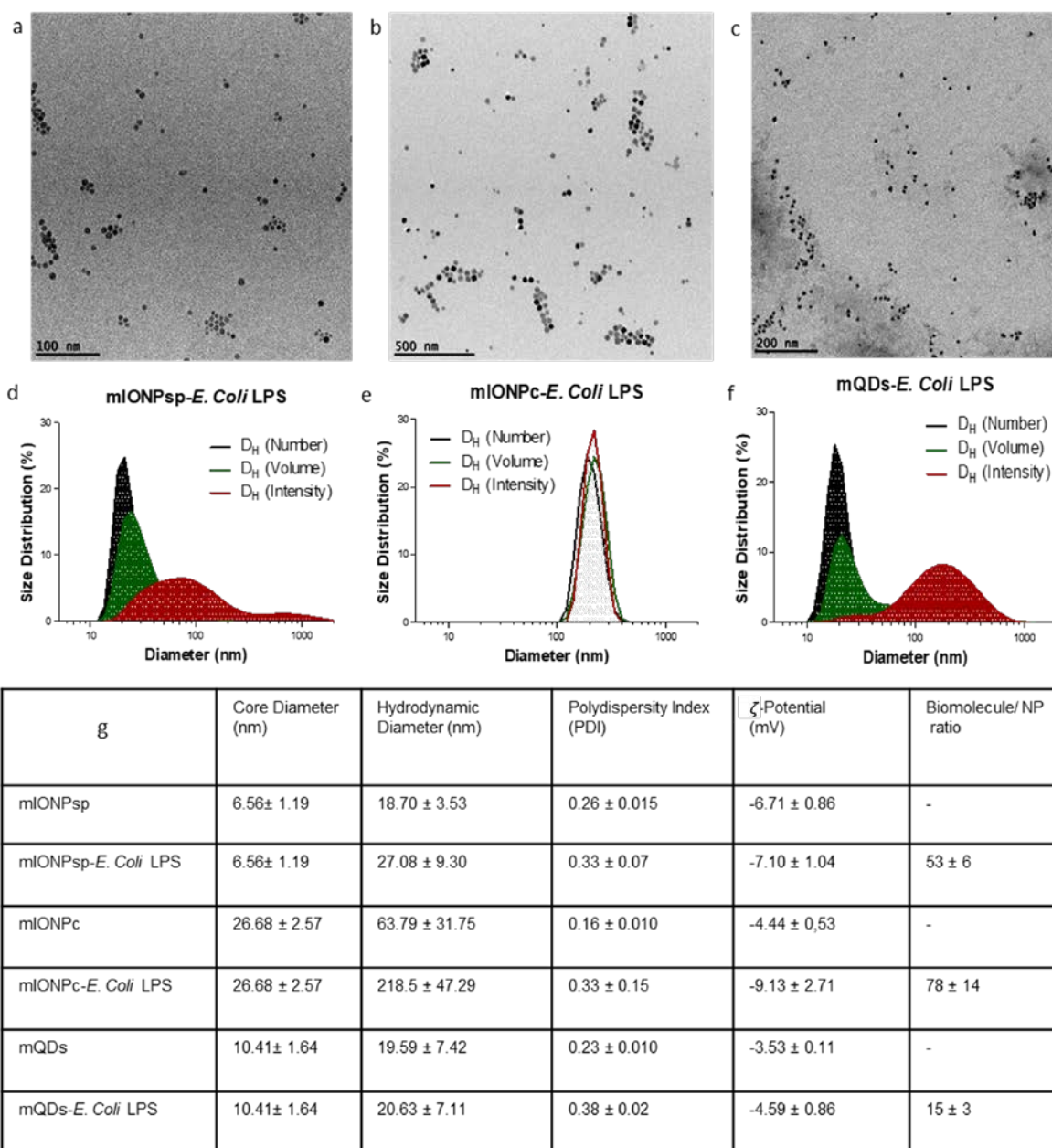
Figure 8: *Size and ζ-potential of mIONPsp, mIONPc and QDs with and without LPS incorporation. TEM images of a) mIONPsp-E. Coli LPS, b) mIONPc-E. Coli LPS and c) mQDs-E. Coli LPS and d), e), f) respective DLS analysis. g) Main characterization data: core diameters from TEM images and counting more than 200 nanoparticles, number-average hydrodynamic diameter and polydispersity index obtained by DLS, ζ-potential and number of biomolecules per nanoparticle based on n > 2 formulation replicates.*

Figure 9: *Quantitation of TLR4 loading in a, b) mIONPsp, c, d) mQDs and e, f) IONPc. After pelleting the mNPs-LOS by three cycles of centrifugation, IL-6 cytokine production in the macrophage cell line J774A.1 after 24 h incubation with the supernatants was compared with the dose-response curves obtained with the corresponding free LOS. Data are presented as mean ± SEM of independent experiments each performed in triplicate.*

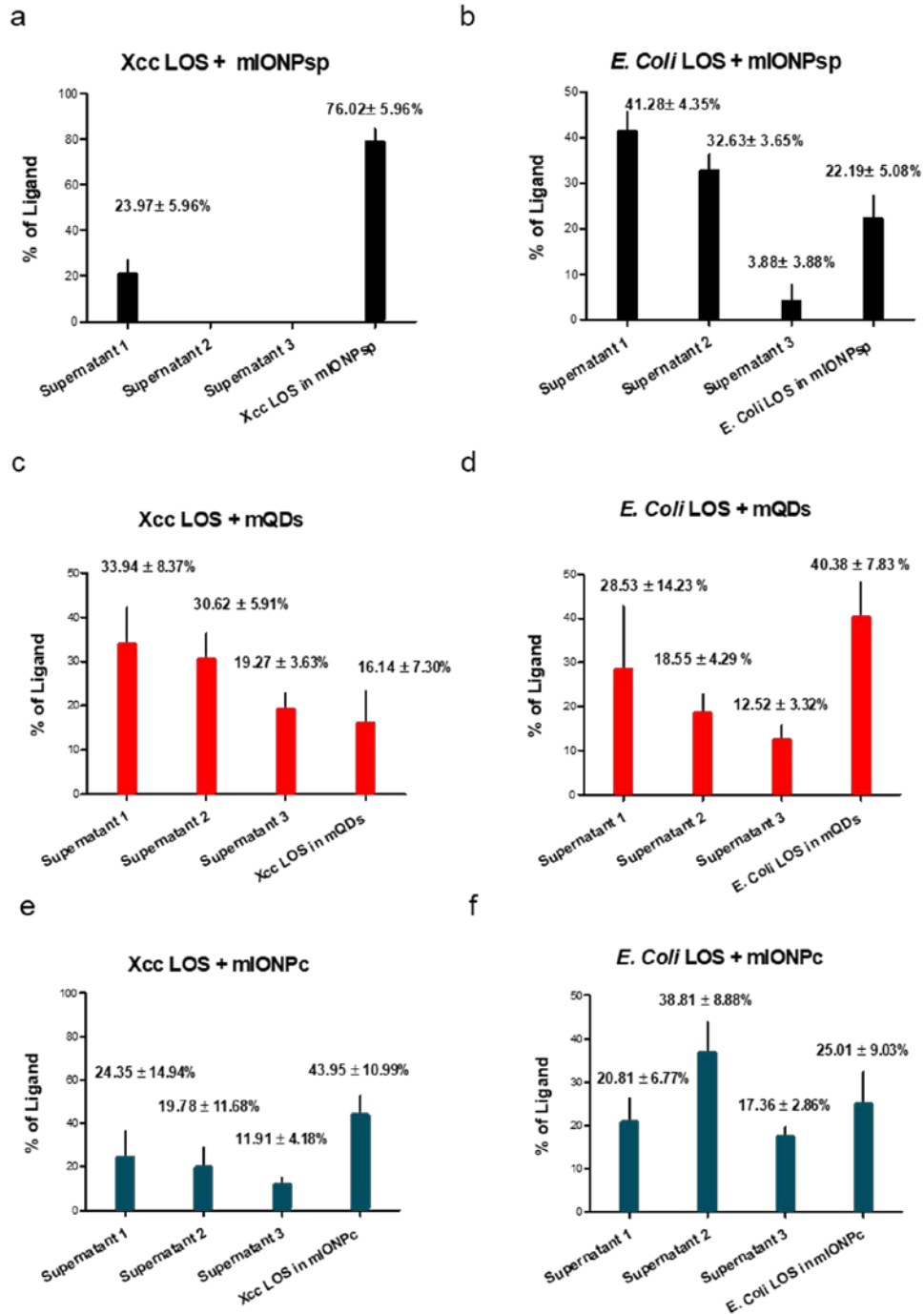To assess the stability of the mIONPsp-*Xcc* LOS over time, their size was analyzed immediately after purification and over a 4-week period in 10 mM PBS. Although the results showed some aggregation over time, the size of the mIONPsp Xcc LOS was still within the ideal range for reaching the lymph nodes (**Figure 10**). To study the *Xcc* LOS molecules release over time, 10 mM PBS solutions of the mIONPsp-*Xcc* LOS were centrifugated at designed time points (week 0, 1 and 2), with the amount of *Xcc* LOS in the supernatants determined as described below. The results showed that only 5% of the *Xcc* LOS molecules are released. In the outer membrane of gram-negative bacteria the negatively charged LPS molecules cover most of the outer surface and divalent cations such as Mg^{2+} and Ca^{2+} are essential to neutralize this negative charge and allow strengthening of the lateral interactions between neighboring LPS molecules, which provides enhanced stability for the external bacterial membrane[45–47]. Similar electrostatic interactions and effects such as increased hydrogen bonding and tighter lipid packing and cross-linking exerted by divalent cation bridging can be expected to take place in the pathogen-mimetic mNP-LOS nanostructures to provide the observed stability.
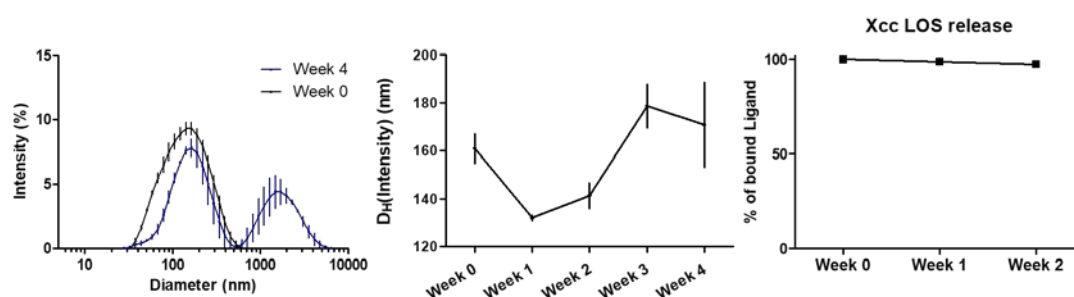
Figure 10: *Stability and Xcc LOS release for mIONPsp-Xcc LOS in 10 mM PBS.*

2.2.2: In vitro activity of the pathogen-mimicking mNPs

Many studies have shown that the immune response to LPS is dictated by their chemical structure. Besides, it has been reported that LPS as amphiphilic molecules form supramolecular aggregates in aqueous environments and that these structures are the biologically active units of LPS.[48] However, the type of supramolecular aggregates structures formed also depends strongly on the chemical structure of the LPS molecules. Incorporation into mNPs ensures the formation of supramolecular structures where multiple copies of the LPS molecules are clustered, and therefore

they would be equally or even more active than the mNP-free preparations. When stimulating the macrophage cell line J774A.1 with the different TLR4 ligands to produce IL-6, the biological activity of *E. coli* LPS showed greater IL-6 production in comparison to equal amounts of *E. coli* LOS or *Xcc* LOS, and lower cell viability. Comparison of IL-6 production and cell viability of the TLR4 ligands compared to TLR4 ligand-loaded mNPs showed that the immunostimulatory properties and cytotoxicity of the two ligands is modulated by each of the mNPs differently. Incorporation into mIONPsp enhanced IL-6 production and significantly reduced cytotoxicity for *Xcc* LOS (**Figure 11***b*), while it did not affect the activity of *E. Coli* LOS. (**Figure 11***a*).

Figure 11: *Immunostimulatory activity and cytotoxicity of a) mIONPsp-E. Coli LOS and b) mIONPsp-Xcc LOS in antigen presenting cells. J774A.1 macrophages were incubated for 24 h at 37 °C with the indicated formulations. Cytokines released in the supernatants were quantified by ELISA and cell viability was determined by the MTT assay. ****P<0.0001, ***P<0.001, **P<0.01, *P<0.05, ns = non significant by (a, b) two-way ANOVA followed by Bonferroni's test. Data show mean ± SEM of 3 independent experiments.*

In contrast, *E. coli* LOS incorporation into the mIONPc lead to reduced IL-6 production and significantly increased cytotoxicity (**Figure 12**a), while incorporation of Xcc LOS into the mIONPc did not affect its toxicity but lowered the immune stimulating capacities of the ligand (**Figure 12**b). The mQDs enhanced IL-6 production of the ligand *E. Coli* LOS without affecting its cytotoxicity (**Figure 13**a), while they did not significantly affect the activity and toxicity of the ligand *Xcc* LOS (**Figure 13**b). On the basis of these results, the mIONPsp-*Xcc* LOS system was selected for further studies.
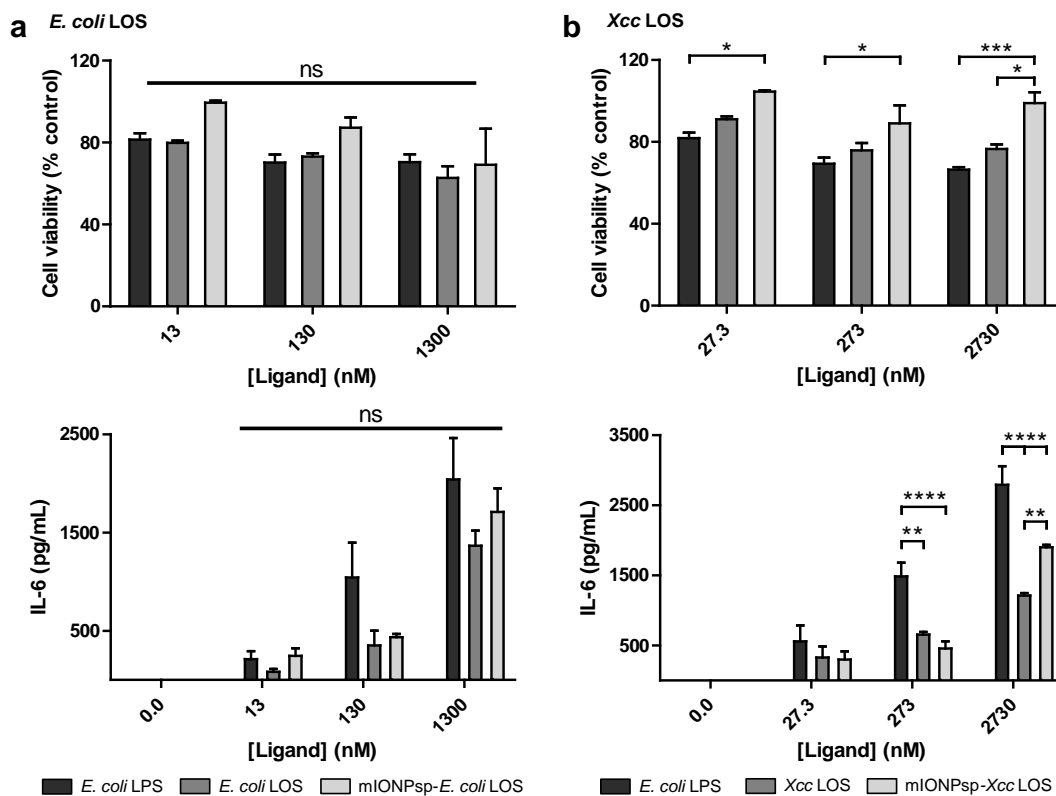

Figure 12: *Immunostimulatory activity and cytotoxicity of a) mIONPc-E. Coli LOS and b) mIONPc-Xcc LOS in antigen presenting cells. J774A.1 macrophages were incubated for 24 h at 37 °C with the indicated formulations. IL-6 released in the supernatants was quantified by ELISA and cell viability was determined by the MTT assay. ****P<0.0001, **P<0.01, *P<0.05, ns = non significant by two-way ANOVA followed by Bonferroni's test. Data show mean ± SEM of 3 independent experiments.*
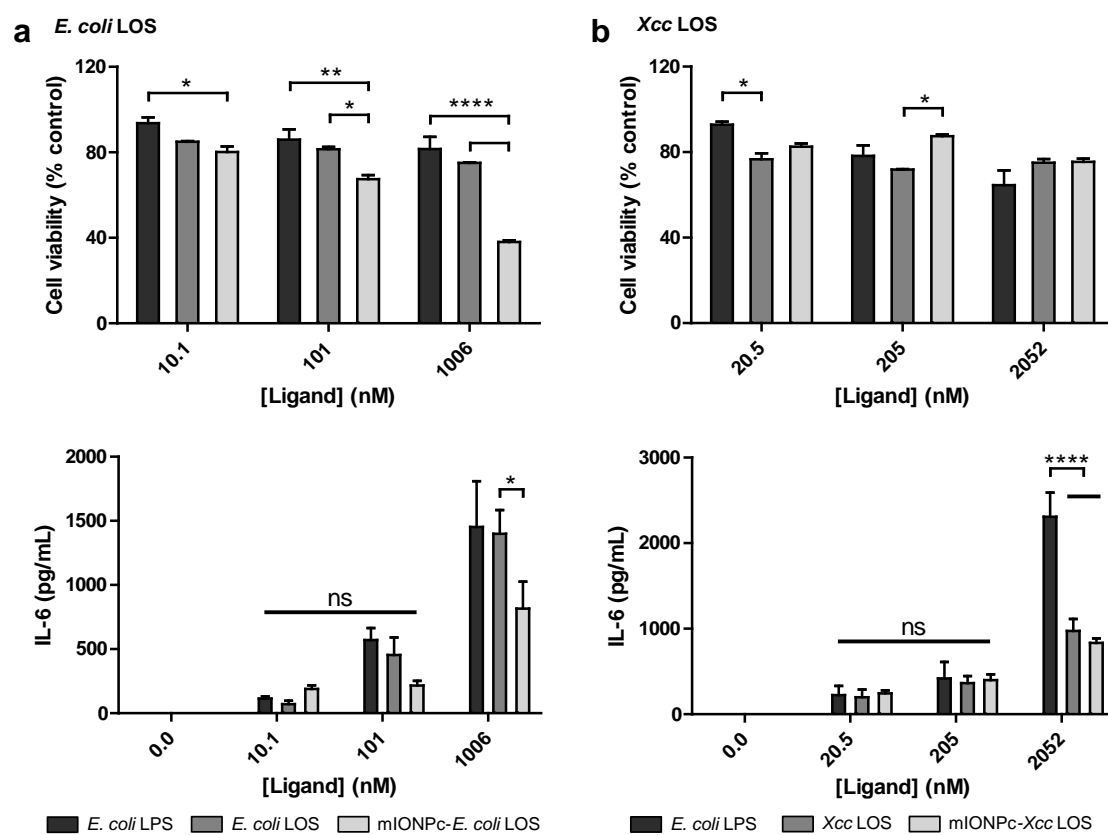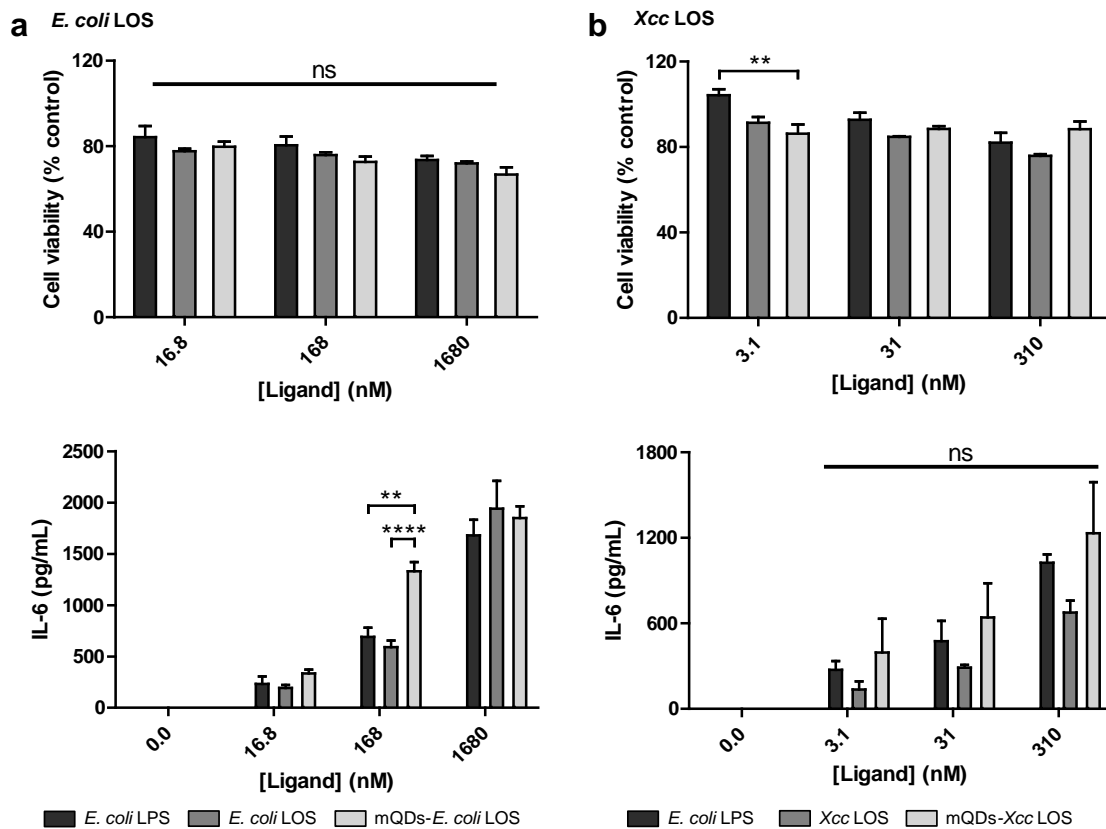
Figure 13: *Immunostimulatory activity and cytotoxicity of a) mQDs-E. Coli LOS and b) mQDs-Xcc LOS in antigen presenting cells. J774A.1 macrophages were incubated for 24 h at 37 °C with the indicated formulations. IL-6 released in the supernatants was quantified by ELISA and cell viability was determined by the MTT assay. ****P<0.0001, **P<0.01, ns = non significant by two-way ANOVA followed by Bonferroni's test. Data show mean ± SEM of 3 independent experiments.*

2.2.3: Uptake of mIONPsp-*Xcc* LOS by antigen presenting cells

The uptake of both drug-free mIONPsp and mQDs was assessed in J774A.1 murine macrophages by fluorescence microscopy. To enable tracking of the mIONPsp during cellular uptake a 5% rhodamine B-labeled phospholipid was incorporated during the micelle synthesis. The mIONPsp(Rho)-*Xcc* LOS was characterized and showed only a slight increase in size and a slight decrease in the ζ-potential compared to the mIONPsp-*Xcc* LOS system (**Figure 14**). In the case of the mQDs, the bright red luminescence (620 nm) was used for tracking. The results show that both mIONPsp and mQDs are uptaken by the cells within 3 h at nanomolar concentrations (**Figure 15**).
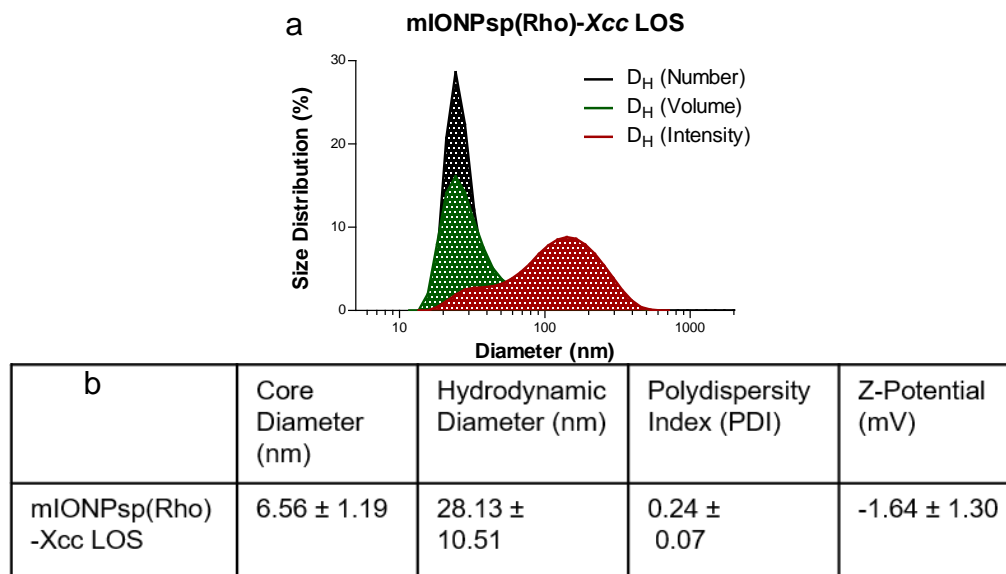
Figure 14: *a) Size and ζ-potential of mIONPsp(Rho)-Xcc LOS and b) main characterization data obtained by DLS and ζ-potential based on n > 3 formulation replicates.*
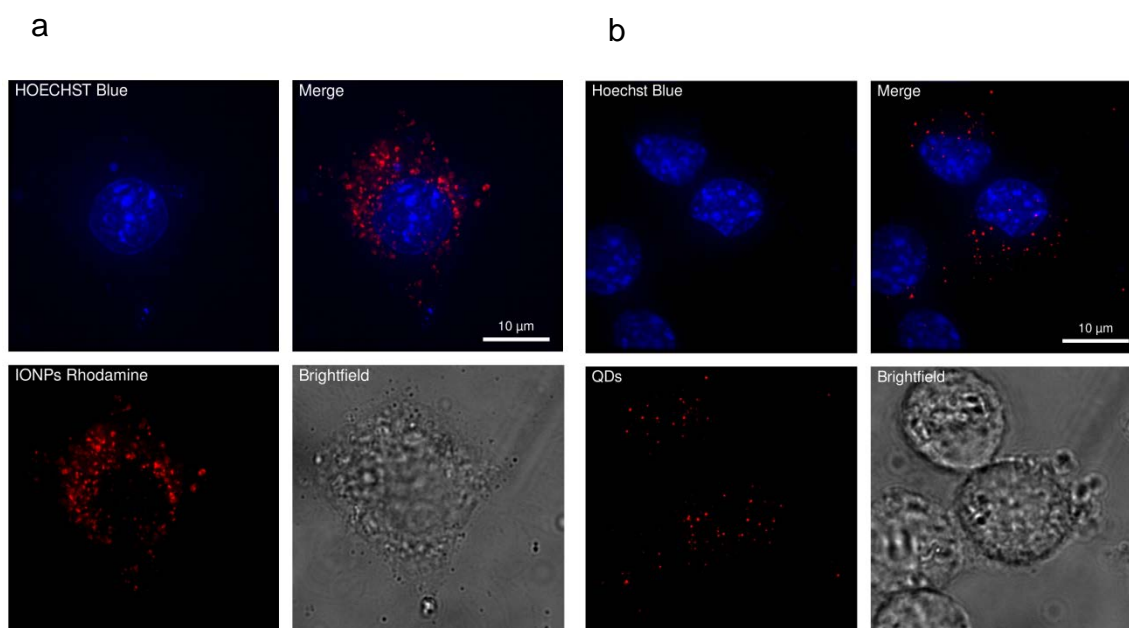

Figure 15: *Stacked fluorescence microscopy images of a) mIONPs(Rho) and b) mQDs, showing uptake of the micelles in cells.*

TLR4 is the only TLR that activates both the MyD88- and TRIF-dependent pathways[49]. LPS binding to TLR4 induces MyD88- and TRIF-dependent pathways

from the plasma membrane and endosomes, respectively. It has been shown that after TLR4 encounters LPS, endosomes showing LPS and TLR4 co-localization appear within 15 min[50]. As expected, mIONPsp(Rho)-*Xcc* LOS co-localized with lysosomes in J774A.1 cells (***Figure 16***).
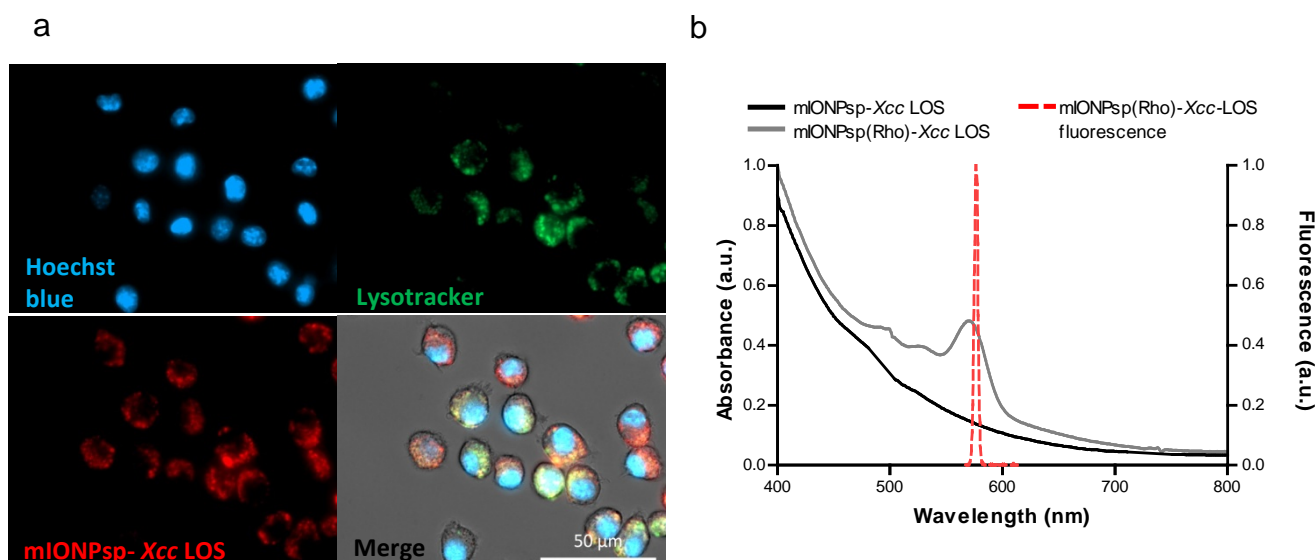
Figure 16: *In vitro uptake and trafficking of rhodamine-labeled mIONPsp-Xcc LOS. micelles. a) Fluorescence microscopy images of J774A.1 showing endocytic uptake of mIONPsp(Rho)-Xcc LOS after 3 h incubation. Cells' nuclei were stained with Hoechst blue and lysosomes and endosomes with Lysotracker green. b) UV-vis absorption and fluorescence spectrum of mIONPsp(Rho)-Xcc LOS.*

2.2.4: Synthesis and characterization of core/shell *NaYF₄: Yb³⁺/ Tm³⁺@NaYF₄* UCNPs

Herein, the steps made towards the preparation of a light-triggered nanoplatform for TLR4 modulation will be discussed.

Hydrophobic core/shell UCNPs were prepared following the procedures already reported in the literature by our research group[36]. Core $NaYF_4$ $Yb^{3+}/$ Tm^{3+} (69.5/30/0.5 mol%) UCNPs were synthesized by thermal decomposition in the presence of oleic acid and 1-octadecene under inert nitrogen atmosphere and using standardized Schlenk techniques and next used as seeds for growing a protective $NaYF_4$ shell, yielding *core/shell* ($NaYF_4$: $Yb^{3+}/$ $Tm^{3+}@NaYF_4$) UCNPs. These UCNPs displayed multiple emission maxima typical of Tm^{3+} electronic transitions: at

345 and 360 nm ($^3P_0 \to {}^3F_4$ and $^1D_2 \to {}^3H_6$), 450 and 475 nm ($^1D_2 \to {}^3F_4$ and $^1G_4 \to {}^3H_6$), 645, 690 and 720 nm ($^1G_4 \to {}^3F_4$ and $^3F_3 \to {}^3H_6$) and at 800 nm ($^3H_4 \to {}^3H_6$)[51] (**Figure 17**). These core-shell UCNPs were characterized by TEM, DLS, X-ray photoelectron spectroscopy (XPS) and infrared spectroscopy (IR). The TEM micrograph shows rod-like hydrophobic nanoparticles with an average length of 39.20 ± 6.64 nm and a uniform size distribution (**Figure 18**).
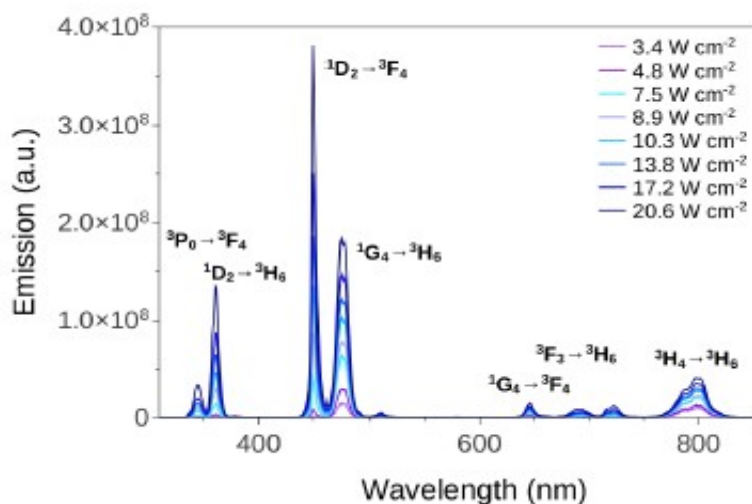
Figure 17: *Upconversion emission pattern of NaYF$_4$: Yb^{3+}/Tm^{3+} @NaYF$_4$ (0.5 mg/mL in THF) upon 980 nm excitation at different laser powers (3.4– 20.6 W/ cm^{-2}). Adapted from reference[36]. Reproduced by permission of The Royal Society of Chemistry.*
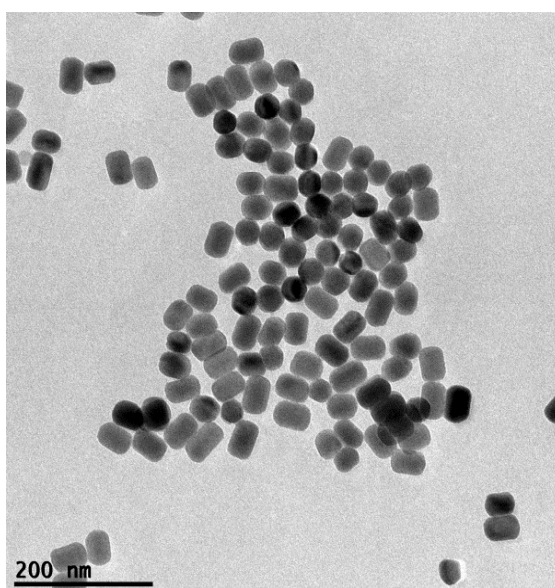
Figure 18: *TEM image of the prepared core/shell NaYF$_4$: Yb^{3+}/ Tm^{3+} @NaYF$_4$ UCNPs.*

XPS analysis was performed to study the composition of the obtained UCNPs. The spectrum confirms the presence of the elements composing the prepared UCNPs being C, O, F, Na, Y, Yb and Tm as assigned by core levels and Auger electrons (**Figure 19**).
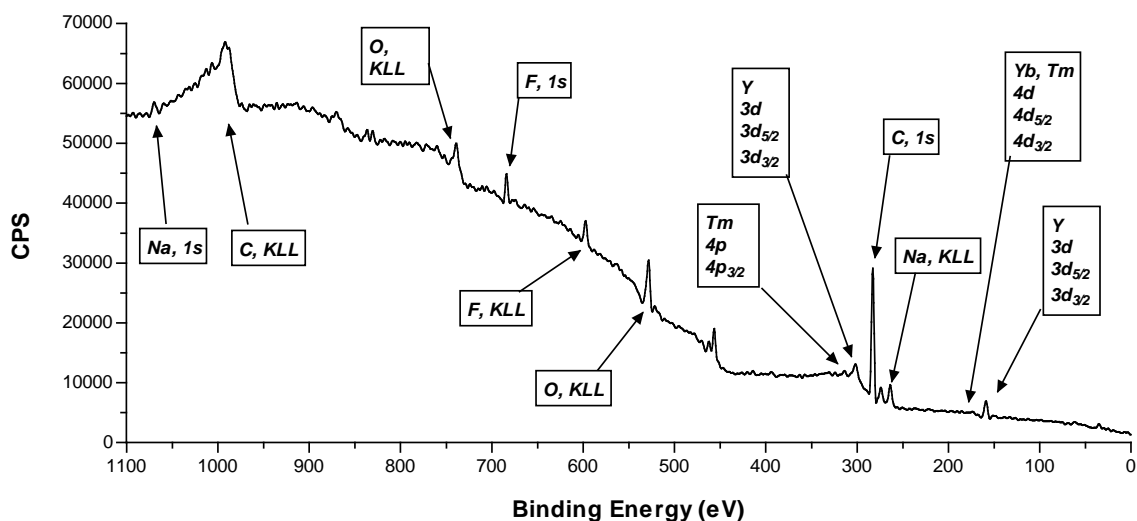
Figure 19: *XPS spectrum of the prepared core-shell NaYF$_4$: Yb^{3+}/ Tm^{3+}@NaYF$_4$ UCNPs.*

The IR spectrum of the UCNPs was recorded and compared with that of the free ligands, and the IR analysis confirms the presence of oleic acid in both core and core-shell UCNPs and reveals its interaction with the nanoparticles (**Figure 20**).
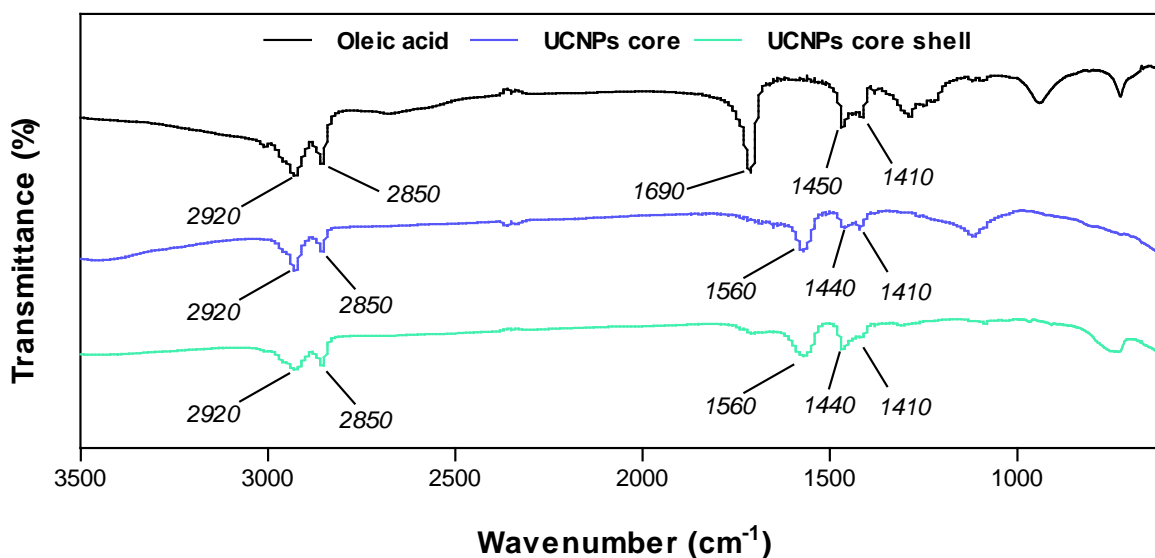
Figure 20: *IR spectrum of oleic acid, core (NaYF$_4$: Yb^{3+}/ Tm^{3+}) and core-shell (NaYF$_4$: Yb^{3+}/ Tm^{3+}@ NaYF$_4$) UCNPs.*

2.2.5: Functionalization of UCNPs with IAXO 102

Both control UCNP-filled micelles (without any bioactive ligand) and UCNPs functionalized with the TLR4 antagonist IAXO 102 were prepared and characterized. UCNPs were solubilized in aqueous solutions using PEGylated phospholipids, adding the hydrophobic IAXO 102 and using the self-assembly process illustrated in **Figure 21**. The resulting mUCNPs were centrifuged and the pelleted mNPs were redissolved in aqueous solution (3 cycles) to remove nanoparticle-free micelles and any unbound ligand.

The characterization of both mUCNPs and mUCNPs-*IAXO 102* was performed by TEM and DLS, showing rod-like particles with uniform size distribution. For mUCNPs, the number-averaged size corresponds to ca. 65 nm (**Figure 22**). To prepare mUCNPs-*IAXO 102*, the same procedure was used but in the presence of the TLR4 ligand IAXO 102. Two different systems were prepared – one with 5% of IAXO 102 (measured in moles) relative to PEG-phospholipid (mUCNPs-*IAXO 102-5%),* and another with 15% of IAXO (mUCNPs-*IAXO 102-15%)* to PEG-phospholipid*.* These systems were characterized by TEM and DLS (**Figure 23** and **Figure 24**). Both systems showed low polydispersity (0.20 and 0.18 for mUCNPs-*IAXO 102-5%* and mUCNPs-*IAXO 102-15%* respectively).
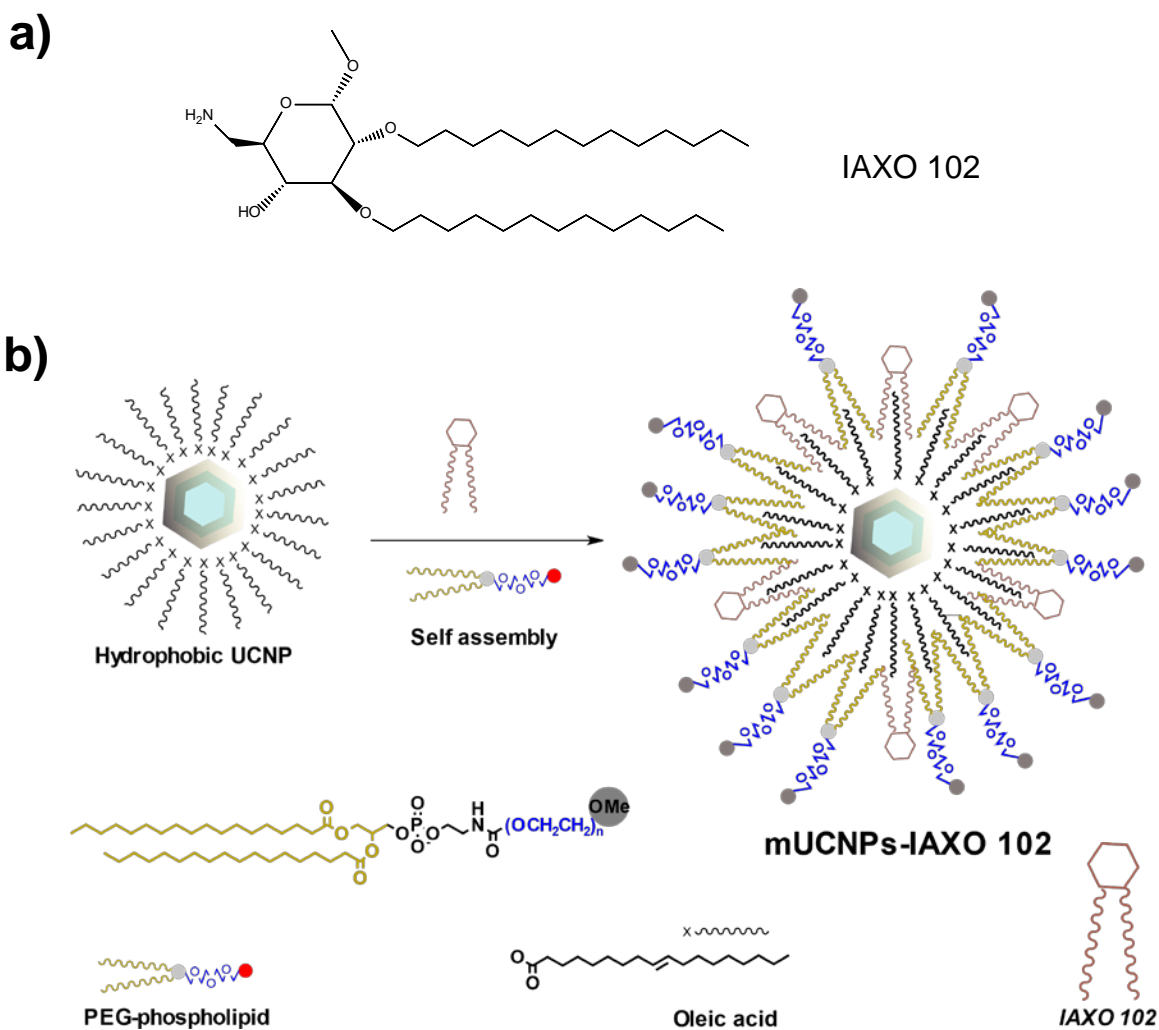
Figure 21: a) Molecular structure of the TLR4 antagonist IAXO 102; b) Generic representation of the interactions between the PEG phospholipids, IAXO 102 and the hydrophobic UCNPs forming mUCNPs-IAXO 102.
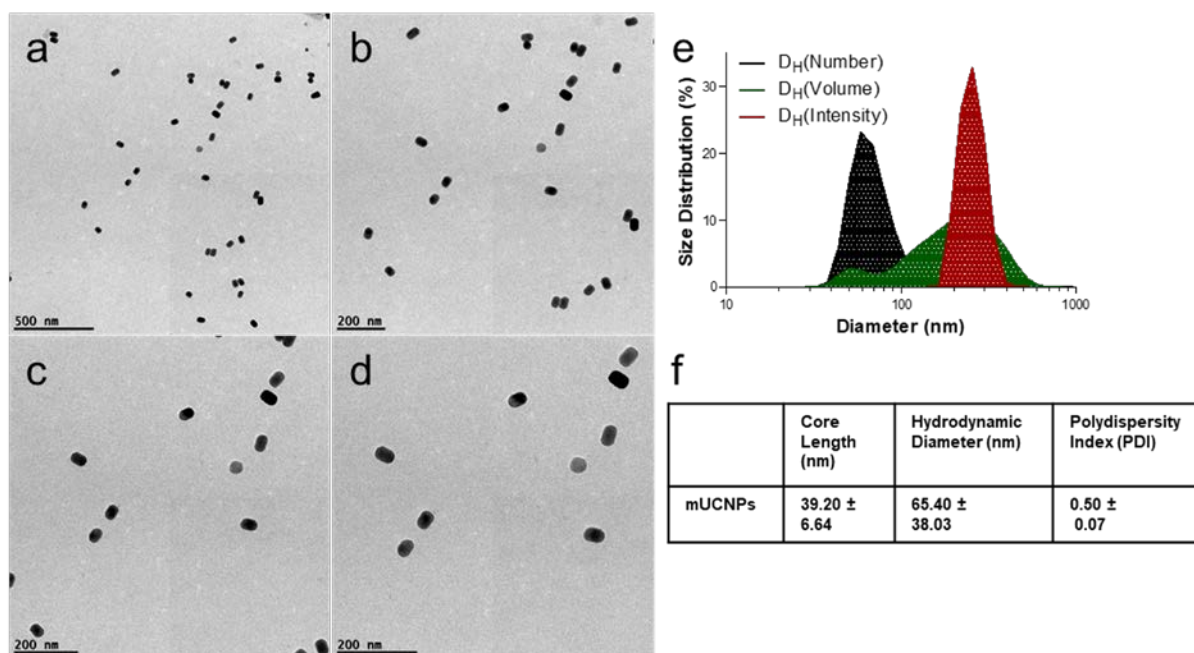
Figure 22: *Characterization of mUCNPs. a-d): TEM images taken at different magnifications (12000x; 15000x; 20000x; 25000x); e) size distribution of mUCNPs; f) table summarizing the main mUCNPs characterization data: UCNPs length from TEM images and counting more than 200 nanoparticles, number-average hydrodynamic diameter and polydispersity index obtained by DLS. Data based on n > 3 formulation replicates.*

The number-averaged hydrodynamic diameter of both the mUCNPs-*IAXO 102* was higher than the hydrodynamic diameter of mUCNPs (81.00 ± 50.34 for mUCNPs-*IAXO 102-5%* and 99.91 ± 41.14 for mUCNPs-*IAXO 102-15%* versus 65.40 ± 38.03 for mUCNPs) (**Figure 23**g, **Figure 24**g and **Figure 22**g respectively). The hydrodynamic diameter of the UCNPs-filled nanosystems is within the range of 20-100 nm ideal for lymph node delivery.
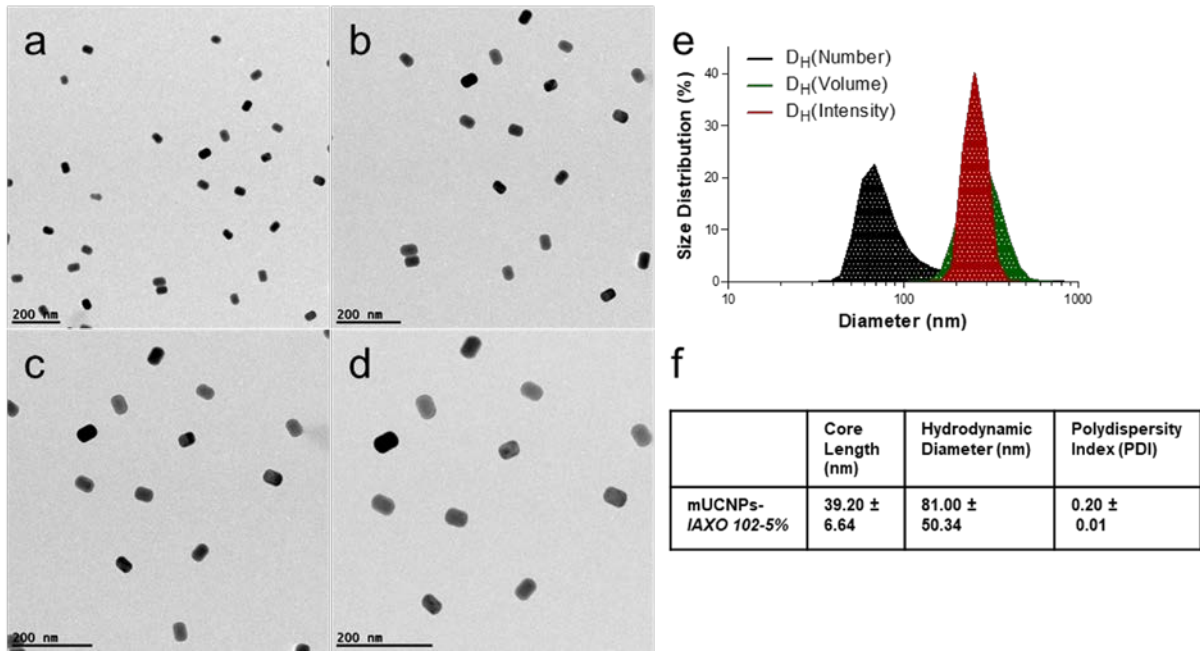
Figure 23: *Characterization of mUCNPs-IAXO 102-5%. a-d) TEM images at different magnifications (15000x; 20000x; 25000x; 30000x); e) mUCNPs-IAXO 102-5% size distribution; f) table summarizing the main mUCNPs-IAXO 102-5% characterization data: UCNPs length from TEM images and counting more than 200 nanoparticles, number-average hydrodynamic diameter and polydispersity index obtained by DLS. Data based on n > 3 formulation replicates.*
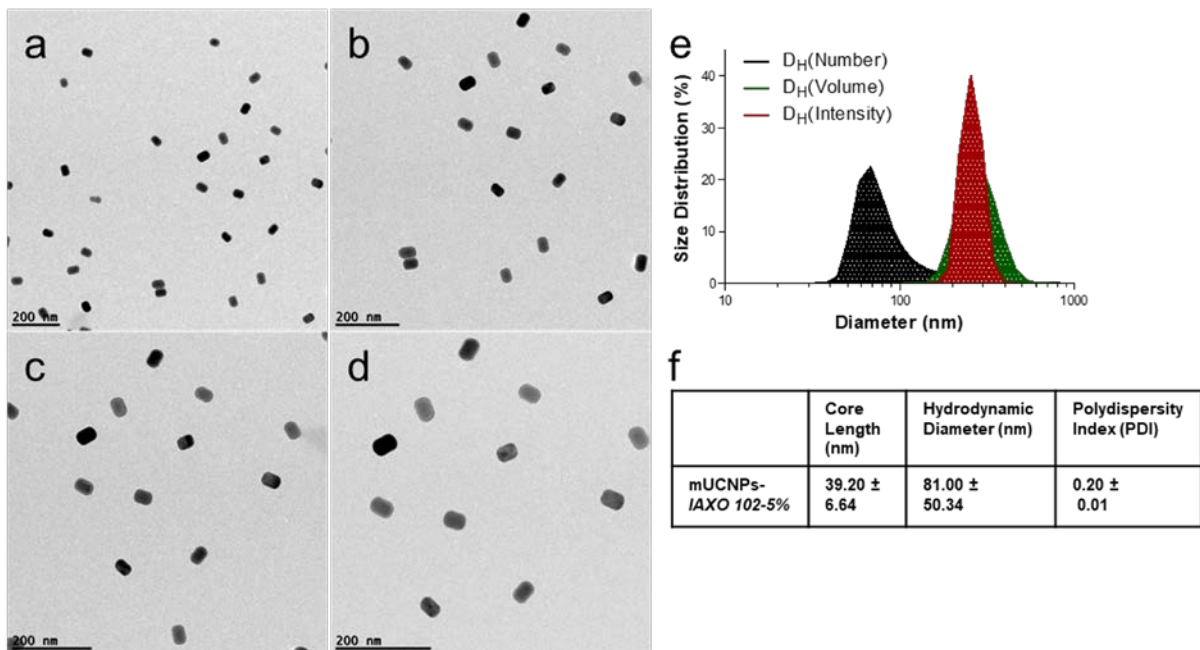
Figure 24: *Characterization of mUCNPs-IAXO 102-15%. a-d) Transmission electron microscopy (TEM) images at different magnifications (15000x; 20000x; 25000x; 30000x); e) mUCNPs-IAXO 102-15% size distribution; f) table*

summarizing the main mUCNPs-IAXO 102-15% characterization data: UCNPs length from TEM images and counting more than 200 nanoparticles, number-average hydrodynamic diameter and polydispersity index obtained by DLS. Data based on n > 3 formulation replicates.

2.2.6: In vitro activity of IAXO 102

The biological activity of IAXO 102 and IAXO 102-functionalized UCNPs as antagonists of LPS was tested in murine J774A.1 macrophages by measuring its capacity to inhibit the L P S - i n d u c e d production of IL-6 and compared to the LPS antagonist polymyxin B (PmB) as a positive control. While the highly cationic PmB forms electrostatic interactions with the negatively charged LPS inhibiting its capacity to bind to TLR4[52], IAXO 102 is expected to compete[53,39] with LPS for the binding sites on the TLR4 hydrophobic pocket. Both mechanisms should decrease the IL-6 release in the supernatants of the LPS stimulated cells. Cells were stimulated with three different concentrations of LPS (66, 6.6 and 0.66 nM) and three different concentrations of PmB and IAXO 102 (both 10, 5 and 1 µM) as antagonists.

Both IAXO 102 and PmB without any LPS stimulation did not show immunostimulatory properties or toxicity in J774A.1 cells at the explored concentrations (***Figure 25***). When administered with LPS, IAXO 102 did not show any antagonist activity. On the contrary, at most of the IAXO 102 and LPS concentrations tested, IAXO 102 seems to turn LPS into a more powerful immunostimulant (***Figure 26***). In contrast, PmB suppressed stimulation by LPS effectively. These results in macrophages are in disagreement with the results reported by Piazza et al.[39], which show effective TLR4 inhibition by compound IAXO 102 in a model using HEK-Blue-4 cells. This model is based on HEK293 cells stably transfected with TLR4, MD2, CD14 genes and engineered to stably express an optimized alkaline phosphatase gene, sAP, which allows monitoring of the activation of TLR4 signal pathway by endotoxin. The difference in the experimental settings played a role, but in the chosen experimental model, no meaningful modulation of the endotoxin's activity was observed despite the promising results obtained by the authors.
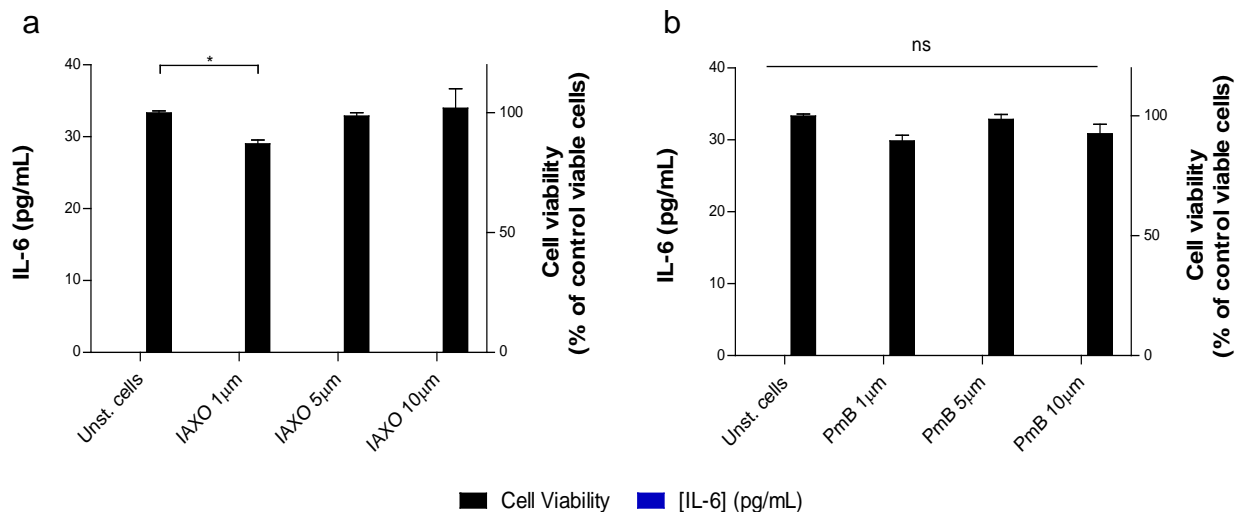
Figure 25: *Administration of IAXO 102 and PmB to J774A.1 macrophages. a) Cytotoxicity and b) immunomodulatory activity of IAXO 102 and PmB in the absence of LPS. *P<0.05, ns = non significant by two-way ANOVA followed by Bonferroni's test. Data shown as Mean ± SEM of triplicates of a representative experiment out of three independent ones.*
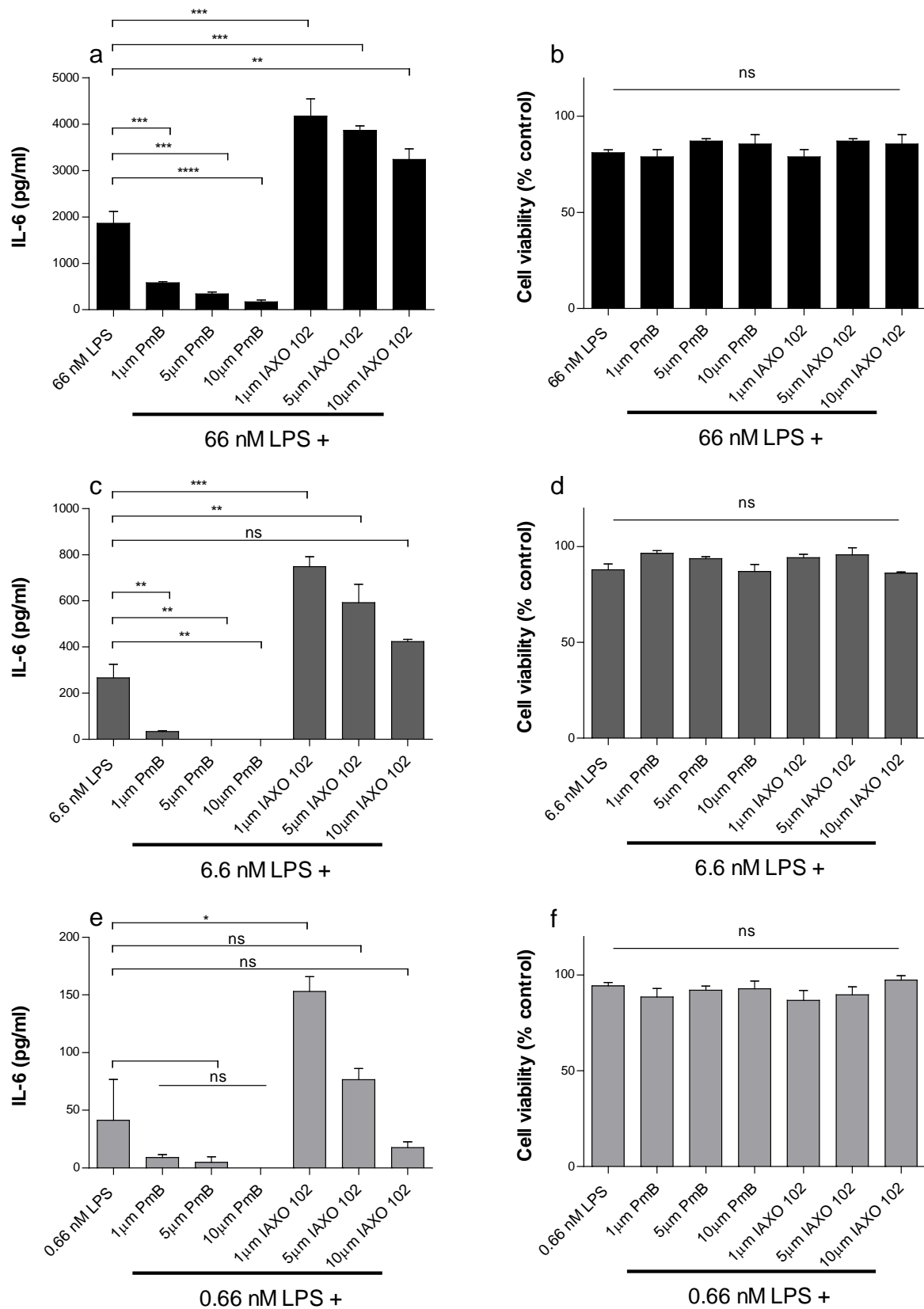
Figure 26: *Cytotoxicity and immunomodulatory activity of LPS are modulated by IAXO 102 and PmB. a, b) IL-6 production and cell Viability in J774A.1 macrophages when stimulated with 66 nm LPS and different concentrations of*

IAXO 102 and PmB; c, d) IL-6 production and Cell Viability in J774A.1 macrophages when stimulated with 6,6 nm LPS and different concentrations of IAXO 102 and PmB; e, f) IL-6 production and Cell Viability in J774A.1 macrophages when stimulated with 0,66 nm LPS and different concentrations of IAXO 102 and PmB; ****P<0.0001, ***P<0.001, **P<0.01, *P<0.05, ns = non significant by two-way ANOVA followed by Bonferroni's test. Data shown as Mean ± SEM of triplicates of a representative experiment out of three independent ones.

2.2.7: In vitro activity of IAXO 102-functionalized UCNPs

The prepared mUCNPs and mUCNPs-*IAXO 102* were tested in J774A.1 mouse macrophages to assess their cytotoxicity and immune-suppressive/stimulatory activity. Prior to using mUCNPs-*IAXO 102,* the immune stimulating activity and cytotoxicity of the drug-free mUCNPs were measured, and the results showed that they are not toxic at the administered concentrations (**Figure 27***a*) and do not induce any IL-6 production (**Figure 27***b*). When administer together with LPS, mUCNPs can slightly increase LPS' toxicity (**Figure 27***c*), on the other hand the immune stimulating activity of LPS is affected by the presence of drug-free mUCNPs which can slightly suppress the IL-6 release (**Figure 27***d*).

J774A.1 cells were thus stimulated with LPS and the two mUCNPs-*IAXO 102* prepared, respectively mUCNPs-*IAXO 102-15%* and mUCNPs-*IAXO 102-5%* (herein named A and B for clarity purposes). At the tested concentrations of mUCNPs-*IAXO 102*, it seems that the IAXO 102-loaded systems and drug-free UCNPs are more effective at suppressing the LPS-induced activity than free IAXO 102. but induce more cell death (**Figure 28**). One hypothesis might be that the mUCNPs could degrade in the lysosomes, releasing the hydrophobic nanoparticles, and the alkyl chains belonging to the oleic acid coating the UCNPs could act on their own as TLR4 modulators by insertion in the hydrophobic pocket of the TLR4.
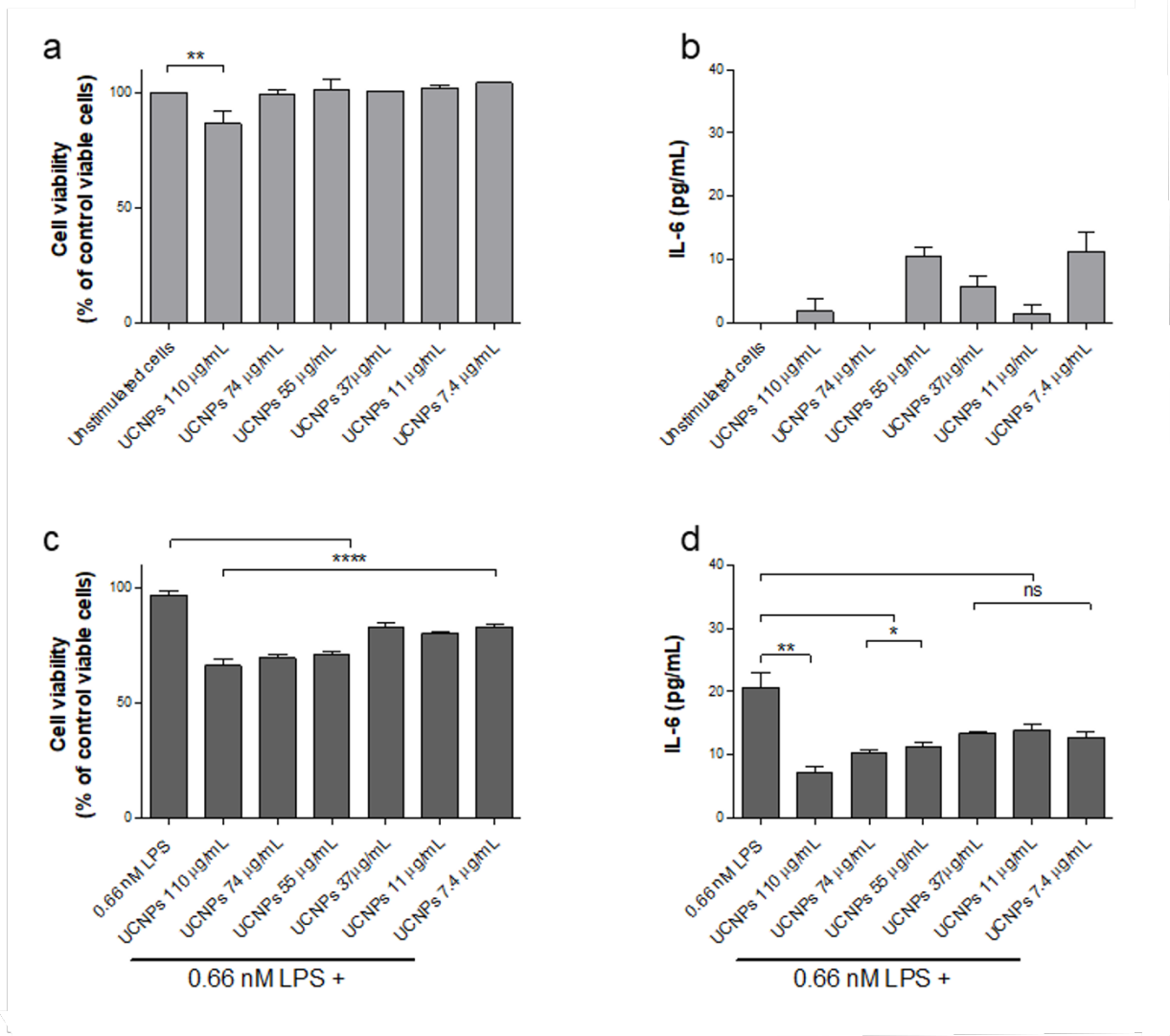
Figure 27: *Effect (IL-6 release and viability) of core-shell mUCNPs on J774.1 mouse macrophage cells. a) toxicity and b) immunostimulatory activity of UCNPs, c) toxicity and d) immunostimulatory activity of UCNPs administered wuth LPS. ****P<0.0001, ***P<0.001, **P<0.01, *P<0.05, ns = non significant by two-way ANOVA followed by Bonferroni's test. Data shown as Mean ± SEM of triplicates of a representative experiment out of three independent ones.*
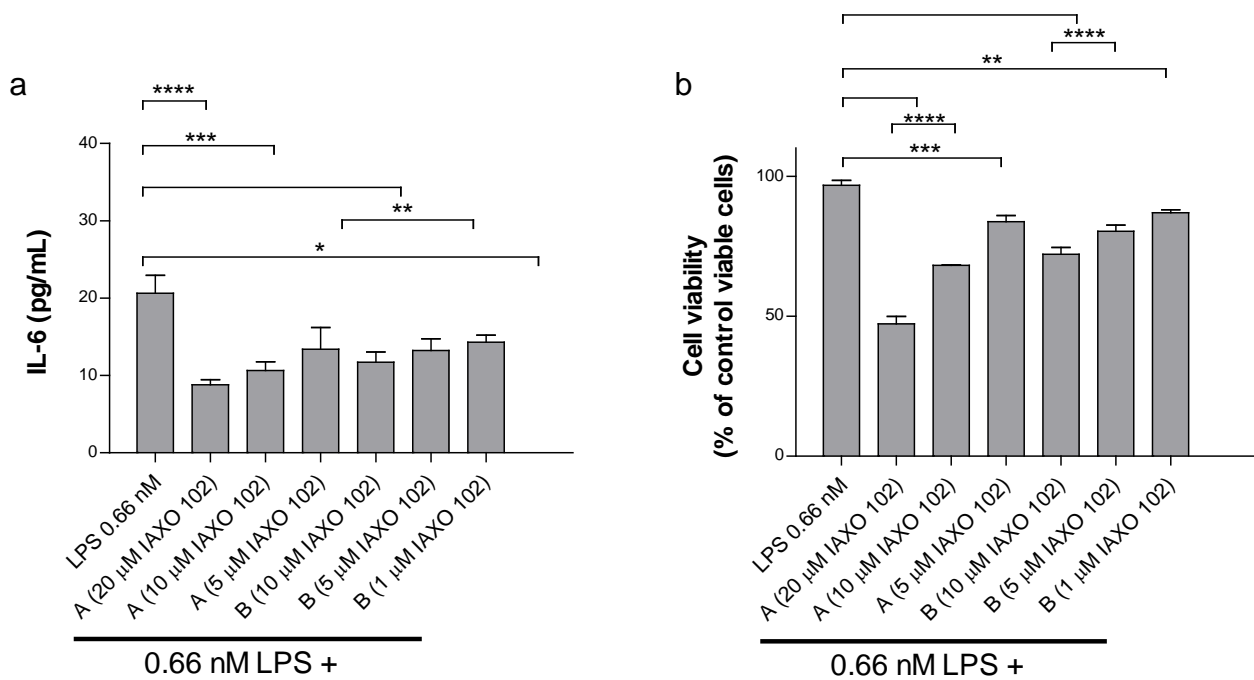
Figure 28: *a) IL-6 release and b) cell viability of mUCNPs-IAXO 102-15% and mUCNPs-IAXO 102-5% on J774.1 mouse macrophage cells. **** P<0.0001, ***P<0.001, **P<0.01, *P<0.05 by two-way ANOVA followed by Bonferroni's test. Data shown as Mean ± SEM of triplicates of a representative experiment out of three independent ones.*

2.3: Conclusions

In summary, a nanoplatform based on pathogen-mimicking TLR4 agonist functionalized structures was designed and developed. The system is comprised of IONPsp encapsulated in phospholipid micelles where the LOS derived from the plant pathogen *Xcc* as TLR4 agonist was adhered by hydrophobic interactions. Unlike MPLA, both E. Coli LOS and the structurally unique *Xcc* LOS allowed effective interaction with IONPsp-, IONPc- and QDs-filled micelles for the generation of stable pathogen-mimicking nanostructures with size, charge and hydrophobicity ideal for lymph node delivery. Each of the new prepared nanosystems, namely mIONPsp-*Xcc* LOS, mIONPsp-*E. Coli* LOS, mIONPc-*Xcc* LOS, mIONPc-*E. Coli* LOS, mQDs-*Xcc* LOS, and mQDs-*E. Coli* LOS were administered to J774A.1 macrophages to select the best adjuvant based on their toxicity profile and immune stimulating capacities. The results showed that each nanoparticle modulates the ligand's activity in a different manner. Amongst the generated nanostructures, the mIONPsp-*Xcc* LOS showed the best size, stability, toxicity profile, and immune response. This system encapsulated the type of IONPs for which previous studies have shown effective *in vivo* tracking by multimodal imaging[10,15] and ability to potentiate other cancer immunotherapies approaches such as DC-based vaccination[54] and macrophage polarization into pro-inflammatory M1 phenotypes[55]. This system was investigated as a cancer vaccine adjuvant (described in chapter 4) together with newly developed antigen-loaded nanoparticles (described in chapter 3).

With the idea to develop a light-triggered nanoplatform for delivery of TLR4 modulators, core-shell $NaYF_4$: Yb^{3+}/ Tm^{3+}@$NaYF_4$ UCNPs were prepared by thermal decomposition and characterized by DLS, TEM, and XPS, obtaining uniform rod-like nanoparticles featuring an upconversion emission at different wavelengths in the UV-Vis range[36], triggered by NIR irradiation at 980 nm. These UCNPs were encapsulated in PEG-phospholipid micelles obtaining water-soluble mUCNPs of ~65 nm, a size suitable for drug delivery. The incorporation of two different ratios of IAXO 102, a TLR4 antagonist, yielded two different nanoplatforms, respectively mUCNPs-*IAXO 102-5% and* mUCNPs-

IAXO 102-15%, featuring hydrodynamic diameters of ~81 and ~99 nm approximately and with a uniform size distribution, ideal for use in drug delivery. Prior to testing the mUCNPs-*IAXO 102*, the antagonist activity of the ligand IAXO 102 was tested in J774A.1 murine macrophages and compared to the well-known LPS inhibitor PmB. As expected, both molecules proved to be non-toxic in J774A.1 cells at the concentrations used. However, it was discovered that while all the PmB concentrations can effectively inhibit 66 nM and 6,6 nM LPS, at these LPS concentrations IAXO 102 seemed to enhance the immune stimulating activity of endotoxin as measured by IL-6 release, thus acting as an agonist, contrarily to what had been seen in the literature[39]. Thus, the activity of IAXO 102 is too complex, since it switches from stimulatory to inhibitory at different concentrations. Interestingly both drug free mUCNPs and the mUCNPs-IAXO 102 systems inhibited the immunostimulatory activity of LPS but with higher toxicity. Taken together, these findings did not encourage any further in vivo study.

2.4: Materials and methods

Materials: Unless otherwise specified all commercially available reagents were used without further purification. Both Xcc LOS and E. Coli LOS were received from the research group of Prof. Alba Silipo at the University of Naples Federico II. The lipooligosaccharide of *Xcc* was extracted and purified from dried cells as described previously[33]. The ligand IAXO 102 was obtained by the group of Prof. Francesco Peri at the University of Milano Bicocca and synthesized as described[39]. Iron (III) acetylacetonate (99 %) was purchased from STREM chemicals; Oleic acid (90 %), Oleylamine (70 %), Dibenzylether (80 %), CdSe/ZnS core/shell quantum dots (λ_{em} 600 nm), Yttrium(III) acetate hydrate (99.9%), Ytterbium(III) acetate tetrahydrate (99.9%), Thulium(III) acetate hydrate (99.9%), 1-octadecene (technical grade, 90%), Sodium hydroxide ($\geq$ 97%), Ammonium fluoride (98%), Tetrahydrofuran (THF), Dimethyl sulfoxide (DMSO) and Polymyxin B (PmB) were all purchased from Sigma Aldrich; 1, 2-hexadecanediol (98 %) was purchased from TCI Europe; 4-biphenylcarboxylic acid (95%) was purchased from Acros; $CHCl_3$ (0,005 % water), Methanol (MeOH) and HNO_3 were purchased from MACRON fine chemicals; 1,2-distearoyl-sn-glycero-3-phosphoethanolamine-N-[methoxy(polyethylene glycol)-2000] (ammonium salt) (DSPE-mPEG) and 1,2 dipalmitoyl-*sn*-glycero-3-phosphoethanolamine-N-(lissaminerhodamine B sulfonyl) (ammonium salt) (Rho-PE) were purchased from Avanti polar lipids. 0.45 µm syringe filters were purchased from Pall life sciences; Pierce LAL chromogenic endotoxin quantitation kit, Hoechst 33342 (Hoechst blue) and Lysotracker green DND-26 were purchased from Thermo Fisher. Dulbecco's Modified Eagle Medium (DMEM), Fetal Bovine Serum (FBS), Penicillin/Streptomycin (P/S) and L-glutamine (L-Glu) were all purchased from Gibco; Cell culture plates were purchased from Nunc; MTT cell proliferation kit was purchased from Roche, IL-6 sandwich ELISA kit was purchased from R&D.

Synthesis of iron oxide nanoparticles (IONP): Hydrophobic spherical IONP (IONPs) and cubic IONP (IONPc) were prepared according to published procedures.[14,21]

Nanoparticle- filled nanomicelles preparation: 1 mg of IONPsp and 2 mg of DSPE-mPEG methoxy were dissolved in 100 µL and 200 µL of chloroform respectively, combined in a 4 mL round-bottomed glass vial with 100 µL of chloroform and let to evaporate overnight at RT. LOS- and LPS- loaded micelles were prepared in the same way, with the exception that 0.2 mg of LOS or LPS were added to the latter 100 µL of chloroform and dissolved thoroughly using a vortex mixer (5 minutes) and an ultrasonic cleaner (30 minutes). Fluorescent micelles were prepared in the same way adding a 5% of 1,2-dimyristoyl-*sn*-glycero-3-phosphoethanolamine-N-lissamine Rhodamine B sulfonyl-ammonium salt to the phospholipids mixture. The flask was placed in a water bath at 80 °C for 30 s, after which micelles were re-dissolved in 1 mL of MilliQ water. This solution was centrifuged at 5000 xg for 5' and passed through a 0.45 µm syringe filter to remove non-soluble particles. Then, the micelles were centrifuged at 108600 xg for 50 minutes; the supernatant was discarded and washed with MilliQ water to remove empty PEG micelles (3 cycles). Finally, the pellet was dissolved in 400 µL of MilliQ water (or 10 mM Phosphate Buffered Saline, PBS, when injected in vivo). Micelles were stored at 4ºC. In order to quantify the concentration of iron, ICP analysis was carried out. Briefly, 10 µL of micelles were digested in concentrated HNO_3 over a minimum of three days. Prior to the measurement, the samples were diluted up to 8 mL in MilliQ water (final acid concentration: 1-2 %). ICP-AES analyses were carried out on a Perkin Elmer Optima 5300 DV (Perkin Elmer, Santa Clara, CA, USA) at CIC BiomaGUNE by the Mass spectrometry platform. A range of calibration standards was prepared using single element 1000 mg/L stock solutions (Fisher Scientific UKLTD) and a Merck multielement standard (ICP Multi element standard solution, VICertiPUR) was employed as a reference standard.

QDs- filled nanomicelles preparation: The procedure reported for the preparation of IONPs- filled nanomicelles was followed, with a variation: after filtering the micelles through a 0.45 µm syringe filter, the micelles were centrifuged at a speed of 108600 xg for 45 min. QDs concentration vas determined by UV-Vis spectroscopy following the procedures reported in the literature[56,57]. UV–Vis absorption spectra were recorded on a V-630Bio Spectrophotometer (JASCO Analytical Instruments).

IONPc- filled nanomicelles preparation: The procedure reported for the preparation of IONPs- filled nanomicelles was followed, with some slight variations: after re-dissolving the micellar film in 1 mL of MilliQ water, the solution was centrifuged at 300 xg for 5 min. Besides, after filtering the micelles through a 0.45 µm syringe filter, they were centrifuged at a speed of 88200 xg for 25 min (3 cycles).

Transmission electron microscopy (TEM) studies were performed using a JEOL JEM-2011 electron microscope operating at 120 kV. The samples were prepared by deposing a drop of a solution of nanoparticles (1 mg/mL in THF) onto Pelco 150 mesh grid (Ted Pella) and allowing it to dry. For the preparation of hydrophilic samples, TEM grids were polarized using a Quorum technologies K100X glow discharge system. Nanoparticles' size was determined from TEM images, measuring a minimum of 200 nanocrystals with the software ImageJ.

Hydrodynamic diameter and ζ-potential of the micelles were measured using a Z-Sizer (Malvern Nano-Zs, UK). To determine the stability, mIONPsp-Xcc LOS were dissolved at a concentration of approx. 5 mM in 10 mM PBS and the hydrodynamic diameter analyzed by Z-Sizer immediately after purification and over a 4 weeks period. To measure the ζ-potential, the samples were dissolved at a concentration of approx. 0, 5 mM in 10 mM NaCl and analyzed by Z-sizer immediately after purification.

Quantification of LOS loading on IONPsp micelles: The amount of LOS incorporated on micelles was measured using a calibration curve prepared plotting the immune stimulating activity of the pure ligand (measured determining the amount of IL-6 released) on cell cultures versus its concentration, and the amount of ligand bound to the nanoparticle was determined indirectly, measuring the amount of ligand that wasn't incorporated to the micelles and remained in the supernatants from the micelles workup. Briefly, in a typical determination, a calibration curve is prepared administering Xcc LOS concentrations ranging from 36 µM to 3.6 nM to cells and the corresponding IL-6 production is measured by Sandwich ELISA and plotted against the ligand's concentration to get a calibration curve, used to extrapolate the concentration of unincorporated Xcc LOS from the supernatants upon

measurements of their immune stimulating activity, by IL-6 concentration. The efficiency of this method was double checked by loading LPS on the mNPs developed and reported in the supporting information section (iron oxide nanospheres and nanocubes and quantum dots) and comparing the results obtained with the "supernatants quantification" method to the ones obtained with a commercial kit (Pierce LAL chromogenic endotoxin quantitation kit) for determination of LPS concentration. The ratio of ligand to nanoparticles was calculated following these calculations for IONPsp: Assuming a completely spherical nanoparticle and the known density of magnetite structure, the number of iron atoms per nanoparticle can be determined:

$V_{IONPsp} = 4/3 \cdot (D/2)^3 \cdot \pi = 1.505 \cdot 10^{-25}$ m^3;

$\rho(Fe_3O_4) = 5.17 \cdot 10^6$ g·m^3;

$m = \rho(Fe_3O_4) \cdot V_{IONPsp} = 7.783 \cdot 10^{-19}$ g;

$n_{Fe} = m/$ MW $(Fe_3O_4) \cdot 3 = 1.009 \cdot 10^{-20}$ mol;

$Fe_{atoms}/IONPsp = n_{Fe} \cdot N_A = 6076$ atoms;

MW (Xcc LOS): 2750 Da and MW (E. Coli LOS): 2000 Da.

In order to calculate the ratio of ligand to IONPc, the same logic was followed, using the side length of nanocubes:

$V_{IONPc} = (l)^3 = 1.899 \cdot 10^{-23}$ m^3;

$\rho(Fe_3O_4) = 5.17 \cdot 10^6$ g·m^3;

$m = \rho(Fe_3O_4) \cdot V_{IONPc} = 9.818 \cdot 10^{-17}$ g;

$n_{Fe} = m/$ MW $(Fe_3O_4) \cdot 3 = 1.272 \cdot 10^{-18}$ mol;

$Fe_{atoms}/IONPc = n_{Fe} \cdot N_A = 766120$ atoms;

MW (Xcc LOS): 2750 Da and MW (E. Coli LOS): 2000 Da.

Quantification of LPS loading on IONPsp, IONPc, and QDs micelles: The analysis was performed using a Pierce LAL chromogenic endotoxin quantitation kit (Thermofisher) following the instructions given by the kit's manufacturer. The assay was performed in aseptic conditions. Briefly, 50 µL of standards or samples were put on a 37ºC 96 well microplate (in duplicates), incubated for 5 min. at 37ºC after which the LAL reagent was added to each well. Following a 10 min. incubation at 37ºC, 100 µL of substrate solution were added, stirred and incubated for 6 min. at 37ºC. Then, 25 µL of stop solution were added and the

absorbance at 405 nm was immediately measured using a Varioskan LUX multimode plate reader (Thermo Fisher). The concentration of LPS in the unknown samples was determined using a calibration curve.

Xcc LOS release studies: Ligand loading on the nanoparticles was measured immediately after preparation. 1 or 2 weeks after, mIONPsp-Xcc LOS nanoparticles were centrifuged at a speed of 108600 xg for 50 min. and the supernatant was removed and analyzed following the fore mentioned procedures for quantification of the ligand loading.

Fluorescence microscopy: J774A.1 cells were seeded in an Ibidi μ-Slide VI$^{0.4}$ at a density of 30000 cells/ well in DMEM supplemented with 10% Fetal Bovine Serum and 1% Penicillin/Streptomycin and let to adhere overnight in an incubator maintained at 37 °C and 5% CO_2. The day after, the medium was removed and cells were administered with 1 μg/ mL Hoechst blue to stain the nuclei and incubated for 30 minutes. Cells were washed with PBS three times in order to get reed of the unbound dye and then stained with ~200 nM mIONPsp(Rho)-Xcc LOS or mIONPs(Rho) or mQDs (the latter at a concentration of ~150 nM) and incubated for three hours. Cells were washed again and stained with 1 mM Lysotracker green, incubated for 30 minutes, washed with PBS and finally images were taken using ZEISS Axio Observer inverted microscope for the experiments carried out at CIC BiomaGUNE and a Zeiss 200M Axiovert for the experiments at UNIBI. In the latter case, a built-in deconvolution program was used to overlap images of cells obtained from different focal planes and deconvolute the images. Fluorescence and absorbance spectrum of the Xcc LOS-loaded micelles were recorded using a Fluorometer Horiba Fluoromaster 3 and UV−Vis absorption spectra were recorded on a V-630Bio Spectrophotometer (JASCO Analytical Instruments) respectively.

Cell viability experiments: The J774A.1 mouse macrophage cell line was obtained from the American Type Culture Collection (ATCC). Cells were grown at 37 °C in a humidified atmosphere of 5 % CO_2 using Dulbecco's Modified Eagle Medium (DMEM, Gibco) supplemented with 10 % Fetal Bovine Serum (FBS, Gibco) and 1 % Penicillin/Streptomycin (P/S, 50 U/mL, Gibco). Cells were

detached when reached 70% confluence by removing them from the culture flask via gentle scraping and then resuspended in medium and seeded at a density of $3 \cdot 10^4$ cells/ well in 96-well plates and allowed to adhere overnight. Then, cells were administered with ligands, micelles or ligand-loaded micelles solutions diluted accordingly in medium, in triplicates, in a final volume of 200 µL (of which 100 from cell seeding and 100 from the administered solution, split into 50 for LPS and 50 for IAXO 102, IAXO 102-loaded mUCNPs or PmB) and incubated for 24h at 37ºC after which supernatants were removed and stored at -20ºC until analysis. Cell viability was determined using a MTT assay (Roche). Briefly, cells were administered with 100 µL/well of a MTT solution diluted in medium and incubated for 1h at 37ºC, after which supernatants were discarded and MTT crystals dissolved in 200 µL/well of Dimethyl sulfoxide (DMSO). The absorbance of the wells was measured using a TECAN Genios Pro 96/384 multifunction microplate reader at 550 nm and data represented as the cell viability compared to control wells.

Quantification of Cytokine Production by ELISA: Cytokines were measured in cells' supernatants using IL-6 (R&D) sandwich ELISA. A 4-parameter logistic standard curve was generated using Graph Pad Prism 5 and used to get the cytokines concentrations. Results are expressed as mean ± SEM in pg/mL or ng/mL, compared to untreated control wells.

Synthesis of Upconverting nanoparticles: Hydrophobic core-shell $NaYF_4$ upconverting nanoparticles doped with Yb and Tm ($NaYF_4$: Yb^{3+}/ Tm^{3+}@$NaYF_4$) were prepared following the procedure reported in the literature by our research group[36].

Synthesis of core $NaYF_4$: Yb^{3+}/ Tm^{3+}: Yttrium(III) acetate hydrate (2.1 mmol, 555 mg), ytterbium(III) acetate tetrahydrate (0.90 mmol, 380 mg) and thulium(III) acetate hydrate (0.015 mmol, 5.2 mg) were added in 1-octadecene (25 mL) and oleic acid (15 mL) in a round-bottomed flask. The suspension was heated up to 120 ºC with a temperature ramp of 3.2 ºC/min under stirring and vacuum. Once the reaction mixture reached such temperature, it was kept in these conditions for 30 min in order to eliminate residual water and oxygen. The

system was then let to cool to 50 ºC under a flow of nitrogen gas. A solution of sodium hydroxide (7.5 mmol, 300 mg) and ammonium fluoride (12.0 mmol, 444 mg) dissolved in methanol (8 mL) was added dropwise to the reaction flask. The reaction mixture was stirred at 50ºC for 30 min and at 70ºC for 30 min under nitrogen. Then, the system was heated up to 300ºC with a temperature ramp of 13.5 ºC/min under stirring and nitrogen and maintained in such conditions for 90 min. Next, the flask was left cooling to room temperature, and nanoparticles were purified by centrifugation (3000 xg, 15 min). The white pellet was washed once with of ethanol (40 mL) and once with THF/ethanol (5/35 mL) and recollected by centrifugation. Upconversion nanoparticles were dried at room temperature overnight.

Synthesis of core-shell $NaYF_4$: Yb^{3+}/ Tm^{3+}@$NaYF_4$: The previously prepared core $NaYF_4$: Yb^{3+}/ Tm^{3+} nanoparticles were used as seeds to grow a $NaYF_4$ shell. Yttrium (III) acetate hydrate (0.9 mmol, 240 mg) was added in 1-octadecene (15 mL) and oleic acid (6 mL) in a round-bottomed flask. The suspension was heated up to 120 ºC with a temperature ramp of 3.2 ºC/min under constant stirring and vacuum, and kept in such conditions for 30 min. Afterwards, the solution was let to cool to 80 ºC and placed under a flow of nitrogen gas. Meanwhile, a suspension of $NaYF_4$:Yb^{3+}/Tm^{3+} (260 mg) in hexane (10 mL) was prepared and added to the reaction flask dropwise. The reaction mixture was heated up to 110 ºC (3.2 ºC/min) under vacuum to eliminate the hexane. After 30 min the solution was let to cool to 50 ºC and a solution of sodium hydroxide (2.2 mmol, 88 mg) and ammonium fluoride (3.5 mmol, 130 mg) in methanol (5 mL) was added to the system drop wise. The flask was kept at 50 ºC for 30 min and at 70 ºC for 30 min under nitrogen to evaporate the entire amount of methanol from the reaction mixture. Afterwards, the reaction flask was heated up at 300 ºC with a temperature ramp of 13.5 ºC/min and kept for 90 min. The solution was then cooled to room temperature. The obtained core-shell nanoparticles were purified by centrifugation (3000 xg, 15 min). The pellet was washed with ethanol and THF and dried overnight.

UCNPs- filled nanomicelles preparation: 2 mg of UCNPs and 2 mg of DSPE-mPEG were dissolved in 200 µL and 200 µL of chloroform respectively, combined in a 4 mL round-bottomed glass vial with 100 µL of chloroform and let

to evaporate overnight at RT. IAXO 102-loaded UCNPs micelles were prepared as above described, with the exception that 0.1 mg or 0.3 mg of IAXO 102 (to prepare mUCNPs-*IAXO 102-r1* and mUCNPs-*IAXO 102-r2* respectively) were added to the latter 100 µL of chloroform. The flask was placed in a water bath at 80 °C for 30 s, and micelles were re-dissolved in 1 mL of MilliQ water. This solution was centrifuged at 5000 xg for 5' and passed through a 0.45 µm syringe filter to remove non-soluble particles. Then, the micelles were centrifuged at 72000 xg for 30 minutes; the supernatant was discarded and washed with MilliQ water to remove empty PEG micelles (3 cycles). Finally, the pellet was dissolved in 400 µL of MilliQ water and micelles were stored at 4ºC. The concentration of UCNPs was measured assuming that 100% of the nanoparticles used ended up in the micelles.

Fourier Transform Infrared (FTIR) FTIR spectra of oleic acid, $NaYF_4$: Yb^{3+}/ Tm^{3+}, $NaYF_4$: Yb^{3+}/ Tm^{3+}@$NaYF_4$, and oleic acid were recorded on a Nicolet FTIR 6700 spectrometer as KBr pellet, obtained by mixing 0.5 mg of core-shell upconverting nanoparticles with 2 mg of dry KBr and using the hydraulic press.

XPS experiments were performed in a SPECS Sage HR 100 spectrometer with a non- monochromatic X-ray source Magnesium Kα line of 1253.6eV energy and an applied power of 250 W. It was calibrated using the 3d5/2 line of Ag with a full width at half maximum (FWHM) of 1.1 eV. All measurements were made in an ultra-high vacuum (UHV) chamber at a pressure below $8 \cdot 10^{-8}$ mbar. To prepare the sample, 3 mg of nanoparticles were dissolved in THF, carefully sonicated and put in a Titanium coated glass slide (previously prepared). The acquisition time was 150 minutes.

Cell viability and cytokine production experiments: The J774A.1 mouse macrophage cell line was obtained from the American Type Culture Collection (ATCC). Cells were grown and split following the procedures already reported in the materials and method section. Then, cells were administered with ligands, micelles or ligand-loaded micelles solutions diluted accordingly in medium, in triplicates, in a final volume of 200 µL (of which 100 from cell seeding and 100 from the administered solution, split into 50 for LPS and 50 for IAXO 102, IAXO 102-loaded mUCNPs or PmB) and incubated for 24h at 37ºC after which supernatants were removed and stored at -20 ºC until analysis. Cell viability

was determined using a MTT assay (Roche). Cytokine production was assessed following the methods previously reported in the materials and methods section.

2.5: References

(1)   Hu, Z.; Ott, P. A.; Wu, C. J. Towards Personalized, Tumour-Specific, Therapeutic Vaccines for Cancer. *Nat. Rev. Immunol.* **2018**, *18* (3), 168.

(2)   McKee, A. S.; Munks, M. W.; Marrack, P. How Do Adjuvants Work? Important Considerations for New Generation Adjuvants. *Immunity* **2007**, *27* (5), 687.

(3)   Vacchelli, E.; Galluzzi, L.; Eggermont, A.; Fridman, W. H.; Galon, J.; Sautès-Fridman, C.; Tartour, E.; Zitvogel, L.; Kroemer, G. Trial Watch: FDA-Approved Toll-like Receptor Agonists for Cancer Therapy. *Oncoimmunology* **2012**, *1* (6), 894.

(4)   Melero, I.; Gaudernack, G.; Gerritsen, W.; Huber, C.; Parmiani, G.; Scholl, S.; Thatcher, N.; Wagstaff, J.; Zielinski, C.; Faulkner, I.; et al. Therapeutic Vaccines for Cancer: An Overview of Clinical Trials. *Nat. Rev. Clin. Oncol.* **2014**, *11* (9), 509.

(5)   Gregory, A. E.; Titball, R.; Williamson, D. Vaccine Delivery Using Nanoparticles. *Front. Cell. Infect. Microbiol.* **2013**, *25* (3), 13.

(6)   Salem, A. K. Nanoparticles in Vaccine Delivery. *AAPS J.* **2015**, *17* (2), 289.

(7)   Zhang, R. X.; Li, J.; Zhang, T.; Amini, M. A.; He, C.; Lu, B.; Ahmed, T.; Lip, H.; Rauth, A. M.; Wu, X. Y. Importance of Integrating Nanotechnology with Pharmacology and Physiology for Innovative Drug Delivery and Therapy - An Illustration with Firsthand Examples. *Acta Pharmacol. Sin.* **2018**, *39* (5), 825.

(8)   Bhatia, S. Nanoparticles Types, Classification, Characterization, Fabrication Methods and Drug Delivery Applications. In *Natural Polymer Drug Delivery Systems*; 2016.

(9)   Yuk, S. A.; Sanchez-Rodriguez, D. A.; Tsifansky, M. D.; Yeo, Y. Recent Advances in Nanomedicine for Sepsis Treatment. *Ther. Deliv.* **2018**, *9* (6), 435.

(10)   Ruiz-De-Angulo, A.; Zabaleta, A.; Gómez-Vallejo, V.; Llop, J.; Mareque-Rivas, J. C. Microdosed Lipid-Coated (67)Ga-Magnetite Enhances Antigen-Specific Immunity by Image Tracked Delivery of Antigen and

CpG to Lymph Nodes. *ACS Nano* **2016**, *26* (10), 1602.

(11) Bocanegra Gondan, A. I.; Ruiz-de-Angulo, A.; Zabaleta, A.; Gómez Blanco, N.; Cobaleda-Siles, B. M.; García-Granda, M. J.; Padro, D.; Llop, J.; Arnaiz, B.; Gato, M.; Escors D.; Mareque-Rivas J.C. Effective Cancer Immunotherapy in Mice by PolyIC-Imiquimod Complexes and Engineered Magnetic Nanoparticles. *Biomaterials* **2018**, *170*, 95.

(12) Barr, T. A.; Krembuszewski, M.; Gupta, M.; Gray, D.; Mareque-Rivas, J. C. Quantum Dots Decorated with Pathogen Associated Molecular Patterns as Fluorescent Synthetic Pathogen Models. *Mol. Biosyst.* **2010**, *6* (9), 1572.

(13) Piazza, M.; Colombo, M.; Zanoni, I.; Granucci, F.; Tortora, P.; Weiss, J.; Gioannini, T.; Prosperi, D.; Peri, F. Uniform LPS-Loaded Magnetic Nanoparticles for the Investigation of LPS/TLR4 Signaling. *Angew Chem Int Ed Engl* **2011**, *141* (4), 520.

(14) Sun S.; Zeng H; Robinson D. B.; Raoux S.; Rice P. M.; Wang S. X.; Li G. Monodisperse MFe_2O_4 (M = Fe , Co , Mn) Nanoparticles. *J.Am.Chem.Soc.* **2004**, *126* (1), 273.

(15) Cobaleda-Siles, M.; Henriksen-Lacey, M.; de Angulo, A. R.; Bernecker, A.; Vallejo, V. G.; Szczupak, B.; Llop, J.; Pastor, G.; Plaza-Garcia, S.; Jauregui-Osoro, M.; Meszaros L. K.; Mareque-Rivas J. C. An Iron Oxide Nanocarrier for DsRNA to Target Lymph Nodes and Strongly Activate Cells of the Immune System. *Small* **2014**, *10* (24), 5054.

(16) Xie, Y.; Bagby, T. R.; Cohen, M. S.; Forrest, M. L. Drug Delivery to the Lymphatic System: Importance in Future Cancer Diagnosis and Therapies. **2009**, *6* (8), 785.

(17) Flask, C.; Weinberg, B.; Farrell, D.; Pagel, M. D.; Ai, H.; Shuai, X.-T.; Gao, J.; Duerk, J. Magnetite-Loaded Polymeric Micelles as Ultrasensitive Magnetic-Resonance Probes. *Adv. Mater.* **2005**, *17* (16), 1949.

(18) Hu, F.; MacRenaris, K. W.; Waters, E. A.; Liang, T.; Schultz-Sikma, E. A.; Eckermann, A. L.; Meade, T. J. Ultrasmall, Water-Soluble Magnetite Nanoparticles with High Relaxivity for Magnetic Resonance Imaging. *J. Phys. Chem. C* **2009**, *113* (49), 20855.

(19) Frey, N. A.; Peng, S.; Cheng, K.; Sun, S. Magnetic Nanoparticles: Synthesis, Functionalization, and Applications in Bioimaging and

Magnetic Energy Storage. *Chem. Soc. Rev.* **2009**, *38* (9), 2532.

(20) Cobaleda-Siles, B. M. Modular Multimodal Iron-Oxide-Based Nanocarriers for Image-Guided Ds-RNA Immunostimulation and Platinum Anticancer Drug Design, UPV/EHU, 2015.

(21) Lee, N.; Choi, Y.; Lee, Y.; Park, M.; Moon, W. K.; Choi, S. H.; Hyeon, T. Water-Dispersible Ferrimagnetic Iron Oxide Nanocubes with Extremely High r 2 Relaxivity for Highly Sensitive in Vivo MRI of Tumors. *Nano Lett.* **2012**, *12* (6), 3127.

(22) Kim, D.; Lee, N.; Park, M.; Kim, B. H.; An, K.; Hyeon, T. Synthesis of Uniform Ferrimagnetic Magnetite Nanocubes. *J. Am. Chem. Soc.* **2009**, *131* (2), 454.

(23) Wang, Y.-X. J. Superparamagnetic Iron Oxide Based MRI Contrast Agents: Current Status of Clinical Application. *Quant Imaging Med Surg* **2011**, *1*, 35.

(24) Barrow, M.; Taylor, A.; Murray, P.; Rosseinsky, M. J.; Adams, D. J. Design Considerations for the Synthesis of Polymer Coated Iron Oxide Nanoparticles for Stem Cell Labelling and Tracking Using MRI. *Chem. Soc. Rev.* **2015**, *44* (19), 6733.

(25) Knop, K.; Hoogenboom, R.; Fischer, D.; Schubert, U. S. Poly(Ethylene Glycol) in Drug Delivery: Pros and Cons as Well as Potential Alternatives. *Angew. Chemie - Int. Ed.* **2010**, *49* (36), 6288.

(26) Mishra, P.; Nayak, B.; Dey, R. K. PEGylation in Anti-Cancer Therapy: An Overview. *Asian J. Pharm. Sci.* **2016**, *11* (3), 337.

(27) Walkey, C. D.; Chan, W. C. W. Understanding and Controlling the Interaction of Nanomaterials with Proteins in a Physiological Environment. *Chem. Soc. Rev.* **2012**, *41* (7), 2780.

(28) Walkey, C. D.; Olsen, J. B.; Guo, H.; Emili, A.; Chan, W. C. W. Nanoparticle Size and Surface Chemistry Determine Serum Protein Adsorption and Macrophage Uptake. *J. Am. Chem. Soc.* **2012**, *134* (4), 2139.

(29) Suk, J. S.; Xu, Q.; Kim, N.; Hanes, J.; Ensign, L. M.; Sciences, H.; Sciences, M. PEGylation as a Strategy for Improving Nanoparticle-Based Drug and Gene Delivery. *Adv. Drug Deliv. Rev.* **2017**, *99*, 28.

(30) Ko, A.; Wui, S. R.; Ryu, J. I.; Do, H. T. T.; Lee, Y. J.; Lim, S. J.; Rhee, I.;

Jung, D. I.; Park, J. A; Choi, J. A; Song M. K.; Lee N. G. Comparison of the Adjuvanticity of Two Adjuvant Formulations Containing De-O-Acylated Lipooligosaccharide on Japanese Encephalitis Vaccine in Mice. *Arch. Pharm. Res.* **2017**, *41* (2), 1.

(31) Ryu, J. I.; Park, S. A.; Wui, S. R.; Ko, A.; Han, J. E.; Choi, J. A.; Song, M. K.; Kim, K. S.; Cho, Y. J.; Lee, N. G. A De-O-Acylated Lipooligosaccharide-Based Adjuvant System Promotes Antibody and Th1-Type Immune Responses to H1N1 Pandemic Influenza Vaccine in Mice. *Biomed Res. Int.* **2016**, *2016*, 3713656.

(32) Han, J. E.; Wui, S. R.; Kim, K. S.; Cho, Y. J.; Cho, W. J.; Lee, N. G. Characterization of the Structure and Immunostimulatory Activity of a Vaccine Adjuvant, de-O-Acylated Lipooligosaccharide. *PLoS One* **2014**, *9* (1), e85838.

(33) Silipo, A.; Molinaro, A.; Sturiale, L.; Dow, J. M.; Erbs, G.; Lanzetta, R.; Newman, M. A.; Parrilli, M. The Elicitation of Plant Innate Immunity by Lipooligosaccharide of Xanthomonas Campestris. *J. Biol. Chem.* **2005**, *280* (39), 33660.

(34) Ryu, K. A.; Stutts, L.; Tom, J. K.; Mancini, R. J.; Esser-Kahn, A. P. Stimulation of Innate Immune Cells by Light-Activated TLR7/8 Agonists. *J. Am. Chem. Soc.* **2014**, *136* (31), 10823.

(35) Aggarwal, P.; Hall, J. B.; McLeland, C. B.; Dobrovolskaia, M. A.; McNeil, S. E. Nanoparticle Interaction with Plasma Proteins as It Relates to Particle Biodistribution, Biocompatibility and Therapeutic Efficacy. *Adv. Drug Deliv. Rev.* **2009**, *61* (6), 428.

(36) Ruggiero, E.; Hernández-Gil, J.; Mareque-Rivas, J. C.; Salassa, L. Near Infrared Activation of an Anticancer Pt IV Complex by Tm-Doped Upconversion Nanoparticles. *Chem. Commun.* **2015**, *51* (11), 2091.

(37) Chen, G.; Qiu, H.; Prasad, P. N.; Chen, X. Upconversion Nanoparticles: Design, Nanochemistry, and Applications in Theranostics. *Chem. Rev.* **2014**, *114* (10), 5161.

(38) Yi, G.; Chow, G. Water-Soluble NaYF4Yb,Er(Tm)/NaYF4/Polymer Core Shell/Shell Nanoparticles with Significant Enhancement of Upconversion Fluorescence. *Chem. Mater.* **2007**, *19* (5599), 341.

(39) Piazza, M.; Rossini, C.; Fiorentina, S. D.; Pozzi, C.; Comelli, F.; Bettoni,

I.; Fusi, P.; Costa, B.; Peri, F. Glycolipids and Benzylammonium Lipids as Novel Antisepsis Agents: Synthesis and Biological Characterization. *J. Med. Chem.* **2009**, *52* (4), 1209.

(40) Liu, H.; Irvine, D. J. Guiding Principles in the Design of Molecular Bioconjugates for Vaccine Applications. *Bioconjug. Chem.* **2015**, *26* (5), 791.

(41) Rao, D. A.; Forrest, M. L.; Alani, A. W. G.; Kwon, G. S.; Robinson, J. R. Biodegradable PLGA Based Nanoparticles for Sustained Regional Lymphatic Drug Delivery. *J. Pharm. Sci.* **2010**, *99* (4), 2018.

(42) Ahsan, F.; Rivas, I. P.; Khan, M. A.; Torres Suárez, A. I. Targeting to Macrophages: Role of Physicochemical Properties of Particulate Carriers—liposomes and Microspheres—on the Phagocytosis by Macrophages. *J. Control. Release* **2002**, *79* (1–3), 29.

(43) Tabata, Y.; Ikada, Y. Effect of the Size and Surface Charge of Polymer Microspheres on Their Phagocytosis by Macrophage. *Biomaterials* **1988**, *9* (4), 356.

(44) Silipo, A.; Molinaro, A.; Lanzetta, R.; Parrilli, M.; Lindner, B.; Holst, O. The Structures of the Lipid A Moieties from the Lipopolysaccharides of Two Phytopathogenic Bacteria, Xanthomonas Campestris Pv.Pruni and Xanthomonas Fragariae. *European J. Org. Chem.* **2004**, *2004* (6), 1336.

(45) Smulders, S.; Kaiser, J.-P.; Zuin, S.; Van Landuyt, K. L.; Golanski, L.; Vanoirbeek, J.; Wick, P.; Hoet, P. H. Contamination of Nanoparticles by Endotoxin: Evaluation of Different Test Methods. *Part. Fibre Toxicol.* **2012**, *9*, 41.

(46) Rice, A.; Wereszczynski, J. Atomistic Scale Effects of Lipopolysaccharide Modifications on Bacterial Outer Membrane Defenses. *Biophys. J.* **2018**, *114* (6), 1389.

(47) Adams, P. G.; Lamoureux, L.; Swingle, K. L.; Mukundan, H.; Montaño, G. A. Lipopolysaccharide-Induced Dynamic Lipid Membrane Reorganization: Tubules, Perforations, and Stacks. *Biophys. J.* **2014**, *106* (11), 2395.

(48) Mueller, M.; Lindner, B.; Kusumoto, S.; Fukase, K.; Schromm, A. B.; Seydel, U. Aggregates Are the Biologically Active Units of Endotoxin. *J. Biol. Chem.* **2004**, *279* (25), 26307.

(49) Akira, S.; Takeda, K. Toll-like Receptor Signalling. *Nat. Rev. Immunol.*

2004, *4* (7), 499.

(50) Husebye, H.; Halaas, Ø.; Stenmark, H.; Tunheim, G.; Sandanger, Ø.; Bogen, B.; Brech, A.; Latz, E.; Espevik, T. Endocytic Pathways Regulate Toll-like Receptor 4 Signaling and Link Innate and Adaptive Immunity. *EMBO J.* **2006**, *25* (4), 683.

(51) Boyer, J.-C.; Cuccia, L. A.; Capobianco, J. A. Synthesis of Colloidal Upconverting NaYF4: Er3+/Yb3+ and Tm3+/Yb3+ Monodisperse Nanocrystals. *Nano Lett.* **2007**, *7* (3), 847.

(52) Morrison, D. C.; Jacobs, D. M. Binding of Polymyxin B to the Lipid A Portion of Bacterial Lipopolysaccharides. *Immunochemistry* **1976**, *13* (10), 813.

(53) Peri, F.; Calabrese, V. Toll-like Receptor 4 (TLR4) Modulation by Synthetic and Natural Compounds: An Update. **2015**, *57* (9), 3612.

(54) Cho, N.-H.; Cheong, T.-C.; Min, J. H.; Wu, J. H.; Lee, S. J.; Kim, D.; Yang, J.-S.; Kim, S.; Kim, Y. K.; Seong, S.-Y. A Multifunctional Core–shell Nanoparticle for Dendritic Cell-Based Cancer Immunotherapy. *Nat. Nanotechnol.* **2011**, *6* (10), 675.

(55) Zanganeh, S.; Hutter, G.; Spitler, R.; Lenkov, O.; Mahmoudi, M.; Shaw, A.; Pajarinen, J. S.; Nejadnik, H.; Goodman, S.; Moseley, M.; Coussens L. M.; Daldrup-Link H. E. Iron Oxide Nanoparticles Inhibit Tumour Growth by Inducing Pro- Inflammatory Macrophage Polarization in Tumour Tissues. *Nat. Nanotechnol.* **2016**, *11* (11), 986.

(56) Kirchner, C.; Liedl, T.; Kudera, S.; Pellegrino, T.; Javier, A. M.; Gaub, H. E.; Stolzle, S.; Fertig, N.; Parak, W. J. Cytotoxicity of Colloidal CdSe and CdSe/ZnS Nanoparticles. *Nano Lett.* **2005**, *5* (2), 331.

(57) Yu, W. W.; Qu, L.; Guo, W.; Peng, X. Experimental Determination of the Extinction Coefficient of CdTe, CdSe, and CdS Nanocrystals. *Chem. Mater.* **2003**, *15* (14), 2854.

CHAPTER 3

Covalent binding of the model antigen ovalbumin (OVA) to IONPsp and JanusNPs:

Here, several ways to improve the delivery of OVA were investigated, by preparing mIONPsp-HyNic-FB-OVA, mJanusNPs-HyNic-FB-OVA and the adjuvant- and antigen- loaded mIONPsp-E. Coli LPS/HyNic-FB-OVA systems using an aniline-catalyzed hydrazone ligation strategy.

3.1: Introduction

The use of nanoparticles for antigen delivery has several advantages over the use of conventional antigens as they can protect antigens from degradation and improve their delivery and presentation to the immune system[1]. Besides, nanostructures can be loaded with multiple antigenic epitopes or both antigen and adjuvant in a single carrier and also reduce systemic side effects[2]. Moreover, coordinated delivery of adjuvant and antigen to the lymph nodes is necessary for the immune system to unleash a strong immune response[3,4,5] and is a desirable feature for every vaccine candidate.

A central aspect of antigen delivery leading to a protective immune response is the antigen presentation to dendritic cells, which will in turn present it on MHC class I or II molecules and subsequently promote T cells expansion. Uto et al. showed that poly(γ-glutamic acid) nanoparticles (γ-PGA NPs) loaded with OVA can be taken up much more efficiently by dendritic cells than OVA alone or its Alum-associated form, and the use of nanoparticles improved the uptake efficiency of up to 30-fold[6].

Another important factor improving antigen delivery is the depot effect, which can provide long-term antigen release from a vaccination site, and polylactide-co-glycolide (PLGA) micro- or nanoparticles have been used for this purpose since they have a history of safe use in humans[7]. However, the literature also reported that antigens encapsulated and released from PLGA micro- or nanoparticles suffered from degradation and that because of low antigen encapsulation efficiency and scale-up issues these particles never moved into clinical trials as controlled-release delivery vehicles for vaccines[7,8,9].

Another type of nanoparticle that has been exploited for antigen delivery are lipid-based vesicles or liposomes. These particles have been investigated intensively in recent years due to being relative ease to make and tune their properties, efficient uptake in APCs and lack of toxicity[10]. However, Epaxal® is the only liposome-based vaccine approved for use in humans against hepatitis A infection[11]. The low stability characteristic of liposomes hinders the application of these particles[12].

Another antigen delivery approach is represented by the use of metallic nanoparticles. Recently, there has been enough evidence to suggest that these might act not only as antigen carriers, but also as immunostimulatory entities, by inducing cytokine production, APCs activation, and humoral immune responses[13].

Another fundamental aspect of antigen delivery by nanoparticles is the strategy employed to conjugate the antigen to nanoparticles, and many different approaches have been reported in the scientific literature. Among them, are the EDC coupling chemistry[14,15,16], and the reductively labile disulphide-based antigen conjugation[17]. Herein, hydrazone ligation was utilized to prepare the nanoparticle-antigen conjugates. The bis-aryl-hydrazone-linking conjugation strategy offers high chemoselectivity, high yields at low concentrations, enhanced reaction rates and easy reaction monitoring. Its selectivity arises from the fact that the linkers, introduced separately in the molecules that have to be conjugated, are not reactive towards the common functional groups found in biological molecules such as amino groups, allowing to avoid cross-linking which could ultimately lead to aggregation.

3.2: Results and discussion

3.2.1: Synthesis and characterization of mIONPsp linked to OVA via hydrazone bond (mIONPsp-HyNic-FB-OVA)

Since mIONPsp-*Xcc* LOS were selected as the best adjuvant system, IONPsp were also chosen for the delivery of the model antigen OVA. The preparation and the characteristics of the hydrophobic IONPsp were already discussed in chapter 2.

To introduce the required functional groups onto the mIONPsp, the terminal amine group of the mIONPsp prepared using 1,2-distearoyl-sn-glycero-3-phosphoethanolamine-N-[amino(polyethylene glycol)-2000] (DSPE-aPEG) was modified to an aromatic aldehyde at a pH of 7 by reaction with the activated ester of the linker succinimidyl 6-hydrazinonicotinate acetone hydrazone (S-HyNic) (**Figure 1a**). The resulting HyNic-modified mIONPsp (mIONPsp-HyNic)

were purified by a desalting column and spin filtration to get rid of the unreacted starting material. The average molar substitution ratio of the mIONPsp with the HyNic linker was *ca*. 10, which was determined by reacting mIONPsp-HyNic with 4-nitrobenzaldehyde and measuring the formation of the bis-aryl hydrazone bond at 345 nm. On the other hand, lysine residues of OVA were modified to an aromatic aldehyde by reacting them with the activated ester of the linker succinimidyl 4-formylbenzoate (4FB) at pH 7 (***Figure 1****a*) and the product was purified by a desalting column and spin filtration. The substitution ratio of the OVA with the 4FB linker was determined by reaction with 2-hydrazinopyridine-2HCl and measuring the formation of the bis-aryl hydrazone at 350 nm, and was of 2-3 molecules of 4FB per OVA (***Figure 1****b*) out of 20 lysine residues. The ligation reaction of the aromatic aldehyde functionalized 4FB-OVA (20-30 µM) with hydrazine activated mIONPsp-HyNic (0.5-3 µM IONPs) carried out at pH 6.2 in the presence of 100 mM aniline as a nucleophile catalyst and monitored by the hydrazone chromophore formation achieved a high level of conjugation (*ca*. 85-90%) in 2 h with an 80% conversion already within the first 10 min of the reaction (***Figure 1****c*). Quantitative analysis of protein content by the commercial test BCA showed conjugation of ~6 molecules of OVA per IONPsp. TEM and DLS studies confirmed that this conjugation strategy preserves the 20-100 nm size for lymph node targeting (***Figure 1****d, e*), and that the mIONPsp-HyNic-FB-OVA are stable for weeks in PBS (***Figure 1****f, g*).
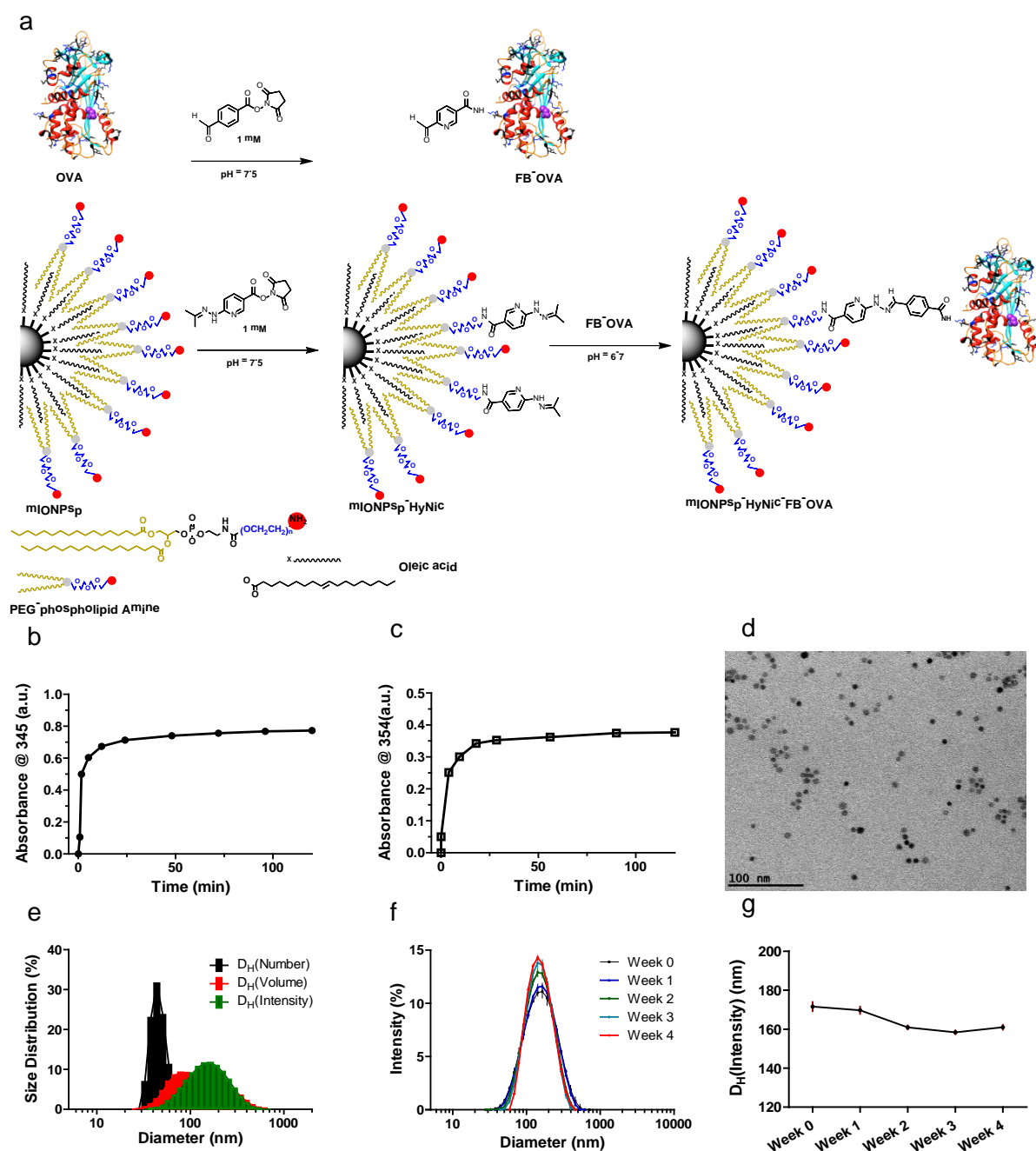
Figure 1. *a) General strategy for the conjugation of the antigen (OVA) to mIONPsp. b, c) UV monitoring of the chemical ligations. b) The substitution ratio of the OVA with the 4-FB linker was determined by reaction of the FB-OVA with 2-hydrazinopyridine-2HCl. c) The formation of the FB-modified OVA and the ligation reaction of FB-OVA (20-30 µM) to mIONPsp-HyNic (0.5-3 µM mIONPsp) in presence of ~100 mM of aniline. d-g) Size and stability of mIONPsp-HyNic-FB-OVA. Representative d) TEM micrograph and e-g) DLS*

analysis of size and size distribution over time. Data are representative of n > 5 formulation replicates.

3.2.2: Uptake of mIONPsp-HyNic-FB-OVA by antigen presenting cells.

The uptake of mIONPsp-HyNic-FB-OVA was assessed in J774A.1 murine macrophages by fluorescence microscopy. To enable tracking of the mIONPsp during cellular uptake a 5% rhodamine B-labeled phospholipid was incorporated during the micelle synthesis. The results show that mIONPsp(Rho)-HyNic-FB-OVA are uptaken and colocalize with the endosomes in the J774A.1 cells (***Figure 2***).
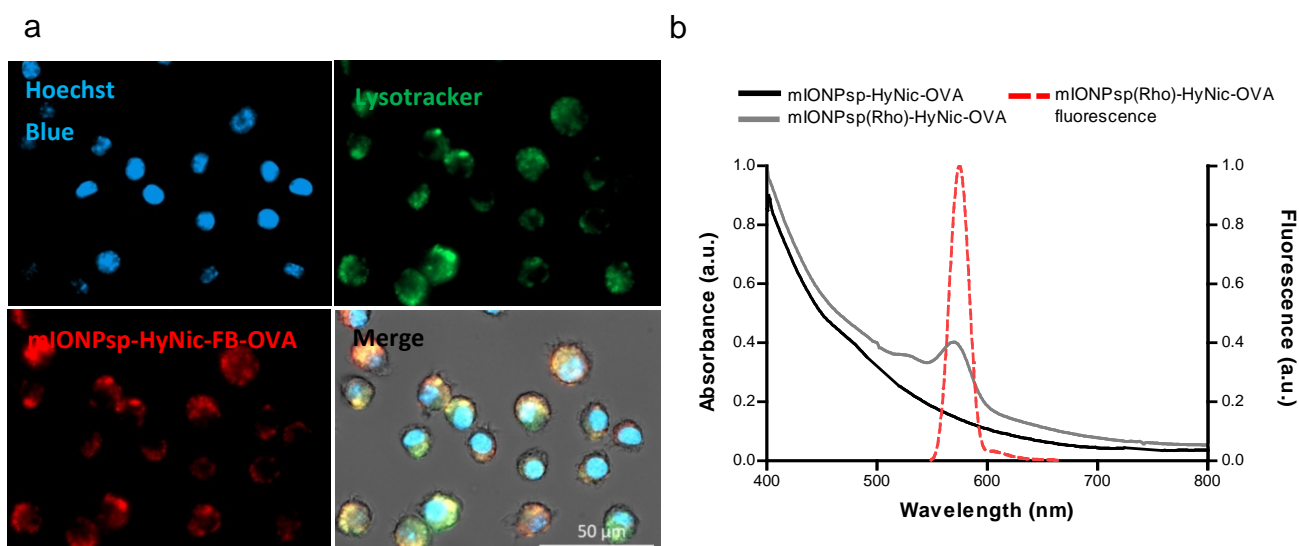
Figure 2. *In vitro uptake and trafficking of rhodamine labeled mIONPsp-HyNic-OVA micelles. a) Fluorescence microscopy images of J774A.1 macrophages showing endocytic uptake of mIONPsp-HyNic-FB-OVA after 3 h incubation. Cells' nuclei were stained with Hoechst blue and lysosomes and endosomes with Lysotracker green. b) UV-vis absorption and fluorescence spectrum of rhodamine-labelled mIONPsp-HyNic-FB-OVA.*

3.2.3: Preparation of hydrophilic Fe₃O₄-Au JanusNPs (mJanusNPs)

Hydrophilic (Fe_3O_4-Au) JanusNPs were synthesized in two consecutive seed-mediated growth steps as previously reported[18] by Dr. Javier Reguera at CIC

BiomaGUNE. In order to obtain JanusNPs, gold nanospheres were prepared and used as seeds for the growth of gold- iron oxide nanodumbbells. Afterwards, these nanodumbbells were used as seeds for the directional growth of asymmetric gold nanostars (**Figure 3**).
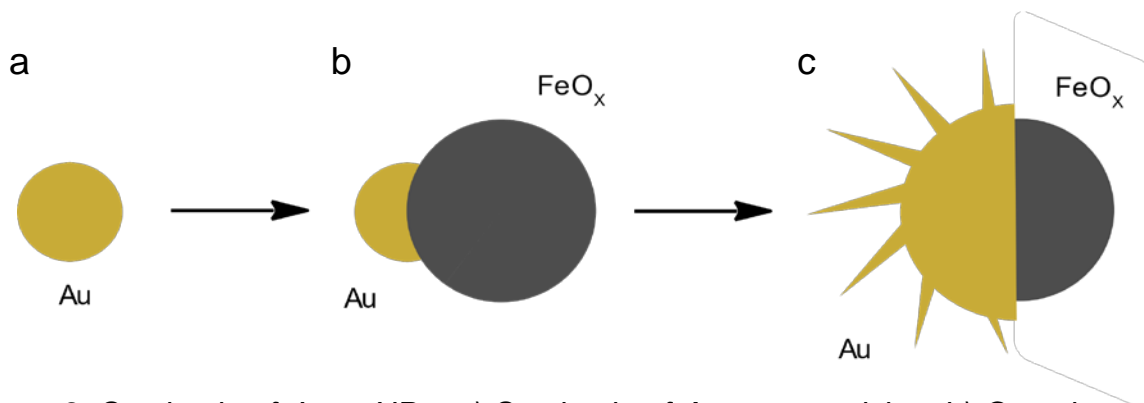
Figure 3. *Synthesis of JanusNPs. a) Synthesis of Au nanoparticles. b) Growth of an IONP and subsequent oxidation. c) Growth of an Au nanostar using the nanodumbbells as seeds.*

The growth of a gold nanostar is performed in presence of polyvinylpyrrolidone (PVP) which acts both as reducing agent and shape-directing capping agent. The nanoparticles were further functionalized selectively with a thiol-functionalized PEG (PEG thiol) and alendronic acid (**Figure 4***a*). The thiol group provides affinity to the gold surface whereas the alendronic acid binds to the iron oxide surface, and both interactions increase the overall colloidal stability of the nanoparticles. Moreover, the amino group of the alendronate ligands can be used for the covalent attachment of ovalbumin. TEM images show uniform nanoparticles with an average equivalent diameter of around 37.4 ± 2.8 nm for the core and featuring a distinctive Janus morphology where the smaller iron oxide lobe protrudes from the gold nanostar (**Figure 4***b, c*). The mJanusNPs showed a low polydispersity of 0.16 and a number-averaged hydrodynamic diameter of 45.67 ± 15.43 nm (**Figure 4***d*) due to the branched morphology of the particle, the organic coating and hydration water around the nanoparticle. Finally, elemental analysis by ICP was used to determine the [Au] and [Fe] concentrations showing a molar ratio of [Au] / [Fe] = 3.83.
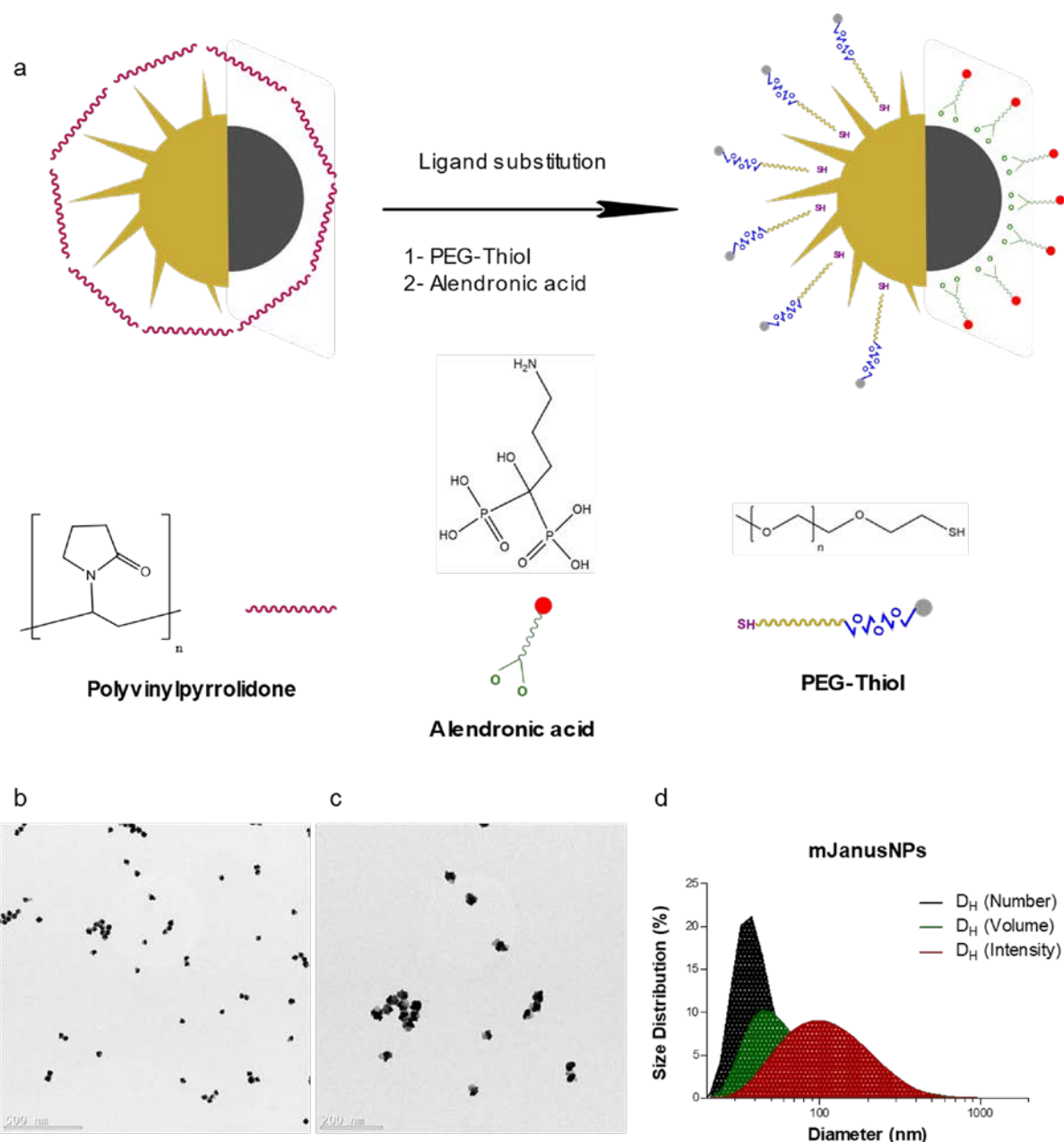
Figure 4. *a) Representation of the ligand substitution reaction. b), c) TEM images at different magnifications and d) Size distribution of mJanusNPs.*

3.2.4: Synthesis and characterization of mJanusNPs linked to OVA via hydrazone bond (mJanusNPs-HyNic-FB-OVA)

In order to contribute to the development of JanusNPs as new vaccine nanoplatforms, OVA was bound to the iron oxide patch of these JanusNPs by using the hydrazone strategy, obtaining a new antigen-loaded nanoplatform. Conjugation of OVA to the linker 4FB yielded 4FB-OVA, and an aromatic

aldehyde was introduced onto the mJanusNPs at the terminal amine group of the alendronic acid on the iron oxide patch at a pH of 7 yielding mJanusNPs-HyNic. By reacting 4FB-OVA with mJanusNPs-HyNic at a pH of 6.2 and in presence of aniline as nucleophile catalyst, mJanusNPs-HyNic-FB-OVA were obtained, which formation could be monitored by UV-Vis following the formation of the chromophore hydrazone (**Figure 5***c*). mJanusNPs-HyNic-FB-OVA showed a number-averaged hydrodynamic diameter of 44.16 ± 14.17 nm, ideal for lymph node delivery (**Figure 5***b*) and a low polydispersity of 0.25. The hydrazone conjugation achieved a loading ratio of ~1 OVA molecule per 2000 Fe atoms and the resulting nanoparticles showed no signs of aggregation for up to a week by visual inspection.
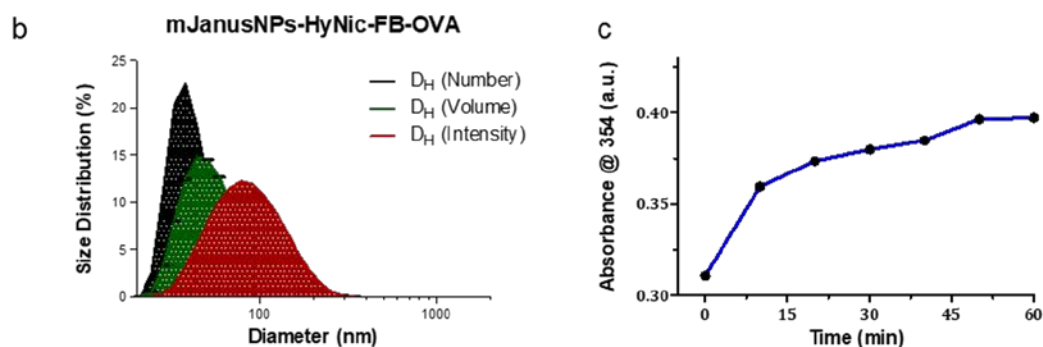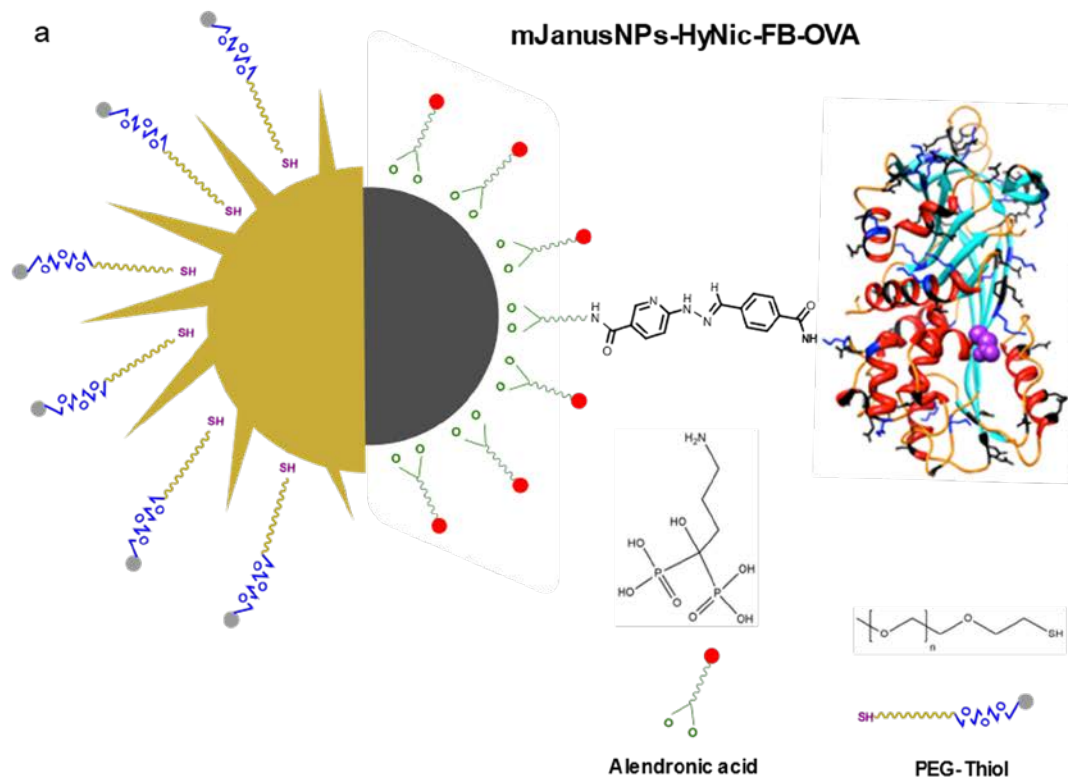
d	Core Diameter (nm)	Hydrodynamic Diameter (nm)	Polydispersity Index (PDI)	Biomolecule/ Iron atoms ratio
mJanusNP	37.4 ± 2.8	45.67 ± 15.43	0.16 ± 0.010	-
mJanusNP-FB-HyNic-OVA	37.4 ± 2.8	44.16 ± 14.17	0.25 ± 0.01	1/ 2000

Figure 5. a) General strategy for the conjugation of OVA to mJanusNPs. b) size distribution of mJanusNPs-HyNic-FB-OVA. c) Monitoring of the conjugation reaction between mJanusNPs-HyNic and FB-OVA in presence of ~100 mM of aniline. d) Table summarizing the main characteristic of mJanusNPs and mJanusNPs-HyNic-FB-OVA.

3.2.5: Co-functionalization of mIONPsp with *E. Coli* LPS and OVA

Next, the attempts made for creating nanoparticles carrying both the antigen and the adjuvant will be discussed. mIONPsp-*E. Coli* LPS were prepared using DSPE-aPEG, and following the same procedures described in chapter 2. Then, the conjugation to OVA was performed using the hydrazone strategy already used for the synthesis of mIONPsp-HyNic-FB-OVA. The resulting nanosystem, mIONPsp-*E. Coli* LPS/HyNic-FB-OVA (***Figure 6***a), was characterized using *TEM*, DLS and by measuring the ζ-potential of the particles (***Figure 6***b, c, d). The mIONPsp-*E. Coli* LPS/HyNic-FB-OVA showed a uniform size distribution with a number-averaged size of 27.08 ± 9.30 nm, which is still within the size range of 20-80 nm ideal for lymph node delivery. The ζ-potential of -7.10 mV, which is more negative than the one of the control nanomicelles, is consistent with the incorporation of the negatively charged *E. Coli* LPS in the micelles and should contribute to promoting accumulation in the lymph nodes, as shown in the literature[19,20]. The OVA payload was quantified using the commercial BCA kit to determine protein concentration and a loading of 2 molecules of OVA per NP was detected. The particles formed were soluble in water and did not show any aggregation for weeks upon visual inspection.

a

mIONPsp-*E. Coli* LPS/HyNic-FB-OVA

PEG-phospholipid

Oleic acid

b

mIONPsp-*E. Coli* LPS/HyNic-FB-OVA

— D_H(Number)
— D_H(Volume)
— D_H(Intensity)

Size Distribution (%)

Diameter (nm)

c

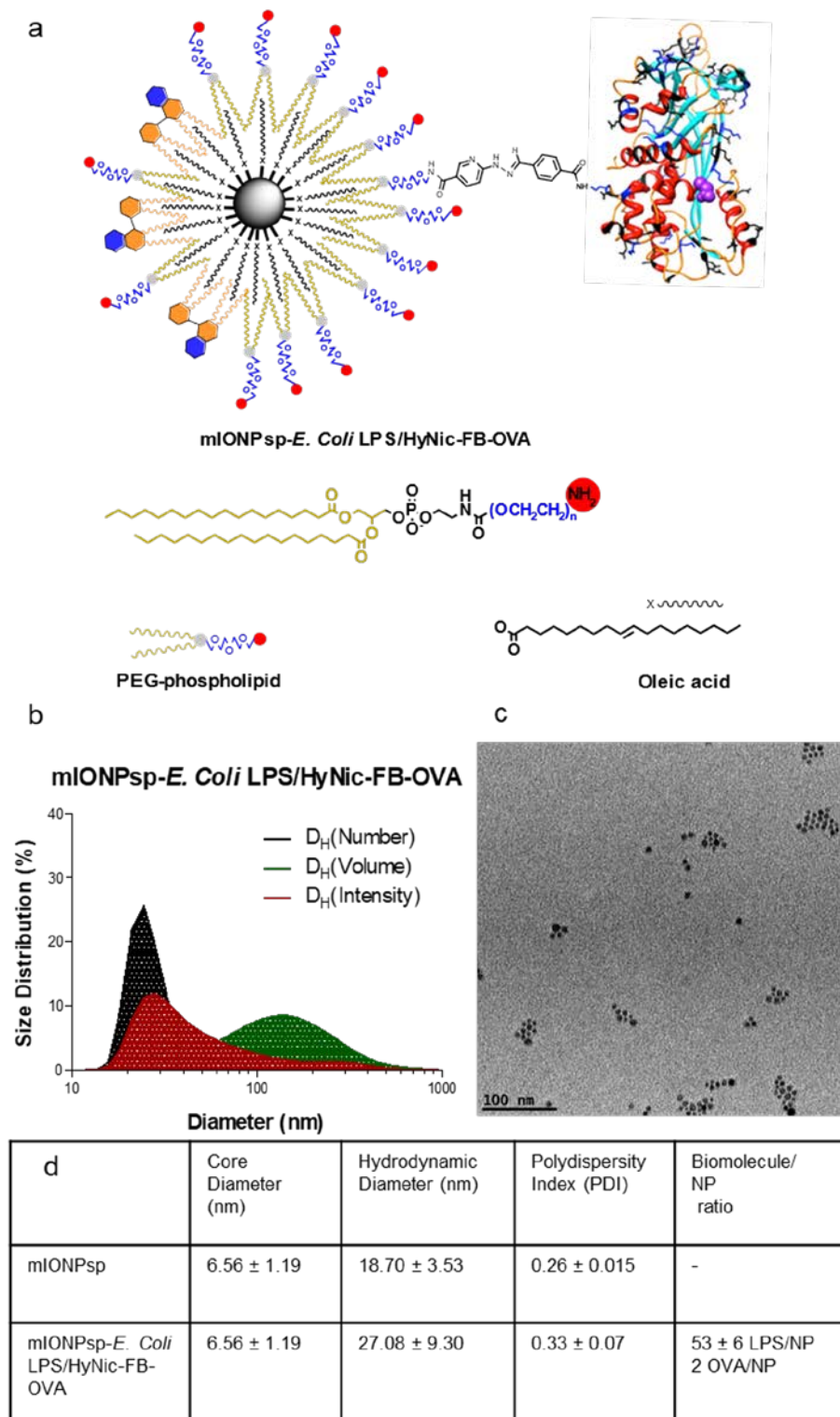| d	Core Diameter (nm)	Hydrodynamic Diameter (nm)	Polydispersity Index (PDI)	Biomolecule/ NP ratio
mIONPsp	6.56 ± 1.19	18.70 ± 3.53	0.26 ± 0.015	-
mIONPsp-*E. Coli* LPS/HyNic-FB-OVA	6.56 ± 1.19	27.08 ± 9.30	0.33 ± 0.07	53 ± 6 LPS/NP 2 OVA/NP

Figure 6. *a) Pictorial representation of the final product and b-d) characterization of mIONPsp-E- Coli LPS/HyNic-FB-OVA. b) DLS analysis of size, c) representative TEM micrograph and d) main characterization data. Data are representative of n > 3 formulation replicates.*

3.2.6: Antigen cross-presentation by mIONPsp-*E. Coli* LPS/HyNic-FB-OVA in bone marrow-derived dendritic cells

MHCI-mediated antigen presentation, also known as cross-presentation, is fundamental in cancer immunotherapy since it allows to initiate CD8+T cell responses, yielding an effective cytotoxic immune response against tumor cells[21].

Since naïve antigen-specific CD8+ T cells cannot directly recognize and eliminate cancer cells, they need to be activated by professional APCs to become active CTLs. Among APCs, DCs can process a variety of antigens and are in charge of activating naïve T cells. On their own, DCs need to acquire and internalize exogenous antigens, and have the capability of presenting it in both MHC class II molecules and MHC class I molecules, the so-called cross-presentation. By this mechanism, tumor antigens can be presented to CD8+ T cells. Upon maturation, DCs migrate to the lymphoid organs where they present the antigen to naïve T cells. The activated T cells subsequently proliferate and leave the lymph nodes in search of cells to kill in an antigen-dependent manner[22]. Although various types of APC can cross-present model antigens in vitro, most studies indicate that DCs are the main cross-presenting APCs in vivo, and that cross-presenting DC subsets thus have a major role in antitumor immune responses[23].

After TLR stimulation, cross presentation by some subsets of mice DC has been observed "ex vivo" and its dependence upon the TRIF signaling pathway induced by this molecule has been reported[24,21]. Loading of the LPS adjuvant and OVA on the same particle could improve the delivery timing and thus boost the immune responses due to an improved cross-presentation. For instance, this was demonstrated using aluminum hydroxide polymer nanoparticles loaded with OVA and CpG as an adjuvant, which resulted in effective cross-presentation of antigen and improved CD8+ T cell responses that led to prolonging survival in B16-OVA tumor-bearing mice[25]. In order to test the possibilities attainable by the delivery of the antigen and adjuvant loaded together on a single particle, cross-presentation experiments were performed at the VIB-UGent Center for Inflammation Research in Ghent. BMDCs were administered and incubated overnight (17 h) with mIONPsp-*E. Coli* LPS,

mIONPsp-HyNic-FB-OVA (here reported as LPS-mIONPsp and OVA-mIONPsp respectively), the combination of mIONPsp-*E. Coli* LPS + mIONPsp-HyNic-FB-OVA, mIONPsp-*E. Coli* LPS/HyNic-FB-OVA (here reported as OVA-LPS-mIONPsp) LPS, OVA, and LPS + OVA. All the formulations used showed a similar activity at inducing both CD86 production and MHC I expression, and the expression of these markers was not affected differently by the use of mIONPsp-*E. Coli* LPS + mIONPsp-HyNic-FB-OVA versus mIONPsp-*E. Coli* LPS/HyNic-FB-OVA. The used concentrations of LPS might have been already quite high to detect differences between the different systems (14 μg/ mL when [OVA] = 2 μg/mL and 1.8 μg/ mL when [OVA]= 250 ng/mL). Song et al reported that a concentration of 1 μg/ mL of LPS can already induce twice as much CD80 and CD54 expression than different PLGA NPs loaded with OVA in dendritic cells[26]. On the other hand, it was found that mIONPsp-HyNic-FB-OVA can slightly enhance CD86 and MHC class I with respect to OVA alone at the highest concentration, a behavior that might be explained by the nanoparticle activating the DCs machinery even when not loaded with any adjuvant or antigen.
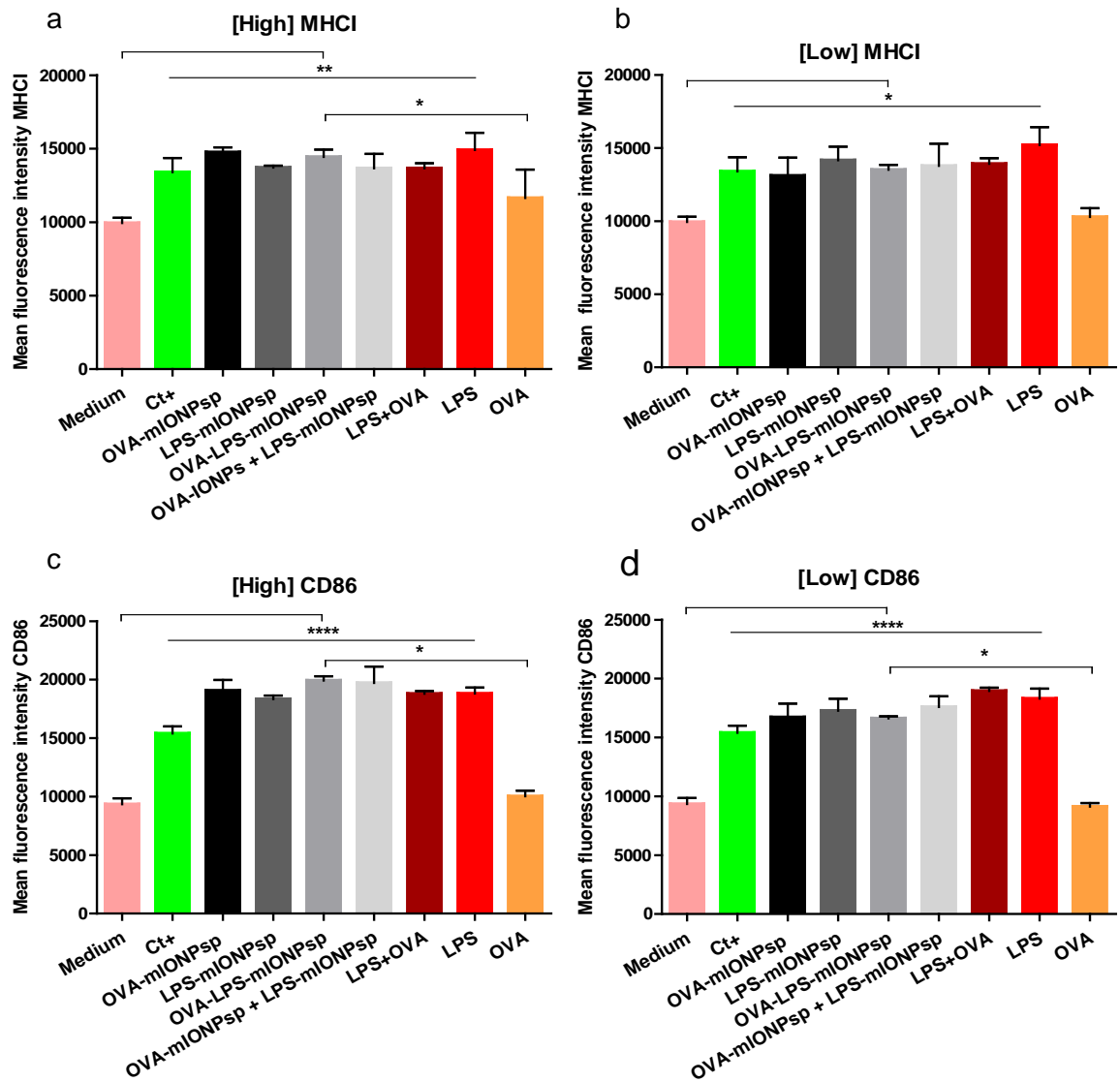
Figure 6: mIONPsp- E. Coli LPS/HyNic-FB-OVA doesn't improve cross-presentation with respect to the mIONPsp-E. Coli LPS + mIONPsp-HyNic-FB-OVA system. a): expression of MHCI at an [OVA]= 2 μg/mL; b): expression of MHCI at an [OVA]= 250 ng/mL; c): expression of CD86 at an [OVA]= 2 μg/mL; d): expression of CD86 at an [OVA]= 250 ng/mL.

3.3: Conclusions

In this chapter different types of nanoplatforms for antigen delivery and co-delivery with TLR4 agonists have been designed, developed and characterized. An aniline-catalyzed hydrazone ligation strategy was used for the conjugation of the tumor antigen OVA to these nanoplatforms, enabling a highly efficient, monitorable and stable covalent conjugation to create multi-functional nanovaccines under physiological conditions at very low concentrations. The simplest platform developed, mIONPsp-HyNic-FB-OVA, was obtained in high yield at micromolar concentrations yielding a stable product which showed uniform size distribution. This construct was rapidly taken up by antigen presenting cells. This system was used in "in vivo" experiments as a nanovaccine together with the mIONPsp-*Xcc* LOS developed in chapter 2 and the obtained results are discussed in the following chapter. A platform where OVA and the adjuvant LPS were bound to the same nanoparticle was also developed and investigated for improving antigen cross-presentation in dendritic cells. Finally, an asymmetrical or "Janus" nanoplatform was developed, mJanusNPs-HyNic-FB-OVA, which combines the properties of iron oxide nanoparticles and gold nanoparticles and allows a different surface chemistry for each material "patch" to be used, allowing different (bio)functionalization. OVA was anchored to the alendronate ligands bound to the IONPs side of the Janus particle using the covalent hydrazone chemistry strategy. This sophisticated nanoplatform was characterized by TEM, DLS and measuring the ζ-potential and OVA payload and represents a highly promising platform for antigen delivery which can be further functionalized and used in different theranostics applications.

3.4: Materials and Methods

Materials: Unless otherwise specified all commercially available reagents were used without further purification. DSPE-aPEG and Rho-PE were purchased from Avanti polar lipids. Hydrogen tetrachloroaurate(III) trihydrate (99.99%) was purchased from Alfa Aesar, oleylamine (80-90%) was purchased from Acros organics, 1- octadecene (90%), oleic acid (90%), iron(0) pentacarbonyl (99.99%), 1,2-hexadecanediol (90%), methoxypolyethylene glycol acetic acid (80%, Mn = 5000 g/mol), 4- mercaptobenzoic acid (90%) and PVP (MW = 10 Kg/mol) were all purchased from Sigma-Aldrich, thiol- terminated PEG (Mn = 750 g/mol), was purchased from Polymer Source. Endo-Ova (Endotoxin-free Ovalbumin) was purchased from Hyglos GmbH; Succinimidyl 6-hydrazinonicotinamide acetone hydrazone was purchased from Solulink; Succinimidyl 4-Formylbenzoate was purchased from Santa Cruz biotechnology; 2-hydrazinopyridine-2HCl was purchased from Fluorochem. Lipopolysaccharides from Escherichia coli O55:B5 and poly(ethylene glycol) methyl ether thiol (average Mn 2000) were purchased from Sigma-Aldrich. 0.45 μm syringe filter were purchased from Pall life sciences; PD MiniTrap G-10 desalting column were from GE Healthcare; Amicon Ultra-0.5 mL Centrifugal filters (100 KDa Molecular weight cut-off) and Amicon Ultra-4mL (10 KDa Molecular weight cut-off) were purchased from Merck; Pierce LAL chromogenic endotoxin quantitation kit, Hoechst 33342 (Hoechst blue) and Lysotracker green DND-26 were purchased from Thermo Fisher. Dulbecco's Modified Eagle Medium (DMEM), Fetal Bovine Serum (FBS), Penicillin/Streptomycin (P/S) and L- glutamine (L-Glu) were all purchased from Gibco; Cell culture plates were purchased from Nunc; Red blood cells (RBC) lysis buffer was purchased from BD Biosciences; 100 mm bacteriological Petri dishes were purchased from Falcon; Granulocyte-macrophage colony-stimulating factor (GM-CSF) was purchased from Peprotech; FC block, Amcyan-labelled L/D staining, APC-labelled anti-CD11c, PE-Cy7-labelled anti-CD86 and PE-labelled MHCI antibodies were all purchased from BioLegend; Ibidi μ-Slides VI$^{0.4}$ were purchased from Ibidi.

Synthesis of iron oxide nanoparticles (IONPsp): Hydrophobic spherical IONP (IONPsp) were prepared as described in chapter 2.

Preparation of Janus NPs: The synthesis of the asymmetric dumbbell seeds was performed as previously reported by a one-pot two-step method[27].

Briefly, for the 20 nm iron oxide part, a solution in 1-octadecane (47 mL) was prepared containing oleic acid (6 mmol, 1.90mL), oleylamine (6 mmol, 1.97mL) and 1,2-hexadecanediol (10 mmol, 2.58g) and stirred for 15 min at 160 ºC under N_2. $Fe(CO)_5$ (2 mL) was then injected and after 3 min a solution containing $HAuCl_4 \cdot 3H_2O$ (0.1 mmol) dissolved in a mixture of oleylamine (0.5 mL) and 1-octadecane (3 mL) was injected and heated up to 310 °C at approximately 3 °C/min. The solution was left to react for 45 min under magnetic stirring. After cooling down, the dispersion was exposed to air for 30 min to cause Fe oxidation. To purify the nanoparticles, 50 mL of isopropanol were added and the solution was centrifuged at 4500 xg for 30 min. The nanoparticles were cleaned two more times after redispersion with hexane and aggregation with isopropanol. Finally, oleylamine (100 µL) was added to store the nanoparticles for long periods of time in a hexane-chloroform solution.

The nanodumbbells were cleaned three times in ethanol and redispersed in chloroform to remove as much as oleylamine as possible. Then, they were redispersed in chloroform at a concentration of approximately 2 mg/mL. A small quantity of carboxyl terminated PEG-PL (PEG-COOH) was added to the solution (to have approximately 2 mg/mL of polymer) and left for 1 h. This step was performed to obtain a good dispersion when the seeds were added to the DMF gold solution.

A solution of $HAuCl_4 \cdot 3H_2O$ (2.184 mL, 50 mM) was added to a solution containing PVP (40 g) dissolved in DMF (400 mL). The solution was left stirring to allow gold salt prereduction from Au^{3+} to Au^+ as described elsewhere[28] (this time was highly dependent on the PVP batch and needed to be adjusted by UV-vis, in this case it was 5 min). The dumbbell nanoparticle solution (at different volumes) was then quickly added and the reaction was left reacting for 1 h, showing a fast color change into blue. The nanoparticles were purified in 4 centrifugation cycles, redispersed 2 times in ethanol and 2 times in water and at a relative centrifugation force of 2500-4000 xg, depending on the nanoparticle size. The nanoparticles were finally redispersed in 40 mL of ultrapure water.

Ligand exchange: Janus nanoparticles were incubated overnight with PEG-thiol (50 ligands/nm^2 assuming a spherical particle). Then the particles were

centrifuged twice at 600 xg for 10 min to remove the unbound PEG-thiol. Alendronic acid (1000 ligands/nm^2) was added to the nanoparticles and they were incubated overnight with 0.83 mM NaOH. Finally, the nanoparticles were centrifuged twice at 600 xg for 10 min and the pellet was redissolved in water. Calculation of the number of ligands/nm^2: The amount of Au was determined by UV-vis using a calibration curve. The [Au] / [Fe] ratio was determined previously by ICP and used to calculate the concentration of Fe. The surfaces of the IONP and Au patch were determined using the known densities and the sizes of the magnetite and Au patches.

IONPsp- filled nanomicelles preparation: 1 mg of IONPsp and 2 mg of PEG phospholipid (DPPE-aPEG) were dissolved in 100 μL and 200 μL of chloroform respectively, combined in a 4 mL round bottomed glass vial with 100 μL of chloroform and let to evaporate overnight at RT. LPS loaded micelles (for mIONPsp-*E. Coli* LPS/HyNic-FB-OVA) were prepared as above described, with the exception that 0.2 mg of or LPS were added to the latter 100 μL of chloroform and dissolved thoroughly using a vortex mixer (5 minutes) and an ultrasonic cleaner (30 minutes). Fluorescent micelles were prepared adding a 5% of 1,2-dimyristoyl-*sn*-glycero-3-phosphoethanolamine-N-lissamine Rhodamine B sulfonyl-ammonium salt to the phospholipids mixture. The flask was placed in a water bath at 80 °C for 30 s, after which micelles were re-dissolved in 1 mL of MilliQ water. This solution was centrifuged at 5000 xg for 5' and passed through a 0.45 μm syringe filter to remove non-soluble particles. Then, the micelles were centrifuged at 108600 xg for 50 minutes; the supernatant was discarded and washed with MilliQ water to remove empty PEG micelles (3 cycles). Finally, the pellet was dissolved in 400 μL of MilliQ water. Micelles were stored at 4ºC. In order to quantify the concentration of iron, ICP analysis was carried out. Briefly, 10 μL of micelles were digested in concentrated HNO_3 over a minimum of three days. Prior to the measurement, the samples were diluted up to 8 mL in MilliQ water (final acid concentration: 1-2 %). ICP-AES analyses were carried out on a Perkin Elmer Optima 5300 DV (Perkin Elmer, Santa Clara, CA, USA) at CIC BiomaGUNE by the Mass spectrometry platform. A range of calibration standards were prepared using single element 1000 mg/L stock solutions (Fisher Scientific UKLTD) and a

Merck multielement standard (ICP Multi element standard solution, VICertiPUR) was employed as a reference standard.

Transmission electron microscopy (TEM) studies were performed using a JEOL JEM-2011 electron microscope operating at 120 kV. The samples were prepared by deposing a drop of a solution of IONPs (1 mg/mL in THF) onto Pelco 150 mesh grid (Ted Pella) and allowing it to dry. For the preparation of hydrophilic samples, TEM grids were polarized using a Quorum technologies K100X glow discharge system. IONPs size was determined from TEM images, measuring a minimum of 200 nanocrystals with the software ImageJ.

Hydrodynamic diameter and ζ-potential of the micelles were measured using a Z-Sizer (Malvern Nano-Zs, UK). To determine the stability, mIONPsp-HyNic-FB-OVA was dissolved at a concentration of approx. 5 mM in 10 mM PBS and the hydrodynamic diameter analyzed by Z-Sizer immediately after purification and over a 4 weeks period. To measure the ζ-potential, the samples were dissolved at a concentration of approx. 0, 5 mM in 10 mM NaCl and analyzed by Z-sizer immediately after purification and over a 4 weeks period.

Conjugation of IONPsp to HyNic (Succinimidyl 6-hydrazinonicotinamide acetone hydrazone): In a typical synthesis, IONPsp micelles (~3- 0.5 µM) were added to a 50 mM NaPi buffer (pH 7.4) and coupled to a 100 mM HyNic solution in CH$_3$CN (420 µL total volume). The reaction mixture was stirred overnight (~14 h) at room temperature and the product was purified using both a desalting column and a 0.5 mL centrifugal filter (100 KDa MW cut-off) (10000 xg, 5 min.) and kept at 4ºC until further use.

Conjugation of Ovalbumin to FB (Succinimidyl 4-Formylbenzoate): a 450 µM Endotoxin-free OVA solution in 50 mM NaPi buffer (pH 7.4) was added to a 100 mM FB solution in DMSO (550 µL total volume) and stirred overnight (~14 h) at room temperature. Purification was carried on using a desalting column and a 4 mL centrifugal filter (10 KDa MW cut-off) (2000 xg, 15 min.). The product was stored at 4ºC.

Covalent attachment of Ovalbumin to IONPsp micelles: HyNic modified IONPsp (~3- 0.5 µM) were first mixed to a 50 mM NaPi buffer (pH 6.2) and conjugated to FB modified OVA (30- 20 µM). Finally, 100 mM Aniline was added (250 µL

total volume). The reaction mixture was stirred overnight (~14 h) at room temperature and the product was purified by a desalting column and a 0.5 mL centrifugal filter (100 KDa MW cutoff) (10000 xg, 5 min.). The obtained product was centrifuged at 17400 g for 20' and the pellet washed with MilliQ water to remove any unbound OVA. The number of OVA molecules bound to the nanoparticle was determined using a commercial BCA kit (ThermoFisher).

Conjugation of JanusNPs to HyNic: (Succinimidyl 6-hydrazinonicotinamide acetone hydrazone): In a typical synthesis, mJanusNPs (~1 mM Fe) were added to a 50 mM NaPi buffer (pH 7.4) and coupled to a 100 mM HyNic solution in CH_3CN (300 µL total volume). The reaction mixture was stirred overnight (~14 h) at room temperature and the product purified using a 0.5 mL centrifugal filter (100 KDa MW cut-off) (600 xg, 10 min.) and kept at 4°C until further use.

Covalent attachment of Ovalbumin to mJanusNPs-HyNic: HyNic modified Janus NPs (~0.5 mM Fe) were first mixed to a 50 mM NaPi buffer (pH 6.2) and conjugated to FB modified OVA (30- 20 µM). Finally, 100 mM Aniline was added (180 µL total volume). The reaction mixture was stirred overnight (~14 h) at room temperature and the product was purified by a desalting column and a 0.5 mL centrifugal filter (100 KDa MW cutoff) (600 xg, 10 min.). The obtained mJanusNPs-HyNic-FB-OVA were centrifuged at 600 xg for 15' and the pellet washed with MilliQ water to remove any unbound OVA. The number of OVA molecules bound to the nanoparticle was determined using a commercial BCA kit (ThermoFisher). In order to quantify the concentration of iron, ICP analysis was carried out, as already reported.

Monitoring of the mJanusNPs-HyNic to 4FB-OVA coupling reaction: 0.5 µM mJanusNPs-HyNic were added to 20 µM 4FB-OVA in 50 mM NaPi buffer (pH 6.2) in a quartz cuvette (500 µL total volume). Aniline (3 µL) was added drop wise to the reaction mixture and the reaction was monitored at a wavelength of 354 nm using a UV-Vis spectrometer.

Estimation of HyNic groups linked to mIONPsp-HyNic micelles: 1.5 µM mIONPs-HyNic micelles were mixed with 0.5 mM 4-nitrobenzaldehyde and 100

mM Aniline in 50 mM pH 6.2 NaPi buffer (500 µL total volume) in a quartz cuvette and thoroughly stirred. The formed hydrazone bond was monitored by UV-Vis at 345 nm and the molar substitution ratio was obtained using the absorption coefficient (ε= 18000) found in the literature.

Estimation of 4-FB groups linked to Ovalbumin: 45 µM functionalized 4FB-OVA was mixed to a 0.5 mM solution of 2-hydrazinopyridine-2HCl and 100 mM Aniline in 50 mM pH 7.4 NaPi buffer (500 µL total volume), put in a quartz cuvette, stirred and finally the absorbance was measured. The reaction kinetics of the hydrazone bond formation were monitored for 120 min at 345 nm using a UV-Vis spectrophotometer and the 4FB-OVA molar substitution ratio was obtained using the extinction coefficient at 24600 for the hydrazone chromophore.

Monitoring of the mIONPsp-HyNic to 4FB-OVA coupling reaction: 3 µM mIONPsp-HyNic were added to 20 µM 4FB-OVA in 50 mM NaPi buffer (pH 6.2) in a quartz cuvette (500 µL total volume). 3 µL of aniline were added drop wise to the reaction mixture and the reaction was monitored at a wavelength of 354 nm using a UV-Vis spectrometer.

Fluorescence microscopy: J774A.1 cells were seeded in an Ibidi µ-Slide VI$^{0.4}$ at a density of 30000 cells/ well in DMEM supplemented with 10% Fetal Bovine Serum and 1% Penicillin/Streptomycin and let to adhere overnight in an incubator maintained at 37 °C and 5% CO_2. The day after, the medium was removed and cells were administered with 1 µg/ mL Hoechst blue to stain the nuclei and incubated for 30 minutes. Cells were washed with PBS three times in order to get reed of the unbound dye and then stained with ~200 nM mIONPsp(Rho)-HyNic-FB-OVA and incubated for three hours. Cells were washed again and stained with 1 mM Lysotracker green, incubated for 30 minutes, washed with PBS and finally images were taken using a ZEISS Axio Observer inverted microscope.

Preparation of mIONPsp- *E. Coli* LPS/HyNic-FB-OVA: 1 mg of IONPsp, 2 mg of PEG phospholipid (PEG-NH$_2$) and 0.2 mg of LPS were dissolved in 100, 200 and 100 µL of chloroform respectively, added to a 4 mL round bottomed glass vial and let to evaporate overnight at RT. Upon adding LPS to the latter 100 µL

of chloroform, it was dissolved thoroughly using a vortex mixer (5 minutes) and an ultrasonic cleaner (30 minutes). The flask was placed in a water bath at 80 °C for 30 s and micelles were re-dissolved in 1 mL of MilliQ water. This solution was centrifuged at 3000 xg for 5' and passed through a 0.45 µm syringe filter to remove non-soluble particles. Micelles were then centrifuged at 108600 xg for 50 minutes; the supernatant was discarded or kept for LPS quantification and washed with MilliQ water to remove empty PEG micelles (3 cycles). Finally, the pellet was dissolved in 200 µL of MilliQ water. Micelles were stored at 4°C.

Quantification of LPS loading on mIONPsp-*E. Coli* LPS/HyNic-FB-OVA micelles: The amount of LOS incorporated on micelles was carried out before conjugation with OVA and measured as previously described for LOS- and LPS- loaded micelles. Briefly, a calibration curve was prepared plotting the immune stimulating activity of the pure ligand on cell cultures versus its concentration and used to determine the amount of ligand bound to the nanoparticle indirectly, measuring the amount of ligand that remained in the supernatants from the micelles' workup. The efficiency of this method was double checked using a commercial kit (Pierce LAL chromogenic endotoxin quantitation kit) and following the instructions given by the kit's manufacturer. The assay was performed in aseptic conditions. Briefly, 50 µL of standards or samples were put on a 37°C 96 well microplate (in duplicates), incubated for 5 min. at 37°C, after which the LAL reagent was added to each well. Following a 10 min. incubation at 37°C, 100 µL of substrate solution were added, stirred and incubated for 6 min. at 37°C. Then, 25 µL of stop solution were added and the absorbance at 405 nm was immediately measured using a Varioskan LUX multimode plate reader (Thermo Fisher). The concentration of LPS in the unknown samples was determined using a calibration curve.

Conjugation of mIONPsp-*E. Coli* LPS to HyNic (Succinimidyl 6-hydrazinonicotinamide acetone hydrazone): The procedure previously described was followed, with slight variations: mIONPsp-*E. Coli* LPS micelles (~0.5- 0.2 µM) were added to a 50 mM NaPi buffer (pH 7.4) and coupled to a 100 mM HyNic solution in CH_3CN (300 µL total volume). The reaction mixture was stirred overnight (~14 h) at room temperature and the product was purified

using both a desalting column and a 0.5 mL centrifugal filter (100 KDa MW cut-off) and kept at 4ºC until further use.

Covalent attachment of Ovalbumin-FB to mIONPsp- *E. Coli* LPS/HyNic micelles: HyNic modified mIONPsp- *E. Coli* LPS (~ 0.5- 0.2 µM) were first mixed to a 50 mM NaPi buffer (pH 6.2) and conjugated to FB modified OVA (30- 20 µM) (prepared as previously described). Finally, 100 mM Aniline was added (180 µL total volume). The reaction mixture was stirred overnight (~14 h) at room temperature and the product was purified by a desalting column and a 0.5 mL centrifugal filter (100 KDa MW cutoff). The obtained product was centrifuged at 17400 xg for 20' and the pellet washed with MilliQ water to remove any unbound OVA. The number of OVA molecules bound to the nanoparticle was determined using a commercial BCA kit (ThermoFisher). In order to quantify the concentration of iron, ICP analysis was carried out, as already reported.

BMDC primary culture establishment: C57BL/6J mice (6–12 weeks old) were sacrificed by cervical dislocation and intact femurs and tibiae of hind limbs were removed aseptically as described elsewhere.[29] After washing the bones in cold PBS (10 mM), the bone marrow was obtained by tearing apart the bones, putting them in a small Eppendorf tube and centrifuging at 2000 xg until it came out. The obtained bone marrow cells were flushed with same buffer using a syringe. After the erythrocytes were lysed with a commercial RBC lysis buffer (BD Biosciences), the cells were washed and resuspended in RPMI-1640 medium supplemented with 10 % FBS, 1 % P/S and 1 % L-glutamine (200 mM, Gibco). On day zero cells were plated at a concentration of $2 \cdot 10^6$ cells per 100 mm bacteriological Petri dish (Falcon) in 10 mL of medium supplemented with 20 ng/mL of murine GM-CSF (Peprotech) and maintained at 37 °C and 5% CO_2. On day 3, 10 mL of complete RPMI-1640 medium containing GM-CSF (20 ng/mL) was added to each Petri dish. On day 6, half of the supernatant was collected, centrifuged and cell pellet resuspended in 10 mL of fresh complete RPMI-1640 with GM-CSF (10 ng/mL) and added again to each Petri dish. Finally, at day 8 of the differentiation process, BMDCs were plated in 96-well plates ($2 \cdot 10^5$ cells/well) and incubated overnight (17h) (in triplicates) with the different stimuli. All experiments were carried out two times.

Analysis of DCs' maturation markers by flow cytometry: After overnight incubation with the different stimuli, 96-well plates containing the BMDCs were centrifuged (400 xg, 5 min, 4°C) and supernatants removed. Cells were washed with cold PBS, centrifuged again and the supernatants were removed. Cells were stained with FC block, Amcyan-labelled L/D staining, APC-labelled anti-CD11c, PE-Cy7-labelled anti-CD86 and PE-labelled MHCI antibodies (all from BioLegend). Cells were incubated with the stains for 20 min after which they were centrifuged and washed using cold PBS. Finally, cells were fixed using BD cytofix-cytoperm solution, washed using BD-wash/perm and finally analyzed. The expression of the different markers was analyzed using the FACS Fortessa flow cytometer. BMDCs were electronically gated based on the forward and side scatter parameters and the not-single events left out based on forward area and height scatter parameters. DCs were gated based on positive staining for CD11c population marker and the expression of the chosen maturation markers was analyzed within this population. Results were expressed as mean ± SEM of the MFI triplicates of each maturation marker representative of two independent experiments.

3.5: References

(1)   Gregory, A. E.; Titball, R.; Williamson, D. Vaccine Delivery Using Nanoparticles. *Front. Cell. Infect. Microbiol.* **2013**, *25* (3), 13.

(2)   Takami Akagi; Baba, M.; Akashi, M. Regulation of Immune Responses by Nanoparticle-Based Vaccine. In *Biodegradable Nanoparticles as Vaccine Adjuvants and Delivery Systems*; 2011; p 31.

(3)   Verma, P.; Biswas, S.; Mohan, T.; Ali, S.; Rao, D. N. Novel Adjuvants and Delivery Vehicles for Vaccines Development: A Road Ahead. *Indian J Med Res.* **2013**, *138* (5), 779.

(4)   Saroja C. H.; Lakshmi P. K.; Bhaskaran S. Recent Trends in Vaccine Delivery Systems: A Review. *Int. J. Pharm. Investig.* **2011**, *1* (2), 64.

(5)   Moyer, T. J.; Zmolek, A. C.; Irvine, D. J. Beyond Antigens and Adjuvants: Formulating Future Vaccines. *J. Clin. Invest.* **2016**, *126* (3), 799.

(6)   Akagi, T.; Toyama, M.; Akashi, M.; Baba, M.; Shima, F.; Uto, T.; Nishi, Y. Comparative Activity of Biodegradable Nanoparticles with Aluminum Adjuvants: Antigen Uptake by Dendritic Cells and Induction of Immune Response in Mice. *Immunol. Lett.* **2011**, *140* (1), 36.

(7)   Hanson, M. C.; Bershteyn, A.; Crespo, M. P.; Irvine, D. J. Antigen Delivery by Lipid-Enveloped PLGA Microparticle Vaccines Mediated by in Situ Vesicle Shedding. *Biomacromolecules* **2014**, *15* (7), 2475.

(8)   O'Hagan, D. T.; Rappuoli, R. Novel Approaches to Vaccine Delivery. *Pharm. Res.* **2004**, *21* (9), 1519.

(9)   De Koker, S.; Lambrecht, B. N.; Willart, M. A.; Van Kooyk, Y.; Grooten, J.; Vervaet, C.; Remon, J. P.; De Geest, B. G. Designing Polymeric Particles for Antigen Delivery. *Chem. Soc. Rev.* **2011**, *40* (1), 320.

(10)   Schwendener, R. A. Liposomes as Vaccine Delivery Systems: A Review of the Recent Advances. *Ther. Adv. Vaccines* **2014**, *2* (6), 159.

(11)   Bovier, P. A. Epaxal®: A Virosomal Vaccine to Prevent Hepatitis A Infection. *Expert Rev. Vaccines* **2008**, *7* (8), 1141.

(12) Boraschi, D.; Italiani, P. From Antigen Delivery System to Adjuvanticy: The Board Application of Nanoparticles in Vaccinology. *Vaccines* **2015**, *3* (4), 930.

(13) Marques Neto, L. M.; Kipnis, A.; Junqueira-Kipnis, A. P. Role of Metallic Nanoparticles in Vaccinology: Implications for Infectious Disease Vaccine Development. *Front. Immunol.* **2017**, *8* (8), 239.

(14) Gregory, A. E.; Williamson, E. D.; Prior, J. L.; Butcher, W. A.; Thompson, I. J.; Shaw, A. M.; Titball, R. W. Conjugation of Y. Pestis F1-Antigen to Gold Nanoparticles Improves Immunogenicity. *Vaccine* **2012**, *30* (48), 6777.

(15) Almeida, J. P. M.; Lin, A. Y.; Figueroa, E. R.; Foster, A. E.; Drezek, R. A. In Vivo Gold Nanoparticle Delivery of Peptide Vaccine Induces Anti-Tumor Immune Response in Prophylactic and Therapeutic Tumor Models. *Small* **2015**, *11* (12), 1453.

(16) Ruiz-de-Angulo, A.; Zabaleta, A.; Gómez-Vallejo, V.; Llop, J.; Mareque-Rivas, J. C. Microdosed Lipid-Coated 67 Ga-Magnetite Enhances Antigen-Specific Immunity by Image Tracked Delivery of Antigen and CpG to Lymph Nodes. *ACS Nano* **2016**, *26* (10), 1602.

(17) Nembrini, C.; Stano, A.; Dane, K. Y.; Ballester, M.; van der Vlies, A. J.; Marsland, B. J.; Swartz, M. A.; Hubbell, J. A. Nanoparticle Conjugation of Antigen Enhances Cytotoxic T-Cell Responses in Pulmonary Vaccination. *Proc. Natl. Acad. Sci. U. S. A.* **2011**, *108* (44), E989.

(18) Reguera, J.; Jiménez De Aberasturi, D.; Henriksen-Lacey, M.; Langer, J.; Espinosa, A.; Szczupak, B.; Wilhelm, C.; Liz-Marzán, L. M. Janus Plasmonic-Magnetic Gold-Iron Oxide Nanoparticles as Contrast Agents for Multimodal Imaging. *Nanoscale* **2017**, *9* (27), 9467.

(19) Liu, H.; Irvine, D. J. Guiding Principles in the Design of Molecular Bioconjugates for Vaccine Applications. *Bioconjug. Chem.* **2015**, *26* (5), 791.

(20) Rao, D. A.; Forrest, M. L.; Alani, A. W. G.; Kwon, G. S.; Robinson, J. R. Biodegradable PLGA Based Nanoparticles for Sustained Regional

Lymphatic Drug Delivery. *J. Pharm. Sci.* **2010**, *99* (4), 2018.

(21) Popovic, Z. V.; Embgenbroich, M.; Chessa, F.; Nordström, V.; Bonrouhi, M.; Hielscher, T.; Gretz, N.; Wang, S.; Mathow, D.; Quast, T.; Schloetel J. G.; Kolanus W.; Burgdorf S.; Gröne H. J. Hyperosmolarity Impedes the Cross-Priming Competence of Dendritic Cells in a TRIF-Dependent Manner. *Sci. Rep.* **2017**, *7* (1), 1.

(22) Bol, K. F.; Schreibelt, G.; Gerritsen, W. R.; De Vries, I. J. M.; Figdor, C. G. Dendritic Cell-Based Immunotherapy: State of the Art and Beyond. *Clin. Cancer Res.* **2016**, *22* (8), 1897.

(23) Joffre, O. P.; Segura, E.; Savina, A.; Amigorena, S. Cross-Presentation by Dendritic Cells. *Nat. Rev. Immunol.* **2012**, *12* (8), 557.

(24) Mouries, J.; Moron, G.; Schlecht, G.; Escriou, N.; Dadaglio, G.; Leclerc, C. Plasmacytoid Dendritic Cells Efficiently Cross-Prime Naive T Cells in Vivo after TLR Activation. *Blood* **2008**, *112* (9), 3713.

(25) Jiang, H.; Wang, Q.; Li, L.; Zeng, Q.; Li, H.; Gong, T.; Zhang, Z.; Sun, X. Turning the Old Adjuvant from Gel to Nanoparticles to Amplify CD8+T Cell Responses. *Adv. Sci.* **2018**, *5* (1).

(26) Song, C.; Noh, Y. W.; Lim, Y. T. Polymer Nanoparticles for Cross-Presentation of Exogenous Antigens and Enhanced Cytotoxic t-Lymphocyte Immune Response. *Int. J. Nanomedicine* **2016**, *11*, 3753.

(27) Reguera, J.; Jiménez De Aberasturi, D.; Winckelmans, N.; Langer, J.; Bals, S.; Liz-Marzán, L. M. Synthesis of Janus Plasmonic-Magnetic, Star-Sphere Nanoparticles, and Their Application in SERS Detection. *Faraday Discuss.* **2016**, *191*, 47.

(28) Barbosa, S.; Agrawal, A.; Rodríguez-Lorenzo, L.; Pastoriza-Santos, I.; Alvarez-Puebla, R. A.; Kornowski, A.; Weller, H.; Liz-Marzán, L. M. Tuning Size and Sensing Properties in Colloidal Gold Nanostars. *Langmuir* **2010**, *26* (18), 14943.

(29) Lutz, M. B.; Kukutsch, N.; Ogilvie, a L.; Rössner, S.; Koch, F.; Romani, N.; Schuler, G. An Advanced Culture Method for Generating Large

Quantities of Highly Pure Dendritic Cells from Mouse Bone Marrow. *J. Immunol. Methods* **1999**, *223* (1), 77.

CHAPTER 4

Anticancer activity of OVA- and LOS- loaded mIONPsp in a mouse melanoma model

In this chapter, the efficacy of the formulation composed by mIONPsp-HyNic-FB-OVA and mIONPsp-Xcc LOS was assessed in a prophylactic setting against B16-F10(OVA) melanoma. Moreover, two formulation composed respectively by mIONPsp-HyNic-FB-OVA co-injected with mIONPsp-E. Coli LPS and mIONPsp-HyNic-FB-OVA co-injected with mIONPsp-Poly(I:C)-imiquimod were tested in a therapeutic setting using the same tumor model.

4.1: Introduction

Immunotherapy has emerged in the last years as one of the main pillars of cancer treatment alongside radiotherapy, surgery, and chemotherapy[1]. An exciting discovery in this field is represented by checkpoint blockade therapy, which has emerged as a promising option for treatment of cancer[2,3,4]. The release of negative regulators of immune activation in tumor cells allows evasion of immune surveillance, and checkpoint blockade can effectively inhibit such mechanisms unleashing the full potential of tumor-reactive T cells[5]. Cancer vaccines constitute an ideal immunotherapeutic partner for checkpoint blockade therapy since they can provide a continuous supply of antigen-specific T cells and long-lasting immune responses[6]. To the best of our knowledge, the adjuvant properties of *Xcc* LOS for vaccine development and immunotherapy have not been investigated previously, while other TLR4 ligands such as LPS and in particular the FDA-approved MPLA have been extensively investigated as vaccine adjuvants[7,8]. TLR agonists, and in particular TRL4 agonists, have the potential to develop Th1 immune responses[9,10,11], but can induce systemic cytokine production leading to acute toxicity[12], and can induce immune inhibitory factors[13]. The combination of checkpoint blockade with TLR4 agonists could compensate for the release of these immune suppressing factors releasing the full therapeutic potential of LPS and LOS. Moreover, TLR ligands have shown ineffective targeting of tumor and lymph nodes[14], and nanoparticle delivery could be used to further improve their therapeutic effectiveness[15,16,17,18].

The use of nanoparticles for vaccine delivery in combinatorial immunotherapy has been already reported in the literature. One example is from Yang et al., who reported imiquimod-loaded PLGA nanoparticles coated with mannose-modified B16-OVA cancer cell membranes (NP-R@M-M) acting as tumor-specific antigens. These nanoparticles showed enhanced uptake in APCs and could effectively target the lymph nodes. When administered in mice bearing B16-OVA tumors, a combination of NP-R@M-M and immune checkpoint inhibition with anti-PD-1 antibodies could improve survival of mice to 45 days with 3/6 mice completely rejecting the tumor from 25-27 days and no mice rejecting the tumor in the case of nanoparticle-treated mice[19] without checkpoint inhibition.

4.2: Results and discussion

4.2.1: Adjuvanticity of mIONPsp-*Xcc* LOS administered with mIONPsp-HyNic-FB-OVA in a prophylactic setting

After having evaluated the potential of *Xcc* LOS and mIONPsp-*Xcc* LOS in vitro, the adjuvanticity of the ligand was assessed in vivo and antigen-specific responses were evaluated. The B16-F10(OVA) subline was chosen for murine tumor immunotherapy studies as a poorly immunogenic, highly aggressive and widely used melanoma model. To compare the adjuvant properties, C57BL/6 mice were immunized subcutaneously with OVA (5 µg) alone or with OVA (5 µg) + *E. coli* LPS (1 µg), OVA (5 µg) + MPLA (1 µg), and OVA (5 µg) + *Xcc* LOS (1 µg) at days 0 and 14. At day 21, mice were challenged with 3×10^5 B16-F10(OVA) cells injected subcutaneously in the right flank, and tumor growth was monitored until they reached the limits of the established endpoint (**Figure 2**a). Despite a weaker capacity of *Xcc* LOS to induce IL-6 production in the J774A.1 macrophages than *E. Coli* LPS (shown in chapter 2 of this thesis), *Xcc* LOS was found to be as effective as *E. coli* LPS and the clinically approved MPLA (**Figure 2**b, c). To evaluate the utility of nanoparticle delivery, another group of mice was immunized with mIONPsp-HyNic-FB-OVA (5 µg OVA) formulated with pathogen-mimicking mIONPsp-*Xcc* LOS (1 µg *Xcc* LOS) as an adjuvant. All animals vaccinated with the TLR4 agonists showed reduced tumor growth and provided survival benefits (median survivals of 34-38 days) compared to the OVA-treated (median survival of 28 days) even with the ultralow adjuvant doses used (1 µg). Compared to the nanoparticle-free treatments, the immunization with mIONPsp-HyNic-FB-OVA formulated with pathogen-mimicking mIONPsp-*Xcc* LOS effectively slowed tumor growth in mice (**Figure 2**d).
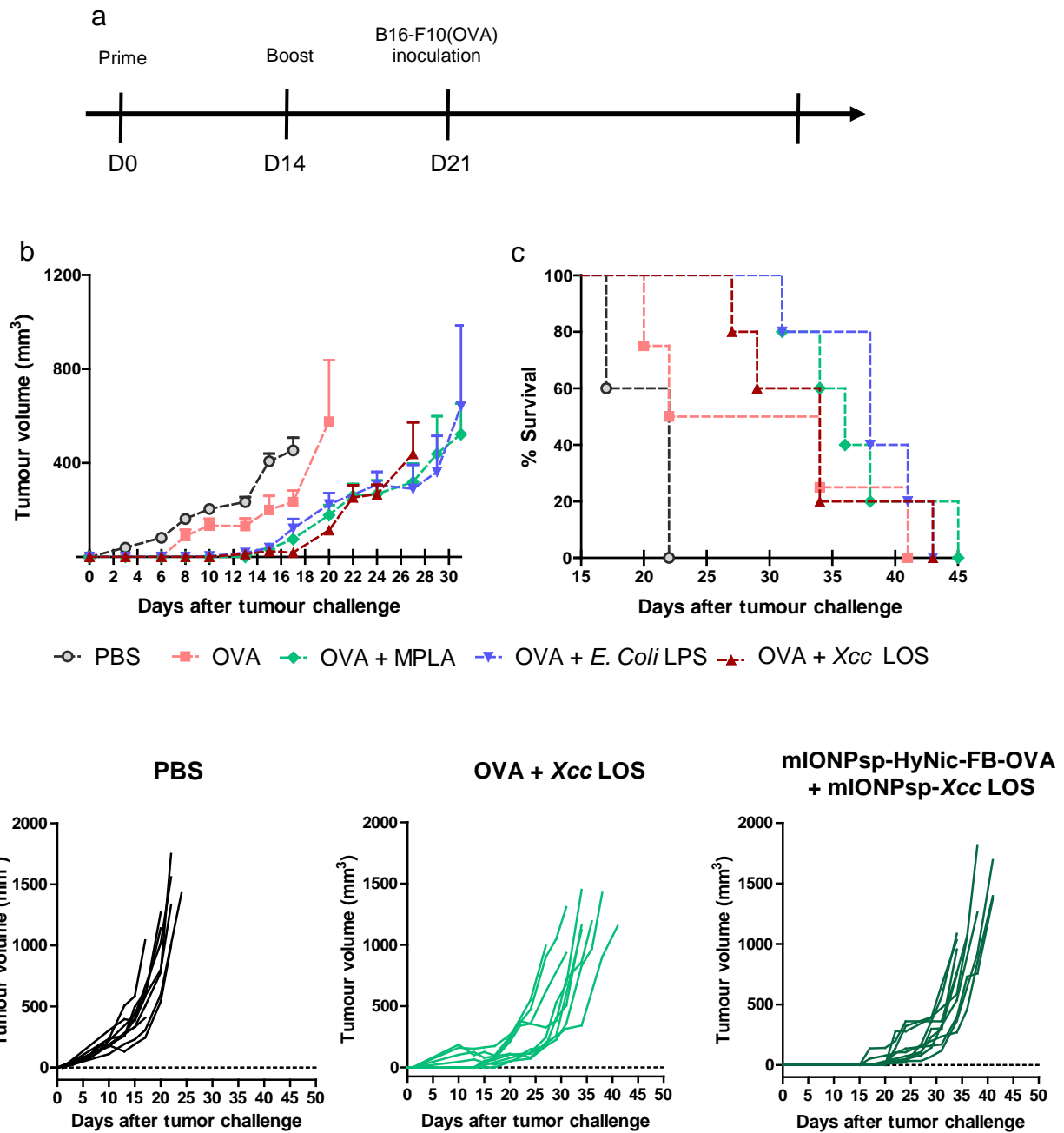
Figure 2: Protective immunity against B10-F10(OVA) melanoma cells induced by the use of the different TLR4 agonists as adjuvants when co-administered with tumor antigen OVA. a) Vaccination scheme. C57BL/6J mice were subcutaneously immunized with the indicated formulations (5 µg of OVA, 1 µg of TLR4 agonist per mouse, 25-70 µg of IONP on day 0 and 14 and subcutaneously challenged with 3×10^5 B16-F10(OVA) cells/mouse on day 21. b-d) Average and individual tumor growth curves and Kaplan–Meier survival curves. The data show mean ± SEM from a representative experiment (n= 5–10) from 2–3 independent experiments.

To understand the enhancement in the anti-melanoma response to the nanovaccines, the induction of tumor antigen-specific CD8^{+} T cells effector and memory response in mice's blood were analyzed. Although generating antibody production has been commonly achieved with conventional vaccine strategies such as Cervarix, generating protective memory CD8^{+} T cells has proven more difficult to achieve[20]. It was therefore analyzed if the immunization with OVA + *Xcc* LOS and mIONPsp-HyNic-FB-OVA formulated with pathogen-mimicking mIONPsp-*Xcc* LOS was able to drive antigen-specific CD8^{+} T cell responses. For this, the frequency of the $OVA_{257-264}$ peptide (SIINFEKL)-specific CD8^{+} T cells was monitored by H-2Kb/SIINFEKL dextramer staining followed by FACS analysis. The highest frequency of SIINFEKL-specific CD8^{+} T cells was found in mice immunized with OVA antigen delivered by mIONPsp-HyNic-FB-OVA and formulated with pathogen-mimicking mIONPsp-*Xcc* LOS (**Figure 3**a).

In the event of infection or vaccination, naive CD8^{+} T cells are primed in secondary lymph nodes by DCs and consequently proliferate and differentiate into 'effector memory' cells (T_{EM}) and 'central memory' (T_{CM}) cells, which exhibit distinct functional abilities playing a different role in adaptive immunity.[21]. Whereas T_{EM} are localized in peripheral non-lymphoid tissues (e.g., lung, liver, intestine), spleen, and blood and can immediately recognize and kill the target virally infected/cancer cells, T_{CM} cells can rapidly traffic into lymph nodes directly from the blood and are thought to provide a sustained and robust CTL recall response to control subsequent disease challenges.
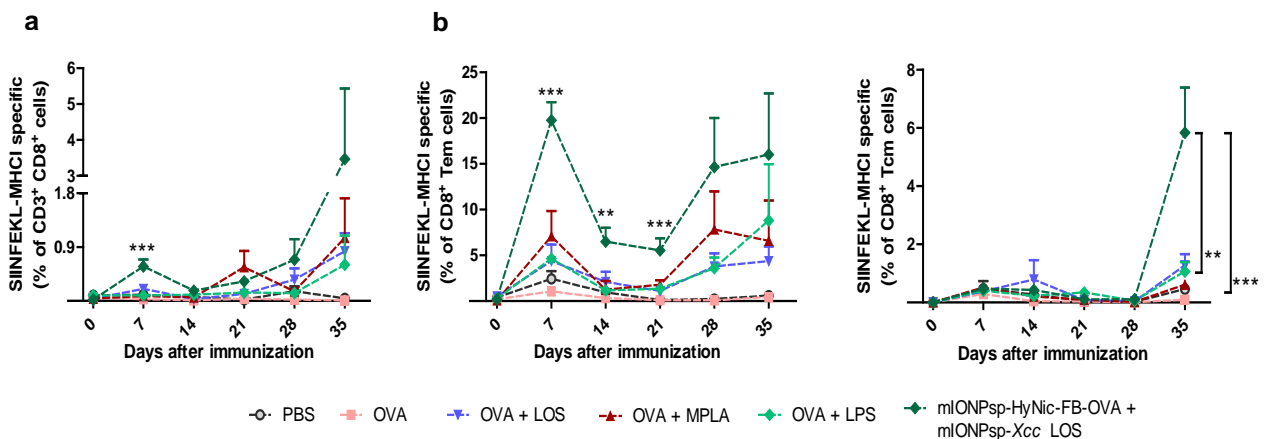

Figure 3. Immunization with the mIONPsp-based vaccines triggers a higher-level tumor antigen-specific cytotoxic T lymphocyte (CTL) effector responses. a)

Analysis of frequency of circulating OVA$_{257-264}$ (SIINFEKL)-specific CD8$^+$ T cells isolated from blood. b, c) Frequency of SIINFEKL-specific CD8$^+$ T$_{EM}$ and T$_{CM}$ cells. T$_{CM}$ cells are defined as CD3$^+$CD8$^+$CD62L$^+$CD44$^+$ and T$_{EM}$ as CD3$^+$CD8$^+$CD62L$^-$CD44$^+$. Data presented as mean ± SEM. n = 5 mice per group. ***P<0.001, **P<0.01, *P<0.05 by two-way ANOVA followed by Bonferroni's test.

The frequency of circulating SIINFEKL-specific CD8$^+$ T$_{EM}$-cells (CD44$^+$CD62L^{low}) and T$_{CM}$-cells (CD44$^+$CD62L^{high}) was analyzed over time (t = 0, 7, 14, 21, 28 and 35 days). mIONPsp-vaccinated mice had a much greater frequency of both antigen-specific T$_{EM}$ and T$_{CM}$ cells. The T$_{EM}$ population peaked at day 7 after the first vaccination and the levels increased drastically on day 35, i.e. after boost and tumor challenge (**Figure 3***b*). The highest frequency of the SIINFEKL-specific CD8$^+$ T$_{CM}$-cells was observed on day 35 (**Figure 3***b*). The results demonstrate that our nanovaccine generates more effectively protective memory CD8$^+$ T cells than the other conventional therapies used.

4.2.2: Combinatorial immunotherapy of PD-L1 checkpoint blockade and mIONPsp-*Xcc* LOS administered with mIONPsp-HyNic-FB-OVA as anticancer vaccine

The B16-F10(OVA) melanoma model used is an ideal candidate for PD-L1 checkpoint inhibition since it is characterized by high PD-L1 expression[22]. The use of anti-PD-L1 blocking antibodies requires multiple doses and PD-L1 is expressed on many immune system cells such as B and T lymphocytes and blocking it can bring to toxicity and uncontrolled auto reactivity[23,24]. Checkpoint blockade was thus performed at the level of the cancer cell using B16-F10(OVA) melanoma cells with silenced PD-L1. This achieves the same effects than knocking out PD-L1 in cancer cells as demonstrated previously. The PD-L1–deficient B16-F10(OVA) cells (B16-F10(OVA) ∆PD-L1) were generated at Navarrabiomed by the research group of David Escors by using CRISPR/Cas9 genome editing and lentiviral particles. This genetically modified cell line, B16-F10(OVA) ∆PD-L1, was used in the prophylactic immunization assay (**Figure 4***a*). C57BL/6 mice were subcutaneously vaccinated with OVA + *Xcc* LOS and

mIONPsp-HyNic-FB-OVA + mIONPsp-*Xcc* LOS (day 0 and 14) and inoculated with 2×10^6 B16-F10(OVA) ΔPD-L1 cells (day 21). All the mice treated with PBS developed melanoma tumors within 10 days. The tumor growth kinetics following inoculation of 2×10^6 B16-F10(OVA) ΔPD-L1 and inoculation of 3×10^5 B16-F10(OVA) cells was very similar for mice treated with PBS. However, in the case of mice immunized with OVA + *Xcc* LOS, mice remained tumor-free for 20 days and 40% did not develop tumor past 100 days after the challenge with B16-F10(OVA) ΔPD-L1 cells, compared to all the mice developing tumor by day 20 after the challenge with the B16-F10(OVA) cells. In the case of mice immunized with mIONPsp-HyNic-OVA + mIONPsp-*Xcc* LOS 100% of the animals were free of tumor 110 days after the challenge with B16-F10(OVA) ΔPD-L1 cells (***Figure 4****b, c, e*). Furthermore, analysis of SIINFEKL-specific CD8$^+$ T cells corroborated the enhanced protection against the melanoma cells (***Figure 4****d*). Hence mIONPsp delivery combined to the permanent PD-L1 checkpoint blockade remarkably improved the efficacy of the vaccination. The immune responses 100 days after the boosting immunization were thus investigated to assess the efficacy and longevity of memory recall responses in the mIONPsp-vaccinated mice. The frequency of circulating SIINFEKL-specific CD8$^+$ T cells was analyzed in the blood previous to the recall immunization and comparing immunized mice with mice of the same age that had not been immunized/challenged with the melanoma cells and no SIINFEKL-specific cells were found neither within the CD8$^+$ nor in the T_{CM} cell population. Mice received a recall immunization 103 days after the boost and the capacity to clear a tumor re-challenge (2×10^6 B16-F10(OVA) ΔPD-L1 cells subcutaneously implanted on the right back on day 122) was investigated (***Figure 5****a*).
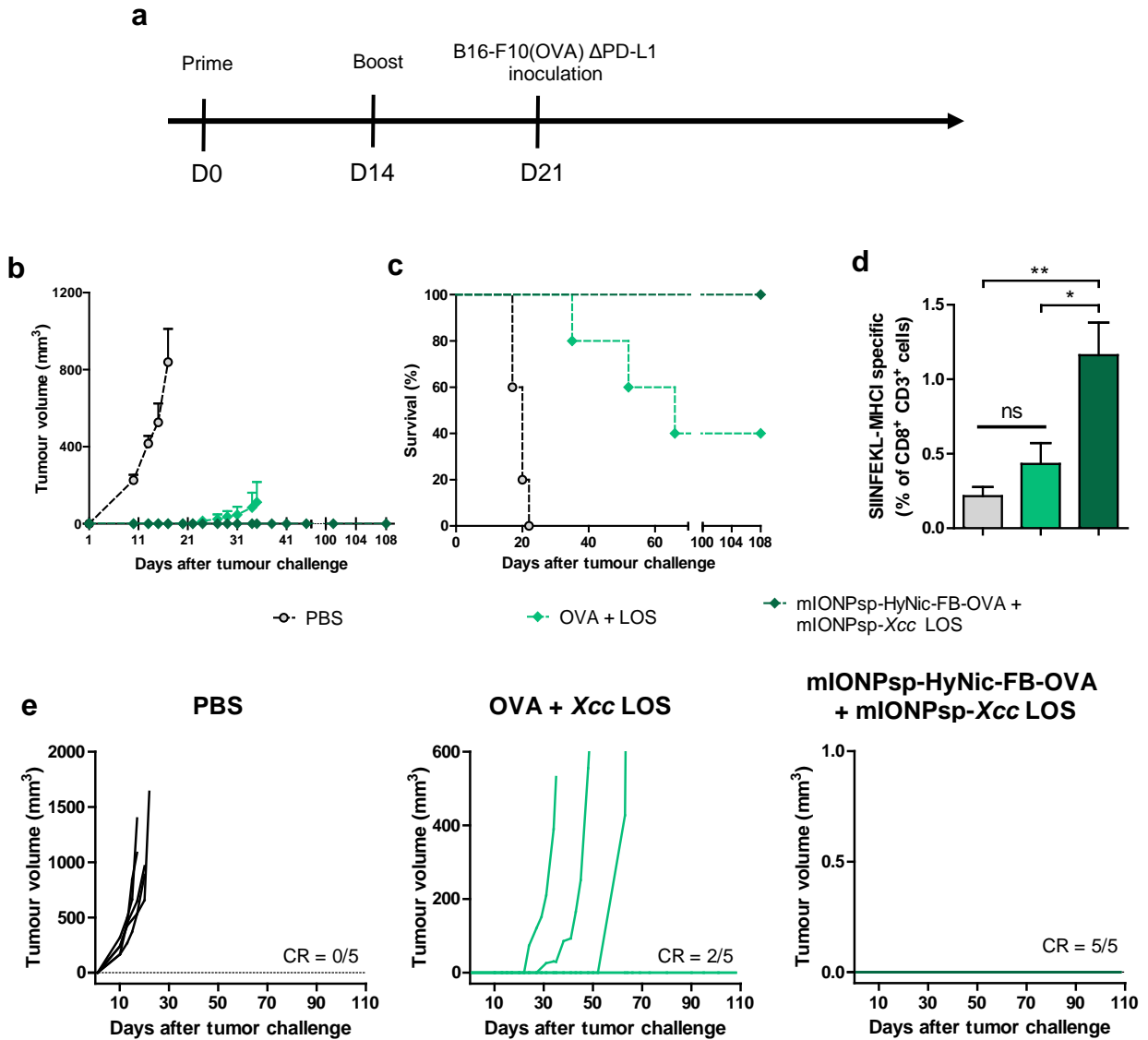
Figure 4. *Protective immunity against B16-F10(OVA) melanoma cells with knocked-down expression of PD-L1 (B16-F10(OVA) ΔPD-L1). a) Vaccination scheme. C57BL/6J mice (n = 5) were subcutaneously challenged with 2 × 10⁶ B16-F10(OVA) ΔPD-L1 cells seven days after the last vaccination with 5 µg of OVA, 1 µg Xcc LOS per mouse, 25 µg of IONP). b-e) Average (b) and individual (e) tumor growth curves and (c) Kaplan–Meier survival curves. d) Circulating SIINFEKL-specific CD8⁺ T cells 35 days after the first immunization (two weeks after tumor inoculation). **P<0.01, *P<0.05, ns = non significant by one-way ANOVA followed by Tukey's test. CR = fraction of complete tumour rejection.*

Whereas the control mice developed melanoma tumors within 10-15 days, 100% of the mIONPsp-vaccinated mice remained tumor-free until the end of the experiment on day 139 (**Figure 5***b*). Further analysis of the T_{EM} subset revealed that mice immunized with mIONPsp-HyNic-FB-OVA + mIONPsp-*Xcc* LOS had high levels of SIINFEKL-specific CD8$^+$ T_{EM} cells even 100 days after the first immunization (**Figure 5***c*). At this point, the frequency of circulating antigen-specific T cells was analyzed to assess the magnitude and quality of the memory response generated after the recall. The frequencies of the SIINFEKL-specific CD8$^+$ T cells in peripheral blood were high 5.9 ± 2.0 % (*n* = 5) (compared to 1.2 ± 0.5% at day 35 after the 1st boost and 1st tumor challenge). The immunization recall (day 117) rapidly increased the antigen-specific T_{EM} and T_{CM} cell percentages up to the frequencies observed on day 35 after first immunization and boost, indicating that mIONPsp-based vaccines induced T cell memory and effective recall responses.

Next, to evaluate the quality of CD8$^+$ T cell responses, cellular extracts from spleens were cultured *ex vivo* by 5h incubation with the antigenic peptide SIINFEKL, and the IFN-γ and TNF-α intracellular production and the degranulation marker CD107a were analyzed by FACS. The data demonstrated that mice immunized with the nanoparticles generate T lymphocytes with enhanced cytolytic activity (**Figure 5***e, f, g*). Also, the cells collected from the spleen showed significantly enhanced ability to release IFN-γ following *ex vivo* re-stimulation with SIINFEKL (over 48 h). Taken together, the results show how a potent and long-lasting antitumor immunity can be achieved when combining and using mIONPsp-based vaccines with PD-L1 abrogation.
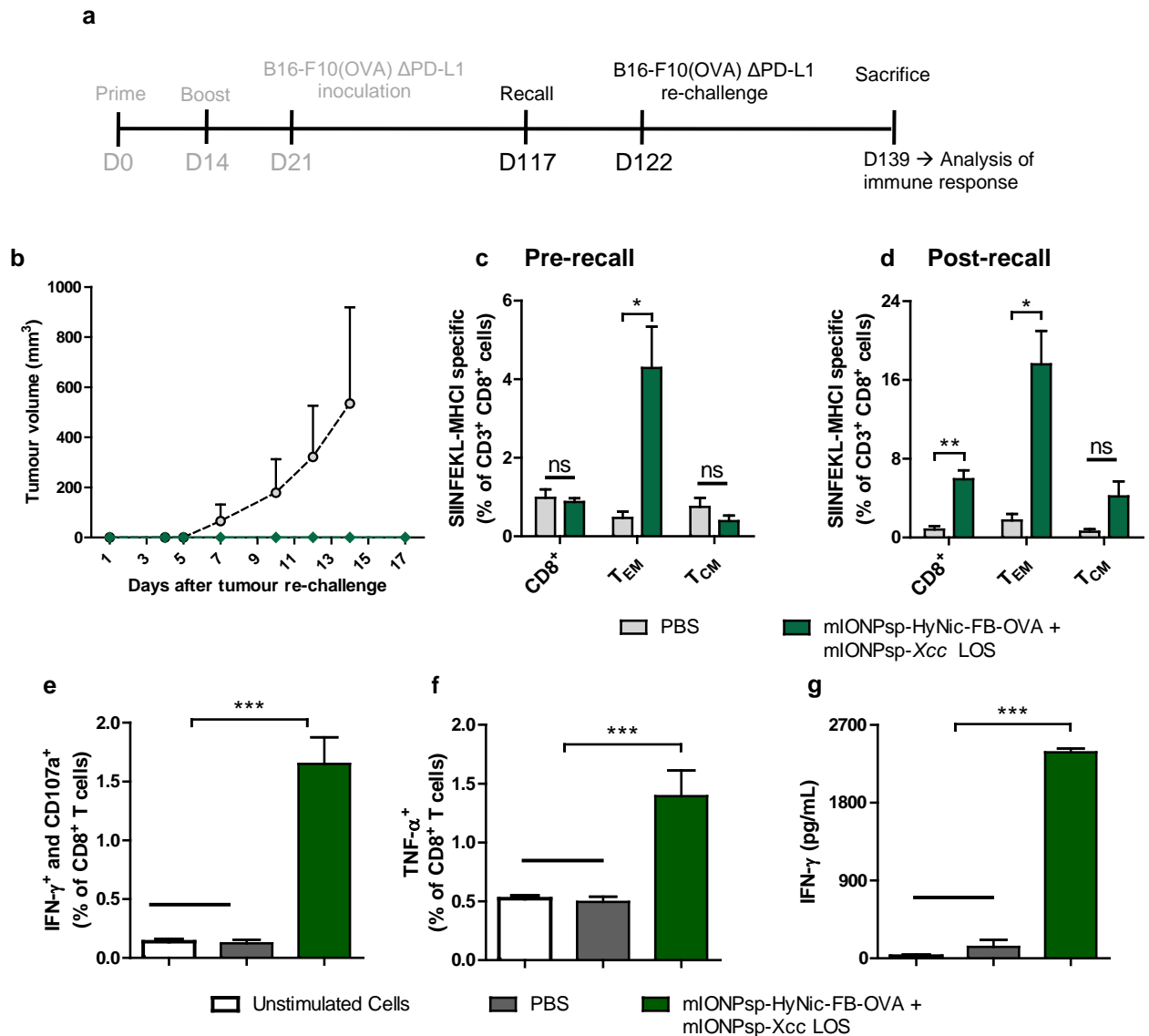
Figure 5. *Tumor protection and rapid activation of the immune system upon recall of mIONPsp-based vaccines (**n** = 5). a) 103 days after the first tumor inoculation, T cell memory was recalled with the nanovaccines (same antigen/adjuvant concentrations). Five days after, a tumor re-challenge with 2 ×10⁶ B16-F10(OVA) ΔPD-L1 cells was carried out. At day 17 after the second tumor challenge, mice were sacrificed and blood and spleens collected for further immune analysis. b) Average tumor growth curves. c, d) SIINFEKL-specific CD8⁺, T$_{EM}$ and T$_{CM}$ cell percentages before (c) and (d) after recall injection. e, f) Intracellular IFN-γ and TNF-α production and CD107a expression after 5 h of incubation with 10 µg/mL of SIINFEKL peptide. g) Extracellular IFN-γ production after 48 h of incubation with the peptide. ***P<0.001, **P<0.01, *P<0.05, ns = non significant by (c, d) two-way ANOVA followed by Bonferroni's test and (e-g) one-way ANOVA followed by Tukey's test.*

4.2.3: Adjuvanticity of mIONPsp-*E. Coli* LPS administered with mIONPsp-HyNic-FB-OVA in a therapeutic setting

The adjuvanticity of LPS has been already explored intensively in vaccine development and immunotherapy as TLR4-dependent vaccine adjuvant, and this ligand showed toxicity and systemic cytokine production leading to undesired side effects and eventually death by sepsis[12]. Hence, the effectiveness of LPS delivery by mIONPsp was assessed in vivo using an ultralow adjuvant dose (5 µg). To compare the anticancer properties of the different nanosystems developed, C57BL/6 mice were injected subcutaneously in the right flank with 3×10^5 B16-F10(OVA) cells at day 0. Then, mice were vaccinated subcutaneously with OVA (10 µg) + *E. coli* LPS (5 µg), OVA (10 µg) + Alum (25 µL) as a conventional therapy, and mIONPsp-HyNic-FB-OVA (10 µg OVA) + mIONPsp-*E. Coli* LPS (5 µg Ligand) at days 7, 10, and 13, and tumor growth was monitored until they reached the limits of the established endpoint (***Figure 6****a, b*). The median survival of *E. Coli* LPS-treated mice was of 26 days and the median survival for mIONPsp-*E. Coli* LPS-treated mice was of 24 days, which overall proved that OVA + *E. Coli* LPS, also when delivered by mIONPsp, worked as weak cancer therapies. Both *E. Coli* LPS- and mIONPsp-*E. Coli* LPS-treated mice showed a similar survival to Alum-treated mice, which boasted a median survival of 22 days (***Figure 6****c*). Moreover, the mice in the OVA + *E. Coli* LPS and mIONPsp-HyNic-FB-OVA + mIONPsp-*E. Coli* LPS groups showed ulceration on the tumor when compared to the control group confirming that *E. Coli* LPS as a therapy shows side effects as reported in the literature[25]. All the treatments used did not cause a weight change in the treated mice (***Figure 7***). The therapy using LPS was not effective at delaying tumor growth when compared to the control group and the OVA + Alum-treated group, and all these treatments showed poor efficiency coupled with significant side-effects.
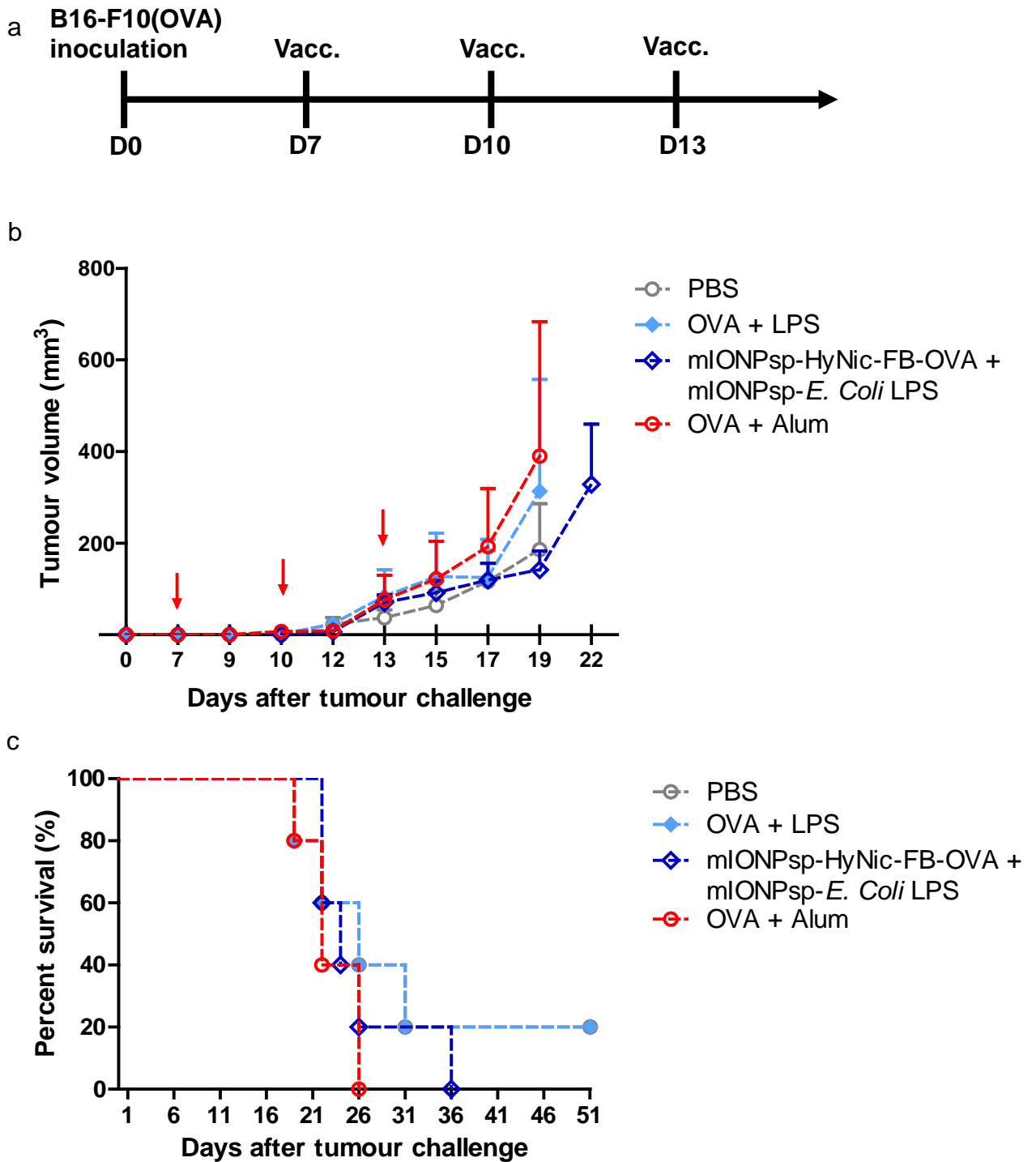
Figure 6. *Therapeutic anticancer effect of different adjuvants administered with OVA antigen. a) Vaccination scheme. C57BL/6J mice were subcutaneously challenged with 3 × 10^5 B16-F10(OVA) cells/ mouse on day 0 and treated with the indicated formulations (10 µg of OVA, 5 µg of E. Coli LPS and 30 µg of IONP per mice on day 7, 10 and 13. b) Average tumor growth and c) Kaplan–Meier survival curves. Data are shown as mean ± SEM from an experiment (n= 5).*
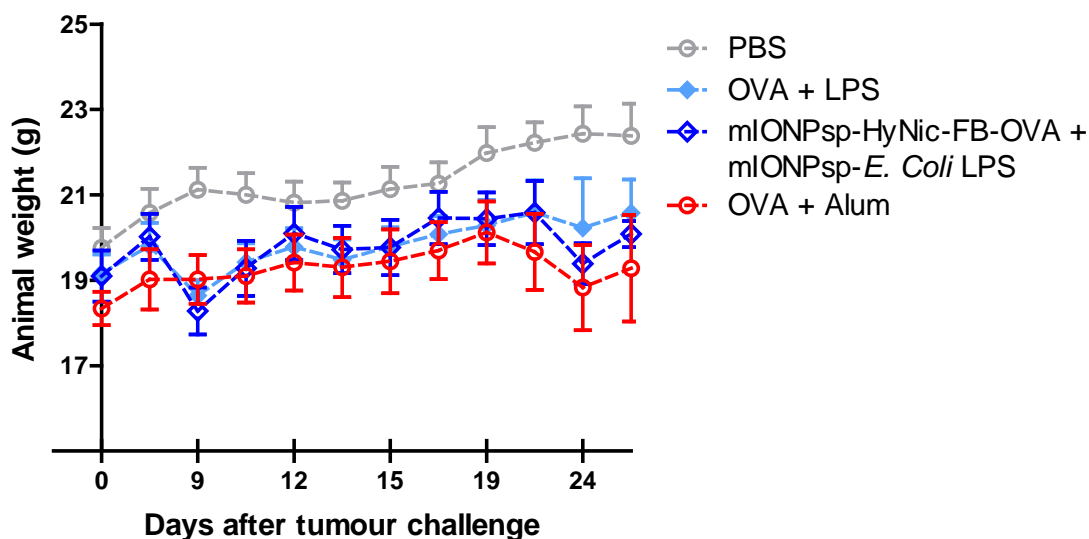
Figure 7. *Animal weight after tumor injection and therapy. Data are shown as mean ± SEM from an experiment (n= 5).*

4.2.4: Formulation of mIONPsp-HyNic-FB-OVA with mIONPsp-Poly(I:C)-imiquimod for improved antigen delivery in a therapeutic setting

Next, the efficacy of the covalent conjugation of OVA to the mIONPsp (mIONPsp-HyNic-FB-OVA) was compared with the mIONPsp-OVA formed by electrostatic interaction previously developed in our laboratory as delivery vehicle for OVA. These electrostatic nanoparticles were conjugated by simply mixing OVA and mIONPsp and were purified using spin filtration to get rid of the unbound OVA, and showed an average OVA loading of 7 OVA/ IONPsp, similar to that of the covalent mIONPsp-HyNic-FB-OVA system. To compare the covalent and electrostatic OVA delivery strategies with IONPsp, a synergistic combination of TLR agonists made up of Poly(I:C) and imiquimod (**Figure 8**), previously shown to be a very potent vaccine adjuvant[22], was chosen.
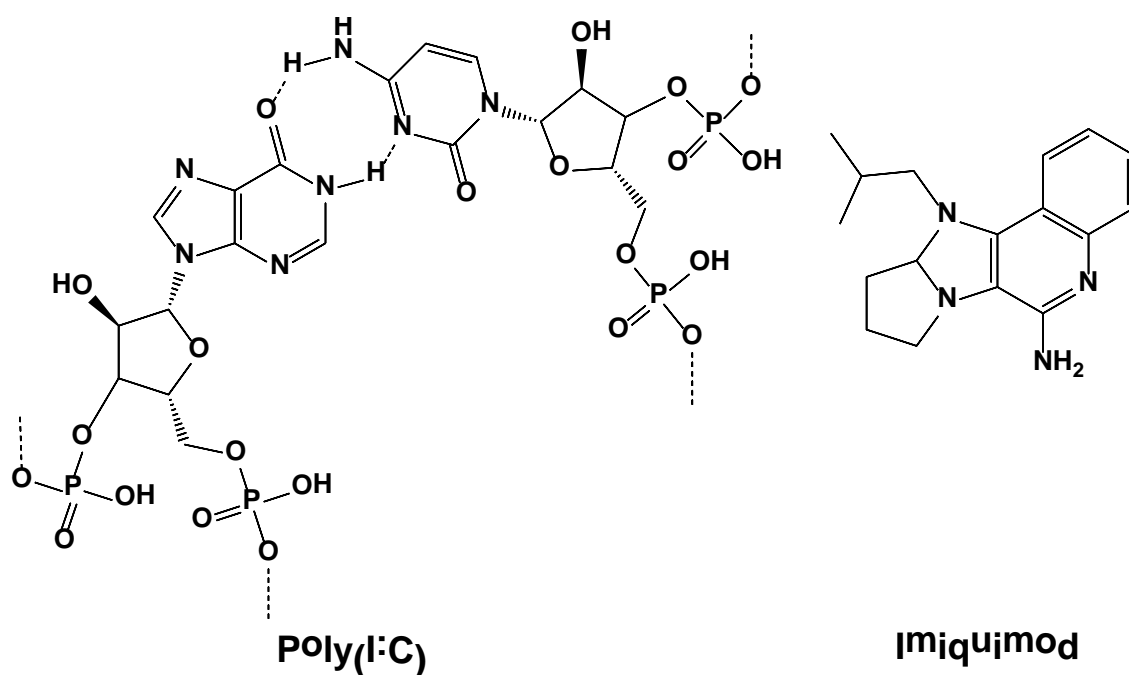
Figure 8. *Poly(I:C) and imiquimod.*

mIONPsp-Poly(I:C)-imiquimod were coupled with the two different OVA-loaded nanoparticles developed, the covalent mIONPsp-HyNic-FB-OVA and the electrostatic mIONPsp-OVA and the two resulting nanovaccines were subcutaneously injected in the B16-F10(OVA) mice tumor model (**Figure 9**a). The FDA-approved adjuvant alum showed a median survival of 22 days and did not work as an effective antitumor therapy when injected with OVA. The use of the electrostatic mIONPsp-OVA as antigen delivery vehicle improved the median survival of the injected mice to 31 days, with 1 mouse out of 5 rejecting the tumor (**Figure 9**b). Compared to the electrostatic mIONPsp-OVA, the covalent mIONPsp-HyNic-FB-OVA significantly delayed tumor growth, with a median survival of 51 days and 3/5 mice tumor-free at day 51 after tumor injection (**Figure 9**c). At the administered concentrations, no meaningful decrease in the weight of mice administered with our treatments was noticed (**Figure 10**).

a B16-F10(OVA) inoculation — Vacc. — Vacc. — Vacc.

D0   D7   D10   D13

b

Tumour volume (mm³) vs Days after tumour challenge

Legend:
- PBS
- mIONPsp-OVA + mIONPsp-Poly(I:C)-imiquimod
- mIONPsp-HyNic-FB-OVA + mIONPsp-Poly(I:C)-imiquimod
- OVA + Alum

c

Percent survival (%) vs Days after tumour challenge

Legend:
- PBS
- mIONPsp-OVA + mIONPsp-Poly(I:C)-imiquimod
- mIONPsp-HyNic-FB-OVA + mIONPsp-Poly(I:C)-imiquimod
- OVA + Alum

***Figure 9**. Therapeutic anticancer effect of the adjuvant mIONPsp-Poly(I:C)-imiquimod administered with* covalent mIONPsp-HyNic-FB-OVA. *a) Vaccination scheme. C57BL/6J mice were subcutaneously challenged with 3 × 10⁵ B16-F10(OVA) cells/ mouse on day 0 and treated with mIONPsp-Poly(I:C)-imiquimod (10 µg of OVA, 4 µg of Poly(I:C), 2 µg of imiquimod and 30 µg of IONP per mouse on day 7, 10 and 13. b) Average tumor growth and c)*

Kaplan–Meier survival curves. Data are shown as mean ± SEM from an experiment (n= 5).
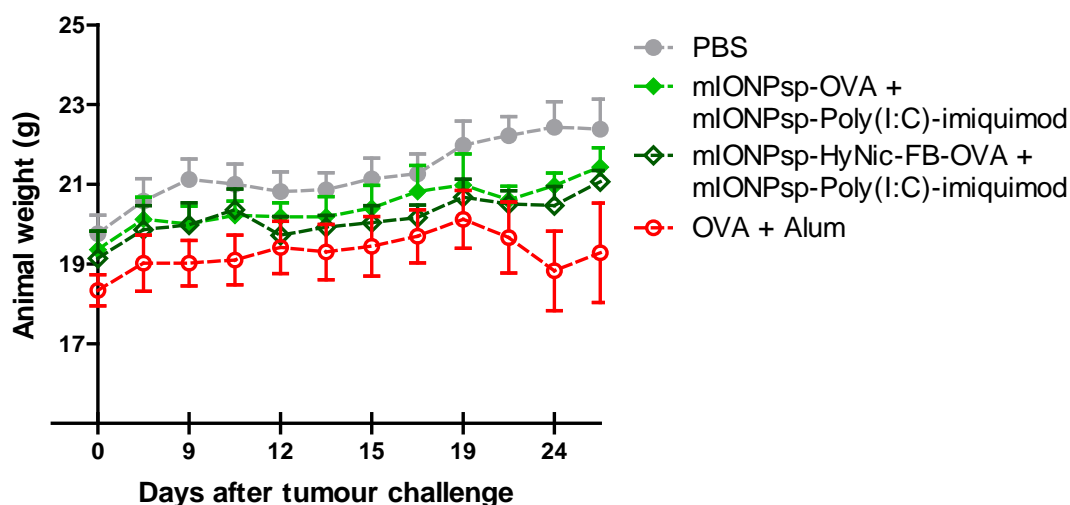
Figure 10. *Animal weight after tumor injection and therapy. Data are shown as mean ± SEM from an experiment (n= 5).*

These results showed that the developed mIONPsp-HyNic-FB-OVA work effectively as an antigen delivery vehicle and that vaccine efficacy is strongly dependent upon the antigen conjugation strategy used. Moreover, the covalent bonding in mIONPsp-HyNic-FB-OVA is acid-labile, which contributes to releasing the antigen payload into the lysosomes at a pH of 5[26]. The mIONPsp-HyNic-FB-OVA is therefore an optimised antigen delivery system based on mIONPsp, which provides significantly more effective antitumor responses.

4.3: Conclusions

After having developed the two adjuvant-loaded nanoparticle-based delivery systems and the antigen loaded mIONPsp-*E. Coli* LPS, mIONPsp-*Xcc* LOS, and mIONPsp-HyNic-FB-OVA, in vivo experiments were performed to evaluate the efficacy of these systems. It was first proved that the adjuvant *Xcc* LOS elicits as potent in vivo immune responses as MPLA (FDA-approved TLR4 agonist) for the development of anti-cancer vaccines. It was also found that the *Xcc* LOS-, *E. Coli* LPS- and MPLA- treated mice had a median survival of 34-38 days, compared to 28 days in OVA-treated mice. Besides, the formulation obtained by combining mIONPsp-*Xcc* LOS with mIONPsp-HyNic-FB-OVA led to enhanced protection against highly aggressive and poorly immunogenic OVA-expressing B16-F10 murine melanomas, slowing down tumor growth when compared to the nanoparticle-free treatments. Moreover, when this formulation was combined with abrogation of PD-L1 expression in the melanoma cells, it achieved complete tumor rejection in 100 % of the immunized mice. This showed the general utility of creating vaccines based on pathogen-mimicking nanostructures and the hydrazone ligation reaction for antigen binding, as well as the importance of PD-L1 blockade for a significant upgrade of vaccines exploiting TLR4 agonists. The developed nanosystems were also tested in a therapeutic vaccination setting with a formulation composed by mIONPsp-*E. Coli* LPS and mIONPsp-HyNic-FB-OVA. mIONPsp-*E. Coli* LPS did not show a strong adjuvanticity at the low concentrations used (5 µg LPS/ mouse). On the other hand, the antigen delivery system developed in this thesis, mIONPsp-HyNic-FB-OVA, was found to work very well and be much more effective than mIONPsp-OVA formed by electrostatic interactions. The covalent mIONPsp-HyNic-FB-OVA system co-administered with mIONPsp-Poly(I:C)-imiquimod as adjuvant led to major improvement of the median survival from 31 to 51 days. Moreover, the covalent mIONPsp-HyNic-FB-OVA improved tumor rejection to 3/5 mice compared with 1/5 in the case of the mIONPsp-OVA. This demonstrates the potential of this covalent binding strategy for antigen delivery using mIONPsp and enhanced antitumor activity.

4.4: Materials and methods

Materials: Unless otherwise specified all commercially available reagents were used without further purification. Endo-Ova (Endotoxin-free Ovalbumin) was purchased from Hyglos GmbH; 1,2-distearoyl-sn-glycero-3-phosphoethanolamine-N-[carboxy(polyethylene glycol)-2000] (DSPE-cPEG) was purchased from Avanti polar lipids, Dulbecco's Modified Eagle Medium (DMEM), Fetal Bovine Serum (FBS), Penicillin/Streptomycin (P/S) L- glutamine (L-Glu) and collagenase/DNase were all purchased from Gibco; Poly(I:C) and Imiquimod were purchased from Invivogen. Cell culture plates and flow cytometry tubes were purchased from Nunc; Matrigel® Matrix from Corning, All the fluorescently labeled antibodies were obtained from BioLegend, unless otherwise specified and SIINFEKL OVA peptide was obtained from Peptides International, red blood cells (RBC) lysing buffer, Golgi Stop and Cytofix/Cytoperm-fixation and permeabilization kit from BD Biosciences.

Preparation of mIONPsp-*Xcc* LOS: synthesis of mIONPsp-*Xcc* LOS was carried out as described in chapter 2 of this thesis.

Preparation of mIONPsp-HyNic-FB-OVA: synthesis of mIONPsp-HyNic-FB-OVA was carried out as described in chapter 3 of this thesis.

Preparation of mIONPsp-*E. Coli* LPS: synthesis of mIONPsp-*E. Coli* LPS was carried out as described in chapter 3 of this thesis.

Preparation of mIONPsp-OVA: mIONPsp were prepared following a similar procedure to the one described in chapter 2 using a different PEG-phospholipid, DSPE-cPEG. Briefly, 1 mg of IONPsp and a mixture of 2 mg of PEG phospholipids (1 mg DSPE-cPEG and 1 mg DPPE-mPEG) were dissolved in 500 μL of chloroform in a 4 mL round bottomed glass vial and let to evaporate overnight at RT. The flask was placed in a water bath at 80 °C for 30 s, after which micelles were re-dissolved in 500 μL of MilliQ water. This solution was centrifuged at 9700 xg for 5' and passed through a 0.45 μm syringe filter to remove non-soluble particles. Then, the micelles were centrifuged at 369000 xg for 45 minutes; the supernatant was discarded and washed with MilliQ water to remove empty PEG micelles (3 cycles). Finally, the pellet was dissolved in 400

µL of MilliQ water (or 10 mM Phosphate Buffered Saline, PBS, when injected in vivo). Characterization of the so-prepared micelles (mIONPsp-Carboxy) was performed using the techniques previously described.

Electrostatic attachment of OVA: The solution of mIONPsp-Carboxy (3 µM) was incubated overnight with endotoxin-free OVA (molar ratio 15:1 OVA to mIONPsp) in a final volume of 300 µL of MilliQ water. The unbound OVA was eliminated by spin filtration at 1844 xg for 5 min (4 cycles) using 100 KDa MWCO Amicons. The pellet (mIONPsp-OVA) was resuspended in the initial volume of nanopure water or PBS and stored at 4 °C.

Preparation of mIONPsp-Poly(I:C)-imiquimod: mIONPsp were prepared following a similar procedure to the one described in chapter 2 using a different PEG-phospholipid (DPPE-mPEG). Briefly, 1 mg of IONPsp and 2 mg of DPPE-mPEG were dissolved in 500 µL of chloroform in a 4 mL round bottomed glass vial and let to evaporate overnight at RT. The flask was placed in a water bath at 80 °C for 30 s, after which micelles were re-dissolved in 1 mL of MilliQ water. This solution was centrifuged at 9700 xg for 5' and passed through a 0.45 µm syringe filter to remove non-soluble particles. Then, the micelles were centrifuged at 369000 xg for 60 minutes; the supernatant was discarded and washed with MilliQ water to remove empty PEG micelles (3 cycles). Finally, the pellet was dissolved in 1 mL of MilliQ water (or 10 mM Phosphate Buffered Saline, PBS, when injected in vivo). Characterization of the so-prepared micelles (mIONPsp-Methoxy 16C) was performed using the techniques previously described.

Electrostatic attachment of Poly(I:C) and imiquimod: Poly(I:C) and imiquimod functionalized mIONPsp were developed through a two-step process as reported in the literature[22]. Poly(I:C) and Imiquimod were dissolved in endotoxin-free water to a final concentration of 1000 µg/mL and 500 µg/mL respectively. After, mIONPsp were mixed with Poly(I:C) and the mixture was stirred overnight at room temperature using a benchtop shaker set at 700 rpm. The excess of unbound Poly(I:C) was removed by three cycles (5 minutes at 1475 xg) of spin filtration with NanoSep 100k (MWCO 100 kDa) centrifugal devices (*Pall Life Sciences*). Then, Poly(I:C)-loaded mIONPsp were

resuspended in an imiquimod solution, keeping the final volume constant. This mixture was stirred and purified as described above. The final pellet was resuspended in MilliQ water or phosphate buffered saline (PBS) and stored at 4 °C.

Assessment of antitumor prophylactic effect: C57BL/6 mice (6−8 weeks old) were immunized subcutaneously in the flanks twice with an interval of 2 weeks between injections (100 µL, 50 µL/flank, 1 µg of TLR4 ligands, 5 µg of OVA and *ca.* 25-70 µg of IONPsp per mice). On day 21 after first immunization, 3.5×10^5 B16-F10(OVA) cells or 2×10^6 B16-F10(OVA) ΔPD-L1 cells diluted in PBS:Matrigel® (1:1) were injected subcutaneously in the right back. Animals were monitored for tumor growth using an electronic digital caliper 779A series (Starrett). Criteria for humane endpoint included tumors greater than 1.5 cm diameter and ulceration. Results were expressed as mean ± SEM of at least 5 mice per group. Blood was taken (50 µL) at several time points after the first immunization for analyzing the generated immune response. In the case of antibodies production, blood was diluted in PBS and centrifuged (13000 xg, 5 min) to separate the serum (supernatant) from blood cells (pellet). Blood sera were stored at -20 °C. In order to analyze the circulating cellular response, blood was diluted up to 4 mL in cold PBS. After centrifugation (1028 xg, 5 min at 4 °C), the pellet was resuspended in 2 mL of commercial RBC lysing buffer and incubated at RT. After washing the cell suspensions twice with 5% FBS in PBS via centrifugation, cells were resuspended in complete RPMI-1640, ready for further analysis. Secondary lymphoid organs such as spleens were also harvested for the analysis of local cellular response. Briefly, spleens were harvested and perfused with tissue dissociating mix (3 mL of collagenase/DNase I diluted in RPMI-1640 medium), cut into small pieces and incubated for 30 min at RT in a sterile Petri dish. The reaction was stopped with 36 µL of 500 mM EDTA and organs were dissociated with the plunger of a syringe. RBC lysis was performed as previously described and the resulting cell suspensions were resuspended in complete RPMI-1640. Primary immune cells were analyzed for CD8+ T cells, T_{CM} and T_{EM} cells specific for the OVA epitope SIINFEKL; extracellular and intracellular TNF-α and IFN-γ production and CD107a degranulation marker expression were also analyzed. The

quantification of extracellular IFN-γ production was performed by seeding 8×10^5 splenocytes/well, followed by incubation over 48 h with 10 µg/mL of SIINFEKL peptide and analyzing the supernatants by sandwich ELISA, as described in the chapter 2. For flow cytometry assays, 1×10^6 splenocytes or peripheral blood cells were placed in round-bottom 96-well plates and stained with different antibodies. SIINFEKL-specific T cells were stained with Brilliant Violet™ 421-labelled anti-CD3, PE-Cy7-labelled anti-CD8, APC-labelled anti-CD44, FITC-labelled anti-CD62L and PE-labelled H-2kb-OVA$_{257-264}$ dextramer (Immudex). SIINFEKL specific cell percentage was analyzed in the CD8$^+$ T cell population (CD3$^+$ and CD8$^+$ double positive); in the T$_{CM}$ cell population (cells showing a phenotype of CD44^{low} and CD62L^{low} within CD3$^+$ and CD8$^+$ double positive population); and in the T$_{EM}$ population (CD44^{high} and CD62L^{low}). To study intracellular TNF-α and IFN-γ and the expression of the degranulation marker CD107a, cells were placed in 100 µL of RPMI-1640 medium in the presence of Golgi Stop, PE-labelled anti-CD107a and 10 µg/mL SIINFEKL peptide. After 5 h of incubation at 37°C, cells were washed twice and stained with the surface markers Brilliant Violet™ 421-labelled anti-CD3, Brilliant Violet™ 510-labelled anti-CD4 and FITC-labelled anti-CD8. Then, cells were fixed and permeabilized using the Cytofix/Cytoperm-fixation and permeabilization kit, after which intracellular cytokine staining was performed (APC-labelled anti-INF-γ and PE-Cy7-labelled anti-TNF-α). T cells were gated based on double positive for CD3 and CD8 markers, excluding CD4$^+$ cells if needed. Results were represented as IFN-γ and CD107a double positive or TNF-α positive cell percentage of total CD3$^+$ CD8$^+$ T cells. Isotype controls were added when needed but were not included in the figures for clarity purposes. Results were expressed as mean ± SEM of 5 mice per group of immunization, analyzed individually and compared to unstimulated wells.

Statistical analysis: All data presented were expressed as mean ± SEM. The differences between the control and the experimental groups were assessed using one- or two-way ANOVA followed by Tukey's test or Bonferroni's test (GraphPad Prism, GraphPad Software, La Jolla, CA). P values of less than 0.05 were considered statistically significant.

Assessment of antitumor therapeutic effect: C57BL/6 mice (6−8 weeks old) were subcutaneously injected 3.5 × 10^5 B16-F10(OVA) cells diluted in PBS:Matrigel® (1:4) in the right flank (Day 0). At day 7, 10 and 13 mice were injected with a dose of therapeutic (50 μL subcutaneously injected in the hock) of PBS, OVA (10 μg) + *E. coli* LPS (5 μg), OVA (10 μg) + Alum (25 μL), mIONPsp-HyNic-FB-OVA (10 μg OVA) + mIONPsp-*E. Coli* LPS (5 μg Ligand), mIONPsp-HyNic-FB-OVA (10 μg OVA) + mIONPsp-Poly(I:C)-imiquimod (10 μg of OVA+ 4 μg of Poly(I:C) + 2 μg of Imiquimod per mouse), mIONPsp-OVA + mIONPsp-Poly(I:C)-imiquimod, 30 μg of IONP per injection. Animals were monitored for tumor growth using an electronic digital caliper 779A series (Starrett). Criteria for humane endpoint included tumors greater than 1.5 cm diameter and ulceration. Results were expressed as mean ± SEM of at least 5 mice per group.

4.5: References

(1)   Farkona, S.; Diamandis, E. P.; Blasutig, I. M. Cancer Immunotherapy: The Beginning of the End of Cancer? *BMC Med.* **2016**, *14* (1), 1.

(2)   Ribas, A.; Wolchok, J. D. Cancer Immunotherapy Using Checkpoint Blockade. *Science*. 2018.

(3)   Alsaab, H. O.; Sau, S.; Alzhrani, R.; Tatiparti, K.; Bhise, K.; Kashaw, S. K.; Iyer, A. K. PD-1 and PD-L1 Checkpoint Signaling Inhibition for Cancer Immunotherapy: Mechanism, Combinations, and Clinical Outcome. *Front. Pharmacol.* **2017**, *23* (8), 561.

(4)   Shukuya, T.; Carbone, D. P. Predictive Markers for the Efficacy of Anti-PD-1/PD-L1 Antibodies in Lung Cancer. *J. Thorac. Oncol.* **2016**, *11* (7), 976.

(5)   Lipson, E. J. Antagonists of PD-1 and PD-L1 in Cancer Treatment. **2016**, *179* (110), 95.

(6)   Hu, Z.; Ott, P. A.; Wu, C. J. Towards Personalized, Tumour-Specific, Therapeutic Vaccines for Cancer. *Nat. Rev. Immunol.* **2018**, *18* (3), 168.

(7)   Didierlaurent, A. M.; Morel, S.; Lockman, L.; Giannini, S. L.; Bisteau, M.; Carlsen, H.; Kielland, A.; Vosters, O.; Vanderheyde, N.; Schiavetti, F.; Larocque D.; Van Mechelen M.; Garçon N. AS04, an Aluminum Salt- and TLR4 Agonist-Based Adjuvant System, Induces a Transient Localized Innate Immune Response Leading to Enhanced Adaptive Immunity. *J. Immunol.* **2009**, *183* (10), 6186.

(8)   Giannini, S. L.; Hanon, E.; Moris, P.; Van Mechelen, M.; Morel, S.; Dessy, F.; Fourneau, M. A.; Colau, B.; Suzich, J.; Losonksy, G.; Martin M. T.; Dubin G.; Wettendorff M. A. Enhanced Humoral and Memory B Cellular Immunity Using HPV16/18 L1 VLP Vaccine Formulated with the MPL/Aluminium Salt Combination (AS04) Compared to Aluminium Salt Only. *Vaccine* **2006**, *24* (33–34), 5937.

(9)   Coffman, R. L.; Sher, A.; Seder, R. A. Vaccine Adjuvants: Putting Innate Immunity to Work. *Immunity* **2010**, *33* (4), 492.

(10)   Ott, P. A.; Hodi, F. S.; Kaufman, H. L.; Wigginton, J. M.; Wolchok, J. D. Combination Immunotherapy: A Road Map. *J. Immunother. Cancer* **2017**, *5* (1), 1.

(11) Dowling, J. K.; Mansell, A. Toll-like Receptors: The Swiss Army Knife of Immunity and Vaccine Development. *Clin. Transl. Immunol.* **2016**, *5* (5), 85.

(12) Baxevanis, C. N.; Voutsas, I. F.; Tsitsilonis, O. E. Toll-like Receptor Agonists: Current Status and Future Perspective on Their Utility as Adjuvants in Improving Anticancer Vaccination Strategies. *Immunotherapy* **2013**, *5* (5), 497.

(13) Lu, H. TLR Agonists for Cancer Immunotherapy: Tipping the Balance between the Immune Stimulatory and Inhibitory Effects. *Front. Immunol.* **2014**, *5*, 83.

(14) Kaczanowska, S.; Joseph, A. M.; Davila, E. TLR Agonists: Our Best Frenemy in Cancer Immunotherapy. *J. Leukoc. Biol.* **2013**, *93* (6), 847.

(15) Ruiz-De-Angulo, A.; Zabaleta, A.; Gómez-Vallejo, V.; Llop, J.; Mareque-Rivas, J. C. Microdosed Lipid-Coated 67Ga-Magnetite Enhances Antigen-Specific Immunity by Image Tracked Delivery of Antigen and Cpg to Lymph Nodes. *ACS Nano* **2016**, *26* (10), 1602.

(16) Yan, S.; Rolfe, B. E.; Zhang, B.; Mohammed, Y. H.; Gu, W.; Xu, Z. P. Polarized Immune Responses Modulated by Layered Double Hydroxides Nanoparticle Conjugated with CpG. *Biomaterials* **2014**, *35* (35), 9508.

(17) de Titta, A.; Ballester, M.; Julier, Z.; Nembrini, C.; Jeanbart, L.; van der Vlies, A. J.; Swartz, M. A.; Hubbell, J. A. Nanoparticle Conjugation of CpG Enhances Adjuvancy for Cellular Immunity and Memory Recall at Low Dose. *Proc. Natl. Acad. Sci. U. S. A.* **2013**, *110* (49), 19902.

(18) Lee, I. H.; Kwon, H. K.; An, S.; Kim, D.; Kim, S.; Yu, M. K.; Lee, J. H.; Lee, T. S.; Im, S. H.; Jon, S. Imageable Antigen-Presenting Gold Nanoparticle Vaccines for Effective Cancer Immunotherapy in Vivo. *Angew. Chemie - Int. Ed.* **2012**, *51* (35), 8800.

(19) Yang, R.; Xu, J.; Xu, L.; Sun, X.; Chen, Q.; Zhao, Y.; Peng, R.; Liu, Z. Cancer Cell Membrane-Coated Adjuvant Nanoparticles with Mannose Modification for Effective Anticancer Vaccination. *ACS Nano* **2018**, *12* (6), 5121.

(20) Butler, N. S.; Nolz, J. C.; Harty, J. T. Immunologic Considerations for Generating Memory CD8 T Cells through Vaccination. *Cell. Microbiol.* **2011**, *13* (7), 925.

(21) Sallusto, F.; Lenig, D.; Förster, R.; Lipp, M.; Lanzavecchia, A. Two Subsets of Memory T Lymphocytes with Distinct Homing Potentials and Effector Functions. *Nature* **1999**, *401* (6754), 708.

(22) Bocanegra Gondan, A. I.; Ruiz-de-Angulo, A.; Zabaleta, A.; Gómez Blanco, N.; Cobaleda-Siles, B. M.; García-Granda, M. J.; Padro, D.; Llop, J.; Arnaiz, B.; Gato, M.; Escors D.; Mareque-Rivas J. C. Effective Cancer Immunotherapy in Mice by PolyIC-Imiquimod Complexes and Engineered Magnetic Nanoparticles. *Biomaterials* **2018**, *170*, 95.

(23) Yamazaki, T.; Akiba, H.; Iwai, H.; Matsuda, H.; Aoki, M.; Tanno, Y.; Shin, T.; Tsuchiya, H.; Pardoll, D. M.; Okumura, K.; Azuma M.; Yagita H. Expression of Programmed Death 1 Ligands by Murine T Cells and APC. *J. Immunol.* **2002**, *169* (10), 5538.

(24) Freeman, G. J.; Long, A. J.; Iwai, Y.; Bourque, K.; Chernova, T.; Nishimura, H.; Fitz, L. J.; Malenkovich, N.; Okazaki, T.; Byrne, M. C.; Horton H. F.; Fouser L.; Carter L.; Ling V.; Bowman M. R.; Carreno B. M.; Collins M.; Wood C. R.; Honjo T. Engagement of the PD-1 Immunoinhibitory Receptor by a Novel B7 Family Member Leads to Negative Regulation of Lymphocyte Activation. *J. Exp. Med.* **2000**, *192* (7), 1027.

(25) Yang, H.; Wang, B.; Wang, T.; Xu, L.; He, C.; Wen, H.; Yan, J.; Su, H.; Zhu, X. Toll-like Receptor 4 Prompts Human Breast Cancer Cells Invasiveness via Lipopolysaccharide Stimulation and Is Overexpressed in Patients with Lymph Node Metastasis. *PLoS One* **2014**, *9* (10), e109980.

(26) Algar, W. R.; Prasuhn, D. E.; Stewart, M. H.; Jennings, T. L.; Blanco-Canosa, J. B.; Dawson, P. E.; Medintz, I. L. The Controlled Display of Biomolecules on Nanoparticles: A Challenge Suited to Bioorthogonal Chemistry. *Bioconjug. Chem.* **2011**, *22* (5), 825.

Conclusions

- Different TLR4-agonists loaded nanoplatforms have been synthesized and characterized taking advantage of the self-assembly process of hydrophobic nanoparticles, PEG-phospholipids and the amphiphilic TLR4 ligands, resulting in IONPsp-, IONPc-, QDs- and UCNPs- filled nanomicelles. These constructs showed a uniform size distribution and their hydrodynamic diameters were within the 20-100 nm range ideal for lymph node uptake, and their negative ζ-potentials and hydrophobicity further contributes to their uptake in the lymph nodes.

- These nanoparticles could modulate the immunostimulatory activity and toxicity of the ligands E. Coli LOS and Xcc LOS in antigen presenting cells, with each of the different nanoplatforms affecting these characteristics differently. Among the different systems developed, mIONPsp-*Xcc* LOS was selected and used for further in vivo studies.

- Hydrophobic UCNPs were synthesized, characterized and used to prepare two different UCNPs-filled nanomicelles loaded with different amounts of the TLR4 antagonist IAXO 102, both showing uniform size distribution and a hydrodynamic diameter within the 20-100 nm range for lymph node delivery. This was able to suppress LPS induced activation of macrophages.

- mIONPsp were covalently bound to the model antigen OVA using hydrazone chemistry, a high-yield, fast, selective and monitorable conjugation reaction. The obtained mIONPsp-HyNic-FB-OVA had a low polydispersity, a hydrodynamic diameter of ~50 nm suitable for lymph node delivery and were stable for weeks in PBS.

- The hydrazone conjugation chemistry was used to bind OVA to mJanusNPs and to prepare mIONPsp-*E. Coli* LPS/HyNic-FB-OVA both characterized by low polydispersity and a hydrodynamic diameter suitable for lymph node delivery.

- Both mIONPsp-*Xcc* LOS and mIONPsp-HyNic-FB-OVA were functionalized with a rhodamine-phospholipid and tracked by fluorescence microscopy and were uptaken in the lysosomes in antigen presenting cells in 3 h at nanomolar concentrations.

- A formulation composed of mIONPsp-Xcc LOS and mIONPsp-HyNic-FB-OVA was investigated in a mice prophylaxis model against the aggressive B16-F10(OVA) melanoma and when coupled to PD-L1 checkpoint blockade led to complete tumor rejection of even after a re-challenge, with FACS analysis confirming induction of antigen-specific T cells and long-lasting antitumor responses.

- A formulation composed of mIONPsp-HyNic-FB-OVA and mIONPsp-Poly(I:C)-imiquimod was injected in mice challenged with B16-F10(OVA) melanoma as a therapy. When compared to the electrostatic mIONPsp-OVA, mIONPsp-HyNic-FB-OVA could enhance the median survival of mice from 31 to 51 days and improve tumor rejection from 1/5 mice to 3/5 mice.

Abbreviations

AD: Alzheimer's disease

AGP: Aminoalkyl glucosamidine-4-phosphates

ALS: Amyotrophic lateral sclerosis

APC: Antigen-presenting cells

BCG: Bacillus Calmette-Guérin

BECC: Bacterial enzymatic combinatorial chemistry

BMDCs: Bone marrow-derived dendritic cells

BMDMs: Bone marrow-derived macrophages

CD14: Cluster of differentiation 14

CpG ODN: CpG oligodeoxynucleotide

CT: Computed tomography

CTLA-4: Cytotoxic T-lymphocyte-associated protein 4

DAMPs: Damage-associated molecular patterns

DCs: Dendritic cells

DLS: Dynamic light scattering

dMMR: Mismatch repair-deficient solid tumors.

DMBA: 7,12-dimethylbenz(a)anthracene

DNP-OVA: Dinitrophenylated-ovalbumin

DOX: Doxorubicin

DPPE-cPEG: 1,2-dipalmitoyl-sn-glycero-3-phosphoethanolamine-N-[methoxy(polyethylene glycol)-2000] (ammonium salt)

DPPE-mPEG: 1,2-Dipalmitoyl-sn-glycero-3-phosphoethanolamine-N-[methoxy (polyethylene glycol)-2000]

DSPE-aPEG: 2-distearoyl-sn-glycero-3-phosphoethanolamine-N-[amino(polyethylene glycol)-2000]

DSPE-mPEG: 1,2-distearoyl-sn-glycero-3-phosphoethanolamine-N-[methoxy(polyethylene glycol)-2000] (ammonium salt)

ED: Effective dose

EDC: 1-ethyl-3-(3-dimethylaminopropyl)carbodiimide

EMA: European Medicines Agency

FDA: American food and drug administration

GLA: Glucopyranosyl lipid A

HMGB1: High-mobility-group box 1 alarmin protein

HNSCC: Head and neck squamous cell carcinoma

IC50: Half maximal inhibitory concentration

IFA: Incomplete Freund's adjuvant

IFNs: Interferons

IL: Interleukin

IONPc: Iron oxide nanocubes

IONPs: Iron oxide nanoparticles

IONPsp: Iron oxide nanospheres

IR: Infrared spectroscopy (IR).

JanusNPs: Janus nanoparticles

Kdo$_2$-Lipid A: 3-deoxy-D-manno-octulosonic acid-lipid A

LAL: Limulus amebocyte lysate

LOS: Lipooligosaccharides

LPS: Lipopolysaccharide

MHC: Major histocompatibility complex

mNPs: Nanoparticle-filled micelles

MPLA: Monophosphoryl lipid A

MRI: Magnetic resonance imaging

MSI-H: Microsatellite instable-high

MyD88: Myeloid differentiation factor 88

NHS: N-hydroxysuccinimide

NK: Natural killer cell

NKT: Natural killer T cell

NSCLC: Non-small cell lung cancer

RCC: renal cell carcinoma

OVA: Ovalbumin

PAMPs: Pathogen-associated molecular patterns

PCho: Phosphorylcholine

PDT: Photodynamic therapy

PD-1: Programmed cell death protein 1

PD-L1: Programmed death-ligand 1

PEG: Poly(ethylene glycol)

PEG thiol: Thiol-functionalized PEG

PLGA: Polylactide-co-glycolide micro- or nanoparticles

PmB: Polymyxin B

Poly(I:C): Polyinosinic: polycytidylic acid

PRRs: Transmembrane pattern recognition receptors

PS: Photosensitizers

PTT: Photothermal therapy

QDs: Quantum dots

RA: Rheumatoid arthritis

Rho-PE: 1,2 dipalmitoyl-*sn*-glycero-3-phosphoethanolamine-N-(lissaminerhodamine B sulfonyl) (ammonium salt)

ROS: Reactive oxygen species

SDS: Sodium dodecyl sulfate

SDR: Static dephasing regime

SNR: Signal to noise ratio

TAAs: Tumor-associated antigens

TEM: Transmission electron microscopy

TICAM2: TIR-containing adapter molecule 2

TILs: Tumor-infiltrating lymphocytes

TIR: Toll-interleukin 1 receptor

TIRAP: TIR-domain containing adaptor protein

TNF-α: Tumor necrosis factor α

TLRs: Toll-like receptors

TLR4: Toll-like receptor 4

TRAM: TRIF-related adaptor molecule

TRIF: TIR-domain-containing adapter-inducing interferon-β

UC: Upconversion

UCNPs: Upconverting nanoparticles

XPS: X-ray photoelectron spectroscopy

γ-PGA NPs: Poly(γ-glutamic acid) nanoparticles

Curriculum vitae

Giordano Traini

giordano.traini@gmail.com

+34 688894917

Publications

Giordano Traini, Ane Ruiz-de-Angulo, Juan Bautista Blanco-Canosa, Kepa Zamacola Bascarán, Antonio Molinaro, Alba Silipo, David Escors, Juan C. Mareque-Rivas- Cancer Immunotherapy of TLR4 Agonist-Antigen Constructs Enhanced with Pathogen Mimicking Magnetite Nanoparticles and Checkpoint Blockade of PD-L1. Full paper in Small (IF 2018: 9.5)**: https://doi.org/10.1002/smll.201803993**

Presentations in conferences and meetings:

MicrobiotaMi 2018, Milan (Italy), 5th to 7th/11/2018:
Giordano Traini, Ane Ruiz-de-Angulo, Juan C. Mareque-Rivas- Cancer immunotherapy of TLR4 agonist-antigen constructs enhanced with pathogen-mimicking magnetite nanoparticles and checkpoint blockade of PD-L1. Poster presentation.

24th World Nano Conference, Rome (Italy), 7th to 8th/05/2018:
Giordano Traini, Ane Ruiz-de-Angulo, Juan C. Mareque-Rivas- Magnetite-filled micelles as a versatile delivery vehicle for a TLR4 mediated cancer nanovaccine. Poster presentation, published in the book of abstracts: Giordano Traini et al., J Nanomater. Mol. Nanotechnol. 2018, Volume 7 DOI: 10.4172/2324-8777-C2-024.

5th "TOLLerant" meeting, Ghent (Belgium), 12th to 15th/12/2017:
Giordano Traini- Nanoparticle filled micelles as versatile delivery vehicles for TLR4 mediated immunotherapy- An update. Oral presentation.

4th "TOLLerant" meeting, Naples (Italy), 5th to 7th/06/2017:
Giordano Traini- Nanoparticle filled micelles as versatile delivery vehicles for TLR4 mediated immunotherapy. Oral presentation.

"TOLLerant" mid-term meeting, Milan (Italy), 12/01/2017:
Giordano Traini- Nanoparticle-based delivery vehicles for TLR4 modulators-Progress, methods and future perspectives. Oral presentation.

3rd "TOLLerant" meeting, Ljubljana (Slovenia), 14th to 16th/12/2016:
Giordano Traini- Nanoparticle-based delivery vehicles for TLR4 modulators. Oral presentation.

2nd "TOLLerant" meeting, Madrid (Spain) 24th to 27th/05/2016:
Giordano Traini- Nanomaterial chemistry for TLR4 modulation. Oral presentation.

Additional events attendances:

1st TOLLerant meeting, Milan (Italy), 21st to 24th/09/2015:
Self-introduction of the PhD fellows and lectures.

CIC BiomaGUNE's international scientific advisory board meeting, 14th to 18th/09/2015:
Lectures and seminars. I helped presenting the poster of my research group, "Nanomaterials for Theragnosis".

Outreach activites:

EXPO Milan- The journey of a molecule within the human body, 24th/09/2015:
I and other PhD fellows gathered a crowd of people to show them an educational video on the interaction of molecules with their receptors within the human body created by the group of Prof. Francesco Peri.

Pint of Science, Donostia- San Sebastian, 15th to 17th/05/2017:
I took part in the organization of the event, by distributing invitations, evaluation questionnaires and setting up the venue for the talks.

Acknowledgements/ Vulio rringraziá

The first thanks goes to Prof. Juan Mareque, the director of this thesis, which followed me along this journey helping me grow and improve. Thanks for accepting me as a PhD student in your research group, thanks for the patience and the dedication shown in guiding me through the path of science and thanks for being a capable advisor. Thanks also to Maria Begoña Ruiz Larrea, my tutor at the university, for being always helpful.

The next thanks goes to the people from TOLLerant. Thanks for having built a network of professionals and, first and foremost, people. Thanks for the great advice you gave me, thanks for cooperating and welcoming me in your laboratories, thanks for sharing your knowledge and your thoughts with me. And thanks to the European Union for having funded this wonderful project.

Thanks to the people from CIC BiomaGUNE. Thanks for making that place a stimulating environment, thanks for all the suggestions, the help given and the coffee breaks.

Thanks to my coworkers, with which we shared the epic quest for achieving our PhD, or whatever achievement may it be. Thanks for the support given and the guidance, and thanks for the interesting lunchtime discussions.

Thanks to my friends which somehow helped me achieving my PhD -you guys know how-, thanks to who left, who's still here, who I know since I was a kid, and who I got to know recently.

Thanks to my family for making me the person I am.

Finally, thanks to my SO. I owe you a second authorship of this document at least.

Lu primu grazie a dè pè lu Prof. Juan Mareque, lu Patrò, che m'è vvinutu 'ppresso ssu camminu che m' ha fattu studiatu e m'ha fatto cresce. Grazie per avemme 'ssundu come dottó su lu gruppu tuu, grazie pe la santa pazienza e l'impegnu che ce sci misto e grazie pe esse un Patrò capace. Grazie a Maria Begoña Ruiz Larrea, la Patrona dell' università, che dè stata sempre n' aiutu.

Lu prossimu a dè pè cossò de TOLLerant. Grazie per avé fattu 'n gruppu de jende capace e soprattutto de persò. Grazie pe avemme iutato, pe fadigá assemo e famme veni llà li lavoratori vostri, spartì quello che saccete e quello che scete pensato. E grazie all Europa per avè misto Li Sordi pe ssu gran progettu.

Grazie pure a le persó de lu CIC BiomaGUNE. Grazie pe fallu 'n postu ddò se 'mpara, pe li suggerimendi, l' aiutu e li caffè.

Grazie a li colleghi, cossò co cui scimo spartito la missìo de diventà studiati, o quello che d'è. Grazie pe l' aiutu, pe 'mparamme e pe le chiacchiere.

Grazie a ll' amici mia pe aiutamme a famme studiatu, quilli che d' è jiti, quilli che d' è rmasti, quilli che conoscio da quanno sò fricu e quilli che so conoscioto poco fa.

Grazie a la famija mia per avemme misto a lu monnu e cresciutu.

Pe 'ffinì, grazie a lla vergara de mojema, duvrisci esse la seconda che ha scritto ssa tesi.